

AD-A194 693

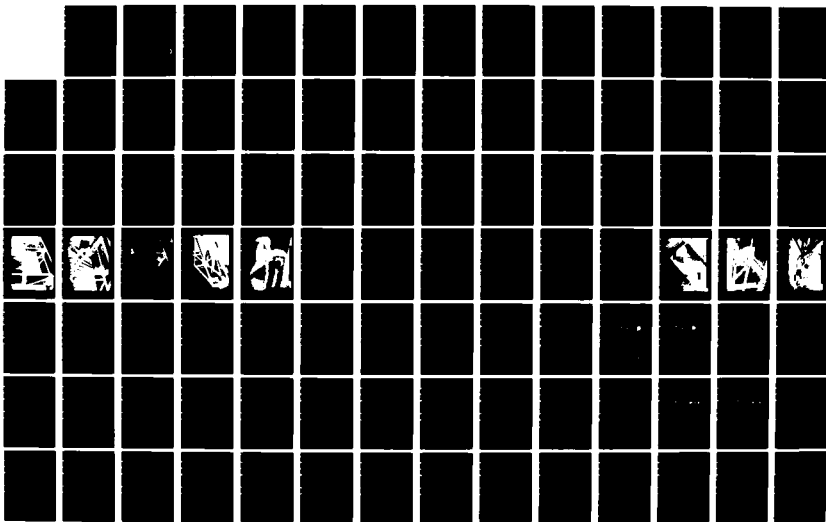
TESTING OF AN INERTIAL REFERENCE SYSTEM CONCEPT TO
MEASURE BLATT-INDUCED (U) TECH REPS INC ABERDEEN MD
ABERDEEN RESEARCH CENTER N H ETHRIDGE ET AL NOV 87
ARC-87-184 BRL-CR-591

1/2

UNCLASSIFIED

F/G 14/2

NL





AD-A194 693

CONTRACT REPORT BRL-CR-591

TESTING OF AN INERTIAL REFERENCE SYSTEM CONCEPT TO MEASURE BLAST-INDUCED DISPLACEMENTS OF VEHICLES

ABERDEEN RESEARCH CENTER (A DIV OF TECH. REPS., INC.) 30 DIAMOND STREET, P.O. BOX 548 ABERDEEN, MD 21001

NOVEMBER 1987

DTIC ELECTE APR 08 1988 S D H

APPROVED FOR PUBLIC RELEASE, DISTRIBUTION UNLIMITED.

US ARMY BALLISTIC RESEARCH LABORATORY ABERDEEN PROVING GROUND, MARYLAND

88 4 3 034

DESTRUCTION NOTICE

Destroy this report when it is no longer needed. DO NOT return it to the originator.

Additional copies of this report may be obtained from the National Technical Information Service, U.S. Department of Commerce, Springfield, VA 22161.

The findings of this report are not to be construed as an official Department of the Army position, unless so designated by other authorized documents.

The use of trade names or manufacturers' names in this report does not constitute indorsement of any commercial product.

ADA194693

REPORT DOCUMENTATION PAGE				Form Approved OMB No. 0704-0188 Exp. Date: Jun 30, 1986	
1a. REPORT SECURITY CLASSIFICATION UNCLASSIFIED		1b. RESTRICTIVE MARKINGS None			
2a. SECURITY CLASSIFICATION AUTHORITY N/A		3. DISTRIBUTION/AVAILABILITY OF REPORT Approved for Public Release, Distribution Unlimited.			
2b. DECLASSIFICATION/DOWNGRADING SCHEDULE N/A					
4. PERFORMING ORGANIZATION REPORT NUMBER(S) ARC-87-104		5. MONITORING ORGANIZATION REPORT NUMBER(S) BRL-CR-591			
6a. NAME OF PERFORMING ORGANIZATION Aberdeen Research Center (A Div of Tech. Reps., Inc.)		6b. OFFICE SYMBOL (if applicable)	7a. NAME OF MONITORING ORGANIZATION U.S. Army Ballistic Research Laboratory ATTN: SLCBR-TB-B		
6c. ADDRESS (City, State, and ZIP Code) 30 Diamond Street, P.O. Box 548 Aberdeen, MD 21001		7b. ADDRESS (City, State, and ZIP Code) Aberdeen Proving Ground, MD 21005-5066			
8a. NAME OF FUNDING/SPONSORING ORGANIZATION		8b. OFFICE SYMBOL (if applicable)	9. PROCUREMENT INSTRUMENT IDENTIFICATION NUMBER DAAA15-86-C-0074		
8c. ADDRESS (City, State, and ZIP Code)		10. SOURCE OF FUNDING NUMBERS			
		PROGRAM ELEMENT NO.	PROJECT NO.	TASK NO.	WORK UNIT ACCESSION NO.
11. TITLE (Include Security Classification) Testing of an Inertial Reference System Concept to Measure Blast-Induced Displacements of Vehicles (U)					
12. PERSONAL AUTHOR(S) Ethridge, Noel H., Dixon, Lisa A., Jackson, Willis F.					
13a. TYPE OF REPORT Final		13b. TIME COVERED FROM 86-7-23 TO 87-3-23	14. DATE OF REPORT (Year, Month, Day)		15. PAGE COUNT
16. SUPPLEMENTARY NOTATION					
17. COSATI CODES			18. SUBJECT TERMS (Continue on reverse if necessary and identify by block number) Inertial Reference Systems, Accelerometers, Angular Rate Sensors, Inertial Tracking Systems, Overturning Test Facility, Vehicle Overturning by Blast, Data Reduction Program		
FIELD	GROUP	SUB-GROUP			
00	11				
19. ABSTRACT (Continue on reverse if necessary and identify by block number) (rsb) This work is the first phase of a project to develop an inertial reference system to measure the displacement of military vehicles exposed to a blast wave in large shock tubes or high-explosive simulations of nuclear weapons. Experimental data describing the movement of military vehicles by blast is required for survivability assessments of such vehicles and for validation of computer models predicting their movement. The sensor array selected for tracking six degrees-of-freedom vehicle movement consisted of three linear accelerometers and three angular rate sensors. For a preliminary evaluation of an inertial reference system using such a sensor array, the capability of two accelerometers and one rate sensor to track displacement and rotation in a plane was investigated. A test facility designed and constructed to simulate the overturning of a vehicle by blast. Off-the-shelf gages were obtained and placed on the rotating component of the test facility, and overturning tests were conducted. A data reduction program was written to predict the (Cont'd)					
20. DISTRIBUTION/AVAILABILITY OF ABSTRACT <input checked="" type="checkbox"/> UNCLASSIFIED/UNLIMITED <input checked="" type="checkbox"/> SAME AS RPT <input type="checkbox"/> DTIC USERS			21. ABSTRACT SECURITY CLASSIFICATION UNCLASSIFIED		
22a. NAME OF RESPONSIBLE INDIVIDUAL Mr. John F. Polk		22b. TELEPHONE (Include Area Code) (301) 278-3361		22c. OFFICE SYMBOL SLCBR-TB-B	

19. ABSTRACT (Continued)

trajectory of the sensor array from the gage readings for comparison with that which actually occurred. The results showed that such a sensor array tracked overturning through 90 degrees and displacement for about two metres with acceptable errors. The requirements for a complete inertial reference system were developed.

FOREWORD

This study was sponsored by the U.S. Army Armament, Munitions, and Chemical Command, Aberdeen Proving Ground, Maryland, under contract DAA15-86-C-0074. The technical monitor for the contract was Mr. Richard J. Pearson of the U.S. Army Ballistic Research Laboratory (BRL), Aberdeen Proving Ground, Maryland.

The authors express appreciation to Mr. Pearson for prompt assistance in obtaining the required government-furnished equipment and for providing access to calibration facilities at the BRL, and to Mr. John H. Keefer, Mr. Sterling A. Dunbar, Mr. G. Thomas Watson, and Ms. Robin S. Bensch for their contributions to the project.

Trade names of materials or products of commercial or non-government organizations are cited in this report only where essential to precision in describing research procedures or evaluation of results. Their use does not constitute official endorsement or approval.

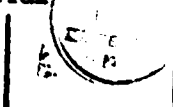
Accession For	
NTIS GRA&I	<input checked="" type="checkbox"/>
DTIC TAB	<input type="checkbox"/>
Unannounced	<input type="checkbox"/>
Justification	
By _____	
Distribution/	
Availability Codes	
Dist	Avail and/or Special
A-1	

TABLE OF CONTENTS

	<u>Page</u>
LIST OF ILLUSTRATIONS.....	7
LIST OF TABLES.....	17
● I INTRODUCTION.....	19
II PROCEDURE.....	20
III INERTIAL REFERENCE SYSTEM.....	20
IV DESIGN AND CONSTRUCTION OF TEST FACILITY.....	27
A. Representative Vehicle Response.....	27
B. Concept for the Test Facility.....	28
C. Modeling of Test Facility.....	32
D. Construction and Assembly.....	38
V INSTRUMENTATION.....	39
A. Selection of Sensors.....	39
B. Calibration of Sensors.....	44
C. Installation of Gages on the Test Facility.....	49
D. Data Acquisition and Reduction System.....	49
VI PROGRAM TO COMPUTE TRAJECTORY OF SENSORS.....	54
VII TEST PROGRAM.....	59
A. Test Procedure.....	59
B. Tests and Results.....	60
C. Discussion of Results.....	127
VIII REQUIREMENTS FOR AN INERTIAL REFERENCE SYSTEM.....	140
IX CONCLUSIONS.....	144
REFERENCES.....	147
APPENDIX A. DATA REDUCTION PROGRAM.....	149
LIST OF SYMBOLS.....	159
DISTRIBUTION LIST.....	163

LIST OF ILLUSTRATIONS

<u>Figure</u>		<u>Page</u>
1	Body-centered and fixed coordinates for rigid body motion.....	22
2	The planar eight accelerometer, four-pair configuration by McMaster (Reference 3).....	26
3	Computed angular velocity of overturning of a truck-shelter combination struck by a 68.9 kPa blast wave from a simulated 1 KT nuclear explosion.....	29
4	Computed accelerations that would be measured by two accelerometers placed at the center of gravity of an overturning truck-shelter combination struck by a 68.9 kPa blast wave from a simulated 1 KT nuclear explosion. The effect of gravity on the accelerometers is included.....	30
5	Concept for a facility to simulate overturning of a military vehicle system by blast.....	31
6	Model representation of quarter wheel after rotation through angle θ	34
7	Acceleration components at the location of the accelerometers on the quarter wheel. Gravitational acceleration g is shown vertical because of the sign convention chosen.....	35
8	Predicted accelerometer waveforms for Cases 1 and 2 for the test facility.....	37
9	The overturning test facility.....	39
10	The quarter wheel in the initial position.....	40
11	The quarter wheel in the overturned position.....	41
12	Rear view of the test facility.....	42
13	The quick-release pin holding the restraint cable.....	43
14	The Humphrey rate sensor and an Endevco accelerometer mounted on the quarter wheel.....	50
15	The precision potentiometer coupled to the end of the rotating axle.....	51
16	The load cell placed to read the force applied by the springs to the cable attached to the quarter wheel.....	52
17	Block diagram of data acquisition and reduction system.....	53

LIST OF ILLUSTRATIONS (Cont'd)

<u>Figure</u>		<u>Page</u>
18	Position and orientation of accelerometers for rotation in a plane by the test facility.....	55
19	Unfiltered acceleration versus time from the initially vertical Endevco accelerometer on Test 29.....	63
20	Filtered acceleration versus time from the initially vertical Endevco accelerometer on Test 29.....	63
21	Unfiltered acceleration versus time from the initially horizontal Endevco accelerometer on Test 29.....	64
22	Filtered acceleration versus time from the initially horizontal Endevco accelerometer on Test 29.....	64
23	Unfiltered angular velocity versus time from the Humphrey rate sensor on Test 29.....	65
24	Filtered angular velocity versus time from the Humphrey rate sensor on Test 29.....	65
25	Unfiltered angle versus time derived from the potentiometer on the axle of the quarter wheel on Test 29.....	66
26	Filtered angle versus time derived from the potentiometer on the axle of the quarter wheel on Test 29.....	66
27	Unfiltered load cell record from Test 29.....	67
28	Filtered load cell record from Test 29.....	67
29	Unfiltered positive phase of acceleration versus time from the vertical accelerometer on Test 29.....	68
30	Filtered positive phase of acceleration versus time from the vertical accelerometer on Test 29.....	68
31	Unfiltered positive phase of acceleration versus time from the initially horizontal accelerometer on Test 29.....	69
32	Filtered positive phase of acceleration versus time from the initially horizontal accelerometer on Test 29.....	69
33	Unfiltered positive phase of the load cell record from Test 29	70
34	Filtered positive phase of the load cell record from Test 29..	70

LIST OF ILLUSTRATIONS (Cont'd)

<u>Figure</u>		<u>Page</u>
35	Comparison of the sensor array trajectory for Test 29 derived from the Endevco accelerometers and the Humphrey rate sensor with the reference trajectory derived from the potentiometer record.....	71
36	Horizontal displacement error versus time of the sensor array for Test 29.....	72
37	Vertical displacement error versus time of the sensor array for Test 29.....	72
38	Comparison of the rotation angle obtained by integration of the rate sensor record with that derived from the potentiometer record for Test 29.....	74
39	Error in the rotation angle obtained by integration of the rate sensor record for Test 29.....	75
40	Unfiltered acceleration versus time from the initially vertical Endevco accelerometer on Test 33.....	76
41	Filtered acceleration versus time from the initially vertical Endevco accelerometer on Test 33.....	76
42	Unfiltered acceleration versus time from the initially horizontal Endevco accelerometer on Test 33.....	77
43	Filtered acceleration versus time from the initially horizontal Endevco accelerometer on Test 33.....	77
44	Unfiltered angular velocity versus time from the Humphrey rate sensor on Test 33.....	78
45	Filtered angular velocity versus time from the Humphrey rate sensor on Test 33.....	78
46	Unfiltered angle versus time derived from the potentiometer on the axle of the quarter wheel on Test 33.....	79
47	Filtered angle versus time derived from the potentiometer on the axle of the quarter wheel on Test 33.....	79
48	Unfiltered positive phase of acceleration versus time from the vertical accelerometer on Test 33.....	80
49	Filtered positive phase of acceleration versus time from the vertical accelerometer on Test 33.....	80

LIST OF ILLUSTRATIONS (Cont'd)

<u>Figure</u>		<u>Page</u>
50	Unfiltered positive phase of acceleration versus time from the initially horizontal accelerometer on Test 33.....	81
51	Filtered positive phase of acceleration versus time from the initially horizontal accelerometer on Test 33.....	81
52	Comparison of the sensor array trajectory for Test 33 derived from the Endevco accelerometers and the Humphrey rate sensor with the reference trajectory derived from the potentiometer record.....	82
53	Horizontal displacement error versus time of the sensor array for Test 33.....	83
54	Vertical displacement error versus time of the sensor array for Test 33.....	83
55	Comparison of the rotation angle obtained by integration of the rate sensor record with that derived from the potentiometer record for Test 33.....	84
56	Error in the rotation angle obtained by integration of the rate sensor record for Test 33.....	85
57	Unfiltered acceleration versus time from the initially vertical Schaevitz accelerometer on Test 45.....	86
58	Filtered acceleration versus time from the initially vertical Schaevitz accelerometer on Test 45.....	86
59	Unfiltered acceleration versus time from the initially horizontal Schaevitz accelerometer on Test 45.....	87
60	Filtered acceleration versus time from the initially horizontal Schaevitz accelerometer on Test 45.....	87
61	Unfiltered angular velocity versus time from the Humphrey rate sensor on Test 45.....	88
62	Filtered angular velocity versus time from the Humphrey rate sensor on Test 45.....	88
63	Unfiltered angle versus time derived from the potentiometer on the axle of the quarter wheel on Test 45.....	89
64	Filtered angle versus time derived from the potentiometer on the axle of the quarter wheel on Test 45.....	89

LIST OF ILLUSTRATIONS (Cont'd)

<u>Figure</u>		<u>Page</u>
65	Unfiltered load cell record from Test 45.....	90
66	Filtered load cell record from Test 45.....	90
67	Unfiltered positive phase of acceleration versus time from the vertical accelerometer on Test 45.....	91
68	Filtered positive phase of acceleration versus time from the vertical accelerometer on Test 45.....	91
69	Unfiltered positive phase of acceleration versus time from the initially horizontal Schaevitz accelerometer on Test 45.....	92
70	Filtered positive phase of acceleration versus time from the initially horizontal Schaevitz accelerometer on Test 45.....	92
71	Unfiltered positive phase of the load cell record from Test 45	93
72	Filtered positive phase of the load cell record from Test 45..	93
73	Comparison of the sensor array trajectory for Test 45 derived from the Schaevitz accelerometers and the Humphrey rate sensor with the reference trajectory derived from the potentiometer record.....	94
74	Horizontal displacement error versus time of the sensor array for Test 45.....	95
75	Vertical displacement error versus time of the sensor array for Test 45.....	95
76	Comparison of the rotation angle obtained by integration of the rate sensor record with that derived from the potentiometer record for Test 45.....	96
77	Error in the rotation angle obtained by integration of the rate sensor record for Test 45.....	98
78	Unfiltered acceleration versus time from the initially vertical Schaevitz accelerometer on Test 46.....	99
79	Filtered acceleration versus time from the initially vertical Schaevitz accelerometer on Test 46.....	99
80	Unfiltered acceleration versus time from the initially horizontal Schaevitz accelerometer on Test 46.....	100

LIST OF ILLUSTRATIONS (Cont'd)

<u>Figure</u>		<u>Page</u>
81	Filtered acceleration versus time from the initially horizontal Schaevitz accelerometer on Test 46.....	100
82	Unfiltered angular velocity versus time from the Humphrey rate sensor on Test 46.....	101
83	Filtered angular velocity versus time from the Humphrey rate sensor on Test 46.....	101
84	Unfiltered angle versus time derived from the potentiometer on the axle of the quarter wheel on Test 46.....	102
85	Filtered angle versus time derived from the potentiometer on the axle of the quarter wheel on Test 46.....	102
86	Unfiltered load cell record from Test 46.....	103
87	Filtered load cell record from Test 46.....	103
88	Unfiltered positive phase of acceleration versus time from the vertical accelerometer on Test 46.....	104
89	Filtered positive phase of acceleration versus time from the vertical accelerometer on Test 46.....	104
90	Unfiltered positive phase of acceleration versus time from the initially horizontal accelerometer on Test 46.....	105
91	Filtered positive phase of acceleration versus time from the initially horizontal accelerometer on Test 46.....	105
92	Unfiltered positive phase of the load cell record from Test 46	106
93	Filtered positive phase of the load cell record from Test 46..	106
94	Comparison of the sensor array trajectory for Test 46 derived from the Schaevitz accelerometers and the Humphrey rate sensor with the reference trajectory derived from the potentiometer record.....	107
95	Horizontal displacement error versus time of the sensor array for Test 46.....	108
96	Vertical displacement error versus time of the sensor array for Test 46.....	108
97	Comparison of the rotation angle obtained by integration of the rate sensor record with that derived from the potentiometer record for Test 46.....	109

LIST OF ILLUSTRATIONS (Cont'd)

<u>Figure</u>		<u>Page</u>
98	Error in the rotation angle obtained by integration of the rate sensor record for Test 46.....	110
99	Comparison of the sensor array trajectory for Test 28 derived from the Endevco accelerometers and the Humphrey rate sensor with the reference trajectory derived from the potentiometer record.....	111
100	Horizontal displacement error versus time of the sensor array for Test 28.....	112
101	Vertical displacement error versus time of the sensor array for Test 28.....	112
102	Comparison of the rotation angle obtained by integration of the rate sensor record with that derived from the potentiometer record for Test 28.....	113
103	Error in the rotation angle obtained by integration of the rate sensor record for Test 28.....	114
104	Comparison of the sensor array trajectory for Test 30 derived from the Endevco accelerometers and the Humphrey rate sensor with the reference trajectory derived from the potentiometer record.....	115
105	Horizontal displacement error versus time of the sensor array for Test 30.....	116
106	Vertical displacement error versus time of the sensor array for Test 30.....	116
107	Comparison of the rotation angle obtained by integration of the rate sensor record with that derived from the potentiometer record for Test 30.....	117
108	Error in the rotation angle obtained by integration of the rate sensor record for Test 30.....	118
109	Comparison of the sensor array trajectory for Test 31 derived from the Endevco accelerometers and the Humphrey rate sensor with the reference trajectory derived from the potentiometer record.....	119
110	Horizontal displacement error versus time of the sensor array for Test 31.....	120
111	Vertical displacement error versus time of the sensor array for Test 31.....	120

LIST OF ILLUSTRATIONS (Cont'd)

<u>Figure</u>		<u>Page</u>
112	Comparison of the rotation angle obtained by integration of rate sensor record with that derived from the potentiometer record for Test 31.....	121
113	Error in the rotation angle obtained by integration of the rate sensor record for Test 31.....	122
114	Comparison of the sensor array trajectory for Test 35 derived from the Endevco accelerometers and the Humphrey rate sensor with the reference trajectory derived from the potentiometer record.....	123
115	Horizontal displacement error versus time of the sensor array for Test 35.....	124
116	Vertical displacement error versus time of the sensor array for Test 35.....	124
117	Comparison of the rotation angle obtained by integration of the rate sensor record with that derived from the potentiometer record for Test 35.....	125
118	Error in the rotation angle obtained by integration of the rate sensor record for Test 35.....	126
119	Comparison of the sensor array trajectory for Test 43 derived from the Schaevitz accelerometers and the Humphrey rate sensor with the reference trajectory derived from the potentiometer record.....	128
120	Horizontal displacement error versus time of the sensor array for Test 43.....	129
121	Vertical displacement error versus time of the sensor array for Test 43.....	129
122	Comparison of the rotation angle obtained by integration of the rate sensor record with that derived from the potentiometer record for Test 43.....	130
123	Error in the rotation angle obtained by integration of the rate sensor record for Test 43.....	131
124	Comparison of the sensor array trajectory for Test 48 derived from the Schaevitz accelerometers and the Humphrey rate sensor with the reference trajectory derived from the potentiometer record.....	132

LIST OF ILLUSTRATIONS (Concluded)

<u>Figure</u>		<u>Page</u>
125	Horizontal displacement error versus time of the sensor array for Test 48.....	133
126	Vertical displacement error versus time of the sensor array for Test 48.....	133
127	Comparison of the rotation angle obtained by integration of the rate sensor record with that derived from the potentiometer record for Test 48.....	134
128	Error in the rotation angle obtained by integration of the rate sensor record for Test 48.....	135
129	Comparison of computed angular velocity for a truck-shelter system struck by blast with that from Test 28 in the test facility.....	136
130	Comparison of computed angle versus time for a truck-shelter struck by blast with that from Test 28 in the test facility...	137
131	Comparison of measured angular velocities from Tests 28, 29, and 30 in the test facility with the same springs and initial load.....	138
132	Comparison of measured angle versus time from Tests 28, 29, and 30 in the test facility with the same springs and initial load.....	139
133	Block diagram of inertial reference system.....	142

LIST OF TABLES

<u>Table</u>		<u>Page</u>
1	Specifications of the Humphrey, Inc., Rate Sensor.....	45
2	Specifications for the Schaevitz Linear Accelerometer at 20 Degrees Celsius.....	46
3	Specifications for the Endevco Accelerometers at 24 Degrees Celsius.....	47
4	Specifications for the Load Cell of Kulite Semiconductor Products, Inc.....	48
5	Tests Performed with Inertial Sensor Arrays in the Test Facility.....	61
6	Errors in Horizontal X and Vertical Y Displacements and Rotation Angle at end of Trajectories in the Test Facility..	141
7	Characteristics of inertial reference system for tracking blast overturning of vehicles.....	145

I. INTRODUCTION

One of the damage mechanisms for military equipment in a nuclear blast environment is the whole body movement that may be produced. Tumbling or overturning of vehicles can cause significant structural damage or render them inoperable until righted. Even if overturning does not occur, a change in orientation may be produced that can put radar and communication equipment out of action until the proper orientation is restored.

Experimental data describing the movement of military equipment during exposure to blast waves simulating those from nuclear explosions is needed for survivability assessments of that equipment. In addition, such data are required for validating computer models of vehicle whole-body movement under long-duration blast loading. Validation of such codes is very important so that the response of U.S. and foreign vehicle systems can be predicted with reliability. It is not practical to obtain vehicle response data experimentally for the full range of targets, yields, and surface conditions of interest to the Army.

Experiments have been conducted previously in which vehicles were exposed to the blast waves from large explosions. The primary instrumentation used on such tests to record whole-body movement has been high-speed photography by cameras mounted on towers near the vehicles. Unfortunately for this technique, the blast wave raises dust from the ground surface which quickly obscures the view of the target. Only at relatively low blast overpressures (less than 70 kPa) have useful displacement versus time data been obtained. At higher overpressures, the dust obscures the targets before significant movement occurs. Dust suppression materials have been applied to the ground surface, but so far they have not prevented dust obscuration. Thus no useful displacement-time data for tracked vehicles has been obtained using photography, and that for wheeled vehicles is limited.

Large nuclear blast simulators have been constructed and used for blast loading of vehicles. However, targets in such simulators may be obscured by a condensation cloud formed by water vapor and possibly carbon dioxide in the driven gas.

A means other than photography is required to measure the displacement versus time of a vehicle struck by a blast wave. One method of interest is the placement of a self-contained inertial tracking system on-board the vehicle. Such a system will use accelerometers and roll rate sensors whose output will be recorded in on-board memories. After the test, a computer program will be used to derive the displacement and rotation versus time for the vehicle from the recorded data.

The objective of this study was to investigate the use of inertial reference systems for measuring blast-induced displacements of military targets.

II. PROCEDURE

The procedure was as follows:

- (1) Review the literature for inertial reference systems and select an appropriate sensor array.
- (2) Design and construct a test facility to translate and rotate a sensor array at approximately the rate that would be experienced during the overturning of a military vehicle.
- (3) Test and evaluate the capability of a sensor array of off-the-shelf components to describe the movement produced by the test facility.
- (4) Develop the requirements for a complete inertial reference system.

III. INERTIAL REFERENCE SYSTEMS

The primary application of inertial reference systems has been for navigation. Gimballed inertial platform systems are by far the most common type of inertial system in military, space, and commercial use. Gyroscopes and accelerometers on the stable platform are inertially stabilized from the body motion, and the stable platform physically represents an inertial reference frame. By double integration of the specific-force indications from the accelerometers, with a correction for gravity, position determination is accomplished. The gimbals isolate the gyroscopes from the possibly large rotation rates of the body in which the system is placed. The state-of-the-art of gimballed systems is such that their navigation performance can approach almost error-free instrument operation to a point where uncertainties in the knowledge of the gravity field become the dominant source of navigational error.

Another type of inertial reference system is the strap-down inertial system. In such a system, the sensors are mounted directly (or perhaps with vibration isolators) on the body. The inertial sensor outputs represent specific accelerations and angular rates coordinated to the body axes. To function, the strap-down systems must utilize a computer-generated transformation matrix to process the angular rate data to relate the attitude of the body frame axes to an arbitrarily specified reference coordinate system with a known relation to inertial space. This attitude determination is then used in the transformation of the acceleration information to the reference coordinate system for derivation of velocities and displacements. A detailed discussion of strap-down systems and transformation algorithms is given in Reference 1.¹

¹ "Strap-Down Inertial Systems," AGARD Lecture Series No. 95, AGARD-LS-95, Advisory Group for Aerospace Research and Development, North Atlantic Treaty Organization, 7 rue Ancelle, 92200 Neuilly sur Seine, France, May 1978. ADA055778

In addition to the added computations, the inertial sensors require a larger dynamic range than gimballed systems. Since they are attached to the body, they are subjected to the entire body dynamic environment, and generally will not perform as well as if they had been isolated from it by gimbals. However, such systems have been pursued for navigation purposes because they can be smaller, easier to maintain, and of less cost.

The system components designed for navigational purposes are generally unsuitable for use in the blast environment because of their cost and susceptibility to shock. The applications other than for navigation found in the literature have used various strap-down systems.

A military vehicle struck by blast may move with six degrees of freedom as a rigid body. The translation is expressed by three independent coordinates which specify the location of a fixed point in the rigid body. The other three degrees of freedom correspond to changes in orientation of the rigid body and can be described by rotational parameters. The rotational motion can be described in terms of direction cosines, quaternions, or Euler's angles.

Figure 1 shows a rigid body moving in space. The 1,2,3 coordinate system is located in the rigid body (body-centered system) and moves with it, while the x,y,z coordinate system is the fixed system. For a rigid body,

$$\ddot{\underline{r}} = \ddot{\underline{R}} + \dot{\underline{\omega}} \times \underline{p} + \underline{\omega} \times (\underline{\omega} \times \underline{p}) \quad (1)$$

where all quantities are vectors (underlining denotes a vector quantity), and

$\ddot{\underline{r}}$ = acceleration of point P relative to origin of fixed system

$\ddot{\underline{R}}$ = acceleration of the origin of the body-centered system

$\underline{\omega}$ = angular velocity of the body-centered system relative to the fixed system

$\dot{\underline{\omega}}$ = time rate of change of angular velocity

\underline{p} = position of point P as measured in the body-centered system.

A measured acceleration contains a component due to gravity,

$$\underline{a} = \ddot{\underline{r}} + \underline{g}, \quad (2)$$

where \underline{a} = acceleration measured by an accelerometer, and

\underline{g} = acceleration due to gravity.

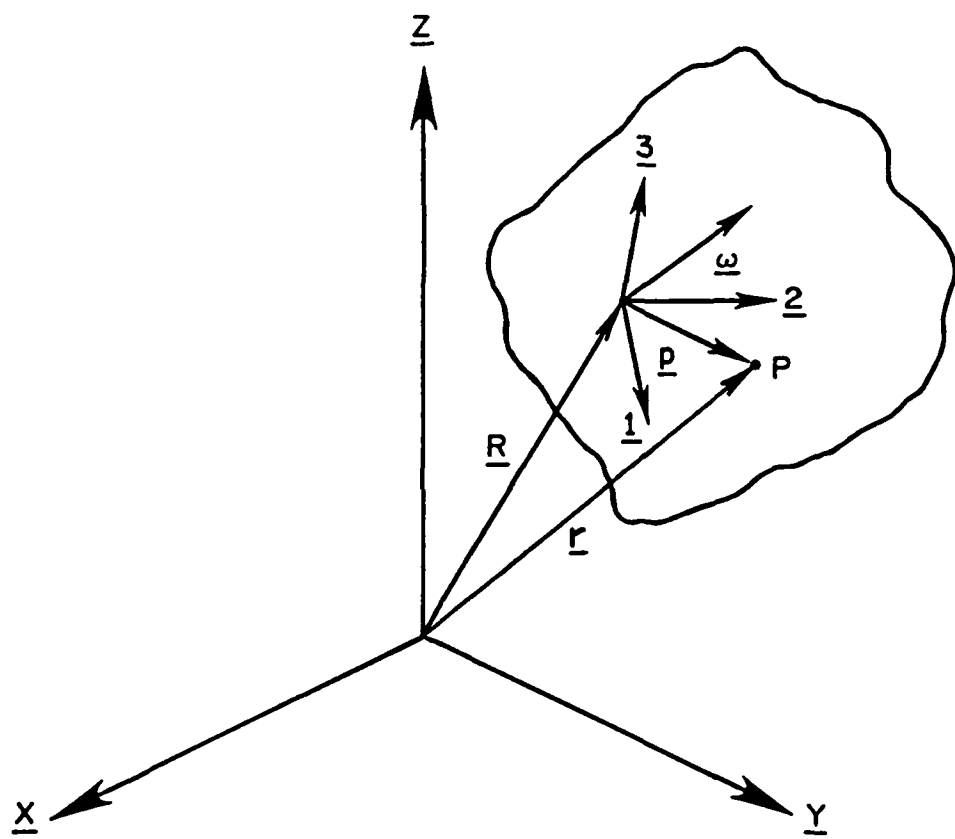


Figure 1. Body-centered and fixed coordinates for rigid body motion.

Then,

$$\underline{a} = \ddot{\underline{R}} + \dot{\underline{\omega}} \times \underline{p} + \underline{\omega} \times (\underline{\omega} \times \underline{p}) + \underline{g} \quad (3)$$

Transforming vectors from the body-centered system to the fixed system, or vice-versa, requires the use of a rotational transformation matrix and translation of the origin of the coordinate system.^{2,3,4}

Once the acceleration has been determined in the fixed coordinate system, velocity is calculated as follows:

$$\underline{v} = \int (\underline{a} - \underline{g}) dt + \underline{v}_0 \quad (4)$$

Position is obtained by integrating the velocity:

$$\underline{r} = \int \underline{v} dt + \underline{r}_0 \quad (5)$$

The initial velocity \underline{v}_0 and initial position \underline{r}_0 must be known in order to perform the integrations.

A variety of sensors and sensor configurations can be placed in the moving rigid body to form a strap-down inertial tracking system. The sensors can be linear accelerometers only, or combinations of three linear accelerometers and rate sensors and angular accelerometers. The applications found in the literature have used mainly arrays of linear accelerometers.

The Naval Biodynamics Laboratory (NBDL) has pursued a program to study human dynamic response to various stimuli including impact and

² Mital, N.K. and King A.I., "Computation of Rigid-Body Rotation in Three-Dimensional Space From Body-Fixed Linear Acceleration Measurements," Transactions of the ASME, Journal of Applied Mechanics, Vol. 46, December 1979, pp 925-930.

³ McMaster, D.K., "The Development of an Accelerometer System for Measuring Pelvic Motion During Walking," Ph.D. Dissertation, University of Oxford, 1979. AD-A088579

⁴ Jeffers, Jr., M.F., "Analytical Methods for Determining the Motion of a Rigid Body Equipped with Internal Motion-Sensing Transducers," DTNSRDC-76-0041, David W. Taylor Naval Ship R&D Center, Bethesda, Maryland, October 1976.

vibration.² In the program it was necessary to measure the acceleration of body components. In a typical test a human volunteer was instrumented and accelerated on a sled that impacted a barrier that produced a controlled deceleration of a duration of 0.25 to 0.30 seconds. A miniature inertial tracking system for installation on the head was developed that used a planar array of six linear accelerometers. This inertial reference system was found to be satisfactory for trajectories where angular displacement was not greater than a quarter of a revolution and the instrumented subject did not strike obstructions that would produce sharp peaks of acceleration.

The requirement for minimal mass limited the choice of sensors, and NBSL conducted a careful evaluation of two types, a subminiature piezoresistive linear accelerometer⁶ and an Endevco angular accelerometer.⁷ The linear accelerometers were usable, but only if they were carefully selected, stringent calibration procedures were followed, and their temperature maintained constant during a test. It was found that the angular accelerometer also should be maintained at the same temperature during a test as was used during its calibration, and should be protected from rapid temperature changes.

The NBSL have proceeded to an inertial reference configuration of nine linear accelerometers in a plane. Three orthogonal triads are located at the vertices of a triangle.

A nine linear accelerometer configuration has also been employed by Mital and King.² The head rotations of anthropomorphic dummies and of cadavers were measured using both the inertial reference system and high-speed photography. In the tests, the dummy or cadaver was accelerated at low levels on a sled and impacted a device that produced a controlled deceleration. The frontal impact produced a peak acceleration of about 18 g's. The maximum rotation of the head was about 120 degrees. The comparison of the inertial reference system results to those from high-speed photography was satisfactory. Mital and King concluded that they had developed an effective and reliable method to compute rigid-body rotation in three-dimensional space from angular accelerations derived from a body-fixed, nine linear accelerometer reference system. The study indicated the advantage of computing the rotation using the accelerometer

⁶ Decker, E. and Willems, G., "An Experimentally Validated 3-D Inertial Tracking Package for Application in Biodynamic Research," Proceedings of the Nineteenth Stapp Car Crash Conference, San Diego, CA, November 1977, pp 899-930.

⁷ Willems, G., "A Detailed Performance Evaluation of Subminiature Piezoresistive Accelerometers," Proceedings of the 23rd ISA International Instrumentation Symposium, 1-5 May 1977, pp 531-540.

⁸ Willems, G., "A Detailed Evaluation of the Endevco Model 7302 Angular Accelerometer," NBSL-838009, Naval Biodynamics Laboratory, New York, NY, 1977, pp 1-33.

data rather than measuring them from film. The latter procedure was slow and very laborious.

McMaster³ developed an inertial reference system using a planar array of eight linear accelerometers (four pair) for determining the three-dimensional motion of the pelvis during walking. The array is shown in Figure 2. He derived the equations for the eight accelerometer, four-pair configuration and the method of solving the equations for angular velocity, angular position, and the translational acceleration, velocity and position. He found it necessary to construct his own accelerometers. The range of interest was ± 5 g's, and the maximum digitization rate required was 200 Hz. He found that temperature effects on the accelerometers were significant and had to be minimized by special techniques. However, the inertial reference system provided results for walking subjects that were satisfactory and consistent with previous studies.

Work done by Jeffers⁴ at the David W. Taylor Naval Ship R&D Center seems more appropriate for the problem of tracking military vehicles struck by blast. The Navy interest was in performing model launching studies of a variety of torpedoes and missiles. High-speed photography was an available technique but required extreme care in implementing, and the analysis was laborious and time consuming. Jeffers derived the appropriate equations for two sensor configurations; three linear accelerometers and three angular rate sensors; and five linear accelerometers and one angular rate sensor. The preferred configuration was three accelerometers and three rate sensors. The formulation considered body-oriented axes that are appropriate for a military vehicle. The method for deriving the rotation and translation parameters from the sensor outputs includes accounting for the initial zeroing of signal level in the gravity field.

Jeffers, in a private communication, stated that limited experiments were performed and the results from the sensors processed using his equations agreed well with results from photography. The angular rate sensor was a prototype Humphrey rate sensor. The program was discontinued, and Jeffers' computer code for processing the data was not documented and published.

These previous studies were restricted in the choice of sensors by requirements for minimum size and mass to permit installation of the sensor array on the subjects of interest and to reduce the influence of the sensor array on the response of the subject. Military vehicles are large in size and mass compared to any reasonable sensor array, and hence there is more freedom of choice for sensors.

The analysis of data from a six accelerometer array was found to be unstable.³ The eight accelerometer, four-pair array of McMaster³ seems preferable to the nine accelerometer array of NBDL or of Mital.² It uses one less accelerometer and does not place more than one accelerometer at the same location. However, the reported experience with accelerometer arrays indicates a need for very accurate gages and great care in calibration and in temperature control. In the analysis of the output

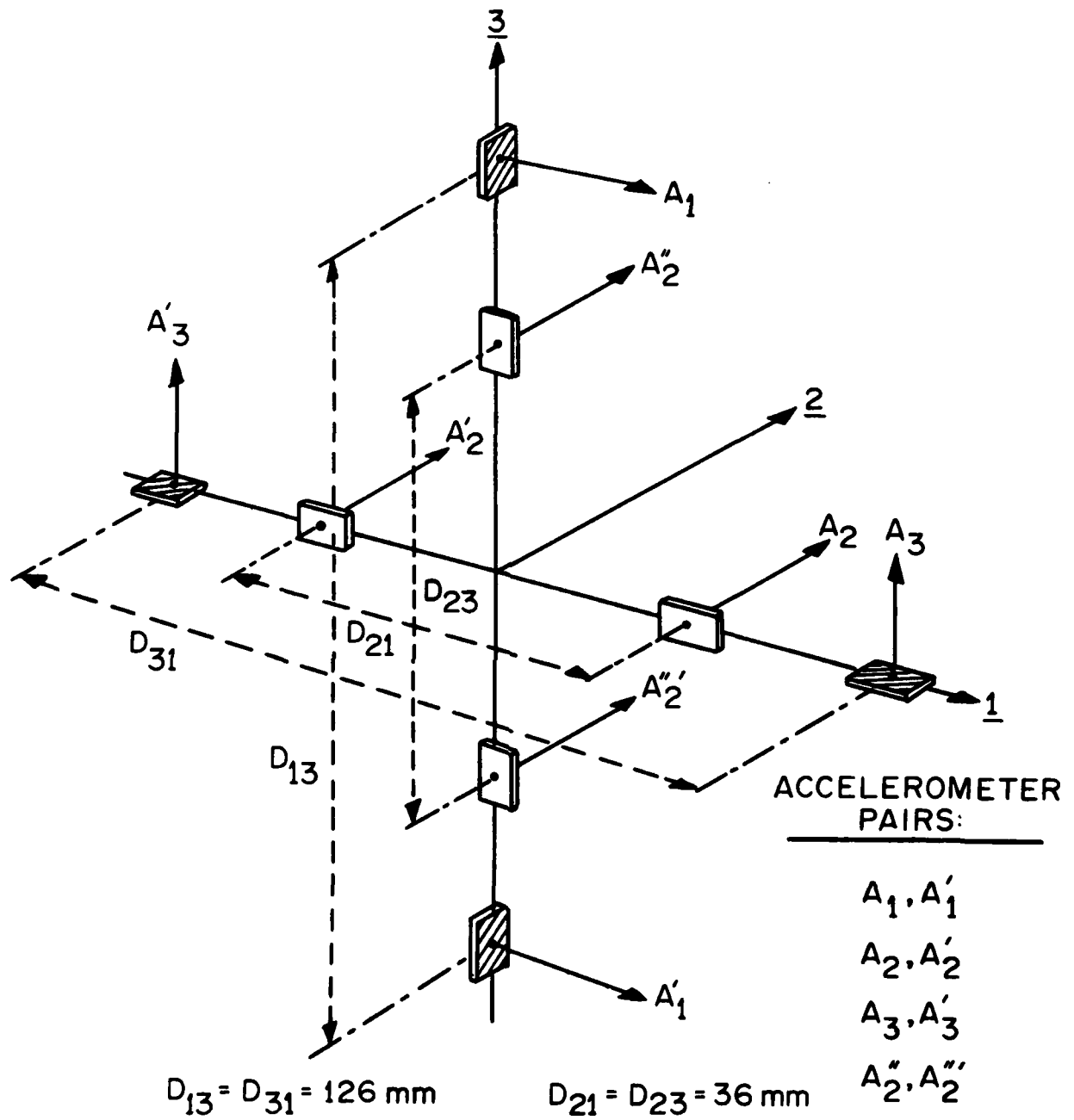


Figure 2. The planar eight accelerometer, four-pair configuration by McMaster (Reference 3).

from such an array, the difference between the records for each pair of accelerometers is used to determine the rotational components.

Difficulties may occur in that each accelerometer is required to sense accurately acceleration due to translational motion, the gravity field, and the rotation of the rigid body. The magnitudes involved may be incompatible with the use of a single sensor to record them.

In the sensor array selected by Jeffers,⁴ consisting of three accelerometers and three rate sensors, the rotational components are determined by direct measurement of angular velocity and by differentiation of the angular velocity to obtain angular acceleration. For maximum reduction of error, three angular accelerometers can be added to the sensor array to make direct measurements of angular acceleration, thus avoiding the necessity for differentiating the angular velocity records. However, adding these accelerometers increases the cost significantly and introduces errors from the accelerometers, so that the reduction in error achieved may not be worthwhile. Although the accelerometers will still be required to sense accurately the translational and gravitational acceleration components, the rotational components will be derived independently from the rate sensors and possibly angular accelerometers. Therefore the accelerometers and rate sensors can be ranged independently of each other, which can lead to improved accuracy.

Based on this review of previous work, the selected sensor array for an inertial tracking system for military vehicles is three linear accelerometers placed in a triad, if possible, and aligned with the primary axes of the military vehicle, and three rate sensors.

The potential for growth of error seems high for any inertial sensor array under blast loading conditions. Before beginning the construction of an inertial tracking system capable of recording the full six degrees of freedom of a rigid body, it seemed necessary to show that tracking could be accomplished with satisfactory accuracy for a system with a minimum of sensors. The array selected for evaluation was that of two linear accelerometers and one rate sensor placed in a configuration to track motion in a plane.

IV. DESIGN AND CONSTRUCTION OF TEST FACILITY

A. Representative Vehicle Response

One military vehicle system of concern for blast survivability and hardening studies is that of a 2 1/2 ton truck carrying an electrical equipment shelter. Such a system has been exposed to blast on large-scale high explosive (HE) tests and in blast simulators.

A calculation of the overturning of such a system by blast from an HE explosion equivalent to a one-kiloton nuclear explosion was available. The code used was BLOM, a single degree-of-freedom code developed at the BRL to calculate blast overturning of vehicles. The blast wave

overpressure was 68.9 kPa (10 psi), atmospheric pressure was 86.7 kPa (12.6 psi), and atmospheric temperature was 12.0 degrees Celsius. The system overturned at this overpressure, but it was not far beyond the limit for overturning.

Figure 3 shows the angular velocity of the system. It has an initial peak of 80 degrees per second, decreases as the center of gravity passes over the axis of rotation, and reaches a maximum of 117 degrees per second at impact with the ground.

Figure 4 shows acceleration versus time as would be sensed by two accelerometers located at the center of gravity; one with the axis initially vertical in the plane of rotation, and the other initially horizontal in the plane of rotation. The effect of the gravity field on the response of the accelerometers was considered in generating the curves.

The lower set of curves shows an initial high magnitude pulse corresponding to the diffraction loading period followed by a lower magnitude, longer duration tail that corresponds to the drag loading phase. After 0.19 seconds the system is rotating under the influence of gravity alone, and the time until impact with the ground is long compared to the positive phases of acceleration. The magnitudes of the accelerations during this period are small compared to the initial peak magnitudes. At the end of blast loading, the system has rotated 13 degrees. Overturning is completed at 1.24 seconds.

The upper set of curves in Figure 4 show that the initial pulse has a duration of about 0.15 seconds. The calculation assumed a perfectly rigid body. In a real system the peak accelerations would be reduced by the flexure of the structure and the pulse width would be somewhat broadened.

To approximate overturning of the truck-shelter system for the case described above, the test facility should provide a loading that produces an initial acceleration pulse of about 10 g's that decreases in 0.015-0.020 milliseconds to about 2 g's, and then decays to zero in 0.15 - 0.2 seconds. Specification of a peak acceleration of about 10 g's instead of the higher values shown in Figure 4 is an attempt to account for the reduction caused by the flexure of a real system. The facility should produce overturning in about 1.2 seconds.

B. Concept for the Test Facility

Figure 5 shows the concept for the test facility to produce a rotation of 90 degrees about an axis perpendicular to the vertical plane. The rotating component is a quarter wheel constructed to minimize its mass and moment of inertia about the rotation axis. The accelerometers are placed at the sensor location shown, and move along the indicated trajectory as the quarter wheel rotates.

The quarter wheel is loaded by coil springs tied to it by a cable. The cable is wrapped around the wheel circumference so that the force moment arm with respect to the rotation axis remains constant. The

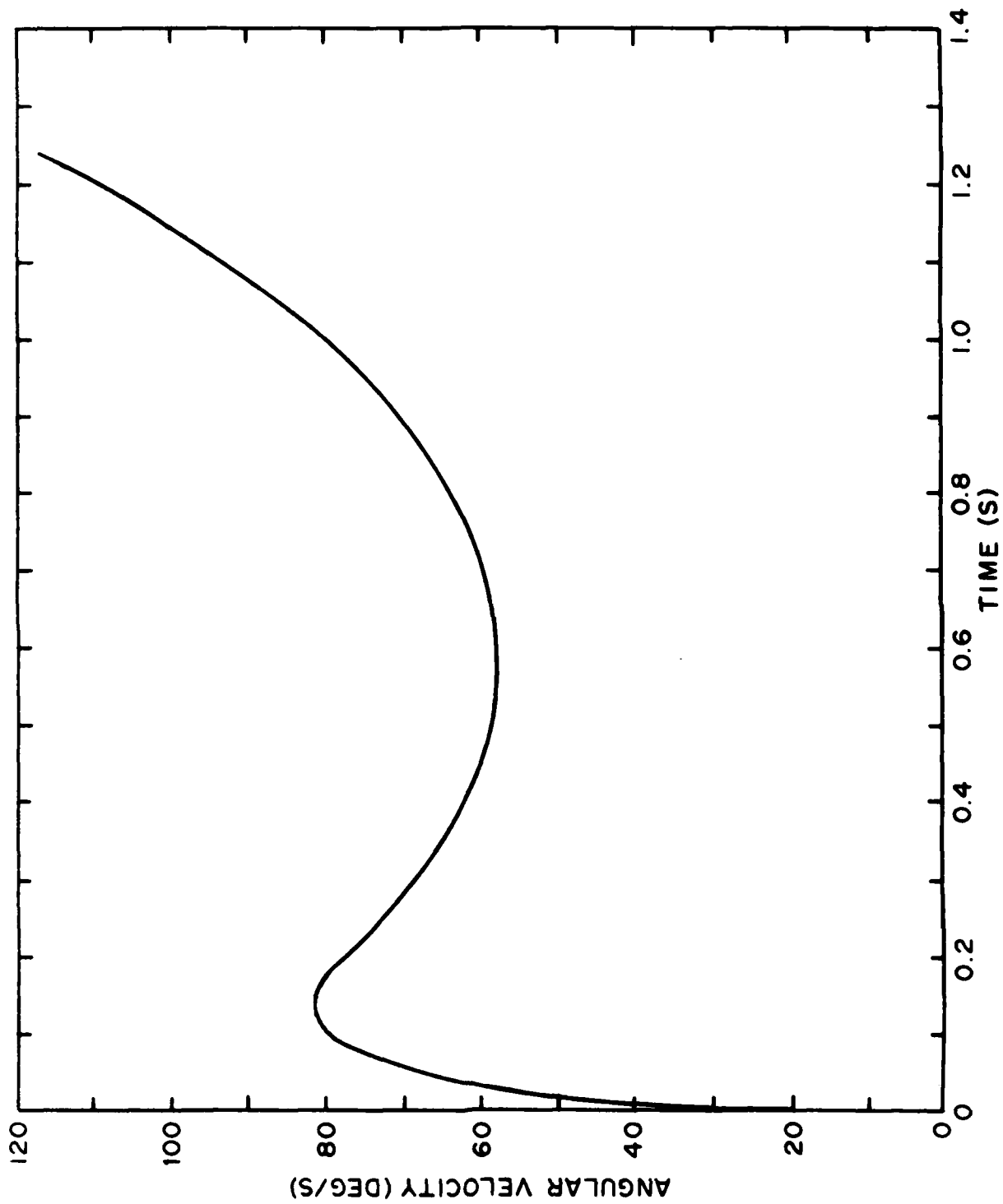


Figure 3. Computed angular velocity of overturning of a truck-shelter combination struck by a 68.9 kPa blast wave from a simulated 1 KT nuclear explosion.

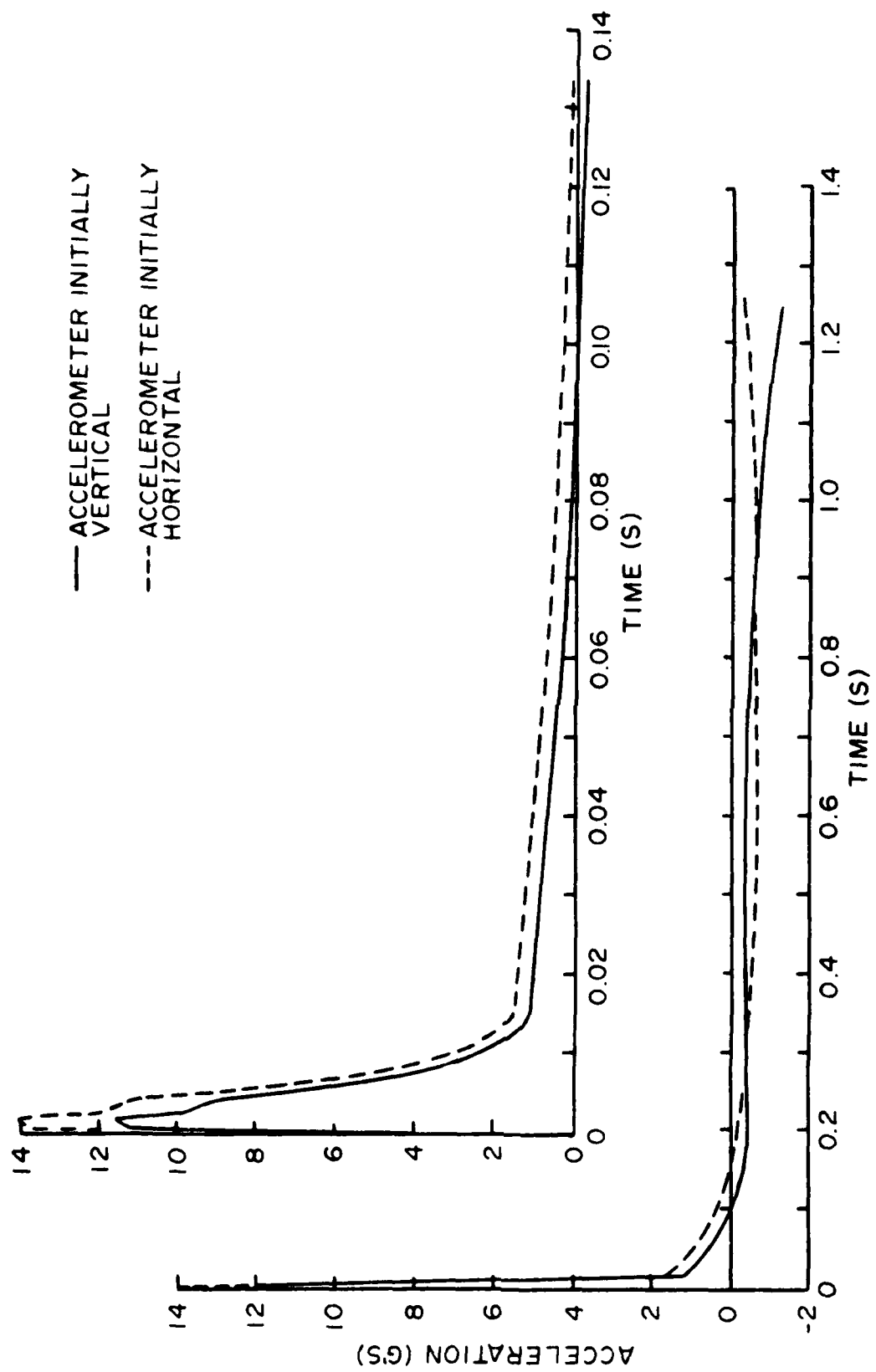


Figure 4. Computed accelerations that would be measured by two accelerometers placed at the center of an overturning truck-shelter combination struck by a 68.9 kPa blast wave from a simulated 1 KT nuclear explosion. The effect of gravity on the accelerometers is included.

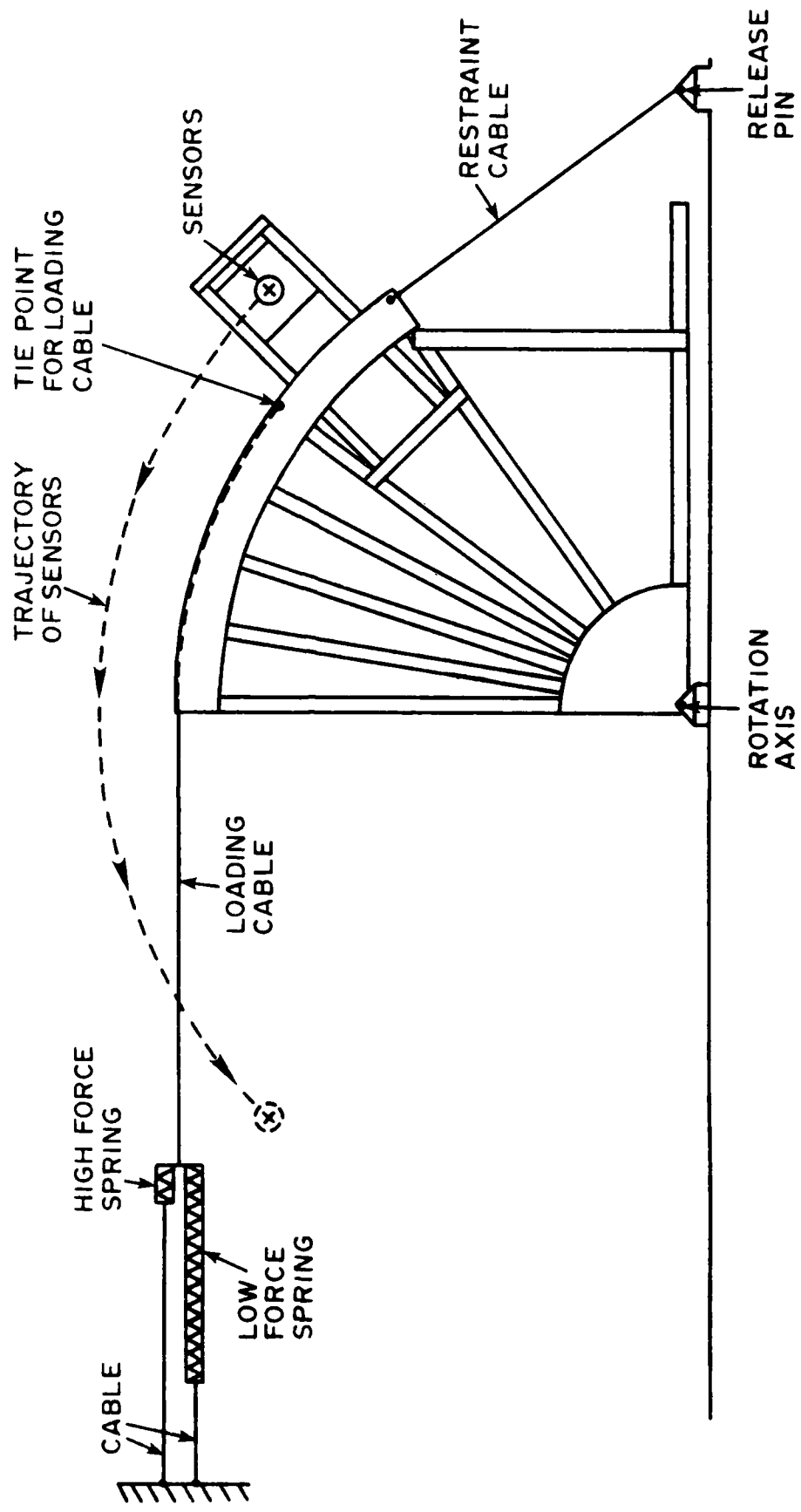


Figure 5. Concept for a facility to simulate overturning of a military vehicle system by blast.

quarter wheel is held in place by the restraint cable. To execute the test, the release pin is pulled free. The high force spring unloads rapidly and simulates blast diffraction loading, and the low force spring simulates drag loading.

C. Modeling of Test Facility

To provide guidance in the design of the test facility, a computer code that modeled the response of the quarter wheel under spring loading was written and utilized. The equation of motion is as follows:

$$\begin{aligned}
 I_{\text{axis}} \ddot{\theta} &= \text{spring moment} - \text{weight moment} \\
 &= H[K_1 (Z_1 - H\theta) + K_2 (Z_2 - H\theta)] - W R_1 \cos(\theta + \theta_1) \\
 &\quad \text{for } Z_1 > H\theta \text{ and } Z_2 > H\theta, \text{ and} \\
 &= H[K_2 (Z_2 - H\theta)] - W R_1 \cos(\theta + \theta_1) \text{ for } Z_1 \leq H\theta \\
 &\quad \text{and } Z_2 > H\theta, \text{ and} \\
 &= -W R_1 \cos(\theta + \theta_1) \text{ for } Z_1 \leq H\theta \text{ and } Z_2 \leq H\theta,
 \end{aligned} \tag{6}$$

where

$$\ddot{\theta} = \frac{d^2\theta}{dt^2}$$

I_{axis} = moment of inertia about axis

θ = angle of rotation in radians from the initial position of the quarter wheel

t = time

H = constant length of force moment arm

K_1 = spring constant for high force spring

Z_1 = maximum extension in length beyond its rest position of high force spring

K_2 = spring constant for low force spring

Z_2 = maximum extension in length beyond its rest position of low force spring

R_1 = radius to center of gravity from axis

θ_1 = initial angle of R_1

m = mass of wheel and sensors

g = acceleration due to gravity

W = weight, mg

The mass of the springs is small compared to the weight of the quarter wheel, and is neglected.

Figure 6 shows a representation of the model of the quarter wheel.

To compute the output of accelerometers placed on the quarter wheel, the components of acceleration due to rotation and to the gravity field must be considered. Figure 7 shows accelerometers placed at the radius R_2 from the axis of rotation.

At the radius R_2 , the magnitudes of the components of acceleration due to rotation are

$$\begin{aligned} a_T &= R_2 \ddot{\theta} \\ a_N &= R_2 \dot{\theta}^2 \end{aligned} \tag{7}$$

where

a_T = acceleration magnitude at radius R_2 that is perpendicular to the radius and tangent to the path of movement

a_N = acceleration magnitude at radius R_2 that is along radius R_2 and normal to the path of movement

R_2 = radius of accelerometers from axis of rotation

$\dot{\theta} = \frac{d\theta}{dt}$, angular velocity

$\ddot{\theta} = \frac{d^2\theta}{dt^2}$, angular acceleration

If the accelerometers are oriented initially so that one has its sensitive axis vertical and the other horizontal, they will sense the components of acceleration due to rotation as follows:

$$\begin{aligned} a_{VR} &= a_T \cos \theta_2 - a_N \sin \theta_2 \\ a_{HR} &= a_T \sin \theta_2 + a_N \cos \theta_2 \end{aligned} \tag{8}$$

where

a_{VR} = acceleration due to rotation sensed by initially vertical accelerometer

a_{HR} = acceleration due to rotation sensed by initially horizontal accelerometer

θ_2 = initial angle of radius R_2 with respect to the horizontal

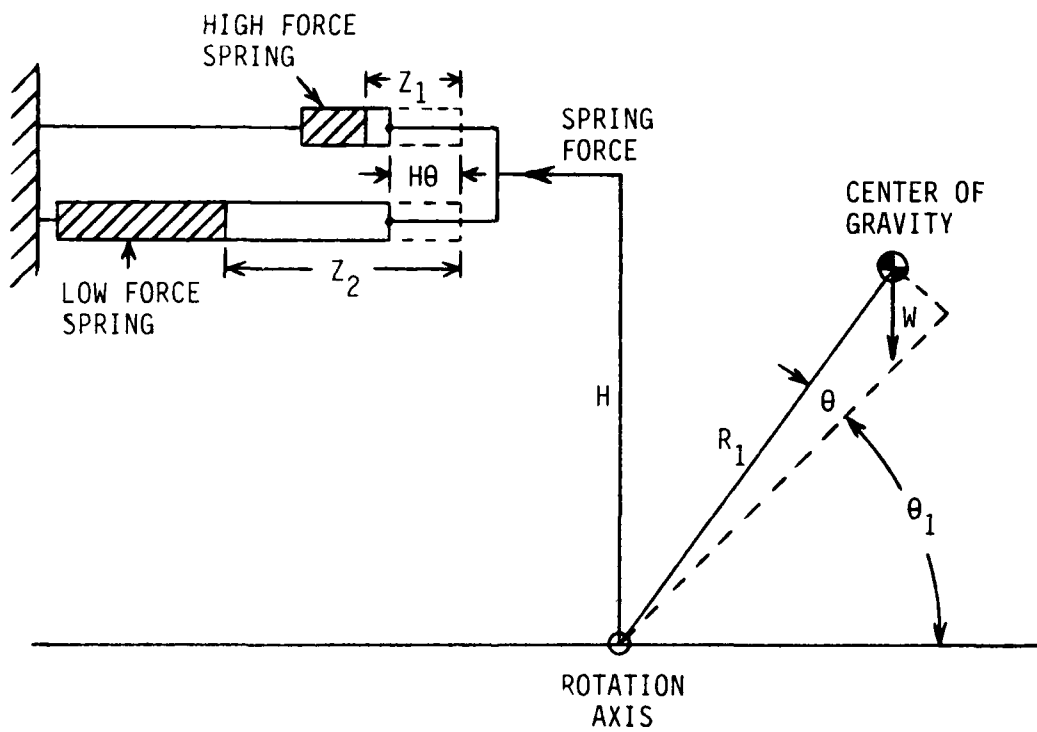


Figure 6. Model representation of quarter wheel after rotation through angle θ .

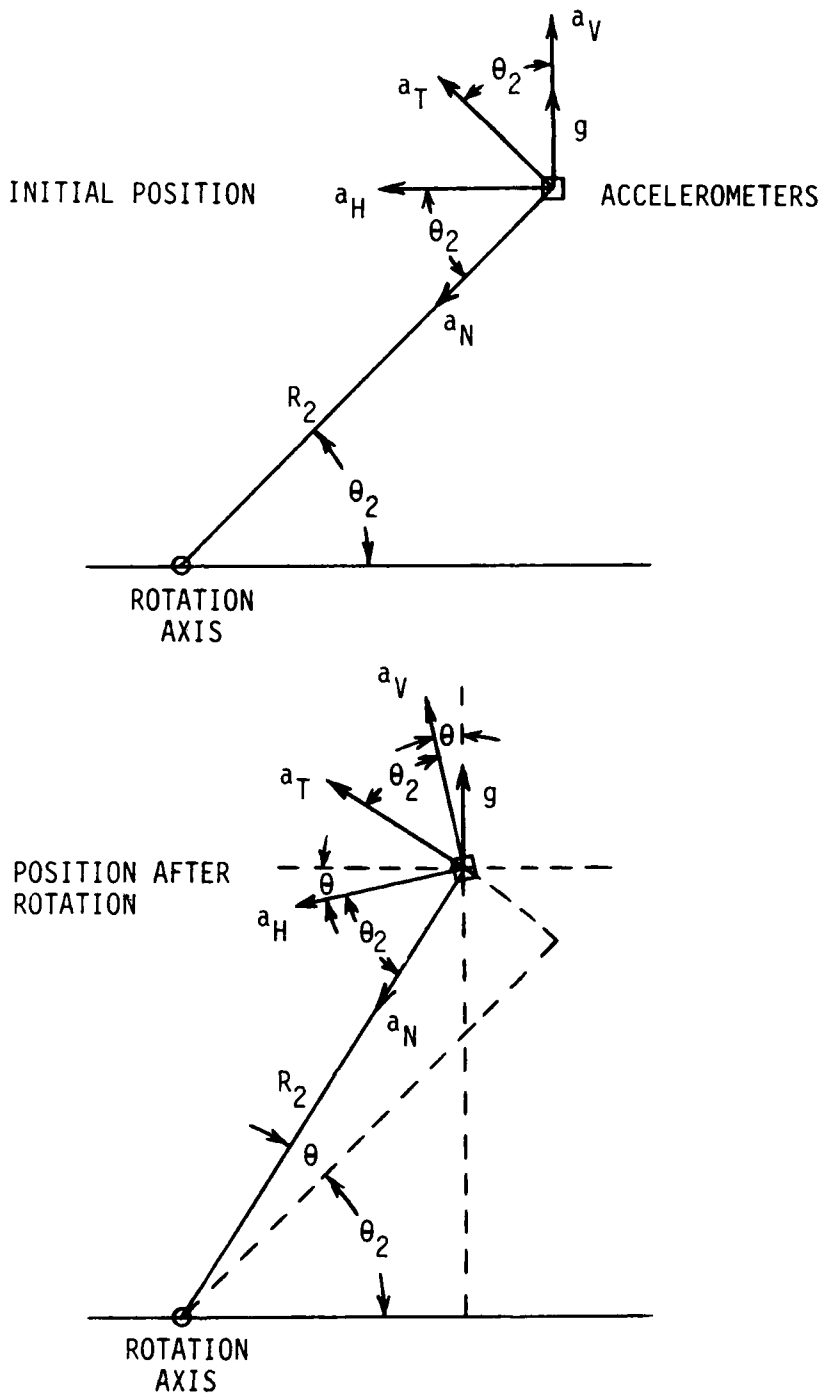


Figure 7. Acceleration components at the location of the accelerometers on the quarter wheel. Gravitational acceleration g is shown vertical because of the sign convention chosen.

The sign convention chosen is such that vertical components in Figure 7 that would cause an accelerometer mass to move down are called positive, and horizontal components that would cause an accelerometer mass to move to the right are called positive.

If the vertical accelerometer is set to read zero initially in the gravity field, then the outputs of the accelerometers due to rotation in the gravity field are computed as follows:

$$a_V = a_{VR} - g (1 - \cos \theta)$$

$$a_H = a_{HR} - g \sin \theta,$$

or

$$a_V = a_{RT} \cos \theta_2 - a_{RN} \sin \theta_2 - g (1 - \cos \theta)$$

$$a_H = a_{RT} \sin \theta_2 + a_{RN} \cos \theta_2 - g \sin \theta,$$

and

$$\begin{aligned} a_V &= R_2 \ddot{\theta} \cos \theta_2 - R_2 \dot{\theta}^2 \sin \theta_2 - g (1 - \cos \theta) \\ a_H &= R_2 \ddot{\theta} \sin \theta_2 + R_2 \dot{\theta}^2 \cos \theta_2 - g \sin \theta, \end{aligned} \tag{9}$$

where

a_V = acceleration sensed by the accelerometer that is initially vertical

a_H = acceleration sensed by the accelerometer that is initially horizontal

Figure 5 shows the configuration selected for the quarter wheel, with aluminum sheet and aluminum channel used for construction. The maximum radius of the wheel as finally designed was 1.22 metres, with a computed mass (with sensors) of 18.1 kilograms and a moment of inertia about the axis of 15.25 kilogram (metres)².

Two cases were finally selected to attempt to achieve in the test facility, Case 1 with peak accelerations of 10 g's, and Case 2 with peak accelerations of 5 g's.

For Case 1 and Case 2, $H = 1.194$ metres, $R_1 = 0.862$ metres, $R_2 = 1.437$ metres, and $\theta_1 = \theta_2 = 45$ degrees.

For Case 1, $K_1 = 73550$ Newtons/metre, $Z_1 = 0.0127$ metres, $K_2 = 1576$ Newtons/metre, and $Z_2 = 0.254$ metres.

For Case 2, $K_1 = 38530$ Newtons/metre, $Z_1 = 0.0127$ metres, $K_2 = 437.8$ Newtons/metre, and $Z_2 = 0.508$ metres.

Figure 8 shows the predicted acceleration versus time waveforms for Cases 1 and 2 for initially vertical and horizontal accelerometers located at radius R_2 at an initial angle of 45 degrees. The primary waveform

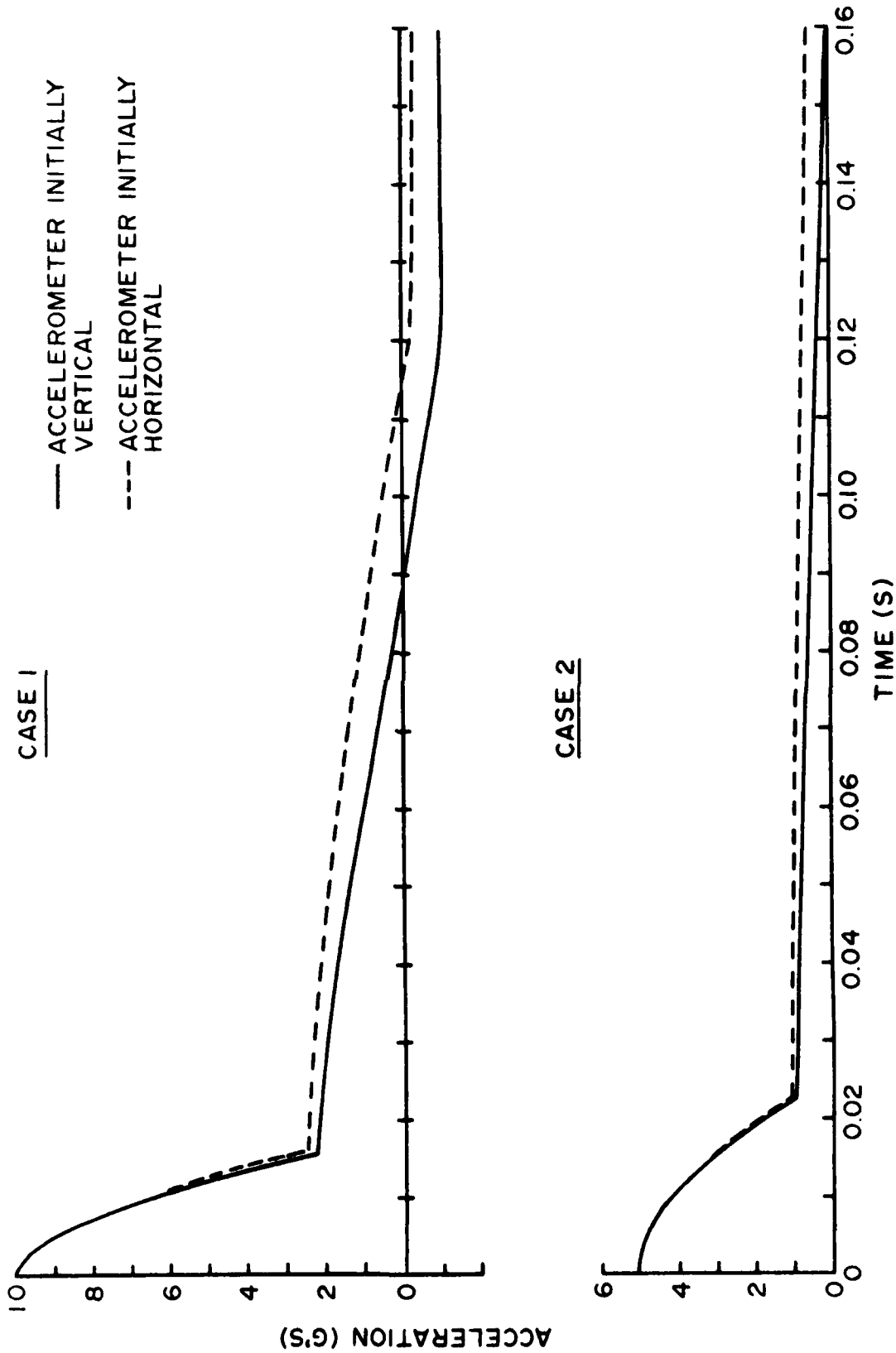


Figure 8. Predicted accelerometer waveforms for Cases 1 and 2 for the test facility.

characteristics of a high magnitude initial pulse of the desired magnitude and duration followed by a low magnitude long duration tail are predicted for Case 1. Case 2 predicts waveforms for a higher yield simulation, where overturning occurs at lower initial g levels and a longer duration wave.

D. Construction and Assembly

The test facility was designed for construction from sheet, channel and angle steel and aluminum. The radius of the quarter wheel is nominally 0.22 metres (4 feet). Figure 9 shows the facility as constructed and assembled. The basic frame is made of steel channel. The quarter wheel is held in the vertical plane by guy cables on each side that are attached to the rotating axle. The springs that apply the load are attached to long threaded rods that pass through a threaded plate at the end of the frame. The springs are extended to apply the loading by unscrewing the threaded rods. The wheel is held in place by a restraint cable that in turn is held by a quick-release pin.

Figure 10 shows the quarter wheel in its initial position. The restraint cable is shown, as well as the guy cables and their attachment to the rotating axle.

Figure 11 shows the quarter wheel in the overturned position. After rotating 90 degrees the wheel strikes packing foam. The magazines seen in the figure are a convenient means to adjust the heights of the initial support and final impact area.

Figure 12 shows a rear view of the facility. The loading cable and its attachment on the wheel can be seen. The wrap-around length of cable is 0.79 metres.

Figure 13 shows the pin that anchors the restraint cable. When the springs have been stretched so that the desired force is acting upon the quarter wheel, this pin is pulled free and wheel rotation begins.

V. INSTRUMENTATION

A. Selection of Sensors

For evaluation of the capability of an inertial reference system for tracking movement in a vertical plane, two linear accelerometers and one gage to measure angular velocity were required for mounting on the quarter wheel. The sensors found for measuring angular velocity were rate gyroscopes, integrating angular accelerometers, and a rate sensor manufactured by Humphrey, Inc.

The Humphrey rate sensor operates on the principle that rotation of the sensor deflects an internal gas jet in proportion to the rotation rate. Deflection of the jet causes it to flow over one of two fine current-carrying wires located on either side of the flow channel. The



Figure 9. The overturning test facility.

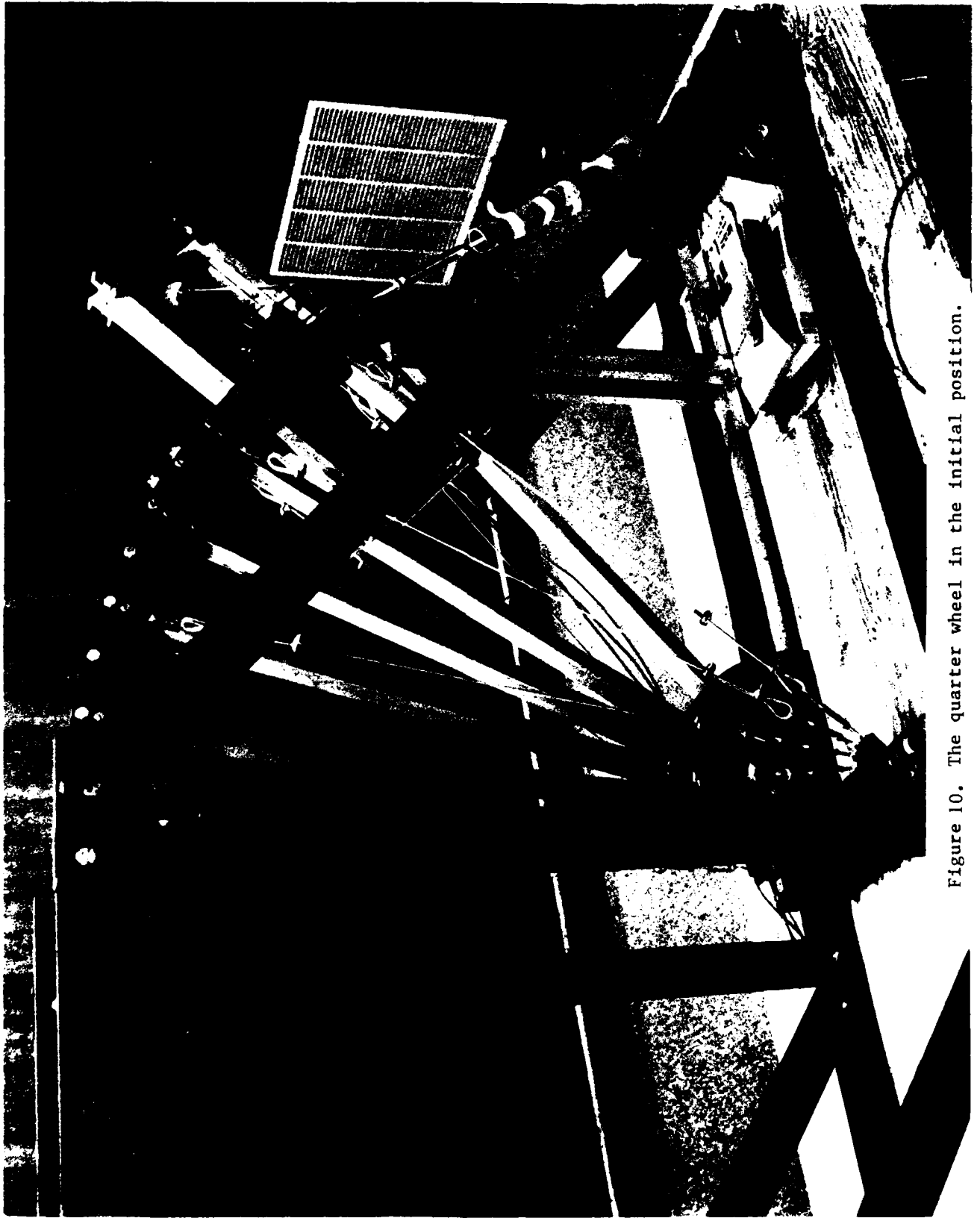


Figure 10. The quarter wheel in the initial position.



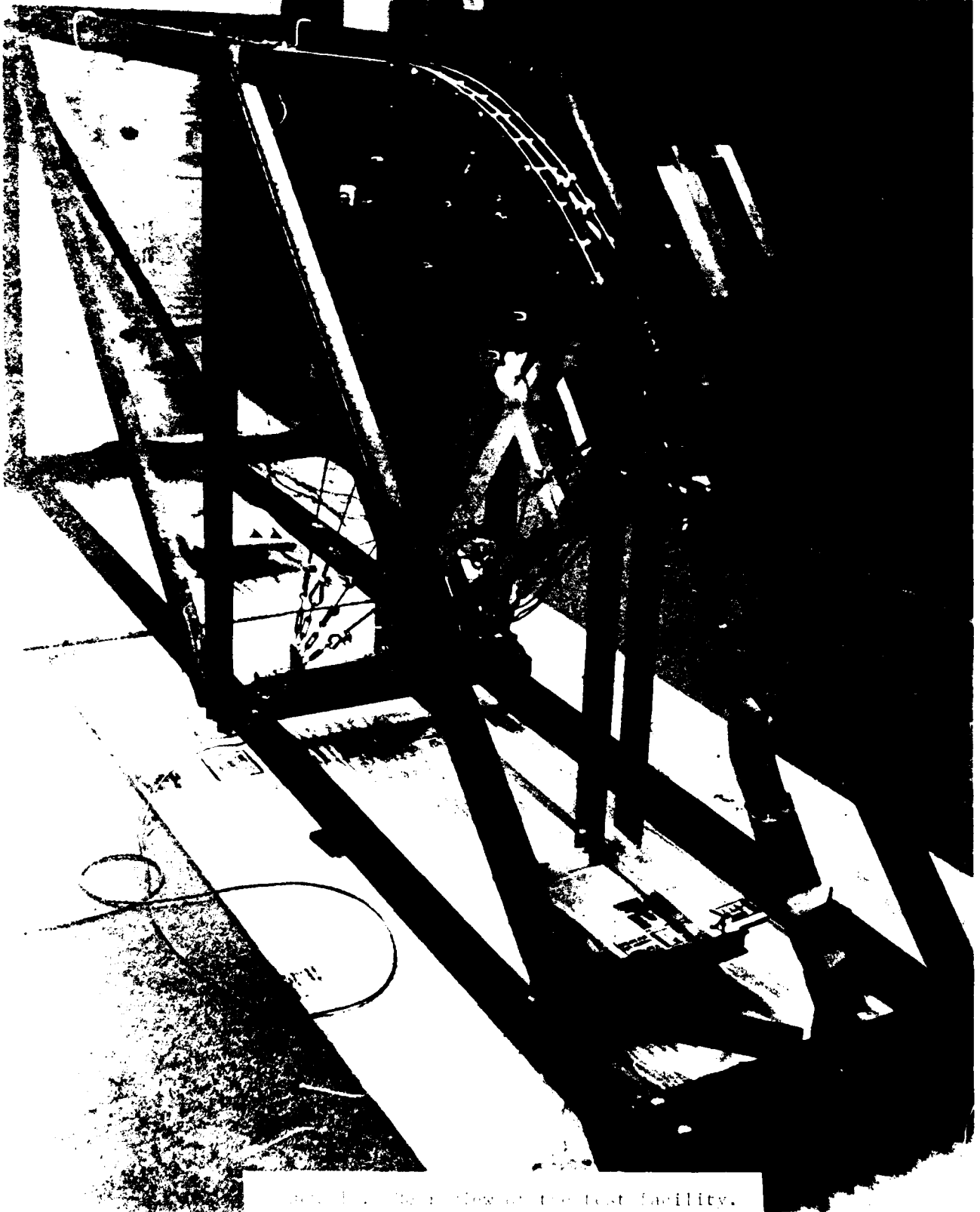
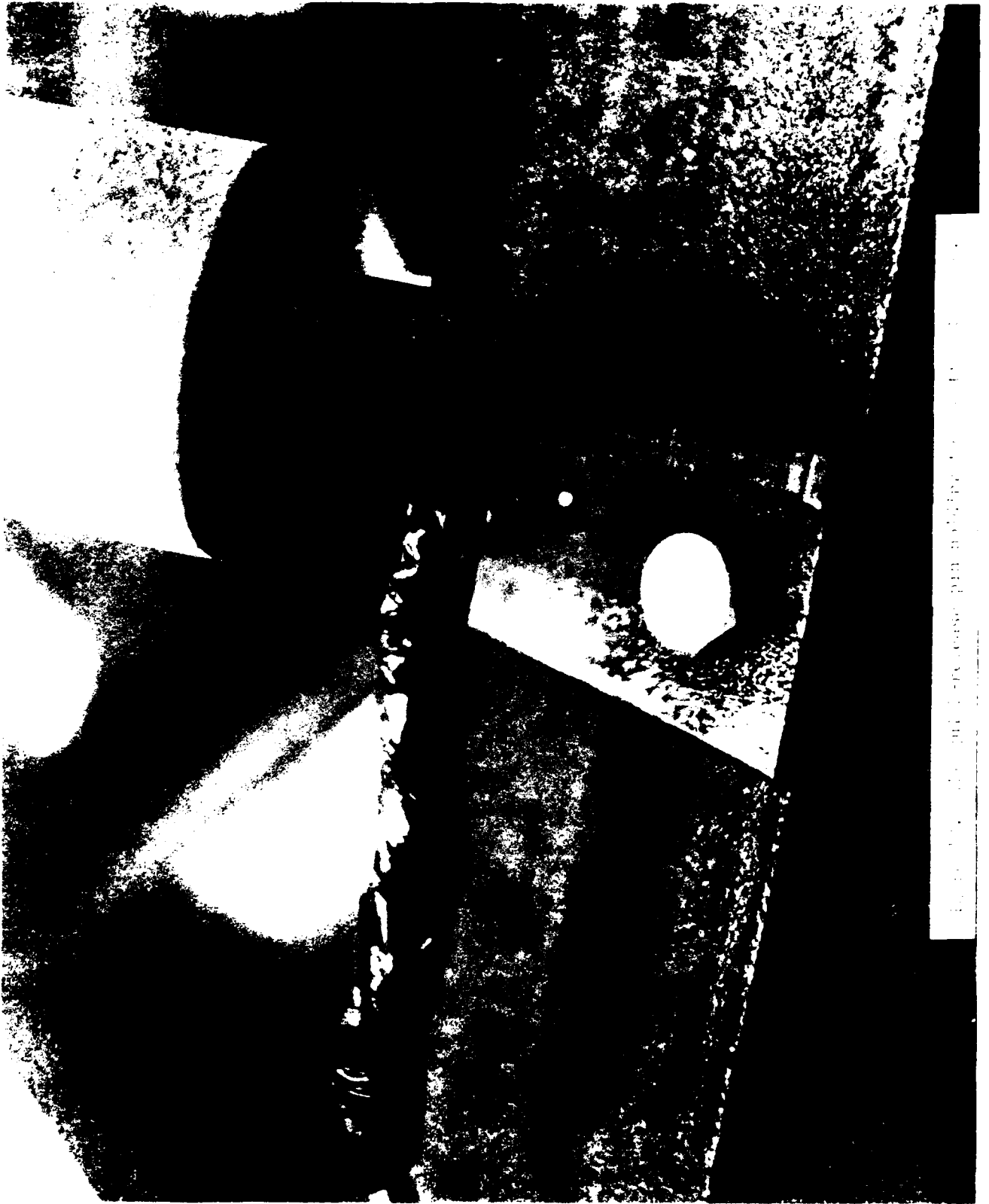


Figure 1. Aerial view of the test facility.



Portrait of a woman, possibly a woman, looking downwards.

Flow past a wire cools the wire and lowers its resistance, unbalancing a bridge circuit containing both wires. The change in the bridge is related to the angular rate of rotation. This sensor offered the best combination of features such as higher natural frequency, damping, accuracy, and resistance to shock and acceleration. The specifications for the Humphrey sensor are shown in Table 1.

The accelerometers selected were closed-loop force balance transducers. These accelerometers typically have errors an order of magnitude or more less than conventional accelerometers. The particular model purchased was the Schaevitz LSB linear accelerometer. In operation, a pendulous mass in the accelerometer develops a torque proportional to the product of its mass unbalance and the applied acceleration. The motion of the mass is detected by a position sensor. The output of the position sensor is applied to a servo amplifier driving a torque motor, and a torque equal and opposite to the acceleration torque is applied so that only minute motion of the mass occurs. The current through the torque motor is proportional to the input acceleration, and is used to produce the output voltage. Table 2 lists the specifications for the Schaevitz accelerometers used in this study.

Standard strain gage accelerometers manufactured by the Endevco Corporation were also available. Table 3 lists the specifications for the model used, which employs piezo-resistive elements in a bridge circuit.

Two other types of sensors were installed on the test facility. A precision potentiometer was placed on the rotating axle of the wheel, and a load cell was placed in-between the springs loading the wheel and the cable connecting them to the wheel.

The potentiometer was placed in an electrical circuit so that a voltage output was generated proportional to the rotation of the axle, and the output was calibrated in terms of rotation angle. The signal from this sensor was intended to provide position in time and space of the accelerometers for reference and comparison with that derived from the accelerometers and rate sensor records.

The load cell was used to indicate the force acting to turn the quarter wheel. It enabled tests to be set up for the acceleration levels of interest and to repeat tests with the same loading. Its output provided an unloading versus time waveform. Table 4 lists the specifications for the Kulite load cell used. The cell is a flat load cell employing a stainless steel diaphragm construction. The transduction element is a four-arm Wheatstone semiconductor bridge, internally compensated for thermal changes.

B. Calibration of Sensors

The accelerometers were statically calibrated with the aid of a Gyrex spin table located at the BRL. The spin table was capable of applying to test specimens a centrifugal force of known magnitude. The acceleration applied to the accelerometers was calculated from the following relation:

TABLE 1. SPECIFICATIONS OF THE HUMPHREY, INC., RATE SENSOR

Model Number: RT03-0136-1
 Serial Number: 101
 Range: ± 200 degrees/second
 Natural Frequency: 25 Hz minimum
 Damping: 0.7 ± 0.2
 Input Voltage: $\pm 12 \pm 2$ volts D.C.
 Input Current: 200 milliamperes maximum
 Calibration at 12 volts, 165 milliamperes:

RATE SENSOR	OUTPUT	DEVIATION
+200 deg/sec	+2.524 volts	+0.000 volts
+160 deg/sec	+2.015 volts	+0.006 volts
+120 deg/sec	+1.506 volts	+0.012 volts
+80 deg/sec	+1.004 volts	+0.012 volts
+40 deg/sec	+0.501 volts	+0.012 volts
+0 deg/sec	+0.001 volts	+0.009 volts
-40 deg/sec	-0.498 volts	+0.006 volts
-80 deg/sec	-1.001 volts	+0.006 volts
-120 deg/sec	-1.498 volts	+0.000 volts
-160 deg/sec	-1.998 volts	-0.003 volts
-200 deg/sec	-2.503 volts	-0.000 volts

Linearity (Calculated): 0.237 percent of full scale
 Scale Factor (Calculated): 0.0126 volts/degree/second
 Noise: 10 millivolts RMS
 Null Signal: ± 50 millivolts
 Acceleration: 100 g's, any axis
 Shock: 100 g's, 11 ± 1 millisecond
 Temperature: -45 degrees C to +77 degrees C
 Mass: 0.31 kilograms nominal

TABLE 2. SPECIFICATIONS FOR THE SCHAEVITZ LINEAR
ACCELEROMETER AT 20 DEGREES CELSIUS

Model:	LSBC-10 Linear Accelerometer
Range:	± 10 g's
Nominal Natural Frequency:	140 Hz
Damping Ratio:	0.6 nominal
Nominal Output Impedance:	2500 ohms
Input Voltage:	± 15 volts D.C. ± 10 percent nominal
Input Current:	25 milliamperes D.C. maximum
Full-Range Open-Circuit Output Voltage:	± 5.0 volts D.C. ± 1 percent
Linearity:	± 0.1 percent of full scale*
Hysteresis:	0.02 percent of full scale maximum
Resolution:	0.001 percent of full scale maximum
Static Cross Axis Sensitivity:	± 0.002 g per g
Bias:	0.1 percent of full scale maximum
Sensitive Axis to Case Alignment:	± 1 degree
Noise Output:	5 millivolts RMS maximum
Operating Temperature:	-55 degrees C to +95 degrees C
Thermal Coefficient of Sensitivity:	0.02 percent per degree C maximum
Shock Survival:	100 g's for 11 milliseconds
Mass:	0.085 kilograms

*Full scale is defined as "minus full range to plus full range"

TABLE 3. SPECIFICATIONS FOR THE ENDEVCO ACCELEROMETERS
AT 24 DEGREES CELSIUS

Model:	2262-25	
Range:	± 25 g's	
Sensitivity at 10 volts excitation, reference 100 Hz:	20 millivolts per g typical, 16 millivolts per g minimum	
Non-Linearity & Hysteresis: (Percent of reading, maximum, to full range)	± 1 percent (above 25 g's, ± 3 percent of reading, maximum, to 50 g's)	
Frequency Response: (± 5 percent maximum, reference 100 Hz)	0 to 650 Hz	
Mounted Resonant Frequency:	2500 Hz	
Damping Ratio:	0.7 \pm 0.15 - 0.10	
Transverse Sensitivity (Max):	3 percent	
Thermal Sensitivity Shift: (Reference 24 degrees C)	<u>Percent</u>	<u>Degrees C</u>
	-5	-18
	-2	-4
	0	24
	-2	66
	-5	93
Zero Measured Output (Max):	± 25 millivolts	
Thermal Zero Shift (Max): (-18 to +93 degrees Celsius)	± 20 millivolts	
Excitation:	10.0 volts D.C.	
Input Resistance:	1800 ohms	
Output Resistance:	1400 ohms	
Mass:	0.028 kilograms	
Acceleration Limits (in any direction):	250 g's static and sinusoidal, 2000 g's shock	
Temperature (Operating):	-18 to 93 degrees Celsius	

TABLE 4. SPECIFICATIONS FOR THE LOAD CELL OF
KULITE SEMICONDUCTOR PRODUCTS, INC.

Model:	TC-2000
Range:	\pm 2224 Newtons (500 pounds)
Diaphragm Thickness:	1.65 millimeters (0.065 inches)
Nominal Deflection:	0.0076 millimeters (0.0003 inches)
Natural Frequency:	12 kHz
Overload:	150 percent of rated capacity
Operational Mode:	Tension and compression
Rated Electrical Excitation:	10 volts DC/AC (RMS)
Max Electrical Excitation:	15 volts DC/AC (RMS)
Input Resistance:	3000 ohms
Full Scale Output:	75 millivolts nominal
Output Resistance:	1000 ohms
Residual Unbalance:	\pm 2 percent
Non-Linearity:	0.5 percent of full scale output
Hysteresis:	0.1 percent of full scale output
Repeatability:	0.1 percent of full scale output
Resolution:	Infinite
Operating Temperature Range:	-40 degrees C to 120 degrees C
Compensated Temperature Range:	25 degrees C to 80 degrees C
Thermal Effect on Zero:	\pm 3 millivolts per 55 degrees Celsius
Thermal Effect on Sensitivity:	\pm 1 percent of full scale output / 55 degrees C
Diameter:	51 millimeters
Thickness:	27 millimeters
Mounting:	Center Stud

$$a = 2.840 \times 10^{-5} N^2 r \quad (10)$$

where

a = acceleration in g's

N = speed in revolutions per minute

r = radius to the seismic mass in inches

Each accelerometer in turn was subjected to accelerations in 5 g increments up to its maximum rated range. The calibration data obtained agreed with those supplied by the manufacturer.

The calibration data supplied by the manufacturer was used for the rate sensor.

The potentiometer for measuring the rotation angle was calibrated by recording the change in output voltage for a rotation of the quarter wheel through 90 degrees.

C. Installation of Gages on the Test Facility

Figure 14 shows an Endevco accelerometer and the Humphrey rate sensor mounted on the quarter wheel. The accelerometer was mounted on a Masonite fiberboard panel 6.35 millimeters thick. The second accelerometer was mounted on the opposite side of the board so that the sensitive masses of the two accelerometers were at the same radius and angle. Several different mounting configurations were used in attempting to minimize mechanical vibrations at the accelerometers. The final test runs were made with the accelerometers mounted in an aluminum bracket, with a layer of lead and a layer of neoprene rubber between the aluminum bracket and the fiberboard. The neoprene rubber was placed against the fiberboard.

The rate sensor was mounted directly to the aluminum channel.

Figure 15 shows the potentiometer that was coupled to the end of the axle to measure rotation angle.

Figure 16 shows the installation of the load cell between the loading springs and the cable that was attached to the quarter wheel.

D. Data Acquisition and Reduction System

The block diagram of a typical channel of the data acquisition and reduction system is shown in Figure 17. The B&F signal conditioners provided excitation voltage and balancing for the Endevco accelerometers. They also provided operating power for the Schaevitz accelerometers. The Kulite load cell, the Humphrey rate sensor, and the potentiometer on the axle were powered by separate power supply modules. The signals from all the transducers were amplified with a Tektronix AM 502 amplifier before being recorded.

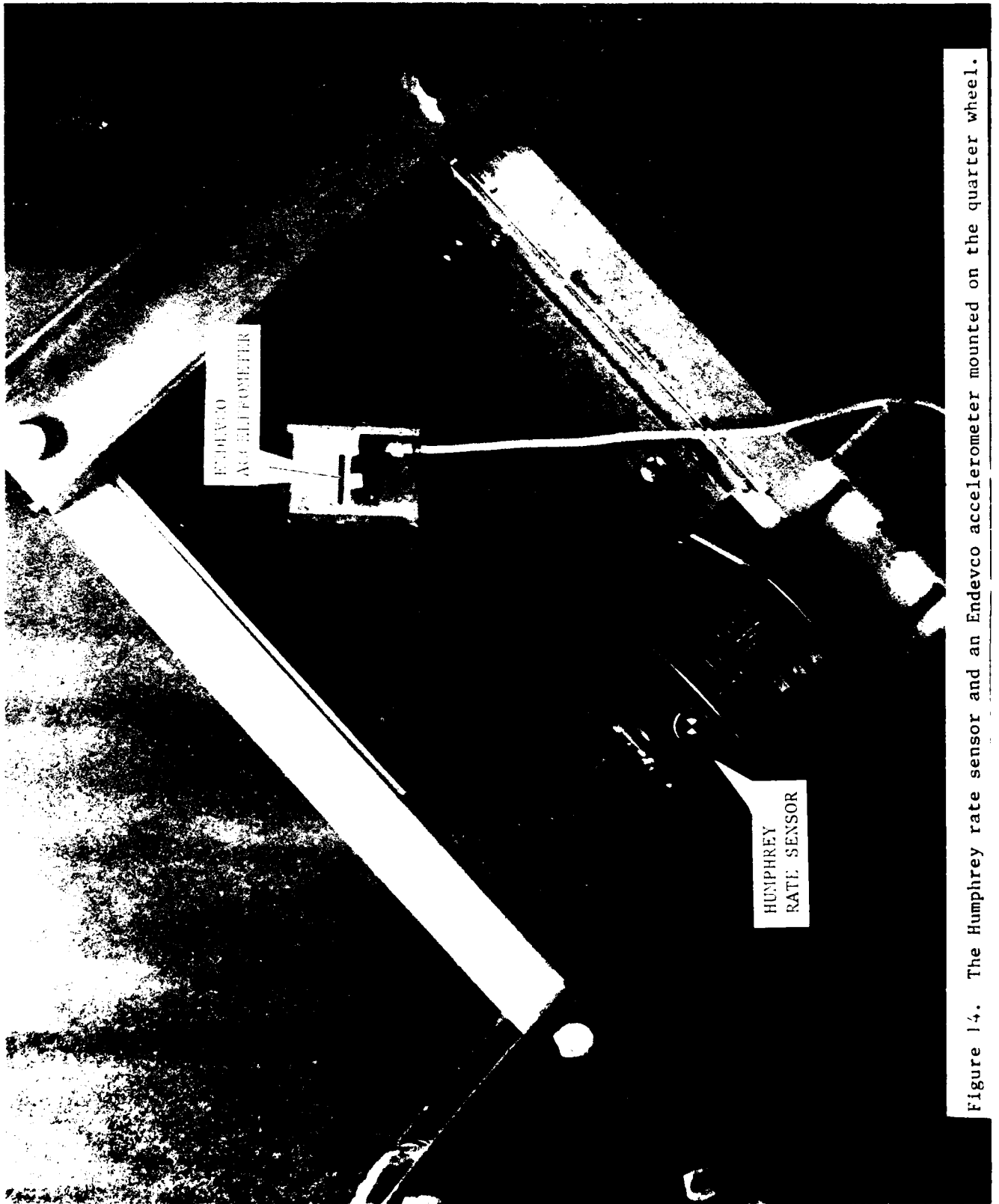


Figure 14. The Humphrey rate sensor and an Endevco accelerometer mounted on the quarter wheel.



Figure 15. The precision potentiometer coupled to the end of the rotating axle.

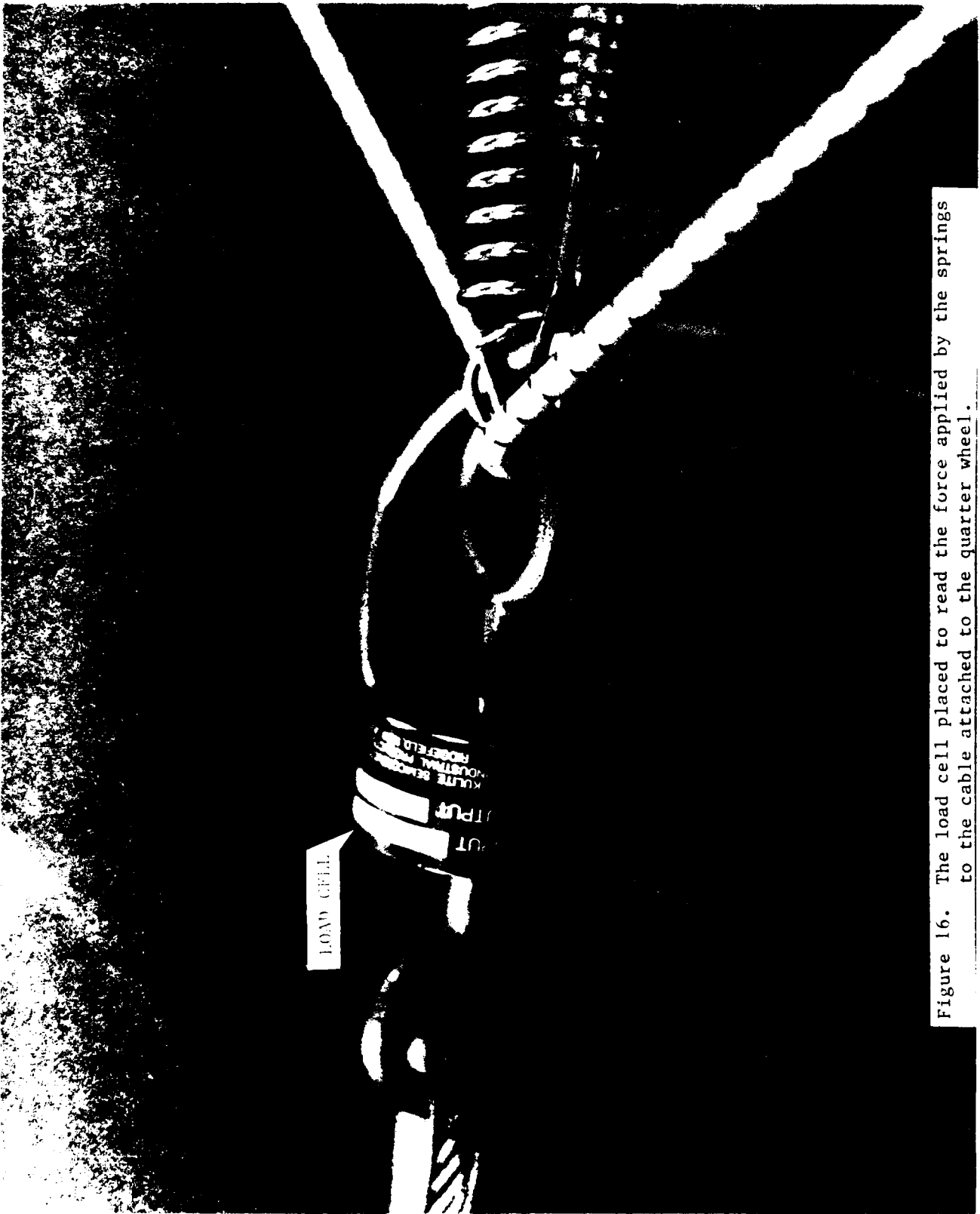


Figure 16. The load cell placed to read the force applied by the springs to the cable attached to the quarter wheel.

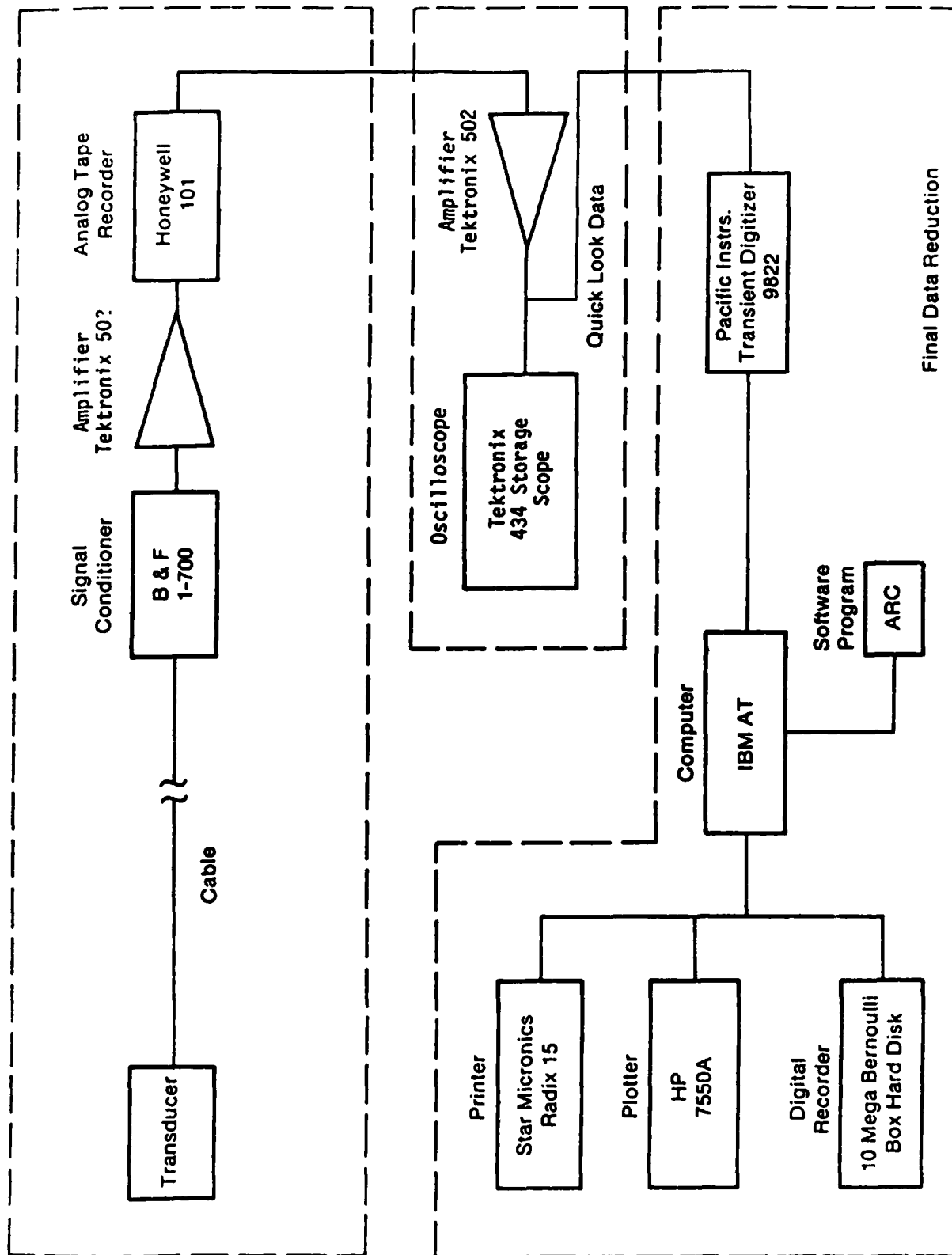


Figure 17. Block diagram of data acquisition and reduction system.

A Honeywell Model 101 FM tape recorder was used to record the signals. It was configured to operate in the intermediate band mode at a tape recording speed of 0.381 metres (15 inches) per second. This configuration provided the optimum signal-to-noise ratio for recording data.

Calibration steps were recorded on the tape prior to each experimental session. The voltage substitution method was used. In this method, a precise voltage representing the known value of the parameter is recorded on the tape for each of the data channels.

The data recorded on tape were played back through a Tektronix AM 502 amplifier into a Pacific Instruments Transient Digitizer at the same tape speed as was used for recording. The data were examined initially unfiltered. For input into a computer code to calculate the trajectory of the sensor array, the data were passed through a low-pass filter in the amplifier set at 100 Hz, and redigitized. These data were transferred to the IBM AT computer for plotting, processing, and permanent storage on a magnetic disk.

VI. PROGRAM TO COMPUTE TRAJECTORY OF SENSORS

A program was written to compute the vertical and horizontal displacement versus time of the sensor array. The program listing is contained in Appendix A.

The program assumes that the accelerometers are initially horizontal and vertical, that they are coincident, and that the vertical accelerometer initially is biased so that its output is zero in the gravity field. Figure 18 shows the geometry involved.

In the program, the angular velocity from the rate sensor is integrated to obtain the angle of rotation. This angle is used to correct the output from the accelerometers for the effect of gravity. It is used also to calculate the horizontal X and vertical Y components of acceleration from the corrected accelerometer records. The X and Y components of acceleration are integrated to obtain X and Y velocities, and integrated again to obtain X and Y displacements. The calculation is repeated, using the rotation angle as determined from the potentiometer on the axle, to obtain displacements without integrating the rate sensor record to obtain the angular velocity.

Integration is accomplished at each time step utilizing the trapezoidal rule. The only control of the accuracy of the integration is by variation of the time step value.

The program begins by reading information describing the test, the gages used, and spring data. Then it reads data required for the computation. These are the radius from the rotation axis to the sensitive masses of the accelerometers, and the horizontal distance from the axis to the vertical line through the sensitive masses of the accelerometers.

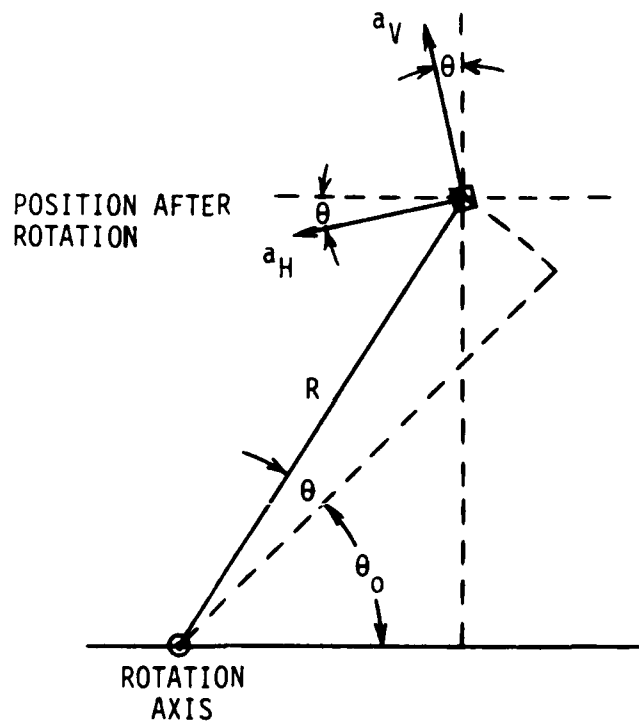
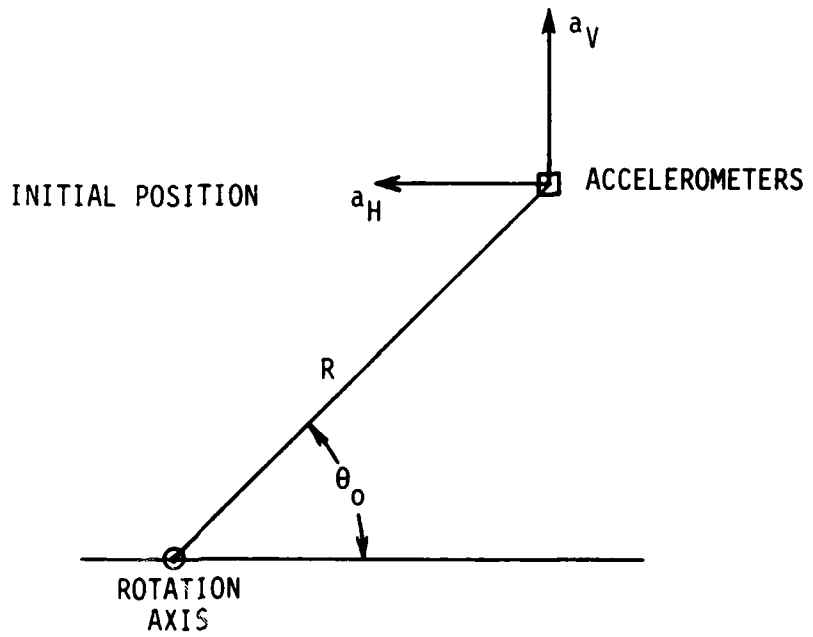


Figure 18. Position and orientation of accelerometers for rotation in a plane by the test facility.

From these values the initial angle of the radius to the accelerometers is computed.

The sensor records fed to the program must be digitized at the same rate so that the time between points is constant for all records. The ordinates of the records are read by the program, and the time for each point is calculated from the input value of the time step. Another input is the number of the time step at which the computation is to stop.

The gravitational constant is defined in the program as 9.800 m/s^2 at Aberdeen, Maryland.

To begin the computation, the initial values of the parameters are defined. All velocities and displacements are set to zero. Starting values for the accelerometers are computed as follows:

$$\begin{aligned}
 a_{Hgl} &= a_{H1} \\
 a_{Vgl} &= a_{V1} \\
 A_{X1} &= (a_{Vgl} \sin\theta_1 + a_{Hgl} \cos\theta_1) g = a_{Hgl}g \\
 A_{Y1} &= (a_{Vgl} \cos\theta_1 - a_{Hgl} \sin\theta_1) g = a_{Vgl}g
 \end{aligned}
 \tag{11}$$

where

- θ_1 = initial value of rotation angle = 0
- g = acceleration due to gravity
- a_{H1} = starting acceleration for the horizontal accelerometer
- a_{V1} = starting acceleration for the vertical accelerometer
- a_{Hgl} = a_{H1} corrected for gravity
- a_{Vgl} = a_{V1} corrected for gravity
- A_{X1} = starting horizontal (X) component of acceleration at accelerometers
- A_{Y1} = starting vertical (Y) component of acceleration at accelerometers

Accelerations described by lower case letters are in terms of g's.

Next the angular velocity is integrated:

$$\theta_{RS2} = (1/2) (\dot{\theta}_{RS2} + \dot{\theta}_{RS1}) (t_2 - t_1) + \theta_{RS1}
 \tag{12}$$

where

t_1 = start time
 t_2 = second time value
 $\dot{\theta}_{RS1}$ = initial angular velocity = 0
 $\dot{\theta}_{RS2}$ = angular velocity at time t_2
 θ_{RS1} = initial angle of rotation = 0
 θ_{RS2} = integrated value for angle of rotation at time t_2

The accelerometer records are corrected for the gravity field using the angle θ_{RS2} :

$$\begin{aligned}
 a_{Hg2} &= a_{H2} + \sin\theta_{RS2} \\
 a_{Vg2} &= a_{V2} + 1 - \cos\theta_{RS2}
 \end{aligned}
 \tag{13}$$

where

a_{H2} = acceleration at time t_2 for the horizontal accelerometer
 a_{V2} = acceleration at time t_2 for the vertical accelerometer
 a_{Hg2} = a_{H2} corrected for gravity
 a_{Vg2} = a_{V2} corrected for gravity

The X and Y components of acceleration at time t_2 are computed from the accelerometer records using the angle θ_{RS2} :

$$\begin{aligned}
 A_{X2} &= (a_{Vg2} \sin\theta_{RS2} + a_{Hg2} \cos\theta_{RS2}) g \\
 A_{Y2} &= (a_{Vg2} \cos\theta_{RS2} - a_{Hg2} \sin\theta_{RS2}) g
 \end{aligned}
 \tag{14}$$

where

A_{X2} = horizontal (X) component of acceleration at accelerometer at time t_2
 A_{Y2} = vertical (Y) component of acceleration at accelerometer at time t_2 .

These accelerations are integrated to obtain X and Y velocities:

$$\begin{aligned}
 u_{X2} &= (1/2) (A_{X2} + A_{X1}) (t_2 - t_1) + u_{X1} \\
 u_{Y2} &= (1/2) (A_{Y2} + A_{Y1}) (t_2 - t_1) + u_{Y1}
 \end{aligned}
 \tag{15}$$

where

u_{x1} = X component of velocity at accelerometers at start time. The value is zero.

u_{x2} = X component of velocity at accelerometers at time t_2

u_{y1} = Y component of velocity at accelerometers at start time. The value is zero.

u_{y2} = Y component of velocity at accelerometers at time t_2

These values of velocity are integrated to obtain the displacements:

$$\begin{aligned} X_2 &= (1/g) (u_{x2} + u_{x1}) (t_2 - t_1) + X_1 \\ Y_2 &= (1/g) (u_{y2} + u_{y1}) (t_2 - t_1) + Y_1 \end{aligned} \quad (16)$$

where

X_1 = starting horizontal displacement of the accelerometers. The value is zero.

X_2 = horizontal displacement of the accelerometers at time t_2

Y_1 = starting vertical displacement of the accelerometers. The value is zero.

Y_2 = vertical displacement of the accelerometers at time t_2

This integration process is repeated by the program using the angle of rotation from the potentiometer record instead of the angle obtained by integrating the rate sensor record.

These same X displacements are calculated also from the radius to the accelerometers and the angle of rotation from the potentiometer record. These values serve as reference values for comparison with those derived using the accelerometers and rate sensors.

$$\begin{aligned} X &= R \cos (\theta_2 - \cos (\theta_{p2} + \theta_0)) \\ Y &= R (\sin (\theta_2 + \theta_0) - \sin \theta_0) \end{aligned} \quad (17)$$

where

R = radius from axis to sensitive masses of the accelerometers

θ_0 = initial angle of R with respect to the horizontal

θ_{p2} = rotation angle at time t_2 derived from potentiometer record

X_2 = horizontal displacement of accelerometers at time t_2

Y_2 = vertical displacement of accelerometers at time t_2

These results for the first integration cycle are printed. The computed values are set by the program as the initial values of the next cycle, and the sequence of computations is repeated until either the number of the time step at which the computation is to stop has been reached or the last data points have been reached, whichever occurs first.

The program provides three descriptions of the displacement versus time of the accelerometers. The most accurate is that derived using the potentiometer record and the radius from the axis to the accelerometers. The second and that of primary interest is derived from the accelerometer and rate sensor records. The third, derived using the accelerometer and potentiometer records, provides results where the dominant errors should be from the accelerometer records.

VII. TEST PROGRAM

The test facility provided capability of movement of about two metres with a rotation of 90 degrees for an inertial sensor array. The sensor array for the tests consisted of two accelerometers and the Humphrey rate sensor. Two types of accelerometers were used. One was the Endevco accelerometer, a piezo-resistive strain gage type with a natural frequency of 2500 Hz. The other was the Schaevitz servo accelerometer, a closed-loop type with a natural frequency of about 140 Hz. These gages are described in more detail in Section V.A.

Two loading functions were used in the program, one producing a peak acceleration of about 10 g's, and the other about 5 g's. Two different sets of springs were used to generate the loading on the quarter wheel. Both loading functions were used in testing sensor arrays containing each type of accelerometer.

A. Test Procedure

Electrical power to the sensors was turned on at least five minutes prior to a test for sensor warming and stabilization. The maximum warm-up time listed by the manufacturer for any gage was two minutes.

Loading on the quarter wheel was provided by a long spring and a short spring connected in parallel in the cable line. First the long spring was connected and the cable centered on the circumference of the wheel. Then the restraint cable was connected. The long spring was stretched to its maximum extension by unscrewing the long threaded rod to which it was attached. The force in the cable was read from a meter monitoring the output of the load cell. The spring was stretched until the force in the cable became that appropriate for the loading function that the spring set was intended to produce. This was either 400 Newtons (90 pounds) or 222 Newtons (50 pounds).

The short, strong spring then was attached to the cable pulling on the wheel and stretched by unscrewing the threaded rod to which it was attached. This spring was stretched until the load cell monitor showed the desired peak force in the cables. The value was either 1334 Newtons

(300 pounds), if the long spring loading was 400 Newtons (90 pounds); or 712 Newtons (160 pounds), if the long spring loading was 222 Newtons (50 pounds).

With the wheel under full loading, a sensitive bubble level was used with turnbuckle adjustments in the restraint cable to set the accelerometers horizontal and vertical. A plumbob was used to define a vertical line through the sensitive masses of the accelerometers. The horizontal distance from the rotation axis to this vertical line was read. The radius from the axis to the accelerometers was measured. These two quantities were used to compute the initial angle of the radius to the accelerometers.

Calibration data for the sensors were fed into the tape recorder. The potentiometer was calibrated by rotating the wheel 90 degrees.

For recording a test, the tape recorder was activated. When the tape was running at the proper speed, a marker signal was placed on the potentiometer channel by a manually operated switch. The pin holding the restraint cable was yanked free, the springs contracted and rotated the quarter wheel.

The trigger signal on the potentiometer channel was used as zero time for all channels. The records were digitized as recorded, and plotted for evaluation. Then the records were played back through a 100 Hz low pass filter and digitized at about 0.5 millisecond intervals. The baseline for a waveform was set using an average of points taken shortly before the initial rise of the waveform. These data were fed into the program described in Section VI and the trajectories of the accelerometers were computed and plotted.

The zero time for the trajectory computation was taken as the earliest positive rise on an accelerometer waveform. Apparently in the pin withdrawal process, a short duration negative acceleration can be produced. This initial disturbance on an accelerometer record was not used in the trajectory computations.

B. Tests and Results

A number of tests were conducted in the test facility using both the Endevco and the Schaevitz accelerometers. Table 5 lists those reported here.

Tests 28, 29, 30, 43, and 45 were run with springs that produced peak accelerations of about 4-4.5 g's. Tests 31, 33, 35, 46, and 48 were run with springs that produced peak accelerations of about 7-9 g's.

The results for tests 29, 33, 45, and 46 will be presented in some detail. Tests 29 and 33 are low and high g tests for the sensor array with Endevco accelerometers, and 45 and 46 are low and high g tests with the Schaevitz accelerometers.

TABLE 5. TESTS PERFORMED WITH INERTIAL SENSOR ARRAYS IN THE TEST FACILITY

Test Number	Long Spring Force (N)	Total Spring Force (N)	XZero* (m)	Radius (in)
Two Endevco accelerometers, one Humphrey rate sensor				
28	214	712	0.963	1.391
29	214	712	0.964	1.391
30	214	712	0.965	1.391
31	400	1334	0.962	1.391
33	400	1334	0.969	1.391
35	400	1334	0.963	1.391
Two Schaevitz accelerometers, one Humphrey rate sensor				
43	222	712	0.982	1.386
45	285	801	0.983	1.386
46	400	1334	0.983	1.386
48	400	1472	0.980	1.386

*XZero is the horizontal distance from the axis to the vertical line through the sensitive masses of the accelerometers.

1. Test 29

This test was done using the Endevco accelerometers. The total force in the cable at initiation of the test was 712 Newtons, and a peak acceleration of about 4.5 g's was produced.

Figure 19 shows the unfiltered vertical acceleration record, and Figure 20 presents the filtered record. The large negative deflection at about 1.6 seconds corresponds to rotation of the quarter wheel 90 degrees, where it impacts a plastic foam stop and bounces. Figures 21 and 22 show the unfiltered and filtered records for the initially horizontal accelerometer.

The records for both accelerometers show an initial negative acceleration. It was assumed that this was produced during the process of releasing the restraint cable by yanking the pin out of the holder. See Figure 13. This negative pulse was omitted from the waveform used in the data reduction program. Zero time was taken as the time for the first positive rise of an accelerometer waveform. This time was used as zero time for the other waveforms as well.

Figures 23 and 24 show the unfiltered and filtered rate sensor records, respectively. Because the rate sensor has a very low natural frequency, it has a time lag in regions of rapidly changing angular velocities. As a result, the waveform initially has negative values.

Figures 25 and 26 show the unfiltered and filtered records for the angle of rotation as derived from the potentiometer on the axis of the quarter wheel. The bounce of the wheel is evident.

Figures 27 and 28 show the unfiltered and filtered records from the load cell. Initially the peak load is on the cable. When the restraint cable pin is pulled, the strong, short spring unloads rapidly. The weaker, long spring unloads at a much slower rate.

Figures 29 and 30 show the unfiltered and filtered positive phases of acceleration from the initially vertical accelerometer. Figures 31 and 32 show the unfiltered and filtered records for the initially horizontal accelerometers for the same time period. Figures 33 and 34 show the unfiltered and filtered load cell waveforms. As expected, the shapes of the acceleration records are similar to that of the load cell.

Figure 35 shows the trajectory of the accelerometers. The solid reference curve is that determined from the radius to the accelerometers and the angle from the potentiometer record. The dashed curve is that derived from the accelerometer and rate sensor records using the programs described in Section VI and listed in Appendix A. Both curves terminate at the same time, which is the last time that the data are uninfluenced by deceleration of the quarter wheel as it impacts the plastic foam stop. Figure 36 shows the horizontal X error versus time. For most of the time, the error is less than 0.03 metres (1.2 inches). At the end point the error is -0.086 metres (-3.4 inches). Figure 37 shows the vertical Y error versus time. It remains less than 0.03 metres (1.2 inches).

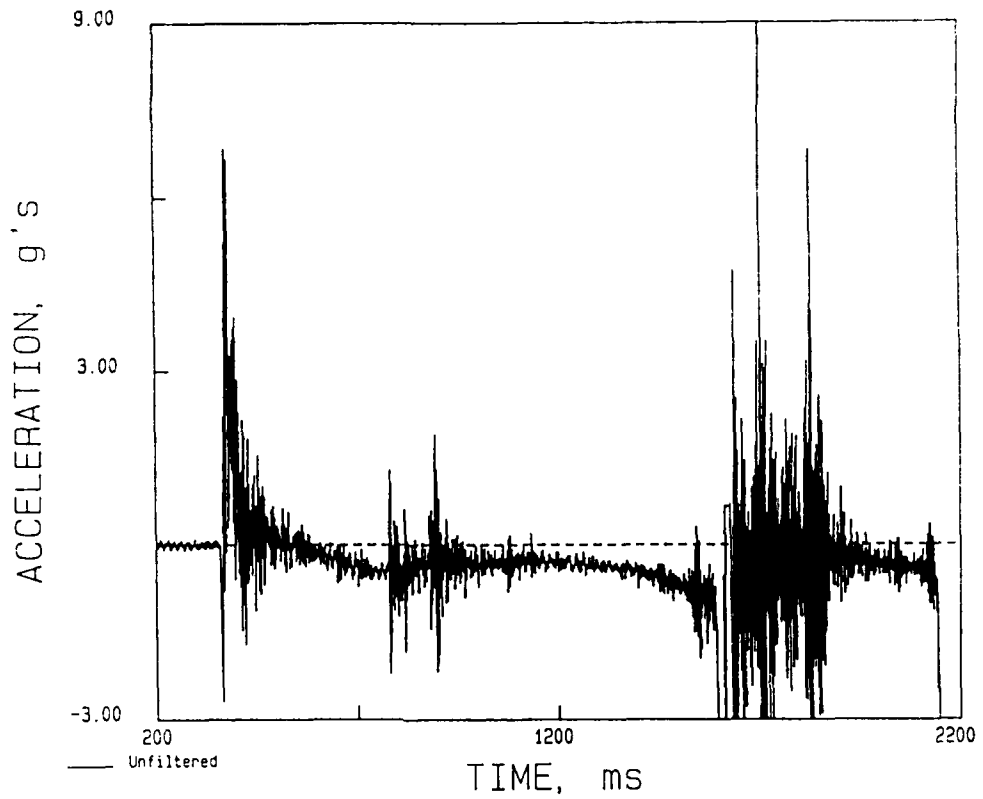


Figure 19. Unfiltered acceleration versus time from the initially vertical Endeveco accelerometer on Test 29.

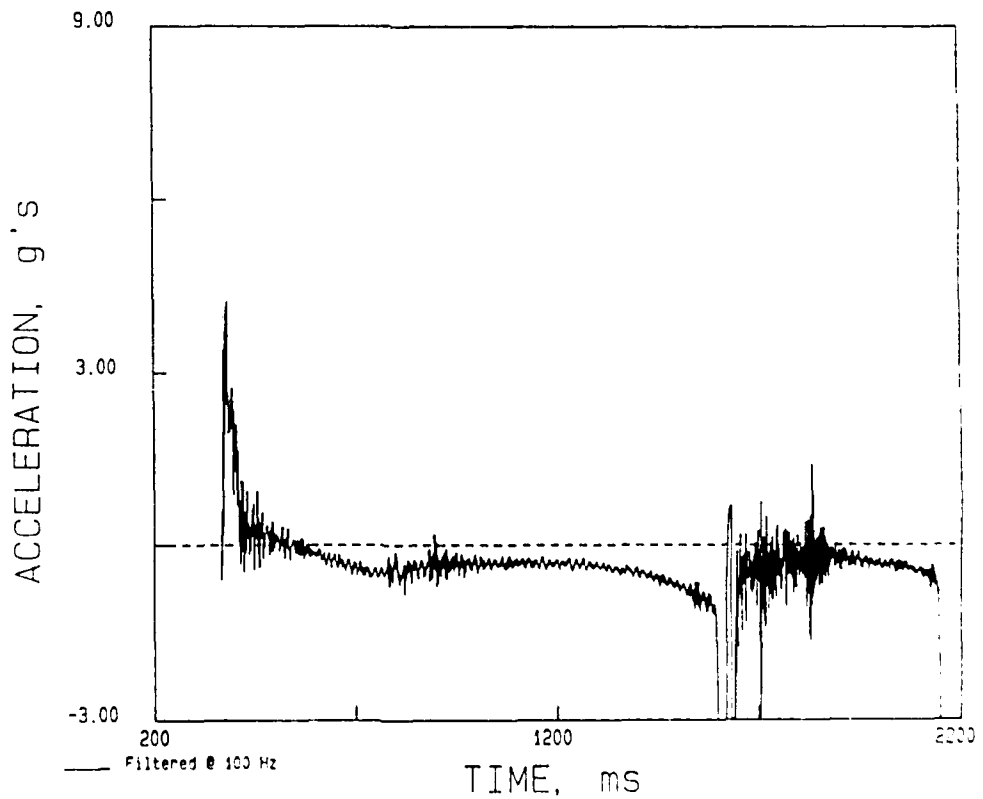


Figure 20. Filtered acceleration versus time from the initially vertical Endeveco accelerometer on Test 29.

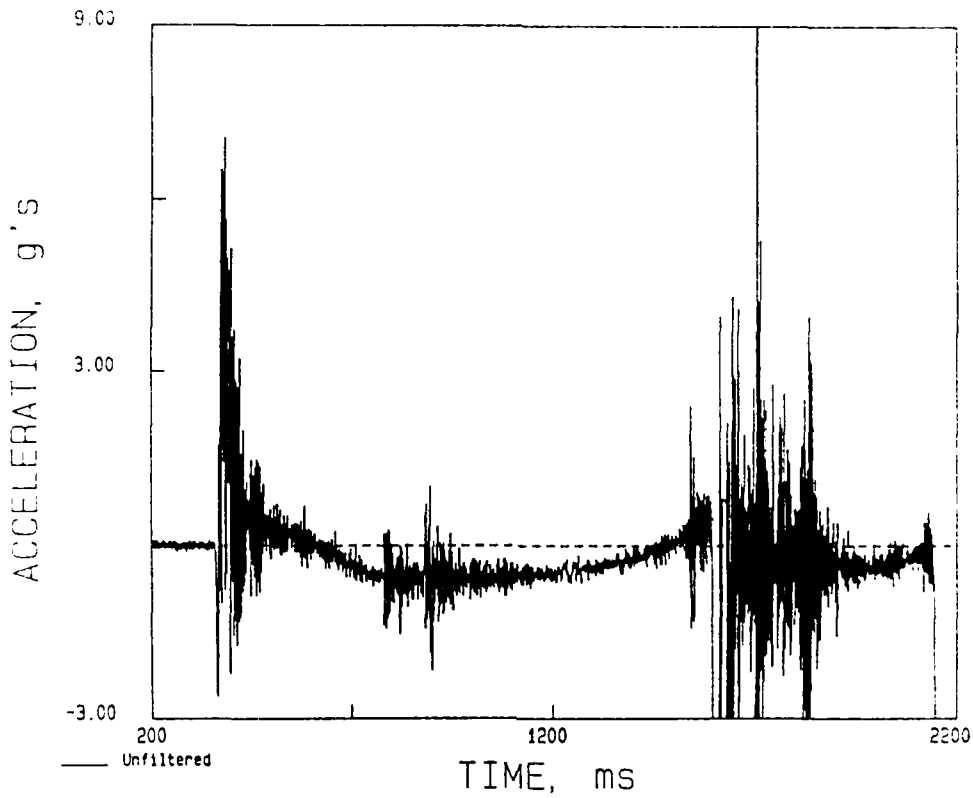


Figure 21. Unfiltered acceleration versus time from the initially horizontal Endevco accelerometer on Test 29.

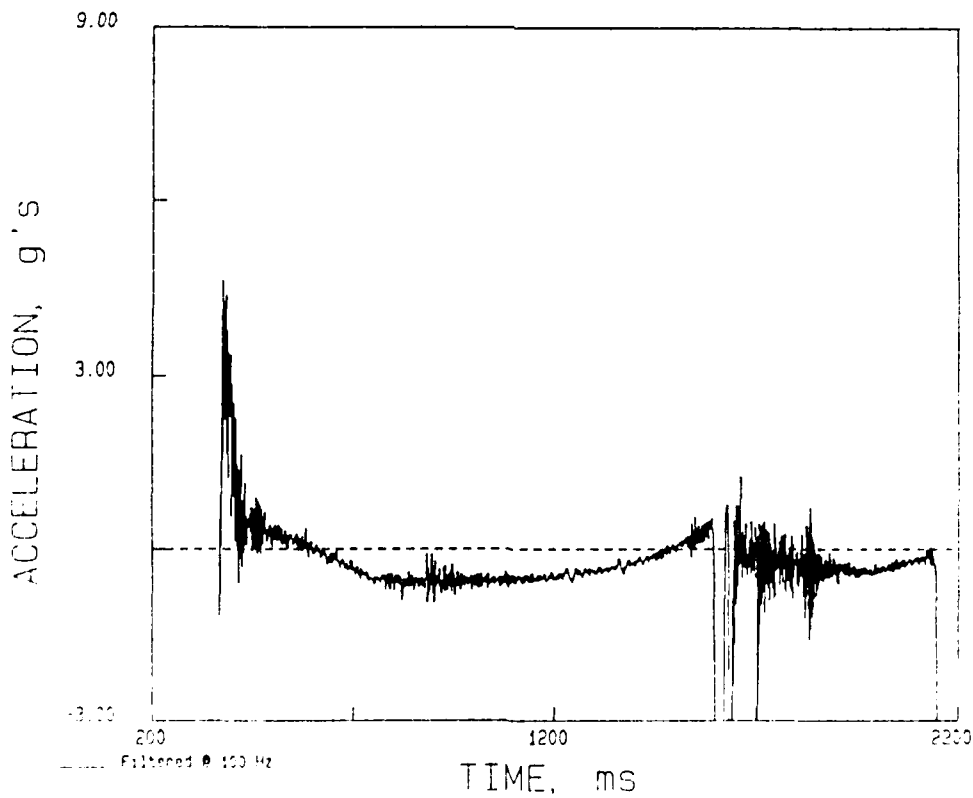


Figure 22. Filtered acceleration versus time from the initially horizontal Endevco accelerometer on Test 29.

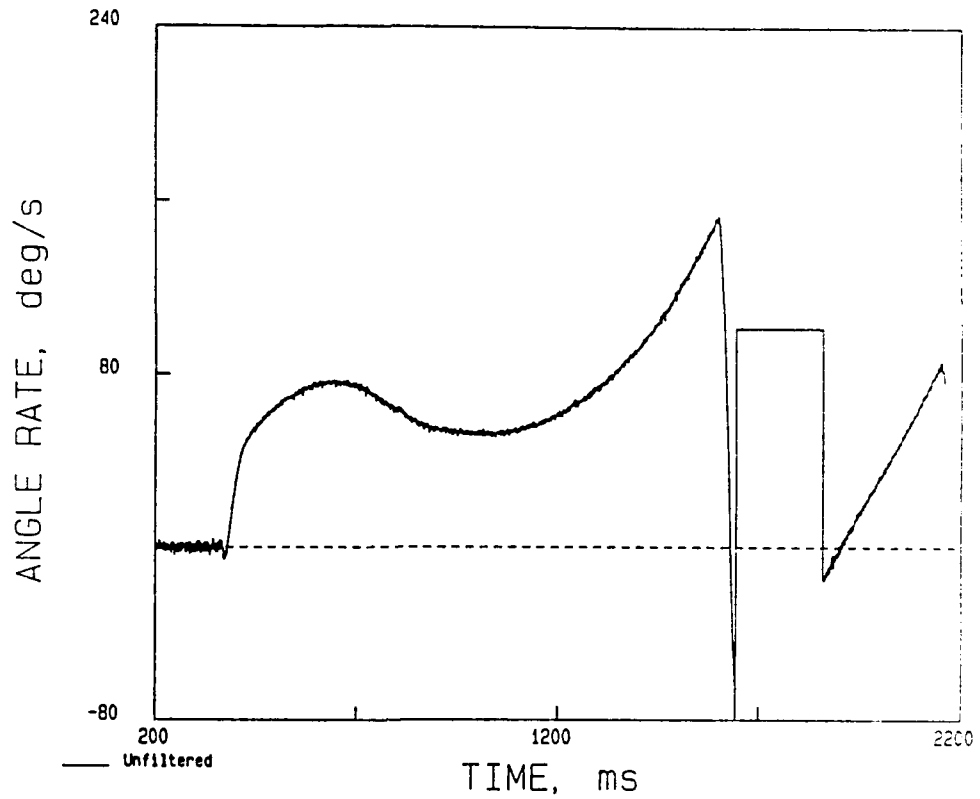


Figure 23. Unfiltered angular velocity versus time from the Humphrey rate sensor on Test 29.

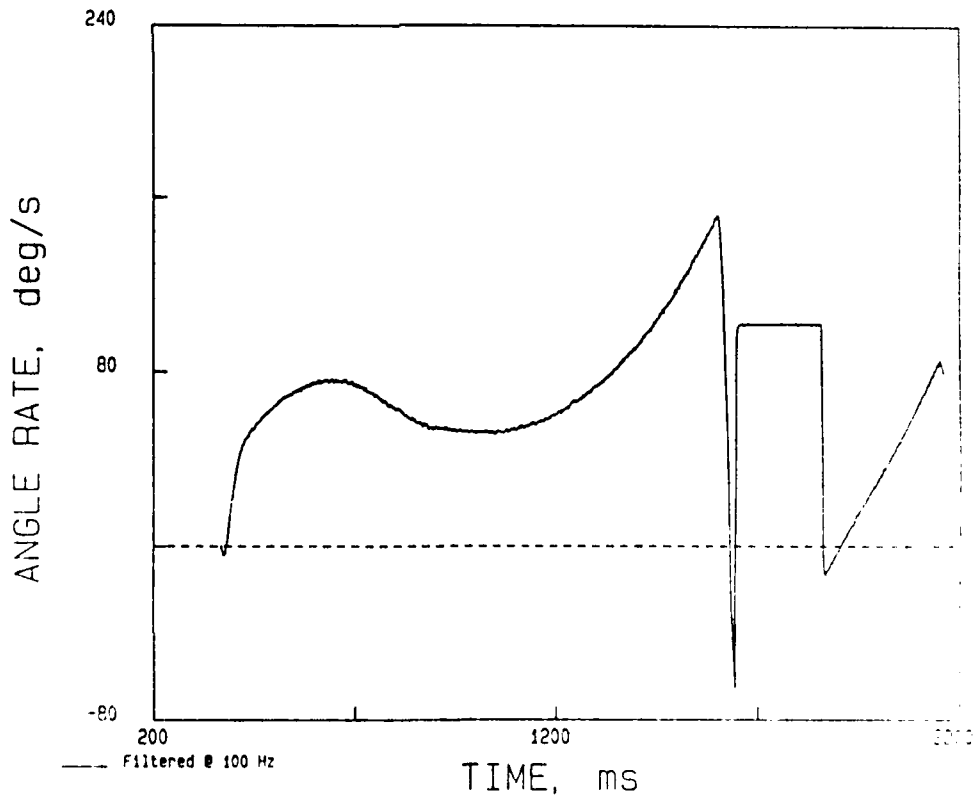


Figure 24. Filtered angular velocity versus time from the Humphrey rate sensor on Test 29.

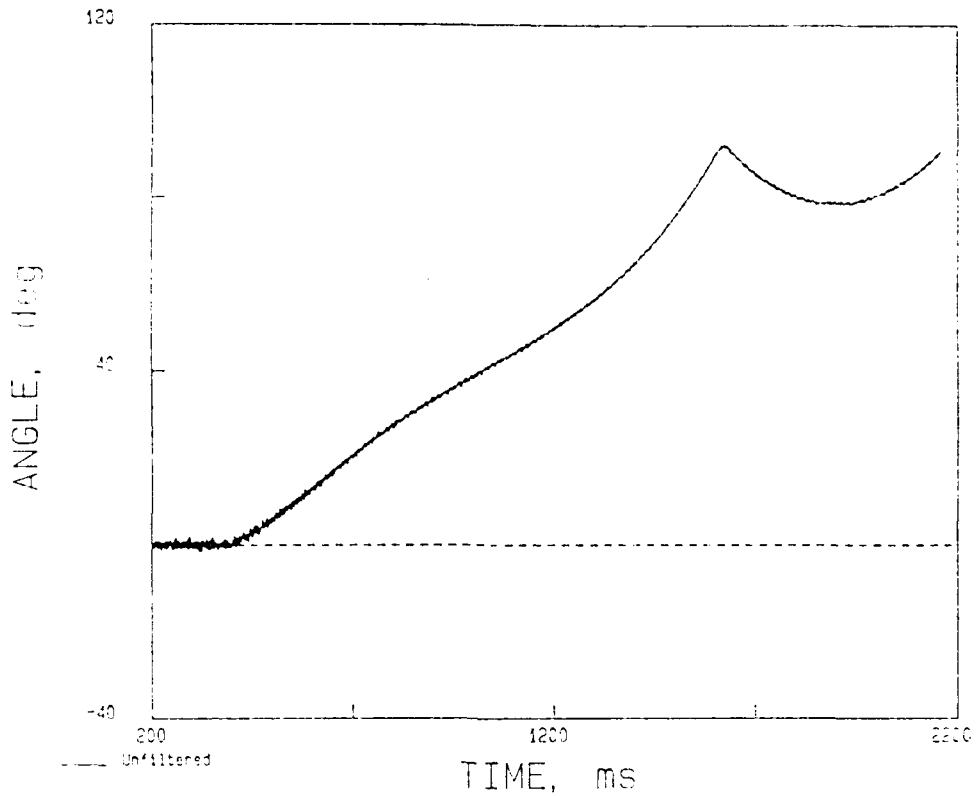


Figure 28. Unfiltered angle versus time derived from the potentiometer on the axle of the quarter wheel on Test 29.

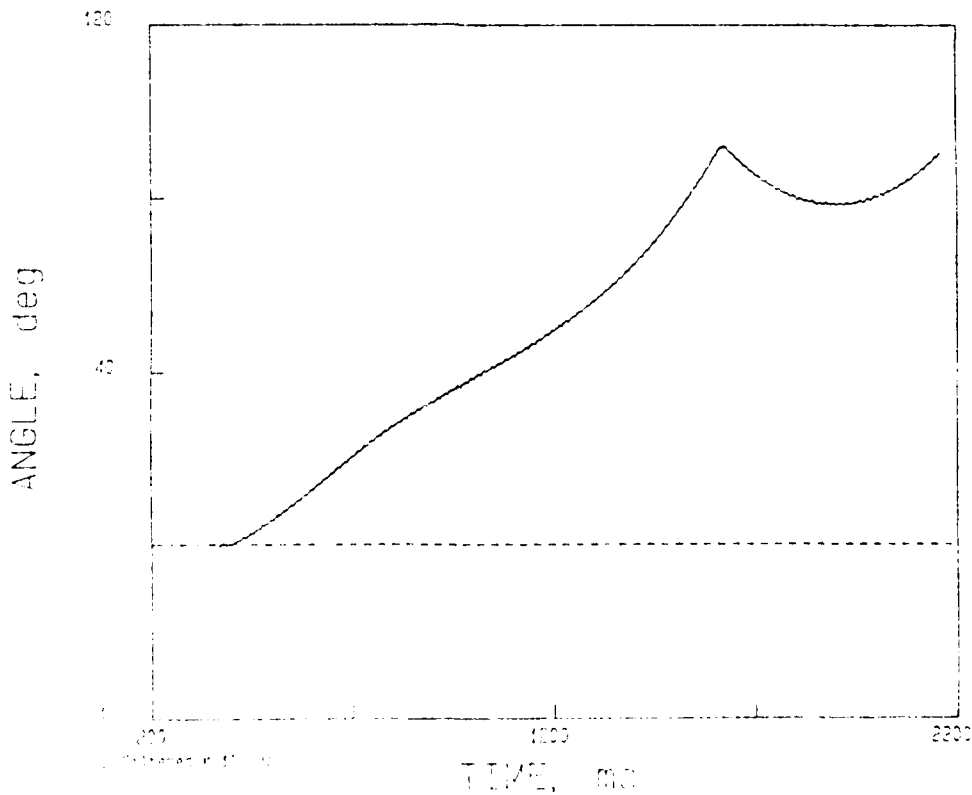


Figure 29. Filtered angle versus time derived from the potentiometer on the axle of the quarter wheel on Test 29.

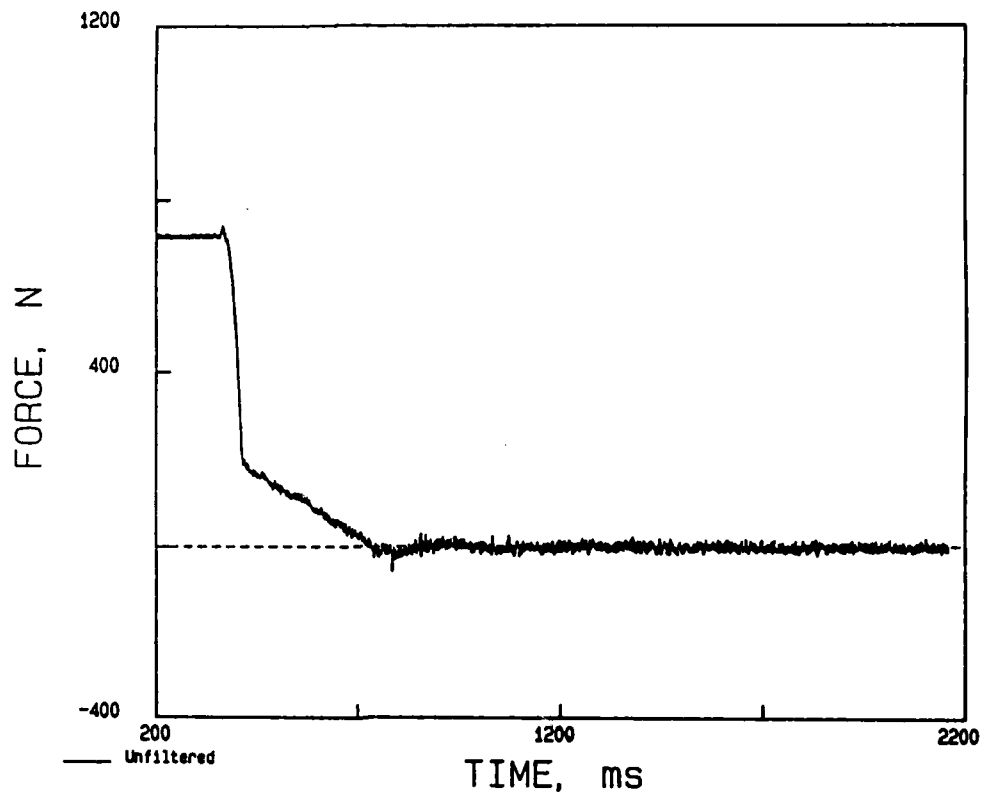


Figure 27. Unfiltered load cell record from Test 29.

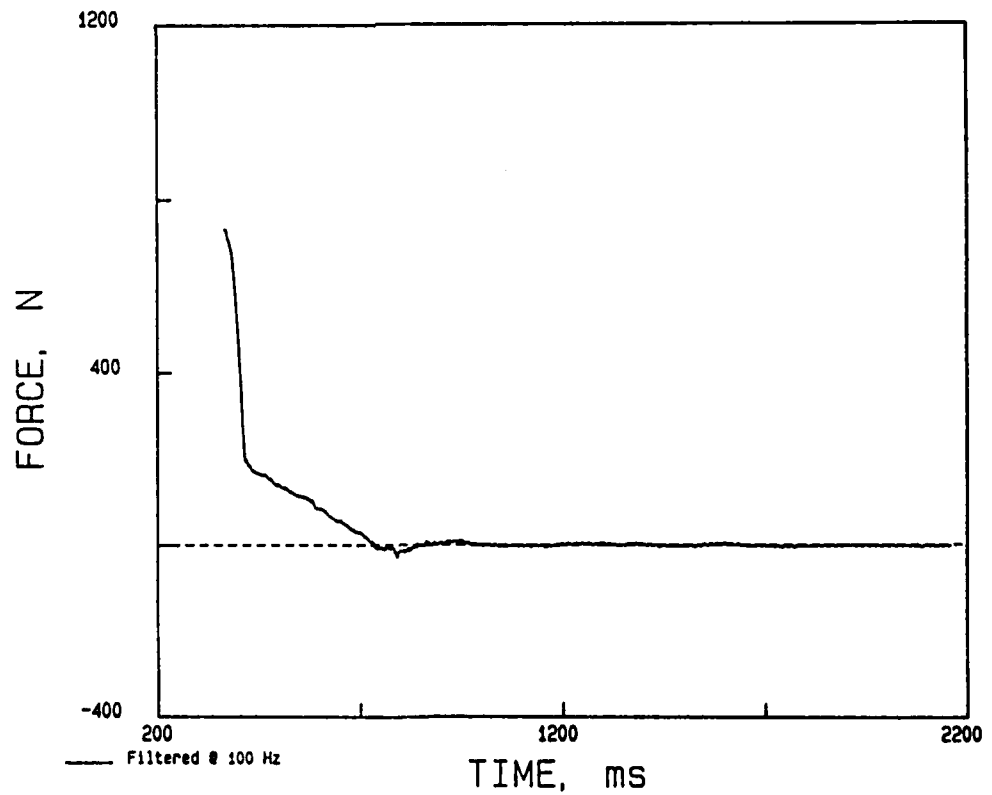


Figure 28. Filtered load cell record from Test 29.

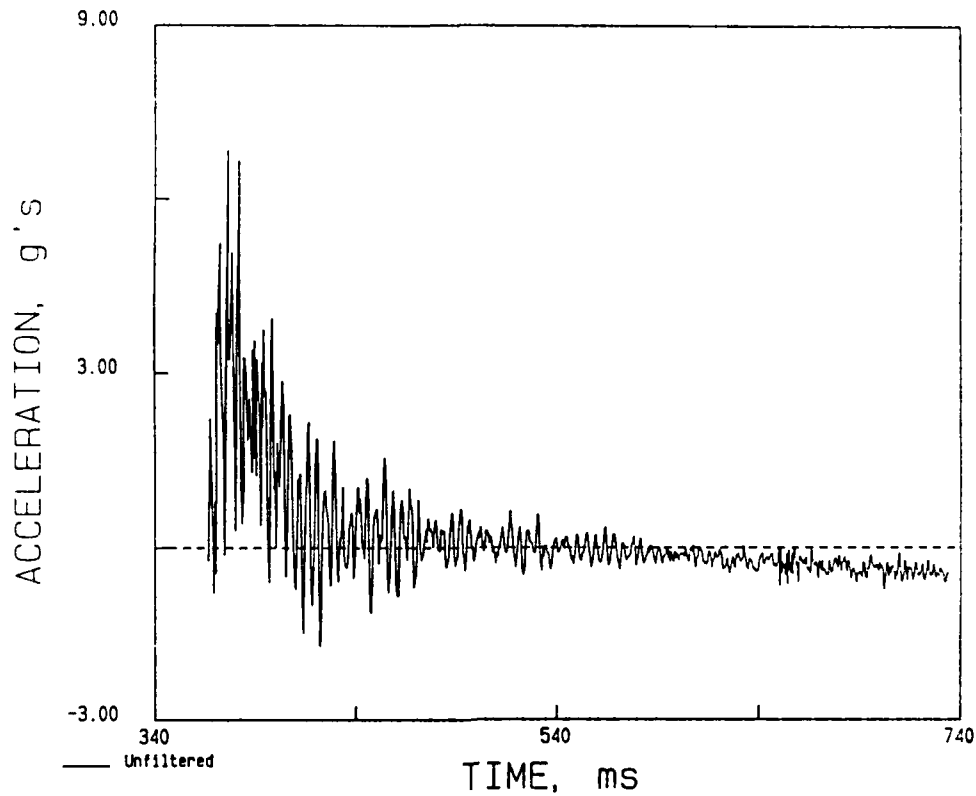


Figure 29. Unfiltered positive phase of acceleration versus time from the vertical accelerometer on Test 29.

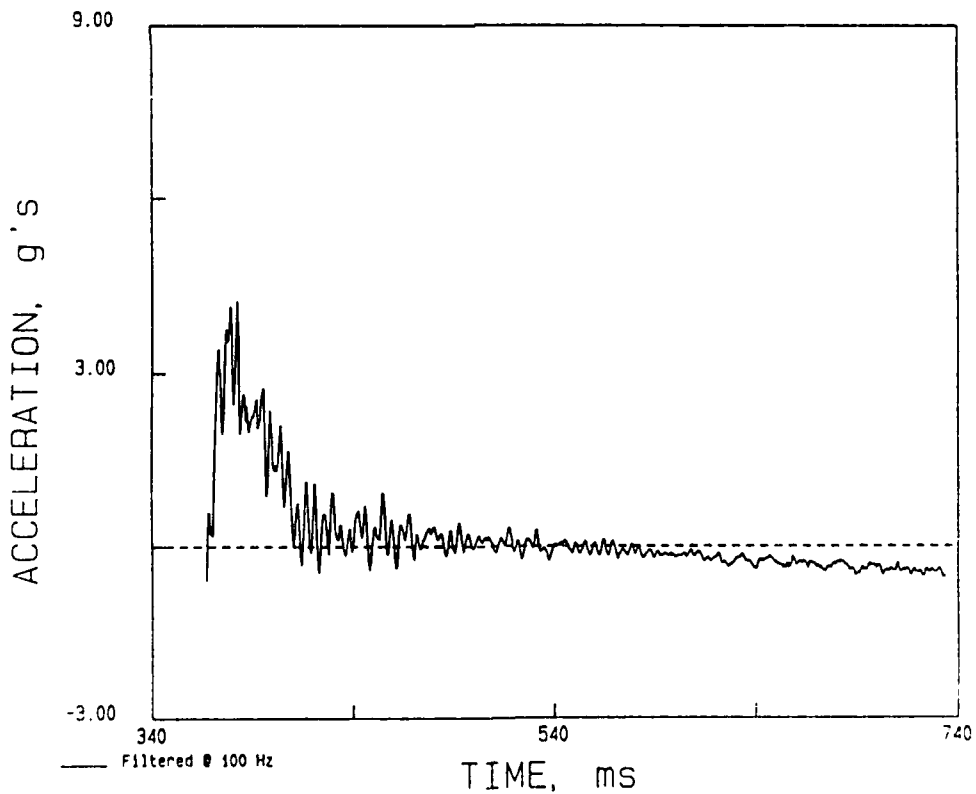


Figure 30. Filtered positive phase of acceleration versus time from the vertical accelerometer on Test 29.

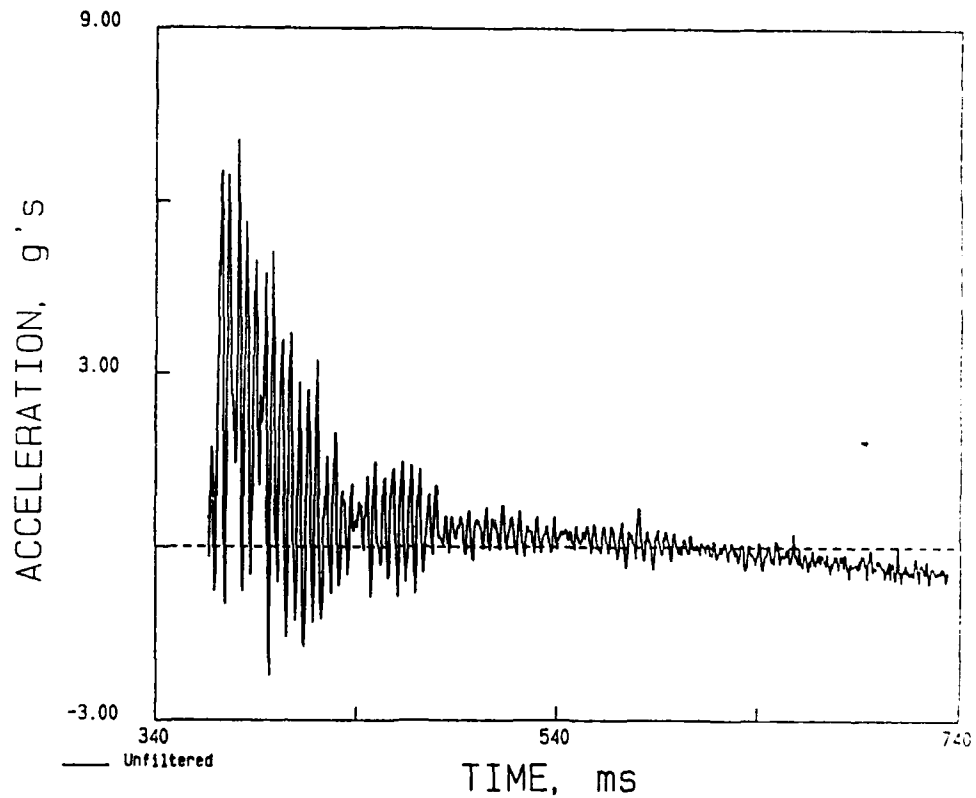


Figure 31. Unfiltered positive phase of acceleration versus time from the initially horizontal accelerometer on Test 29.

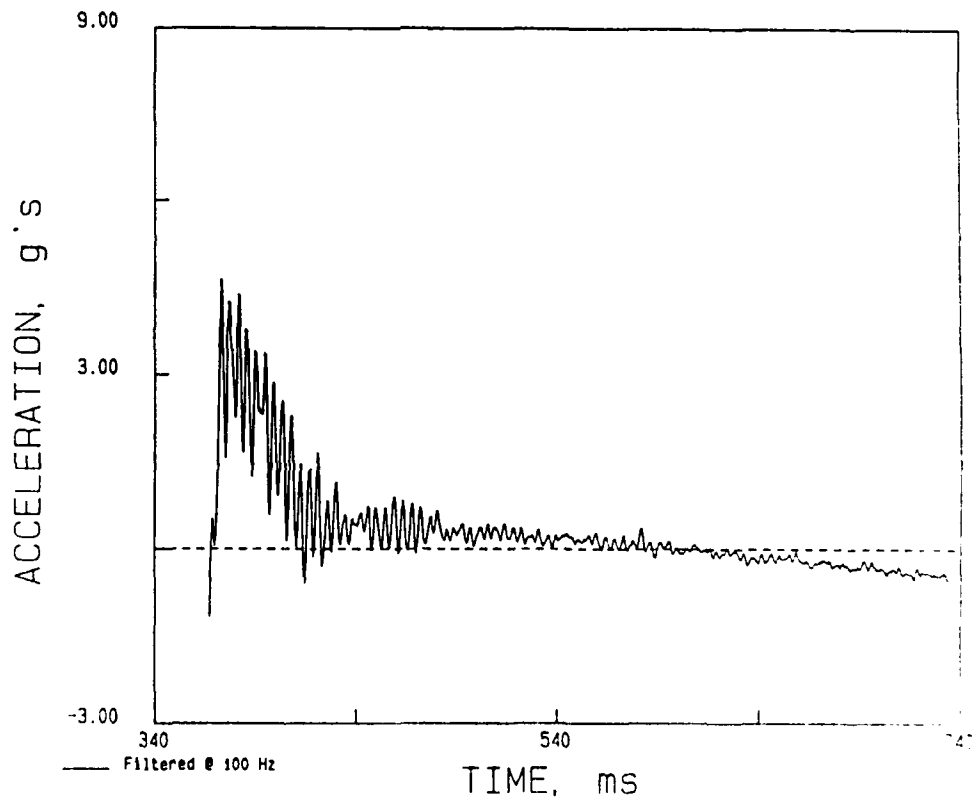


Figure 32. Filtered positive phase of acceleration versus time from the initially horizontal accelerometer on Test 29.

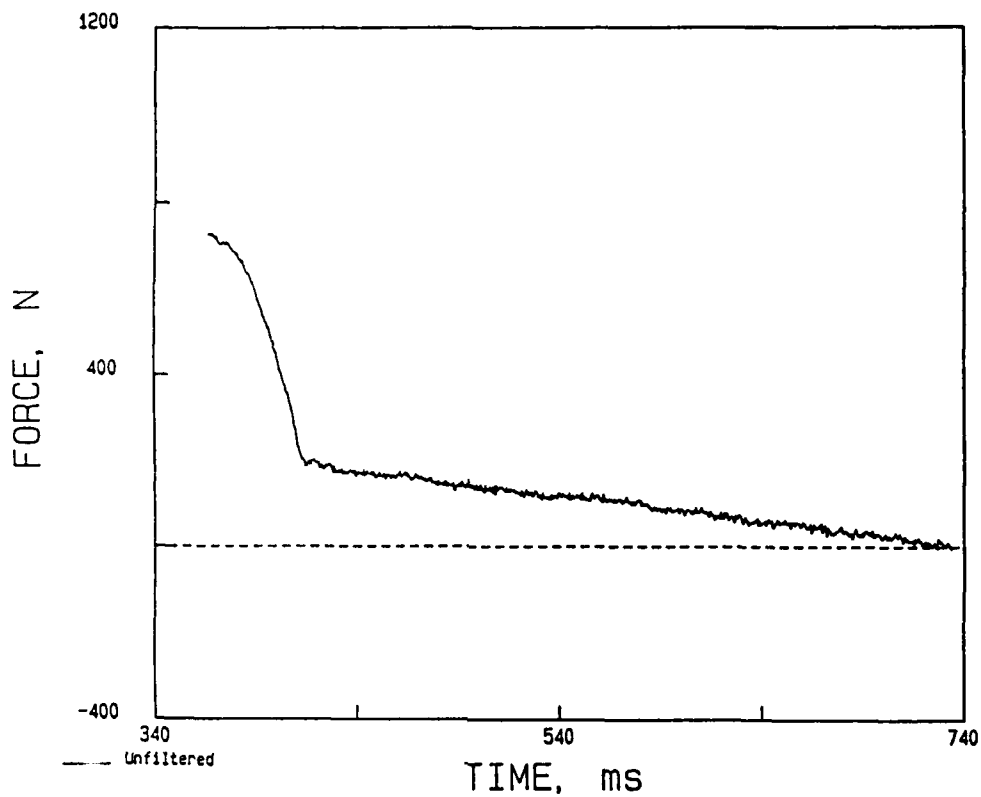


Figure 33. Unfiltered positive phase of the load cell record from Test 29.

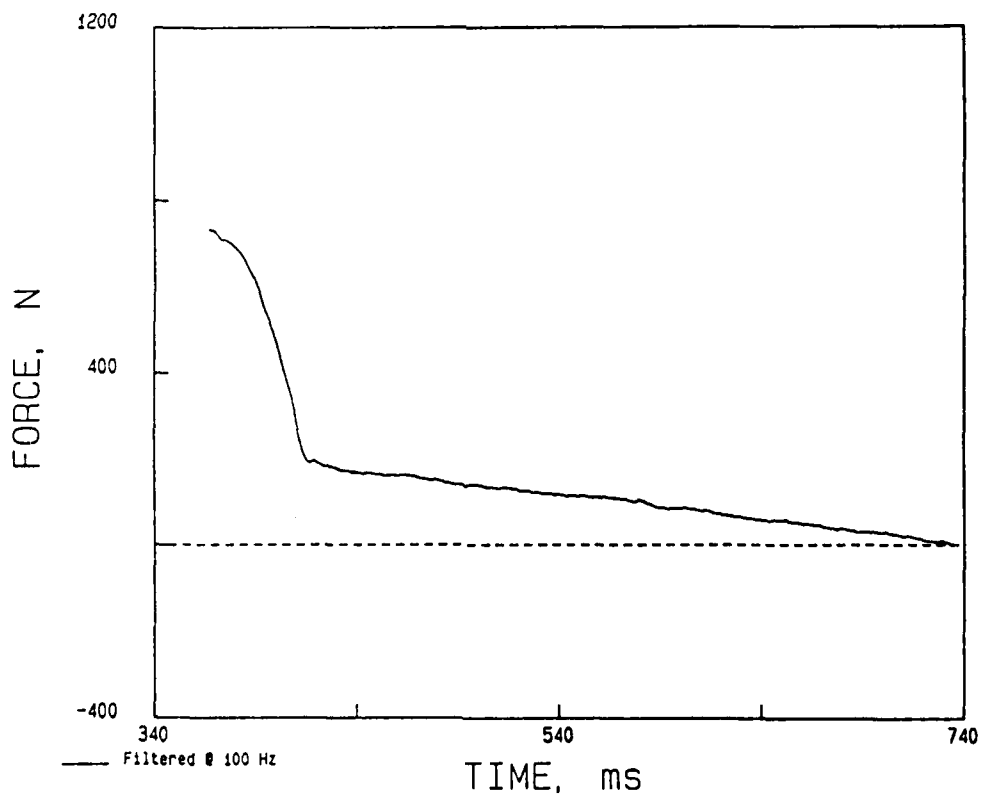


Figure 34. Filtered positive phase of the load cell record from Test 29.

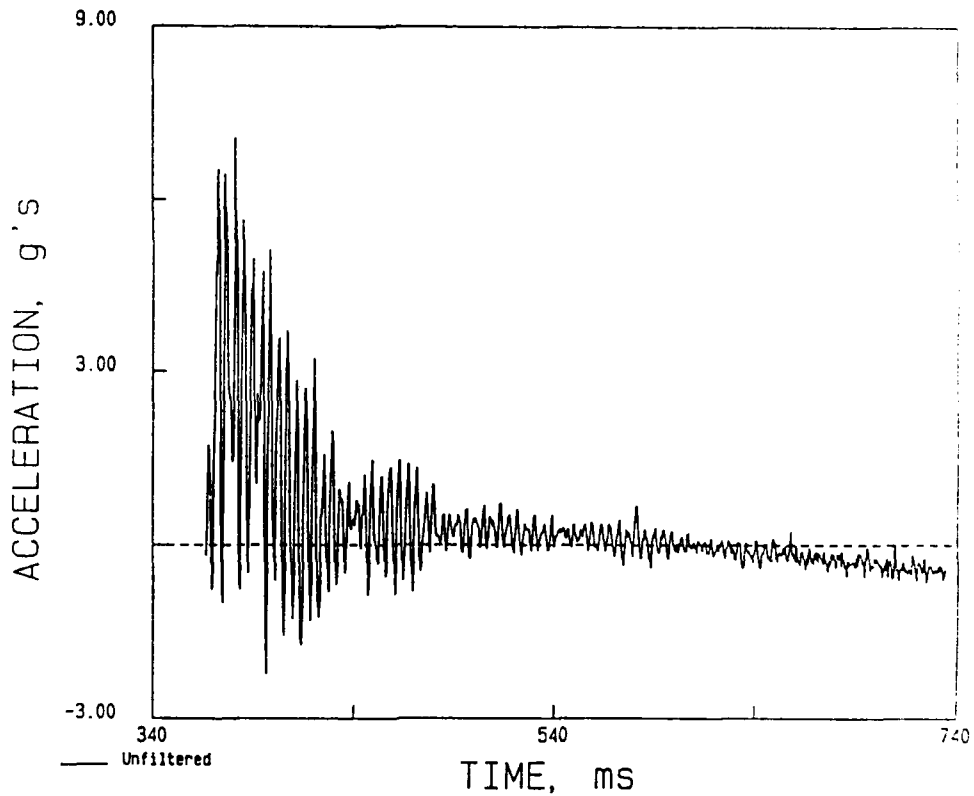


Figure 31. Unfiltered positive phase of acceleration versus time from the initially horizontal accelerometer on Test 29.

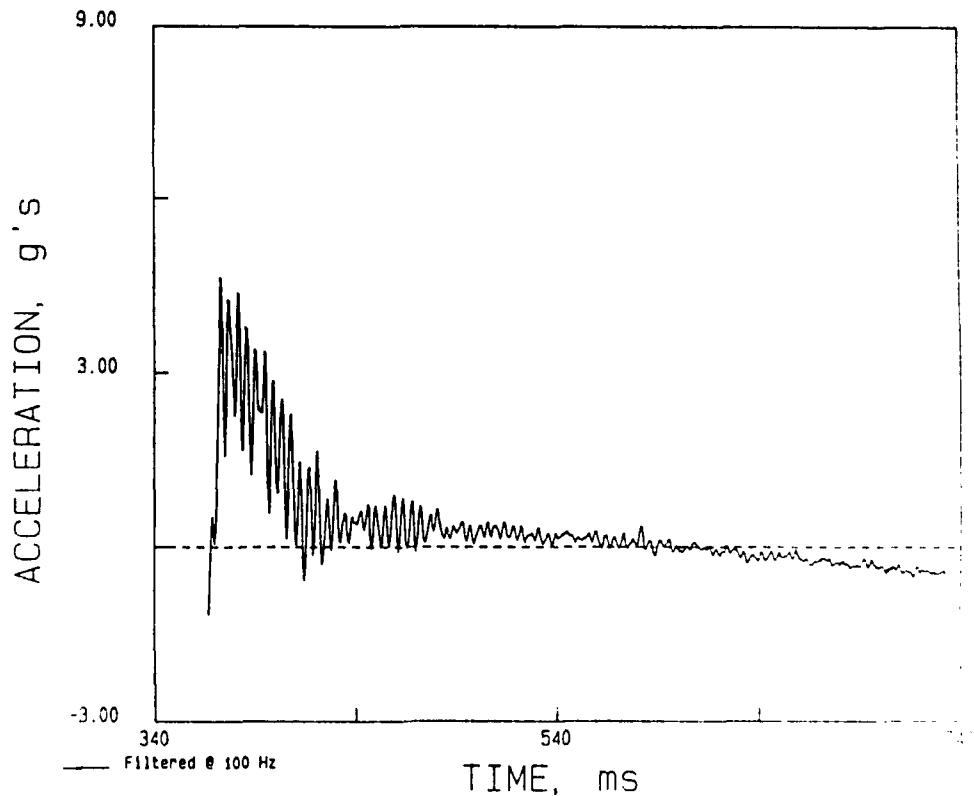


Figure 32. Filtered positive phase of acceleration versus time from the initially horizontal accelerometer on Test 29.

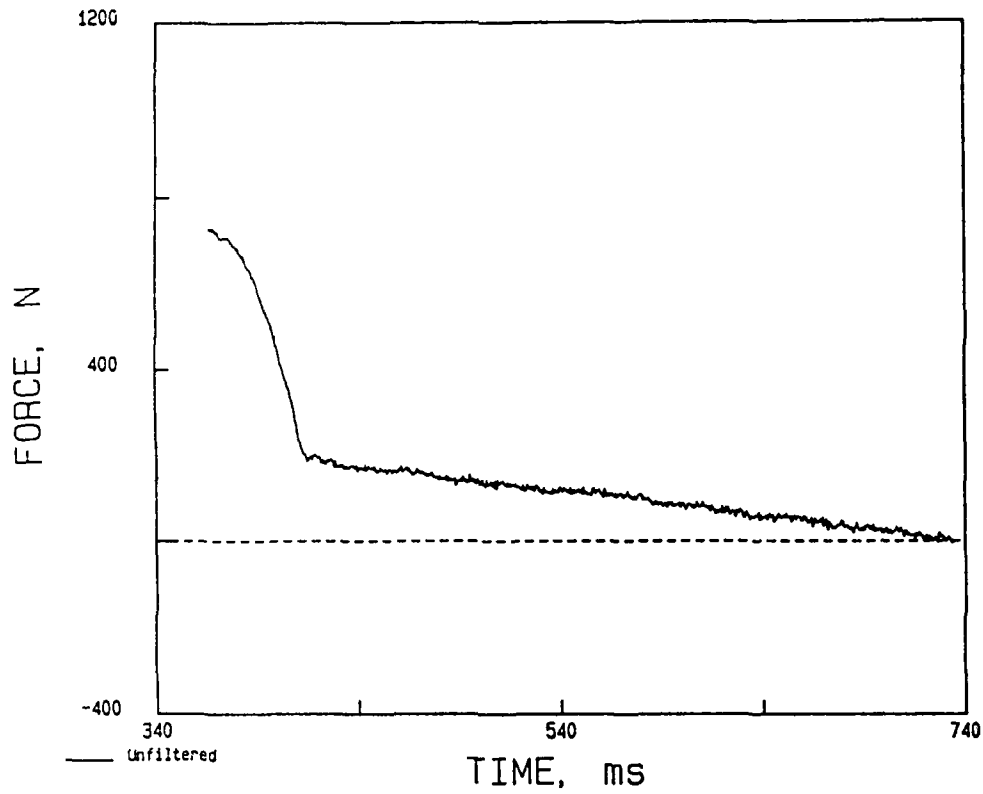


Figure 33. Unfiltered positive phase of the load cell record from Test 29.

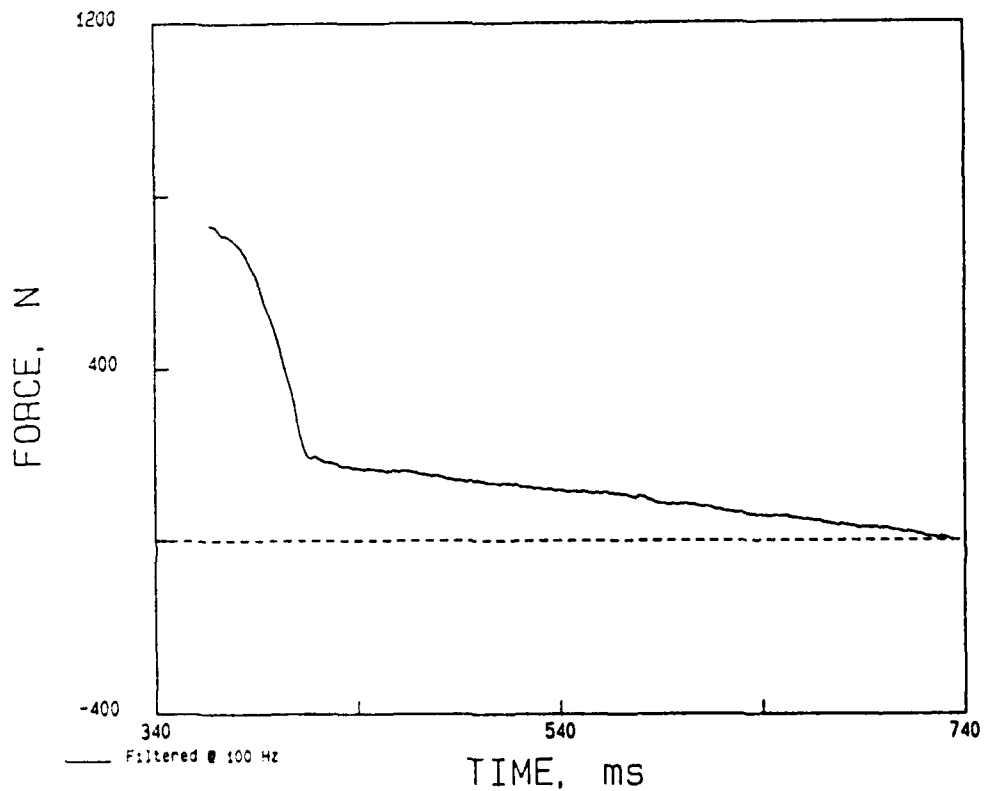


Figure 34. Filtered positive phase of the load cell record from Test 29.

TRAJECTORY OF SENSORS - 29

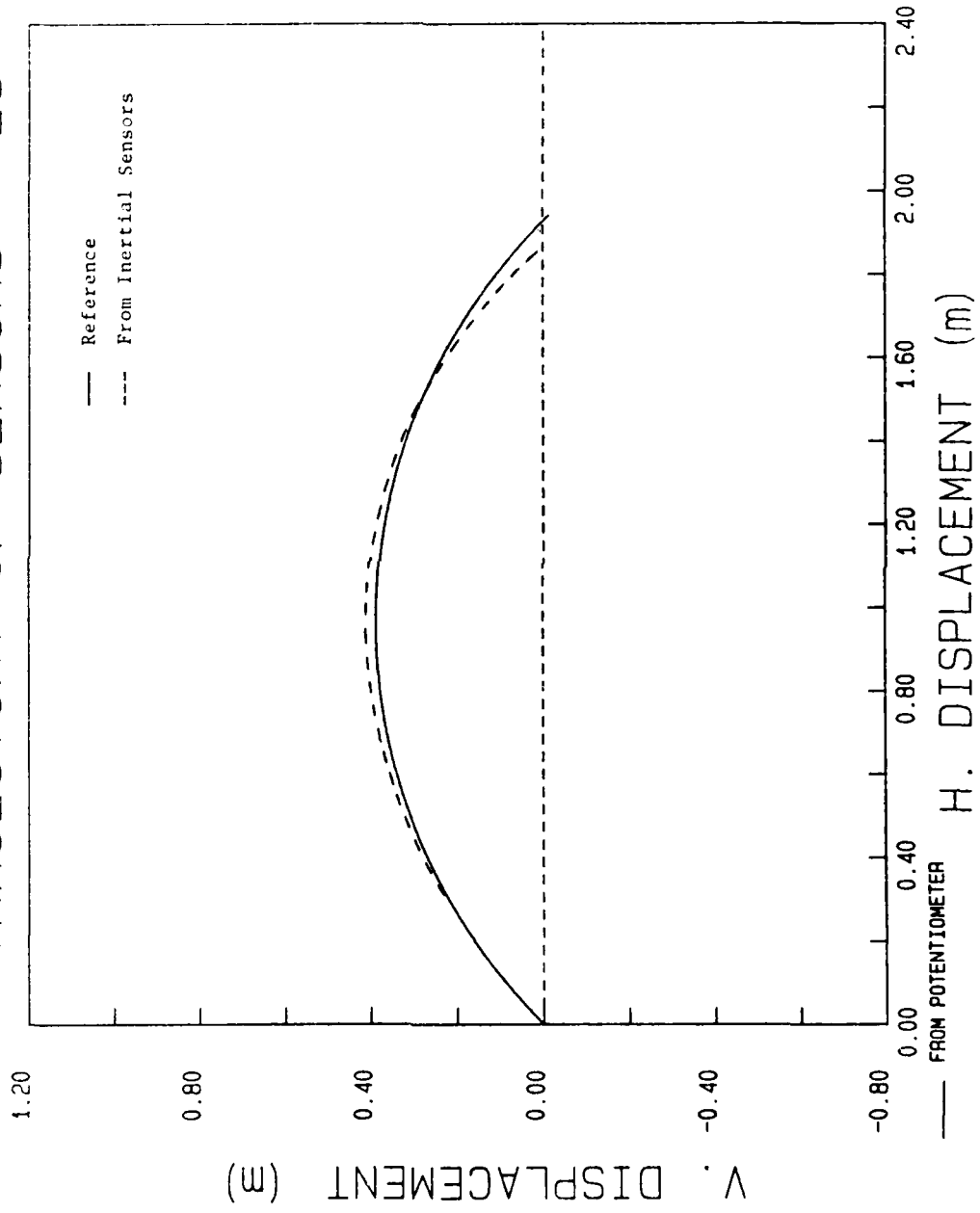


Figure 35. Comparison of the sensor array trajectory for Test 29 derived from the Endevco accelerometers and the Humphrey rate sensor with the reference trajectory derived from the potentiometer record.

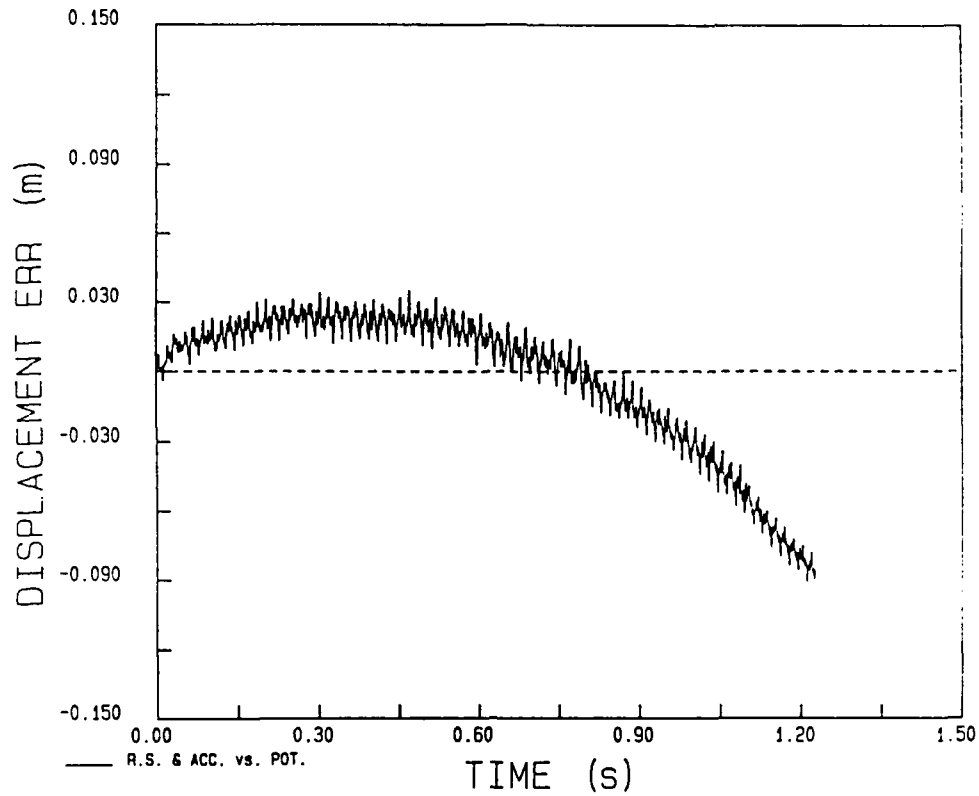


Figure 36. Horizontal displacement error versus time of the sensor array for Test 29.

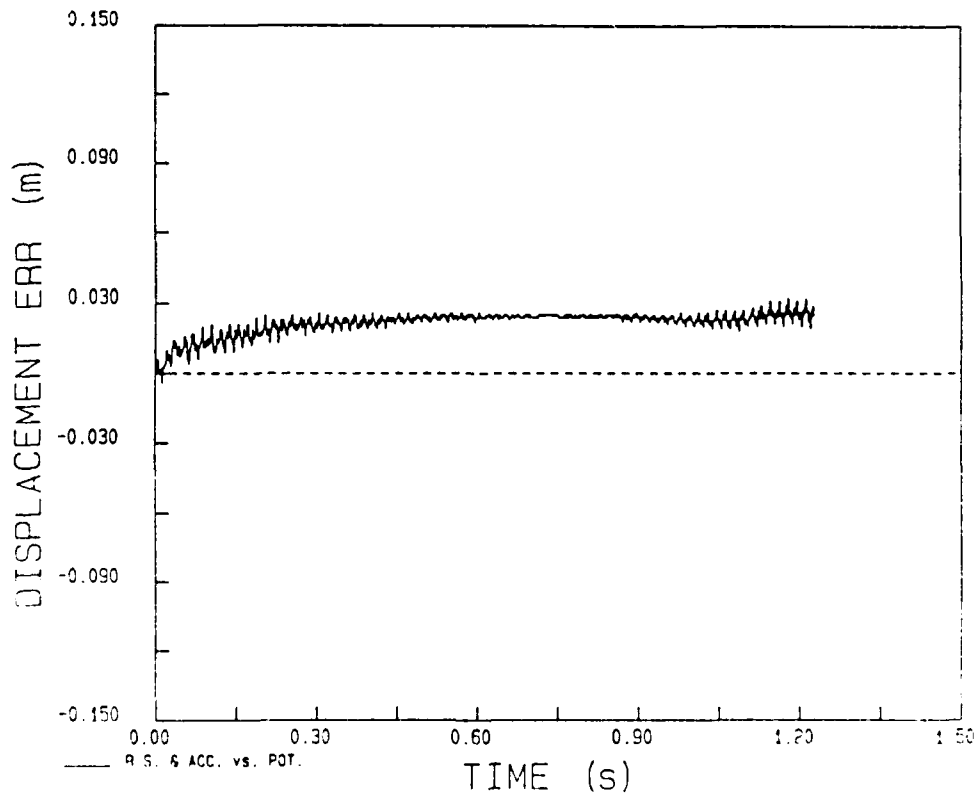


Figure 37. Vertical displacement error versus time of the sensor array for Test 29.

The dashed line in Figure 38 is the angle of rotation as determined by integrating the filtered rate sensor record. The solid curve is the angle derived from the potentiometer record. The agreement is excellent. Figure 39 shows the angular error versus time. It remains less than one degree for most of the time, and is always less than two degrees in magnitude.

2. Test 33

This test was done using the Endevco accelerometers. The total force in the cable at initiation of the test was 1334 Newtons, and a peak acceleration of about 8 g's was produced.

Figures 40 through 51 show unfiltered and filtered records for the accelerometers, rate sensor, and potentiometer. The load cell record was bad, and it is not included.

Figure 52 shows the trajectory of the accelerometers. The solid curve is that determined from the radius and angle from the potentiometer record. The dashed curve is that derived from the accelerometer and rate sensor records using the computer program listed in Appendix A.

Figure 53 shows the horizontal X error versus time. Figure 54 shows the vertical Y error versus time. Both are 0.03 metres or less. The agreement is good.

Figure 55 compares the angle of rotation as determined by integrating the rate sensor record with that derived from the potentiometer record. Figure 56 shows the error in angle versus time. For most of the time, the error is less than 2 degrees in magnitude. It reaches a maximum of about -3.4 degrees at impact.

3. Test 45

This test was done using the Schaevitz accelerometers. The total force in the cable at initiation of the test was 801 Newtons, and a peak acceleration of about 4.4 g's was produced.

Figures 57 through 72 show unfiltered and filtered records for the accelerometers, rate sensor, potentiometer, and load cell. The magnitude of the oscillations appearing on the Schaevitz accelerometer records are considerably less than those on the Endevco accelerometer records.

Figure 73 shows the trajectory of the accelerometers. The solid curve is that determined from the radius and angle from the potentiometer record. The dashed curve is that derived from the accelerometer and rate sensor records using the computer program listed in Appendix A. Figures 74 and 75 show the horizontal and vertical displacement errors. At impact they are -0.051 and 0.108 metres, respectively.

Figure 76 compares the angle of rotation as determined by integrating the rate sensor record with that derived from the

POTENTIOMETER - 29

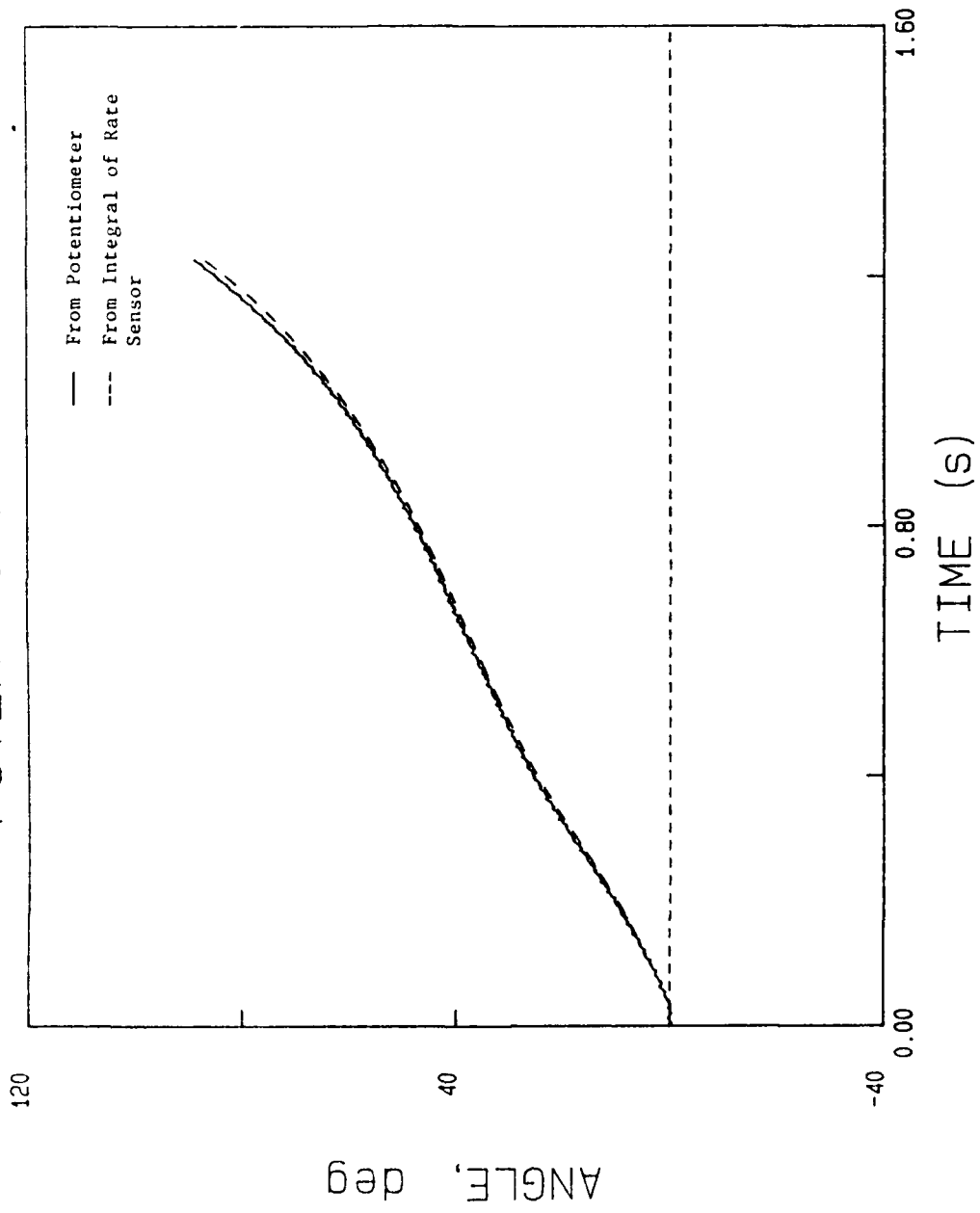


Figure 38. Comparison of the rotation angle obtained by integration of the rate sensor record with that derived from the potentiometer record for Test 29.

ANGULAR ERROR - 29

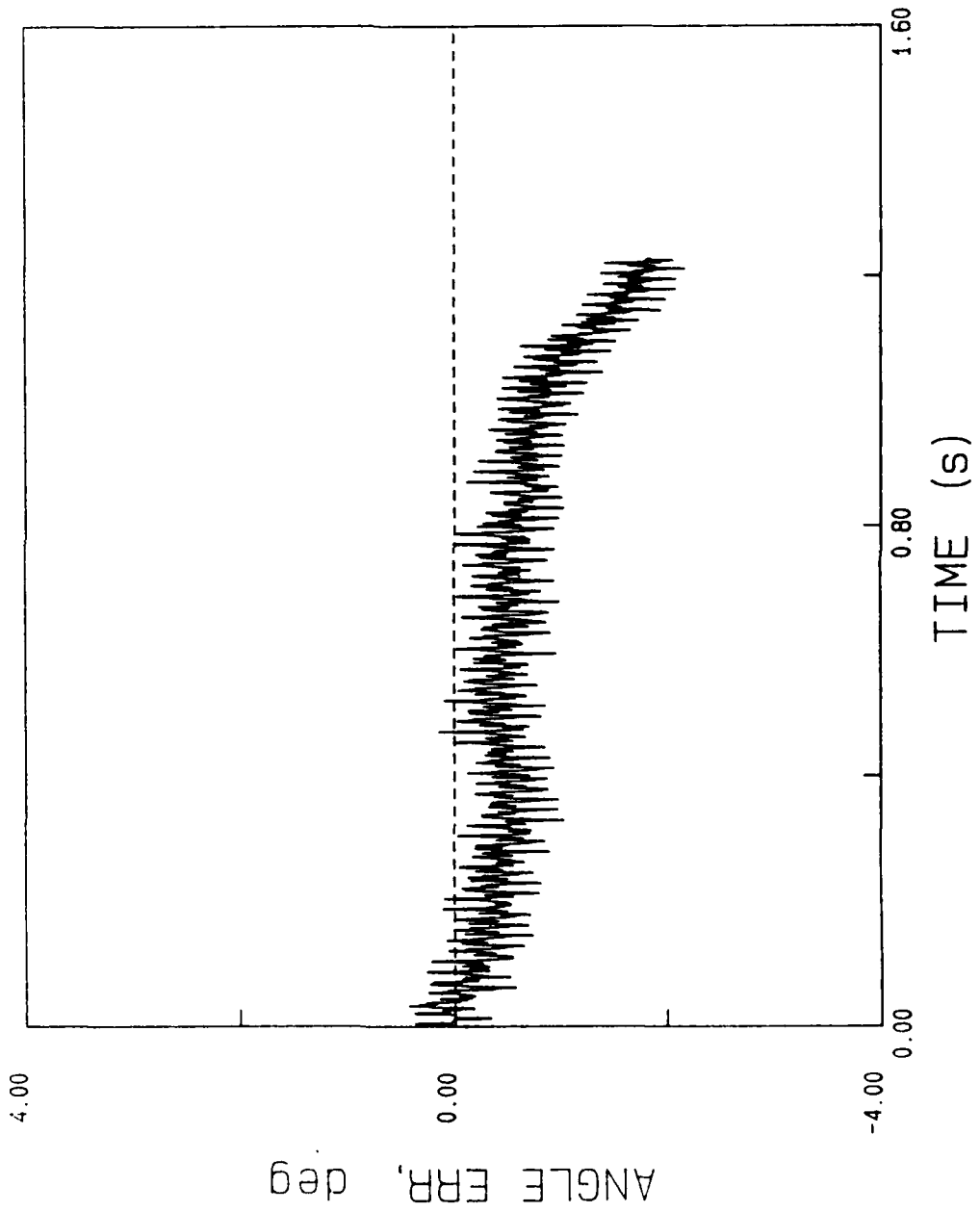


Figure 39. Error in the rotation angle obtained by integration of the rate sensor record for Test 29.

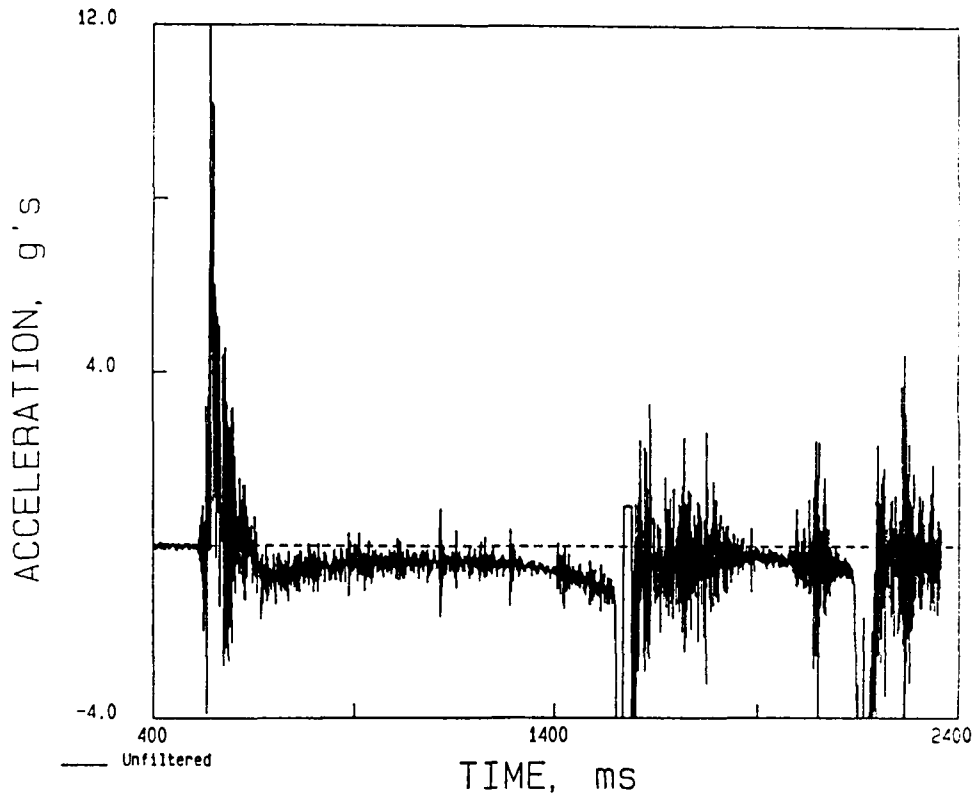


Figure 40. Unfiltered acceleration versus time from the initially vertical Endeveco accelerometer on Test 33.

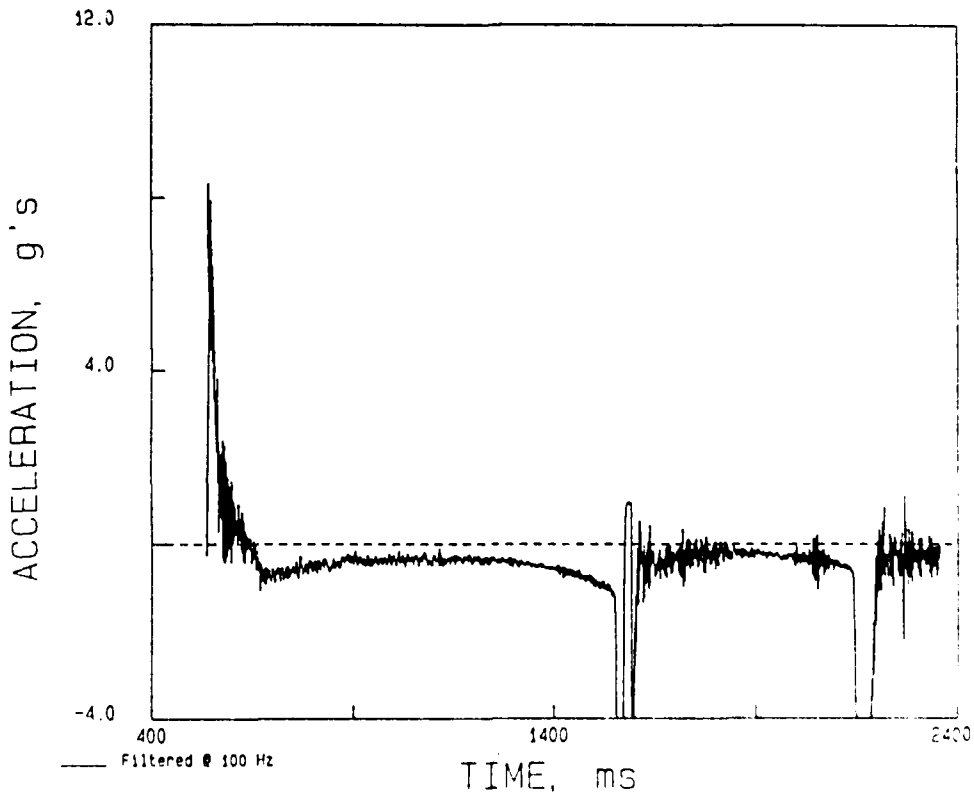


Figure 41. Filtered acceleration versus time from the initially vertical Endeveco accelerometer on Test 33.

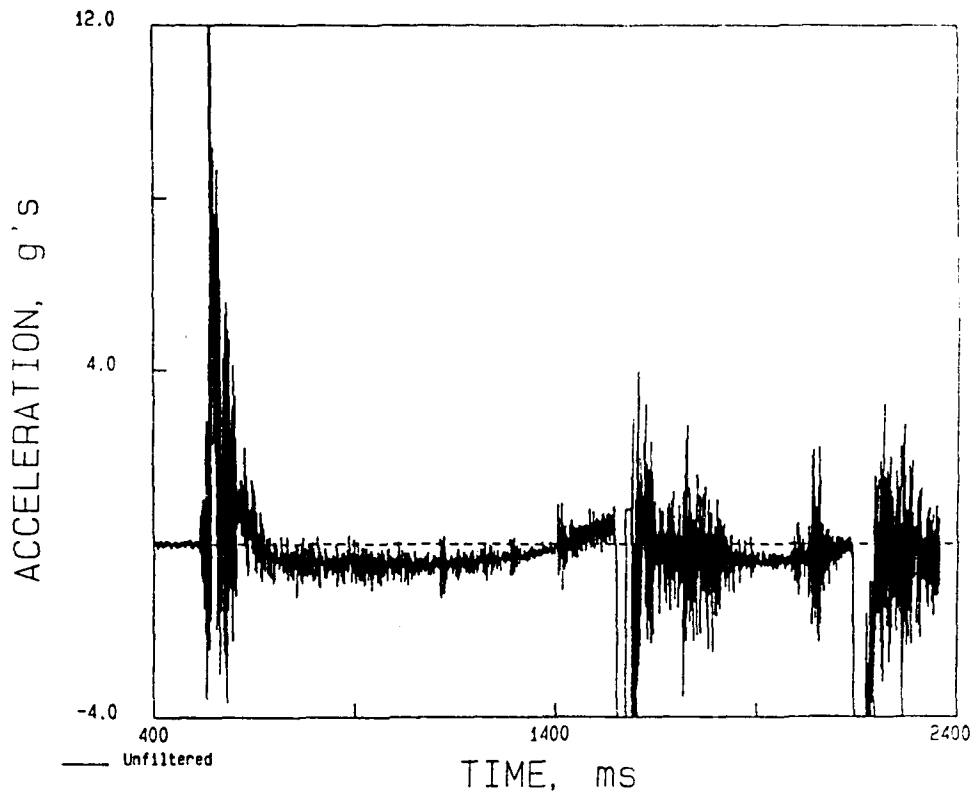


Figure 42. Unfiltered acceleration versus time from the initially horizontal Endeveco accelerometer on Test 33.

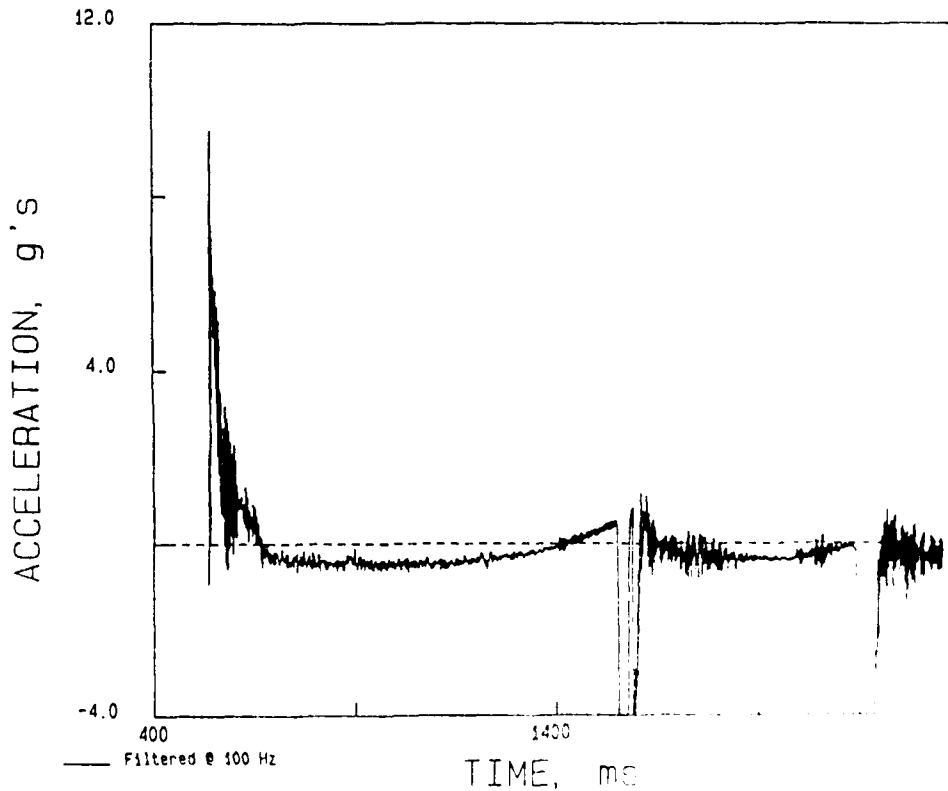


Figure 43. Filtered acceleration versus time from the initially horizontal Endeveco accelerometer on Test 33.

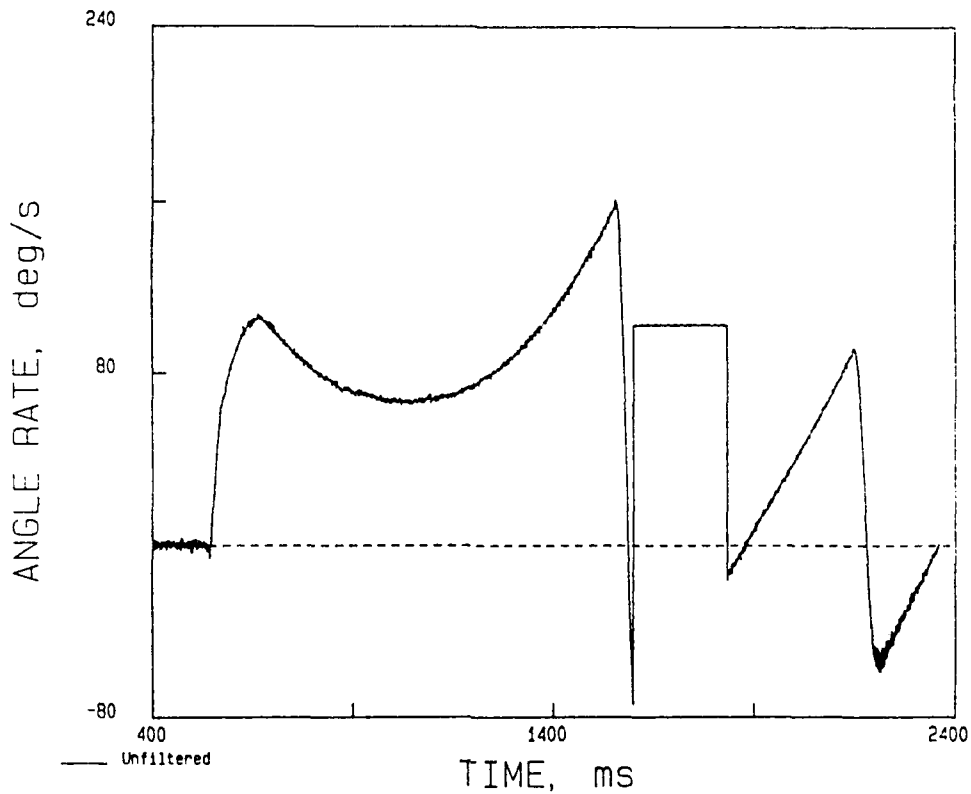


Figure 44. Unfiltered angular velocity versus time from the Humphrey rate sensor on Test 33.

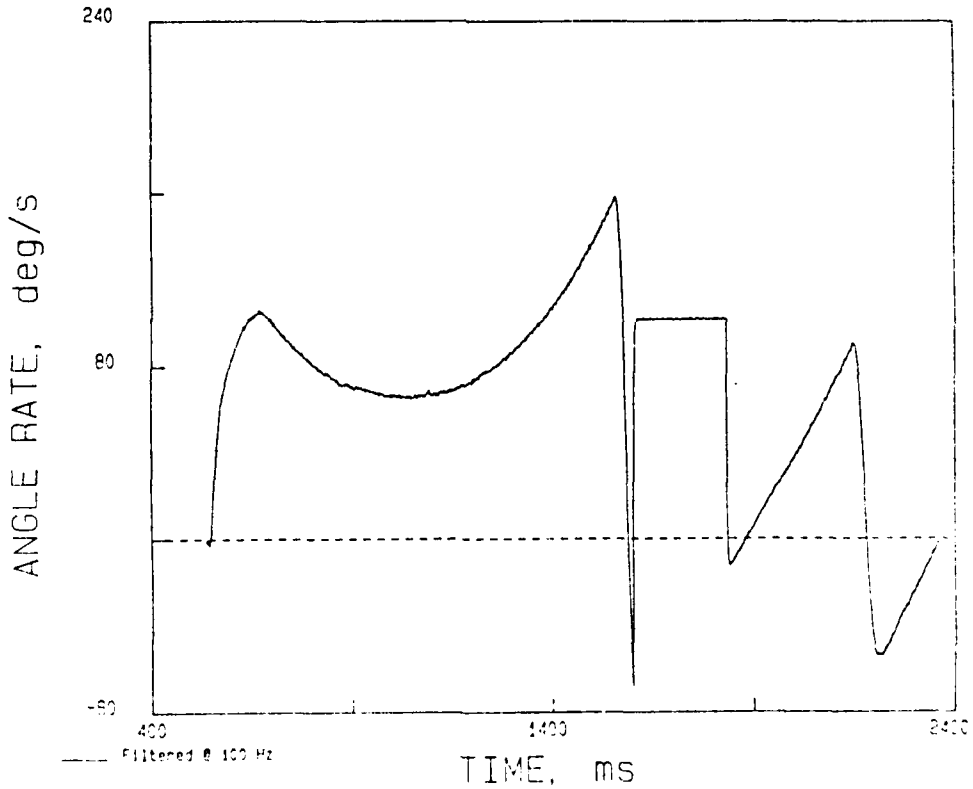


Figure 45. Filtered angular velocity versus time from the Humphrey rate sensor on Test 33.

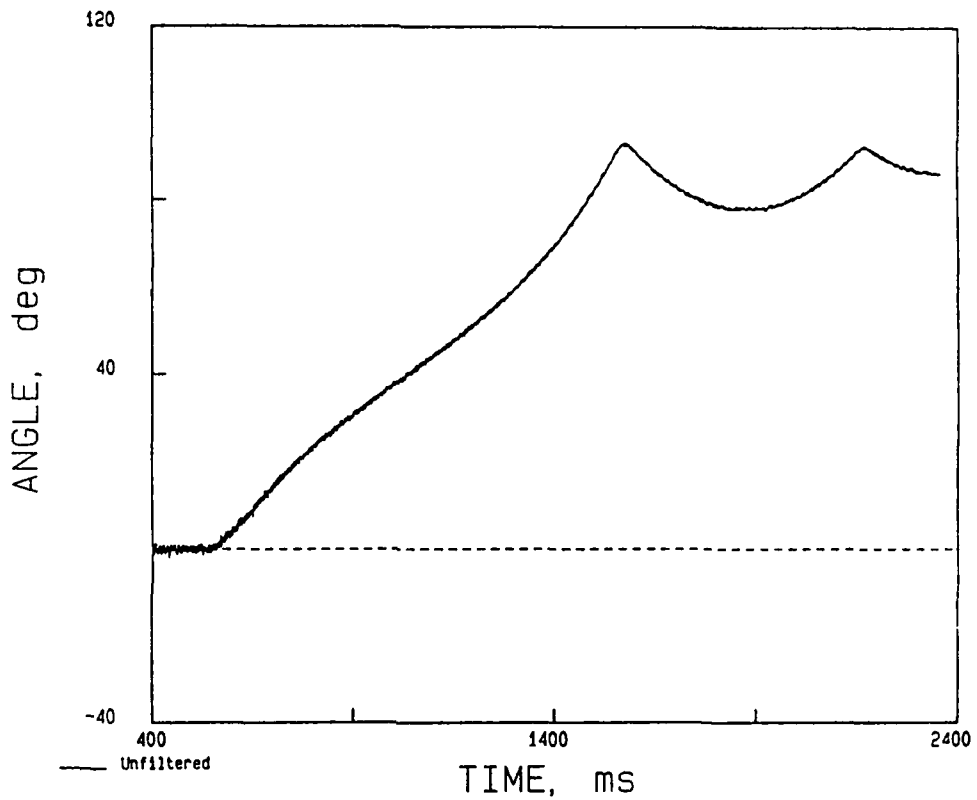


Figure 46. Unfiltered angle versus time derived from the potentiometer on the axle of the quarter wheel on Test 33.

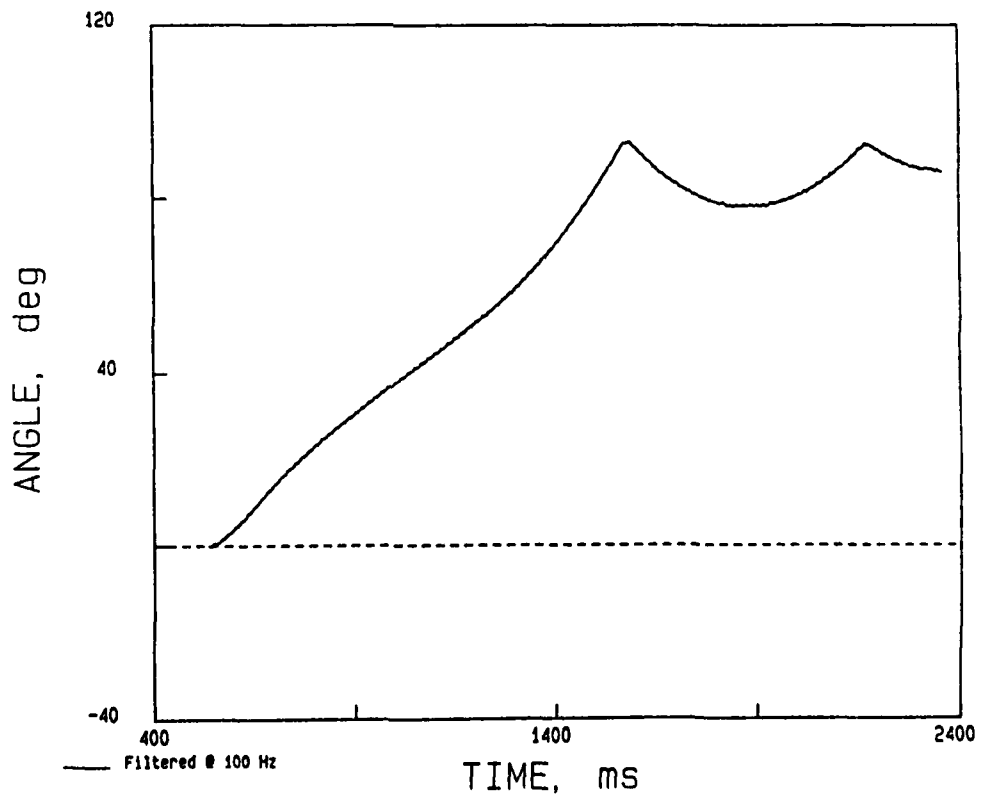


Figure 47. Filtered angle versus time derived from the potentiometer on the axle of the quarter wheel on Test 33.

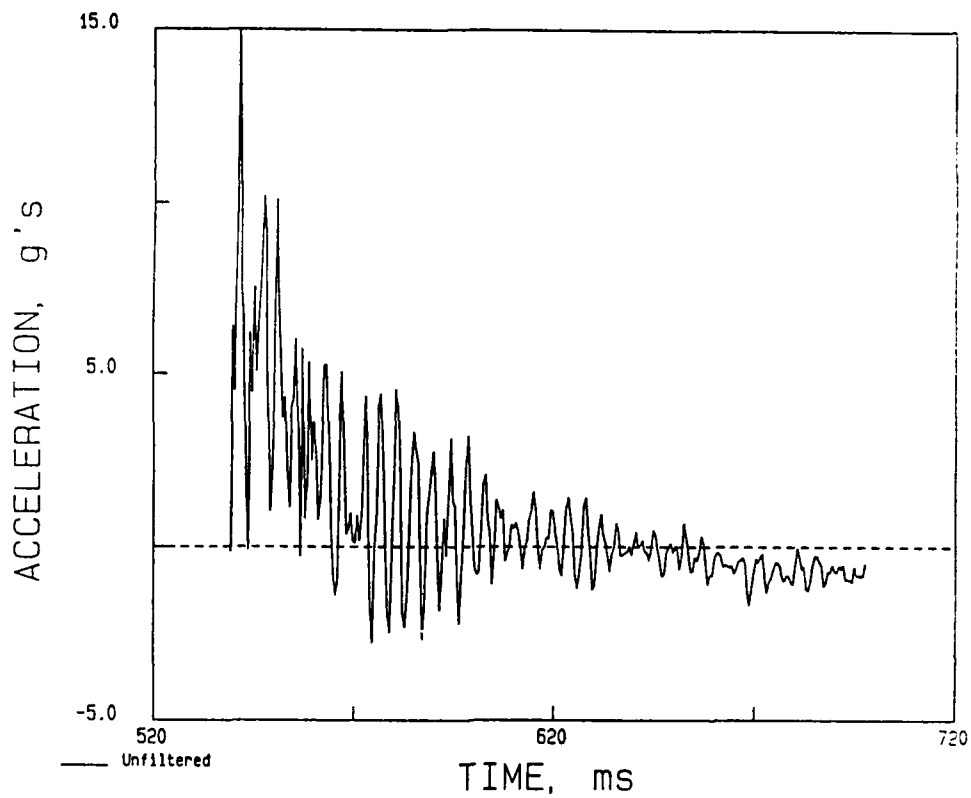


Figure 48. Unfiltered positive phase of acceleration versus time from the vertical accelerometer on Test 33.

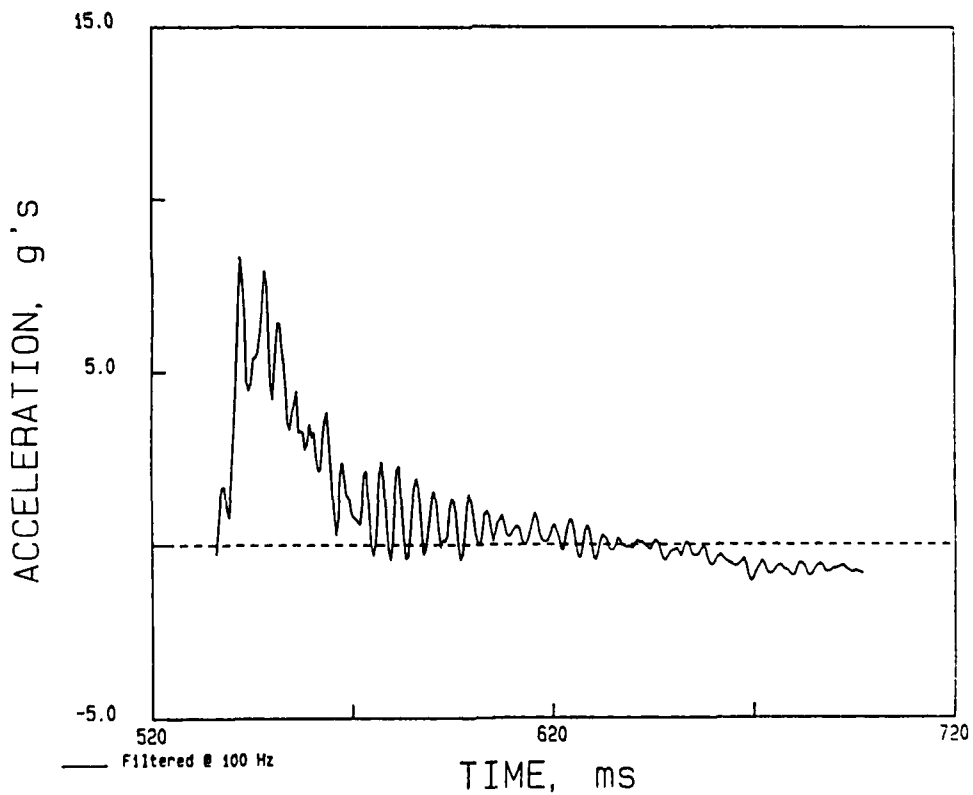


Figure 49. Filtered positive phase of acceleration versus time from the vertical accelerometer on Test 33.

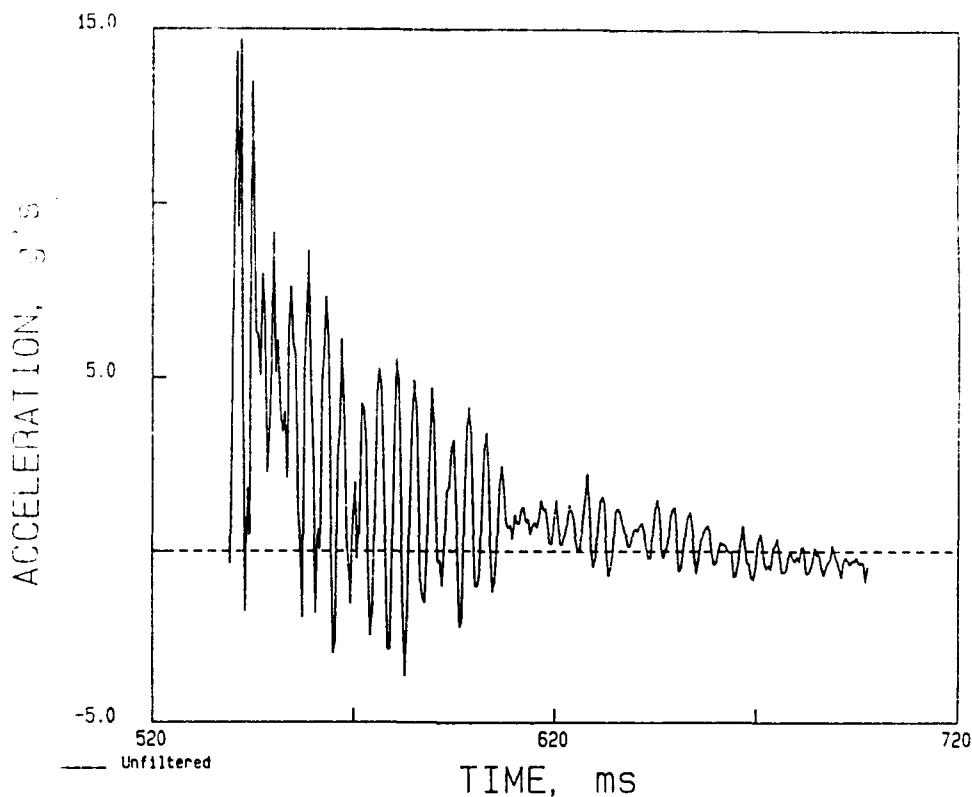


Figure 50. Unfiltered positive phase of acceleration versus time from the initially horizontal accelerometer on Test 33.

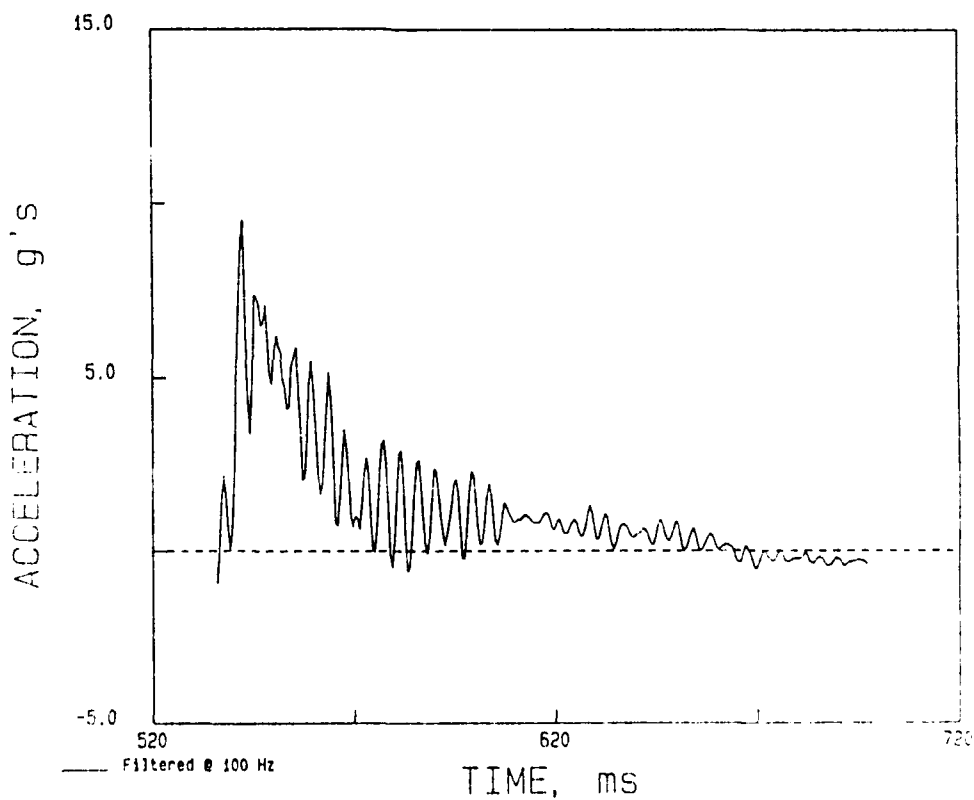


Figure 51. Filtered positive phase of acceleration versus time from the initially horizontal accelerometer on Test 33.

TRAJECTORY OF SENSORS - 33

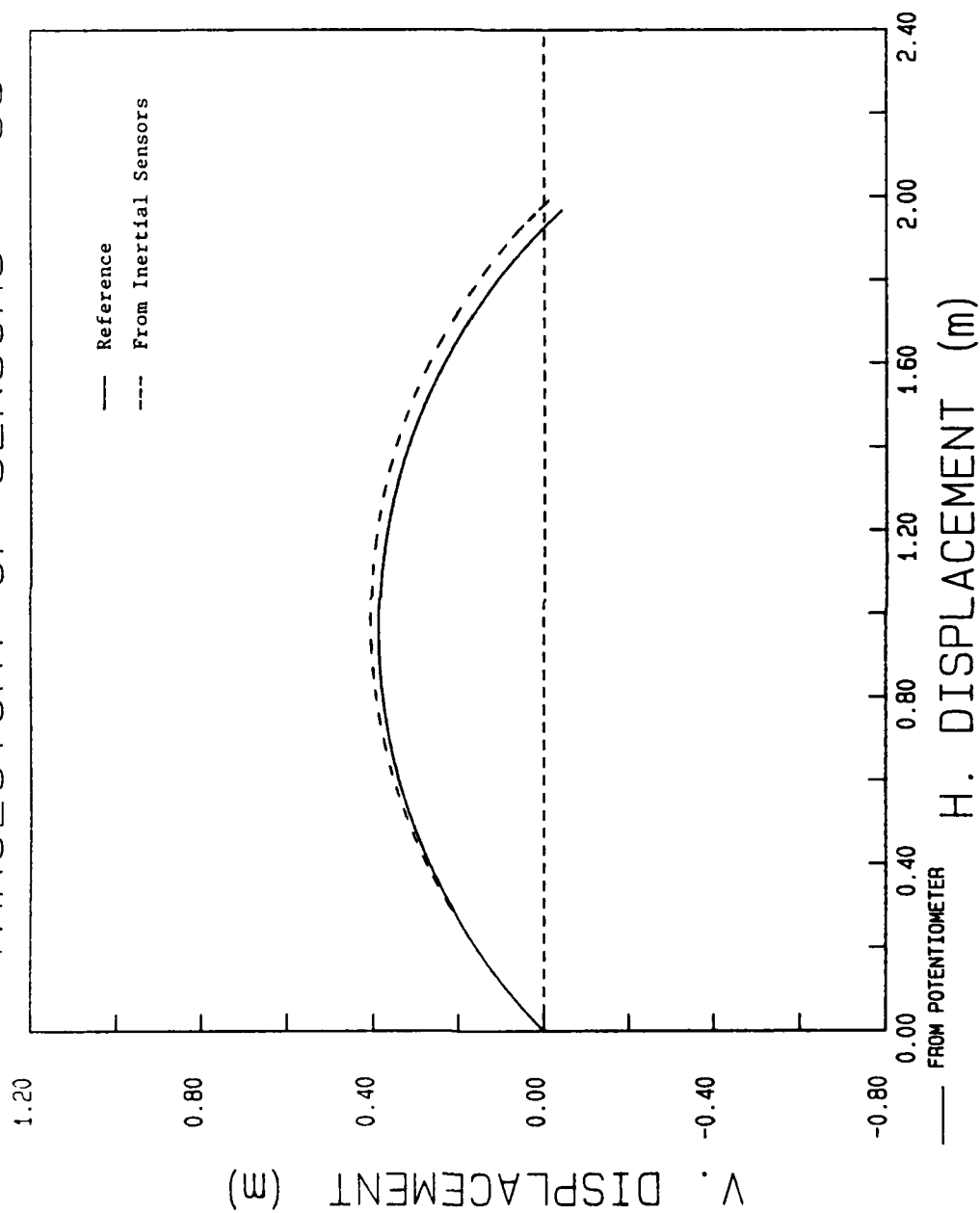


Figure 52. Comparison of the sensor array trajectory for Test 33 derived from the Endevco accelerometers and the Humphrey rate sensor with the reference trajectory derived from the potentiometer record.

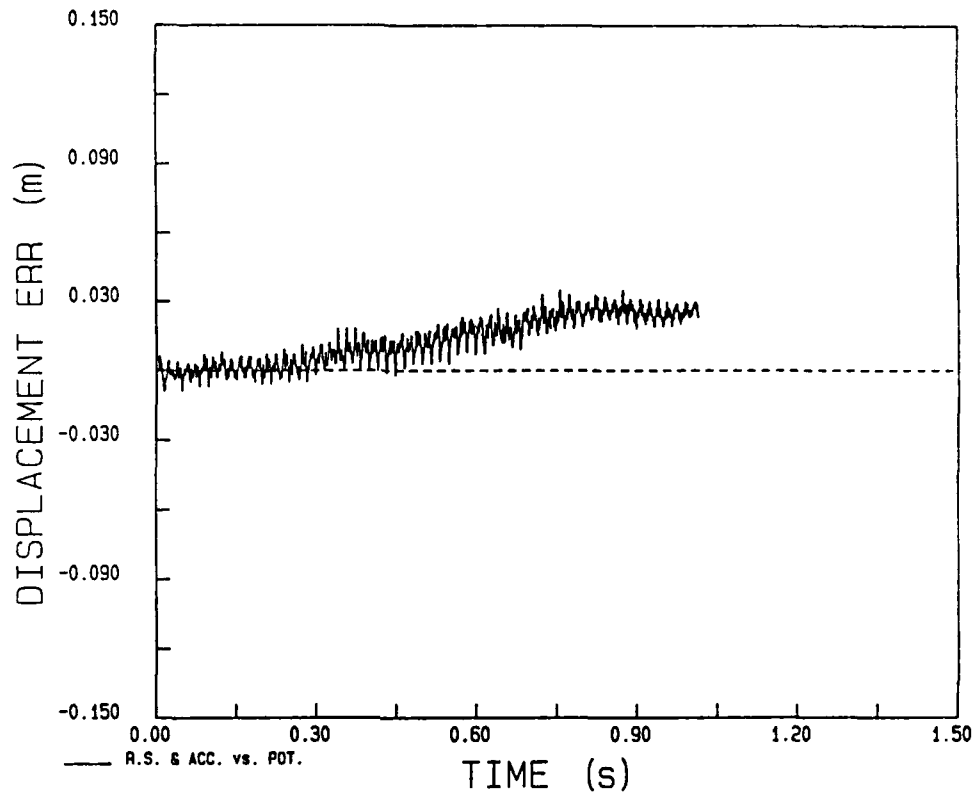


Figure 53. Horizontal displacement error versus time of the sensor array for Test 33.

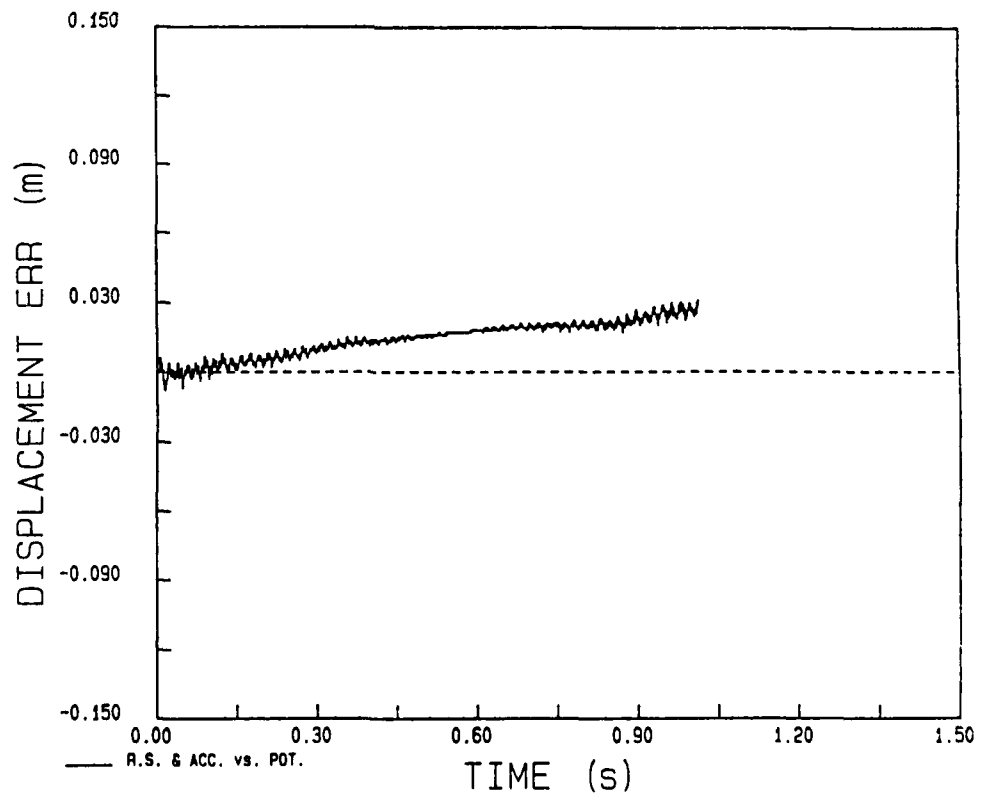


Figure 54. Vertical displacement error versus time of the sensor array for Test 33.

POTENTIOMETER 33

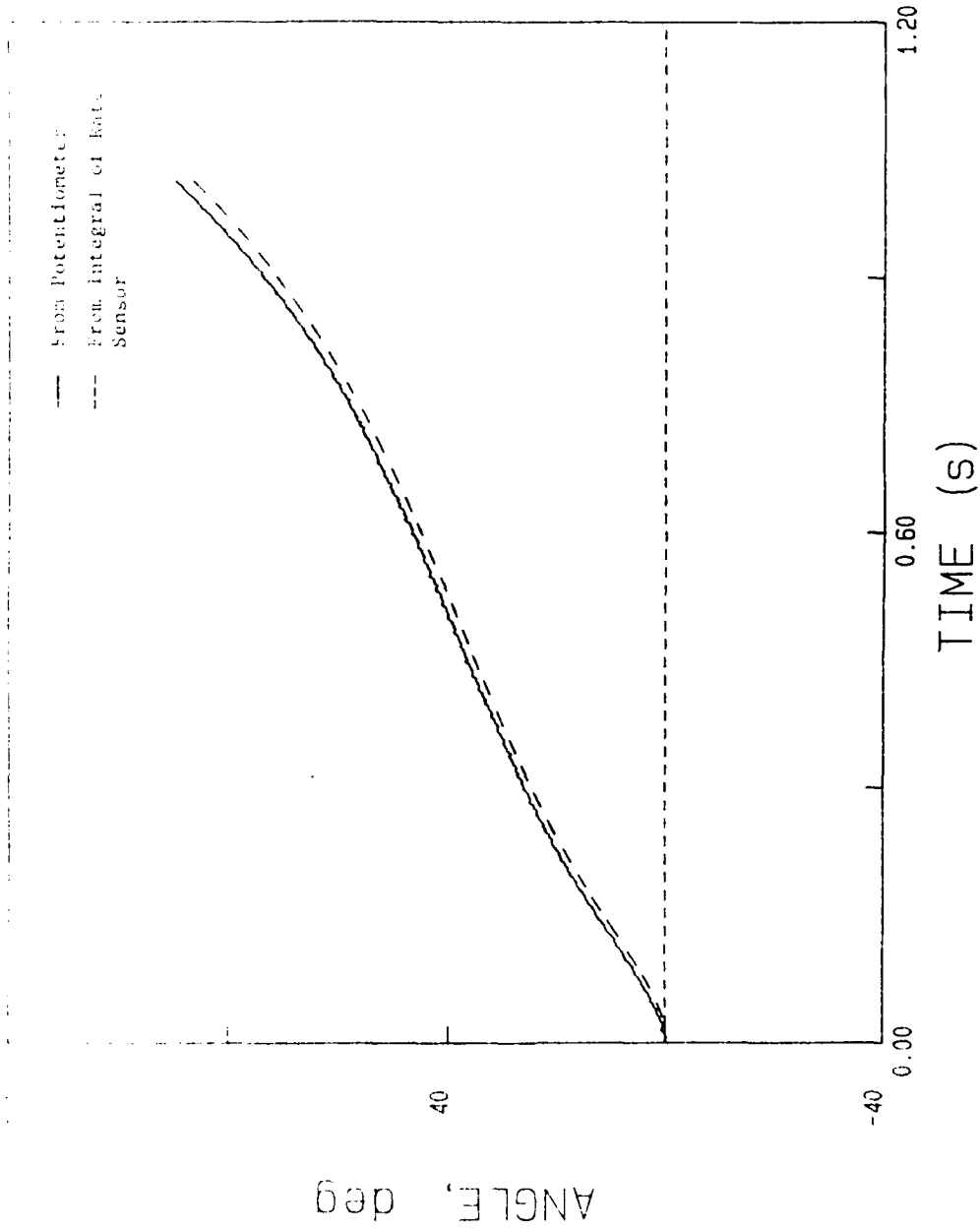


Figure 55. Comparison of the rotation angle obtained by integration of the rate sensor record with that derived from the potentiometer record for Test 33.

ANGULAR ERROR - 33

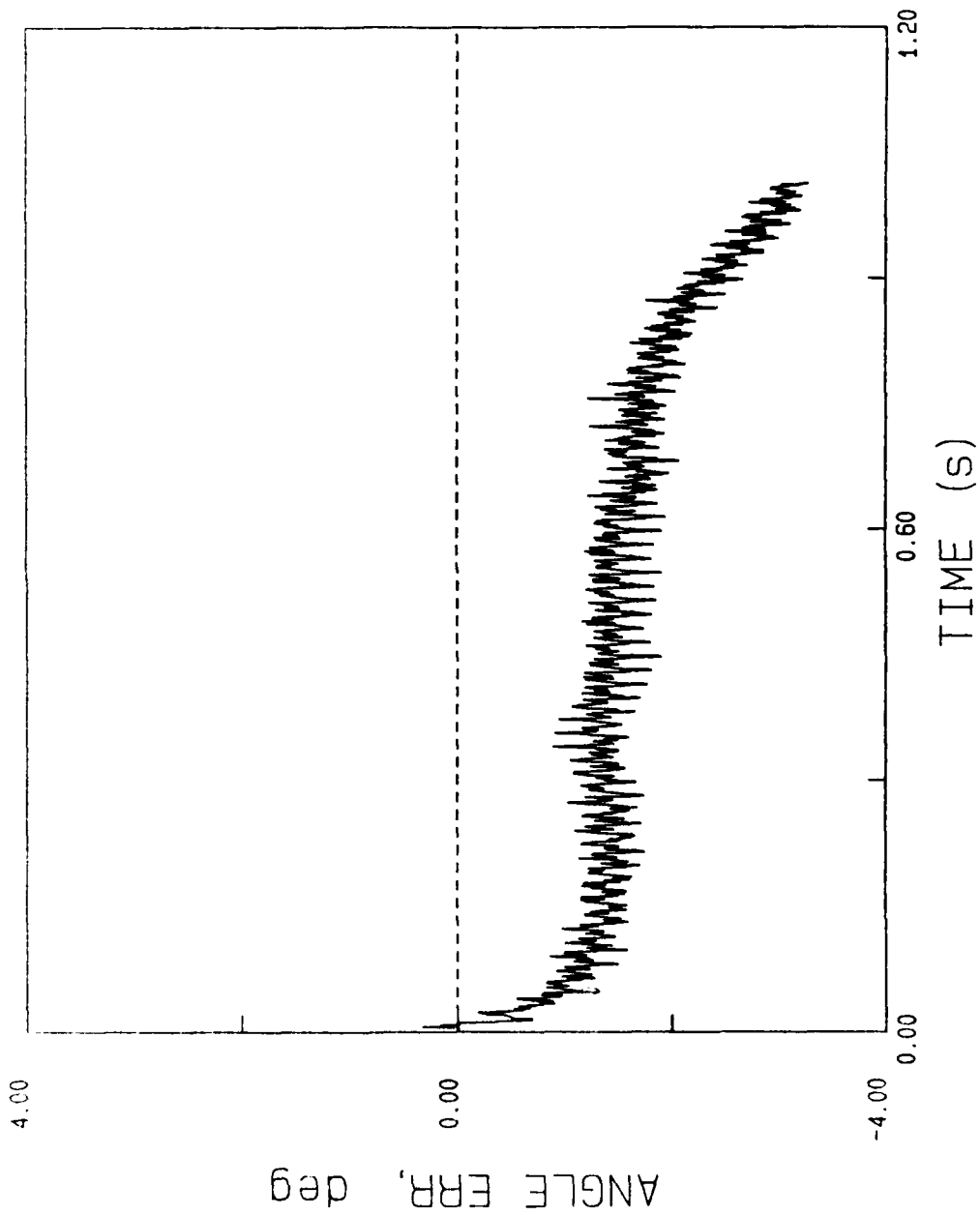


Figure 56. Error in the rotation angle obtained by integration of the rate sensor record for Test 33.

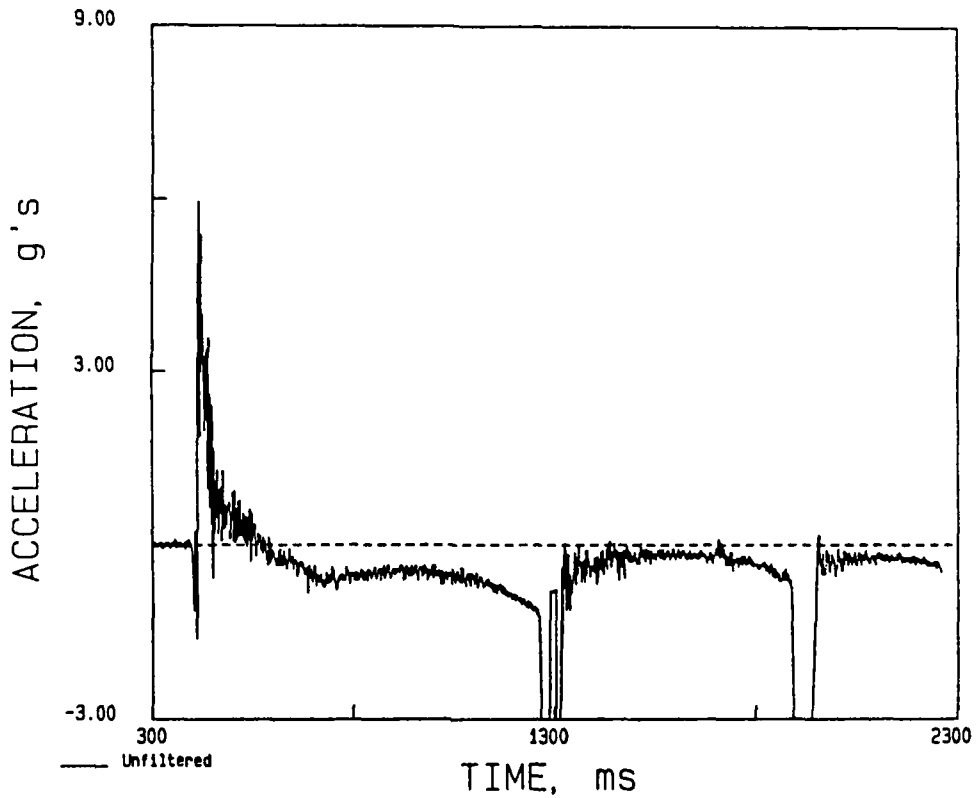


Figure 57. Unfiltered acceleration versus time from the initially vertical Schaevitz accelerometer on Test 45.

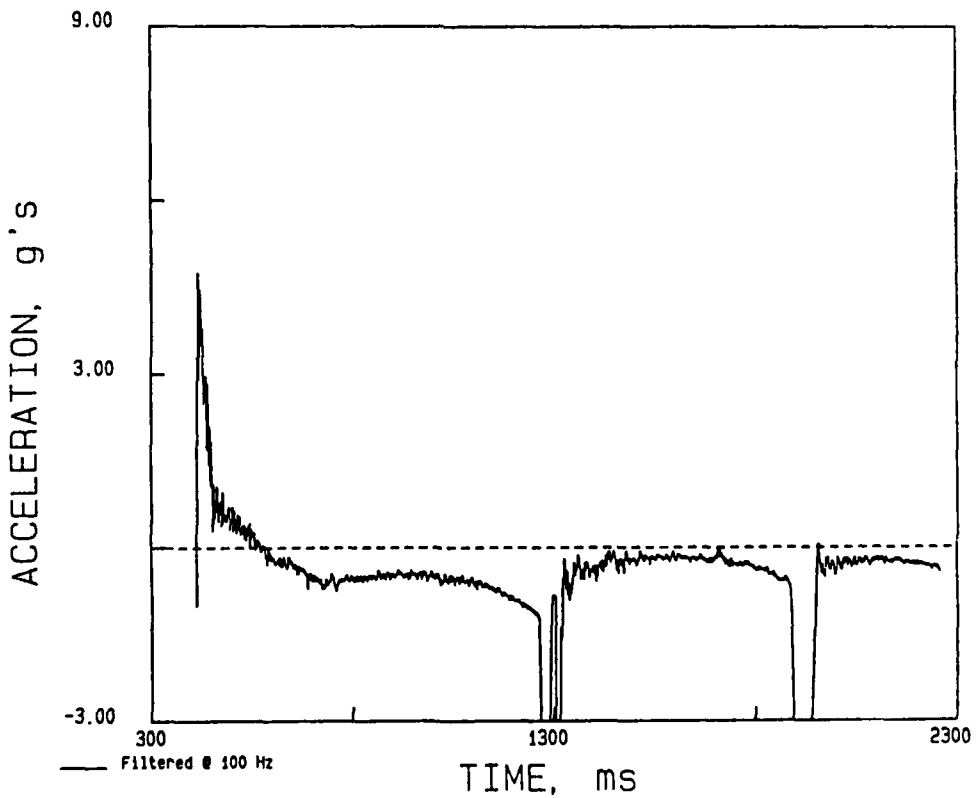


Figure 58. Filtered acceleration versus time from the initially vertical Schaevitz accelerometer on Test 45.

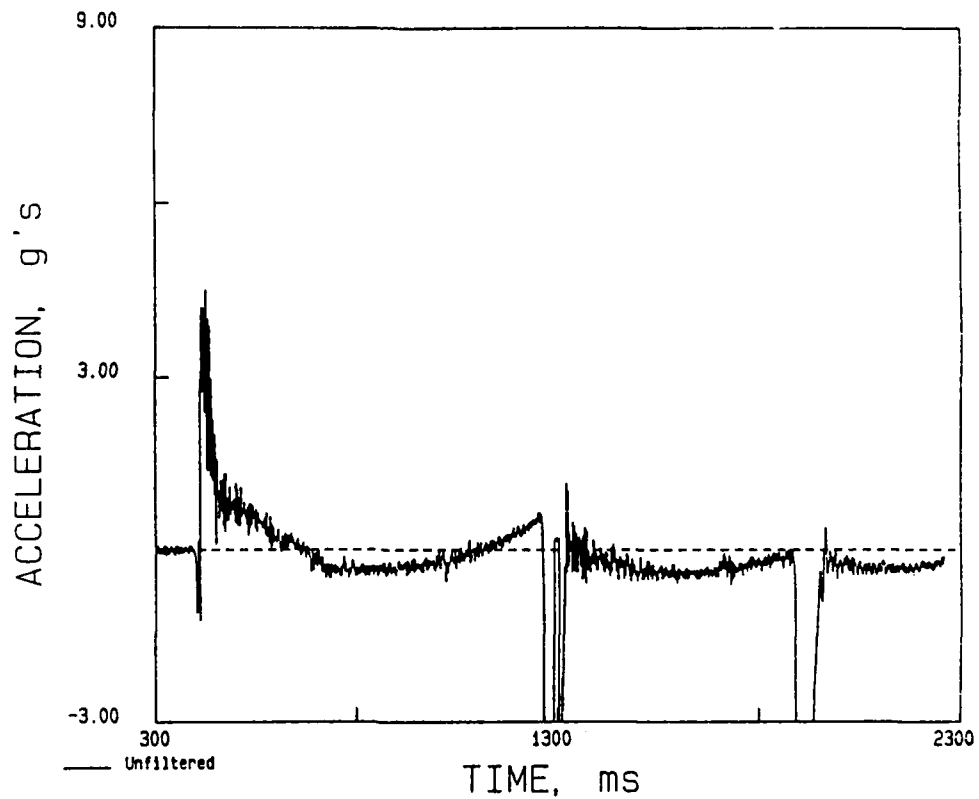


Figure 59. Unfiltered acceleration versus time from the initially horizontal Schaevitz accelerometer on Test 45.

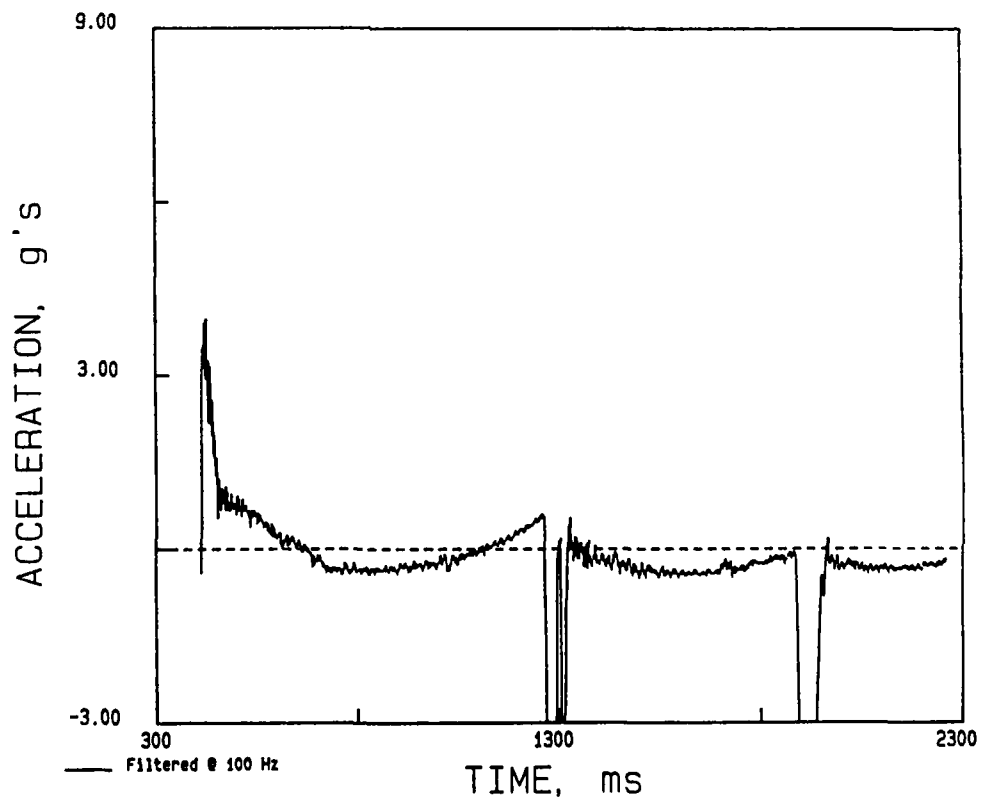


Figure 60. Filtered acceleration versus time from the initially horizontal Schaevitz accelerometer on Test 45.

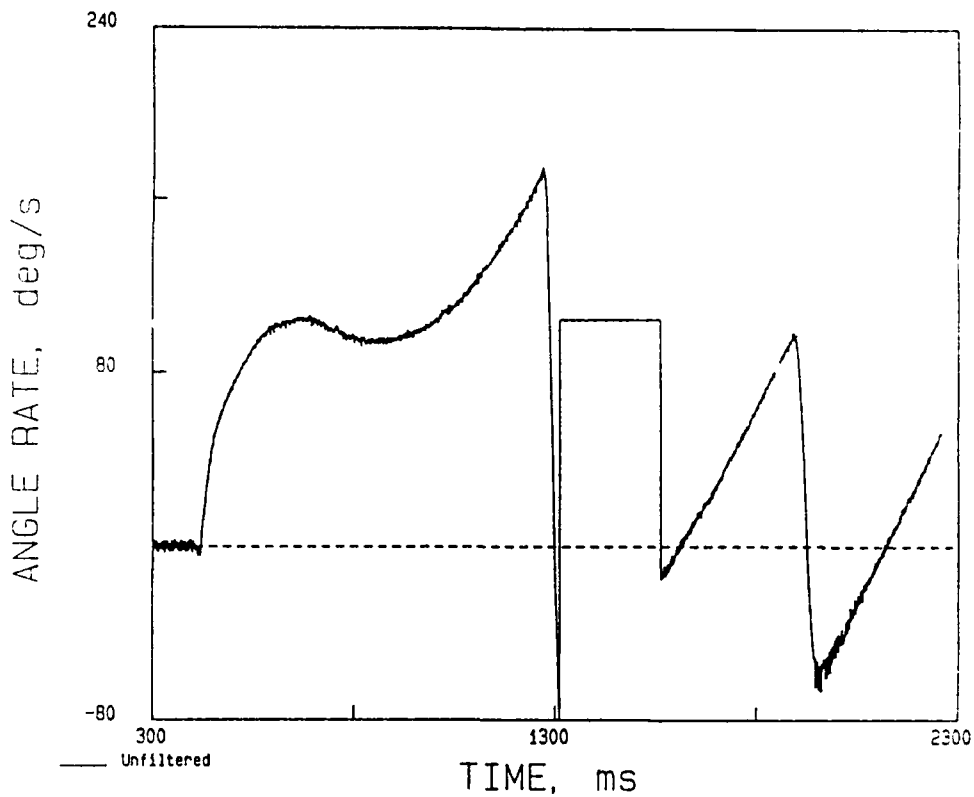


Figure 61. Unfiltered angular velocity versus time from the Humphrey rate sensor on Test 45.

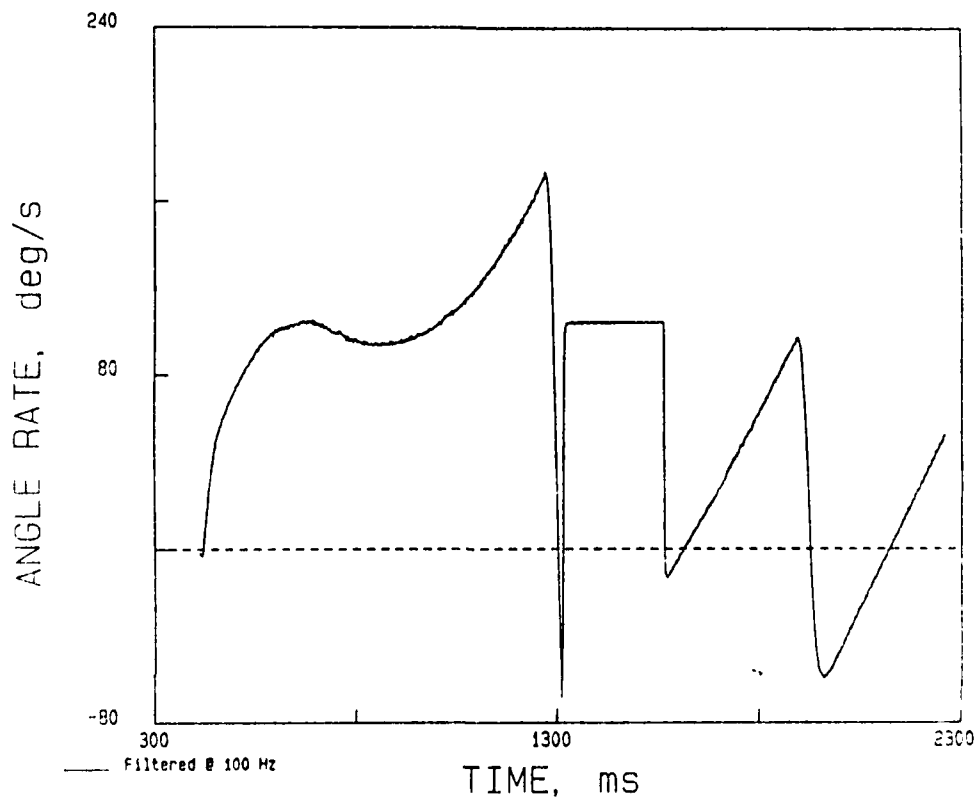


Figure 62. Filtered angular velocity versus time from the Humphrey rate sensor on Test 45.

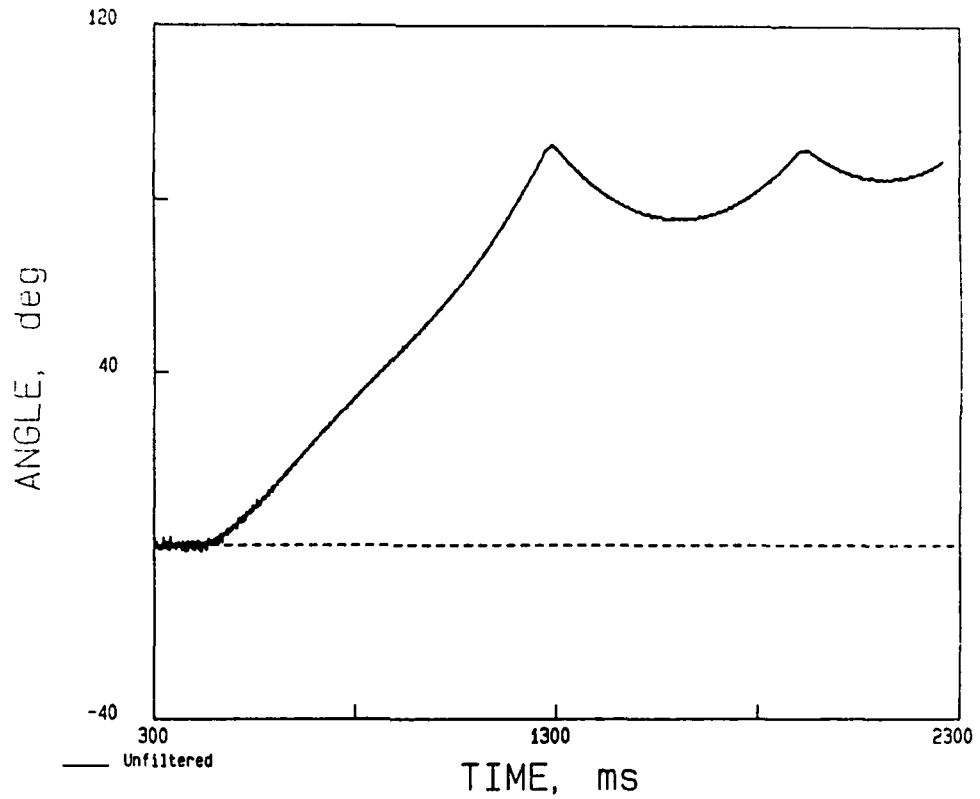


Figure 63. Unfiltered angle versus time derived from the potentiometer on the axle of the quarter wheel on Test 45.

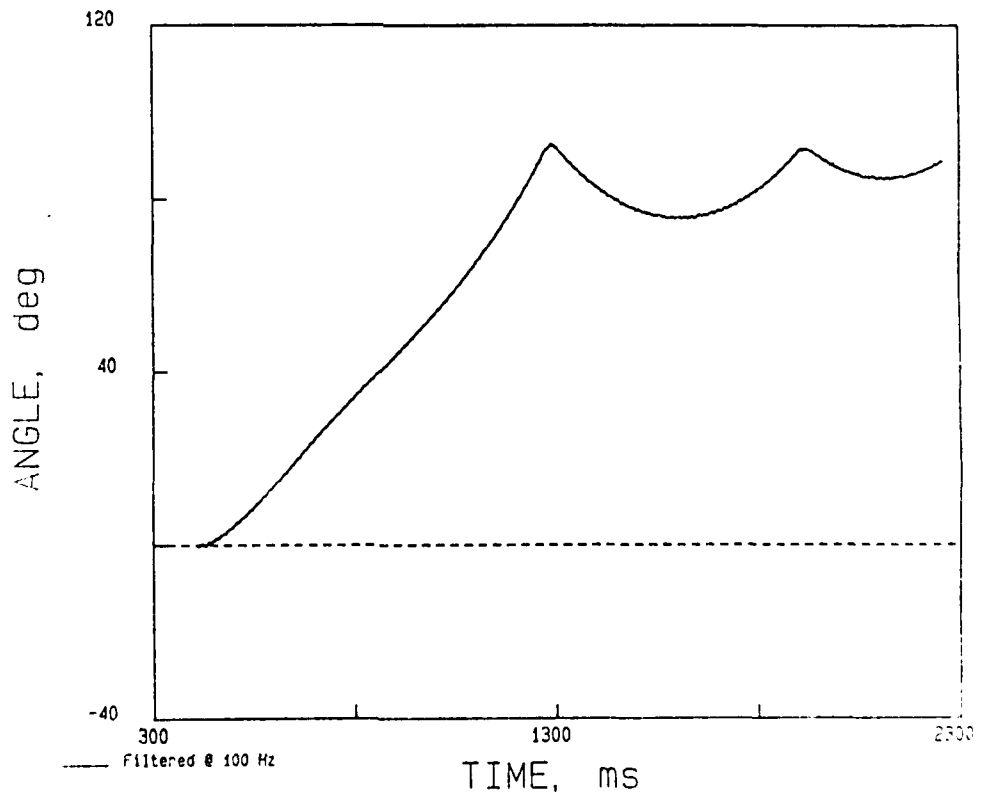


Figure 64. Filtered angle versus time derived from the potentiometer on the axle of the quarter wheel on Test 45.

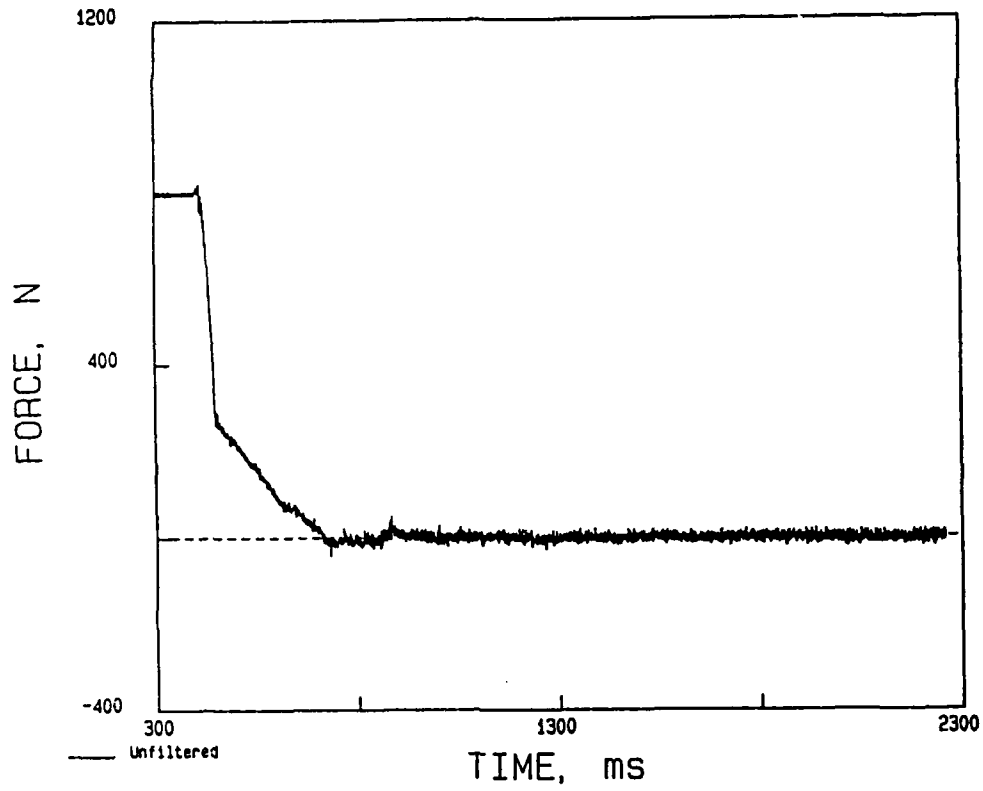


Figure 65. Unfiltered load cell record from Test 45.

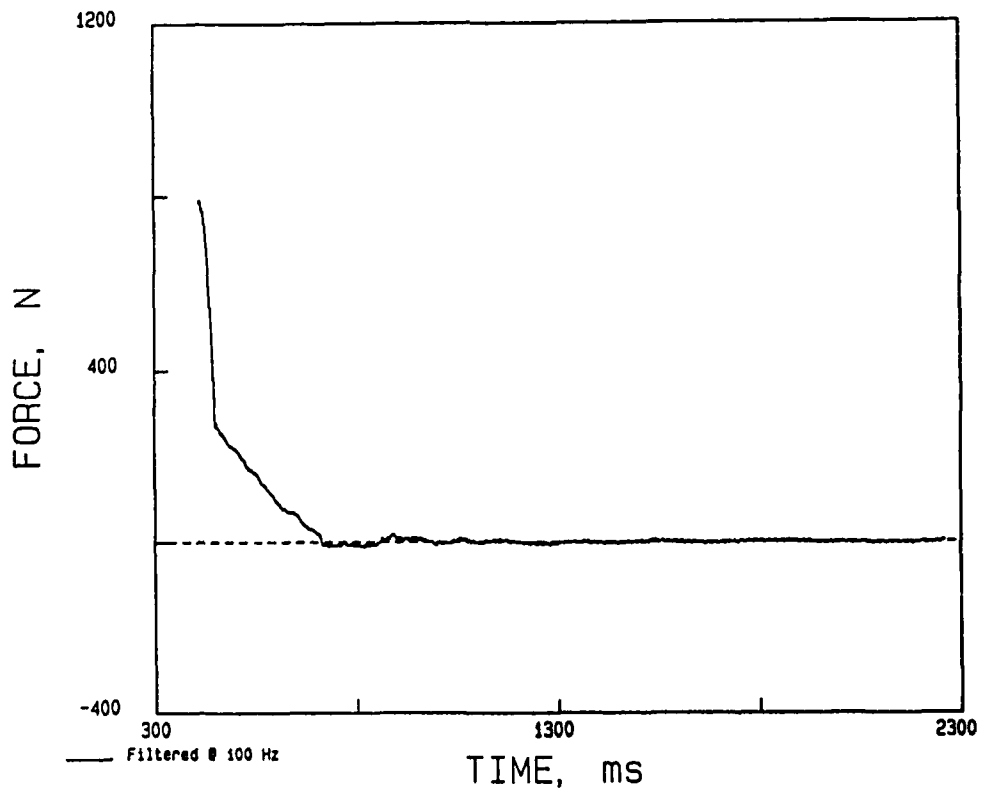


Figure 66. Filtered load cell record from Test 45.

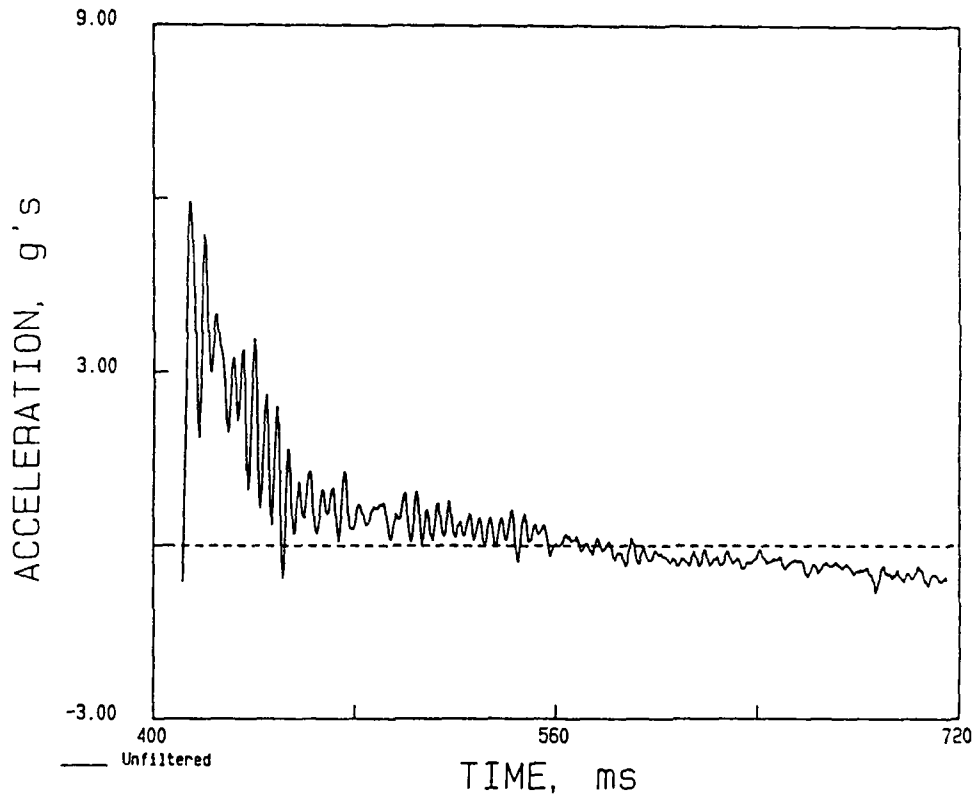


Figure 67. Unfiltered positive phase of acceleration versus time from the vertical accelerometer on Test 45.

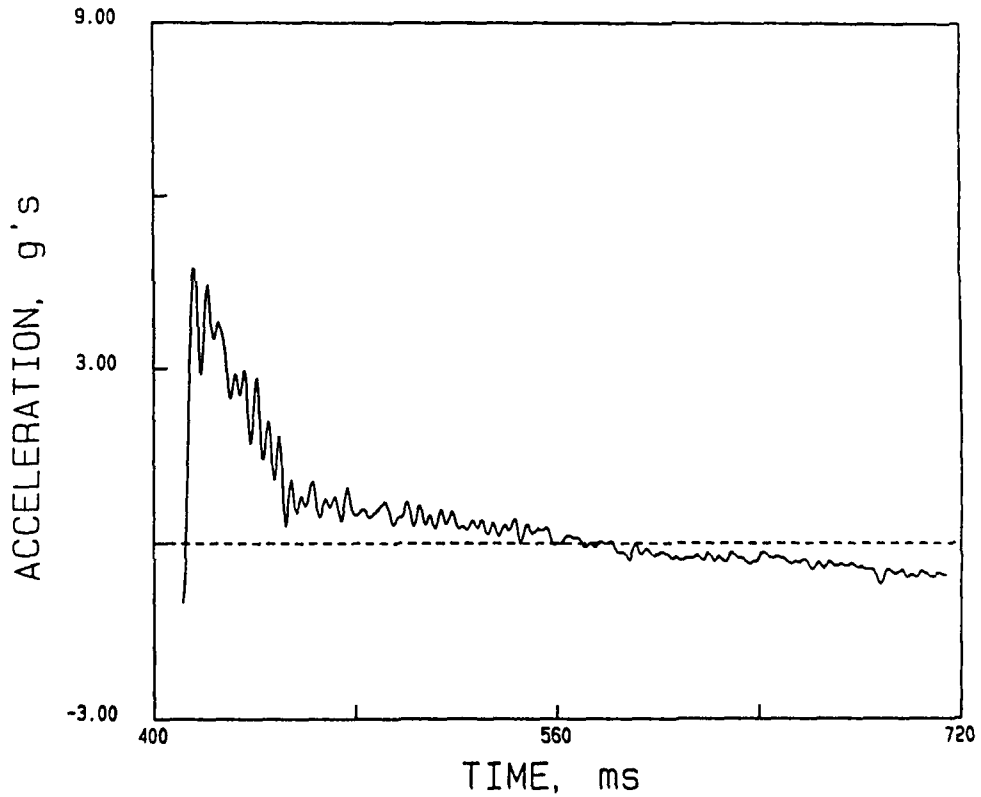


Figure 68. Filtered positive phase of acceleration versus time from the vertical accelerometer on Test 45.

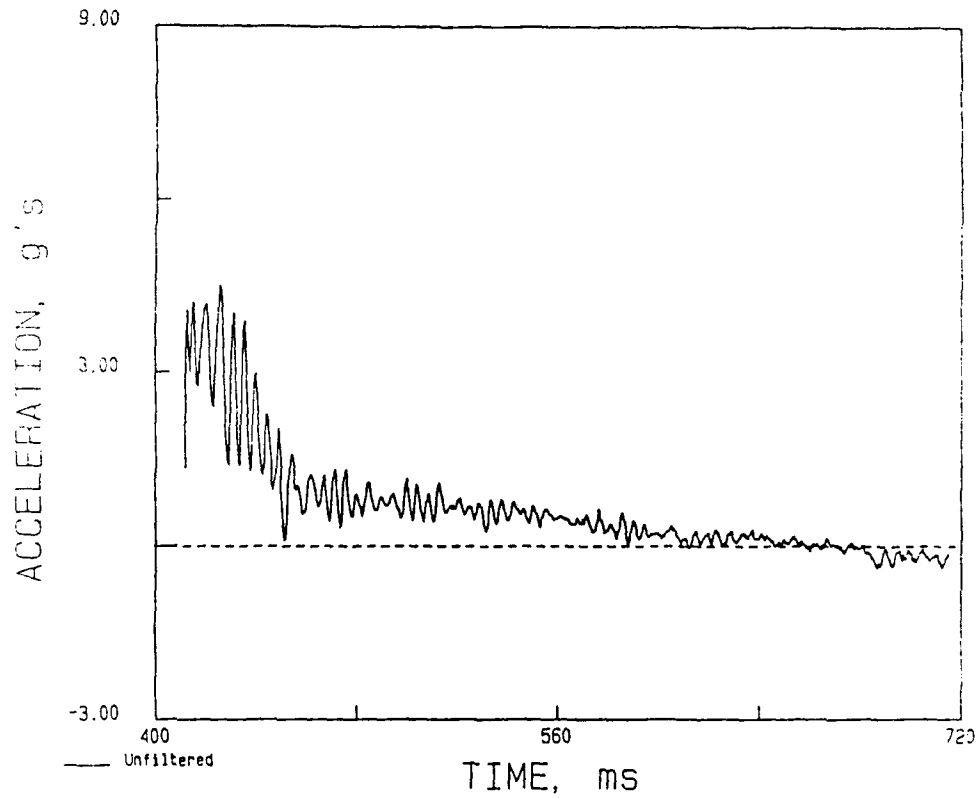


Figure 69. Unfiltered positive phase of acceleration versus time from the initially horizontal Schaevitz accelerometer on Test 45.

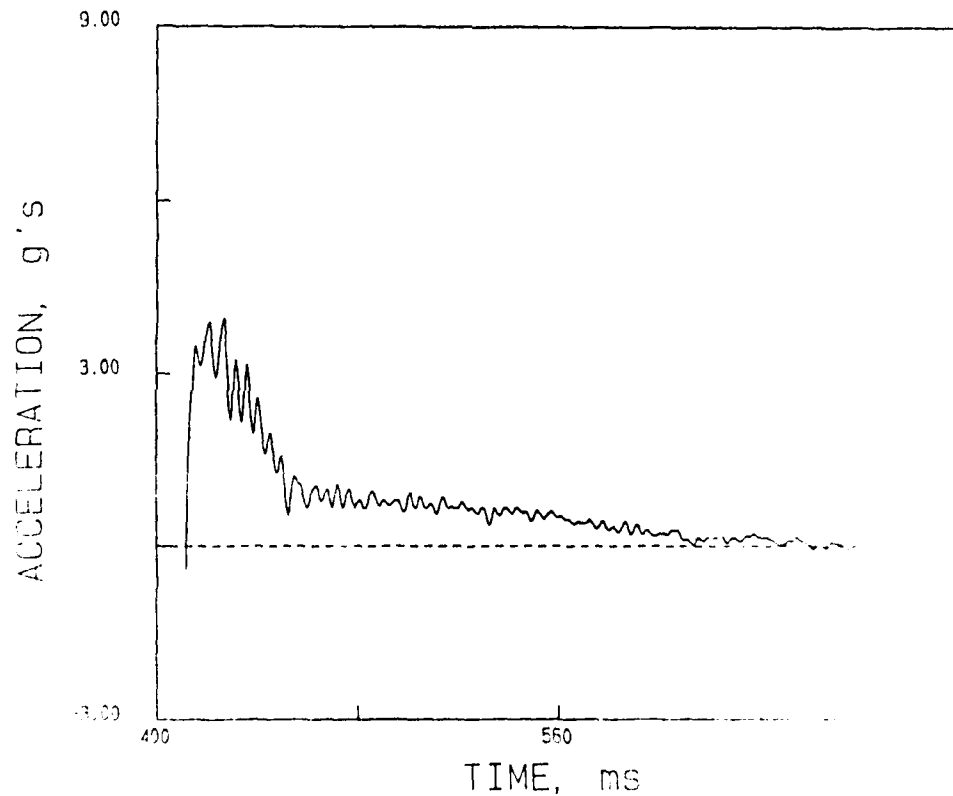


Figure 70. Filtered positive phase of acceleration versus time from the initially horizontal Schaevitz accelerometer on Test 45.

AD-A194 693

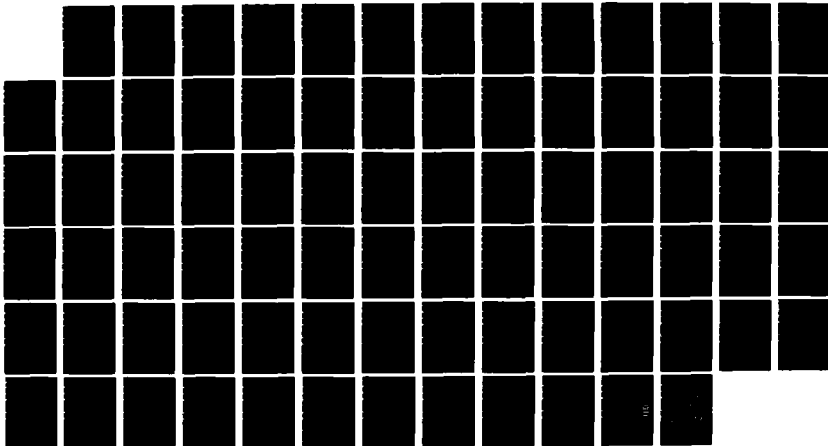
TESTING OF AN INERTIAL REFERENCE SYSTEM CONCEPT TO
MEASURE BLATT-INDUCED (U) TECH REPS INC ABERDEEN MD
ABERDEEN RESEARCH CENTER N H ETHRIDGE ET AL NOV 87
ARC-87-104 BRL-CR-591

2/2

UNCLASSIFIED

F/G 14/2

ML





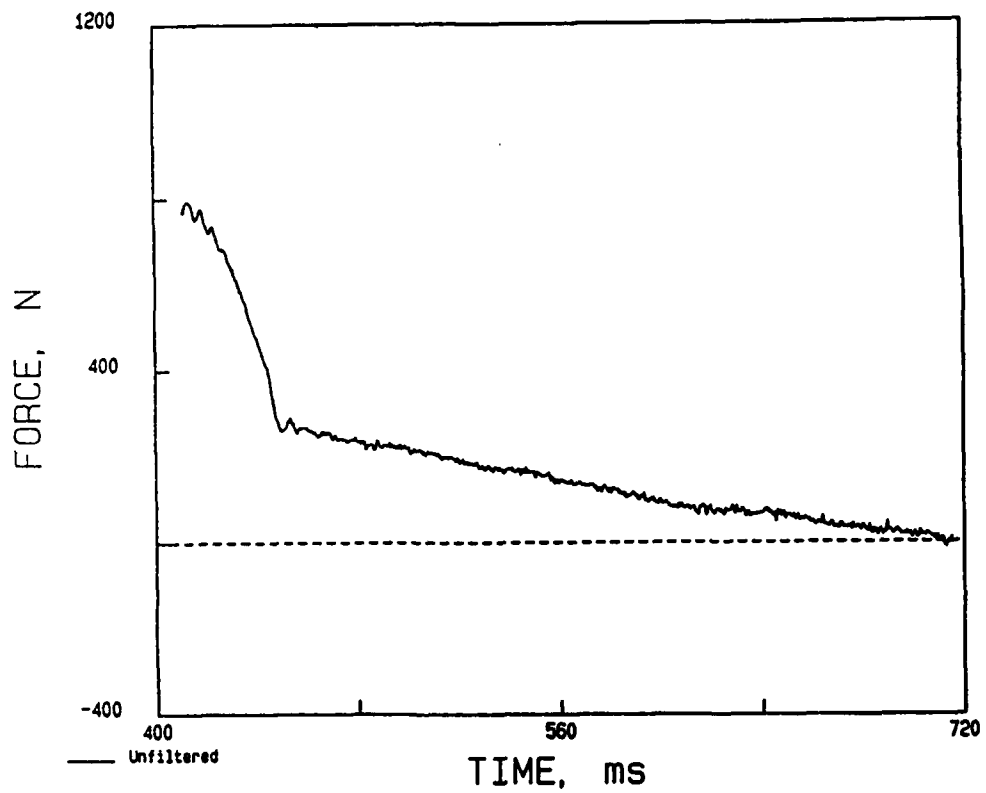


Figure 71. Unfiltered positive phase of the load cell record from Test 45.

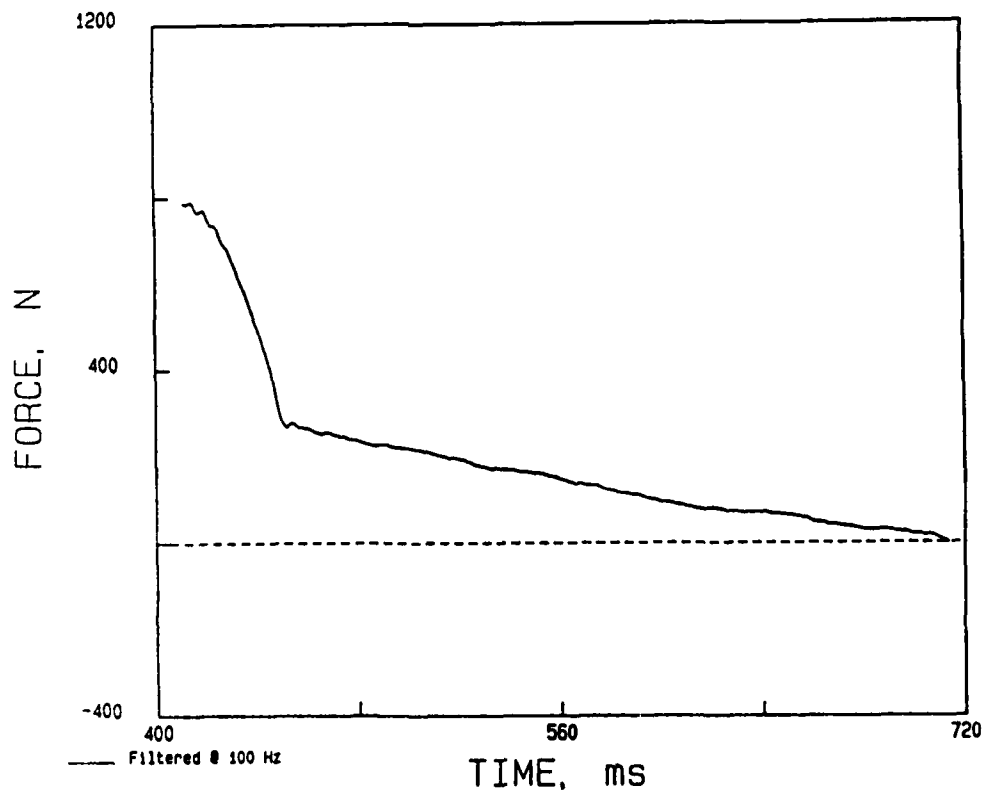


Figure 72. Filtered positive phase of the load cell record from Test 45.

TRAJECTORY OF SENSORS - 45

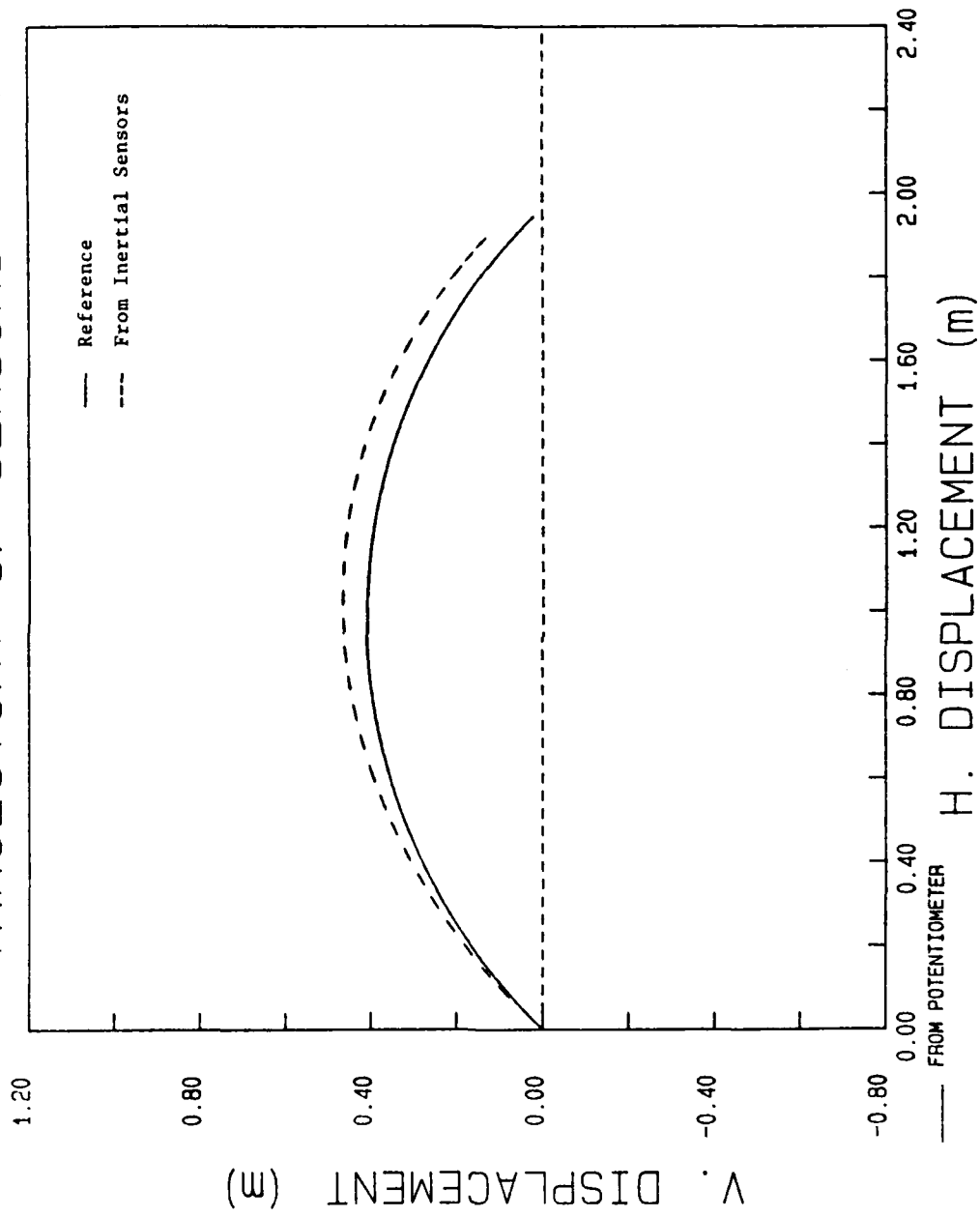


Figure 73. Comparison of the sensor array trajectory for Test 45 derived from the Schaevitz accelerometers and the Humphrey rate sensor with the reference trajectory derived from the potentiometer record.

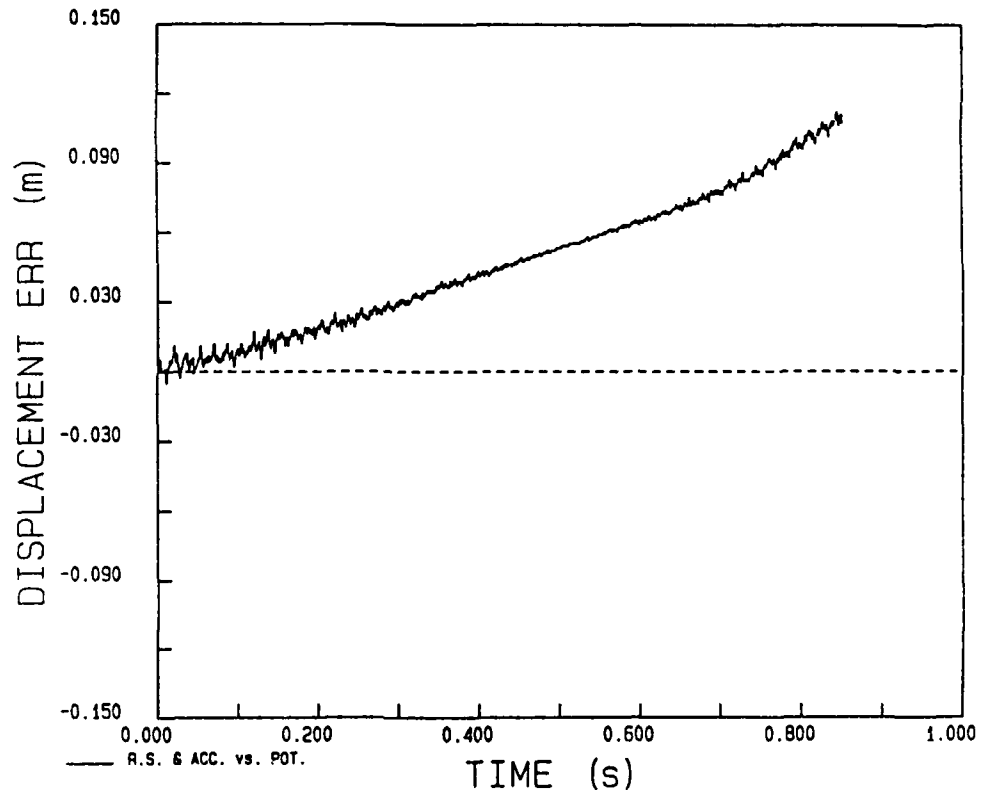


Figure 74. Horizontal displacement error versus time of the sensor array for Test 45.

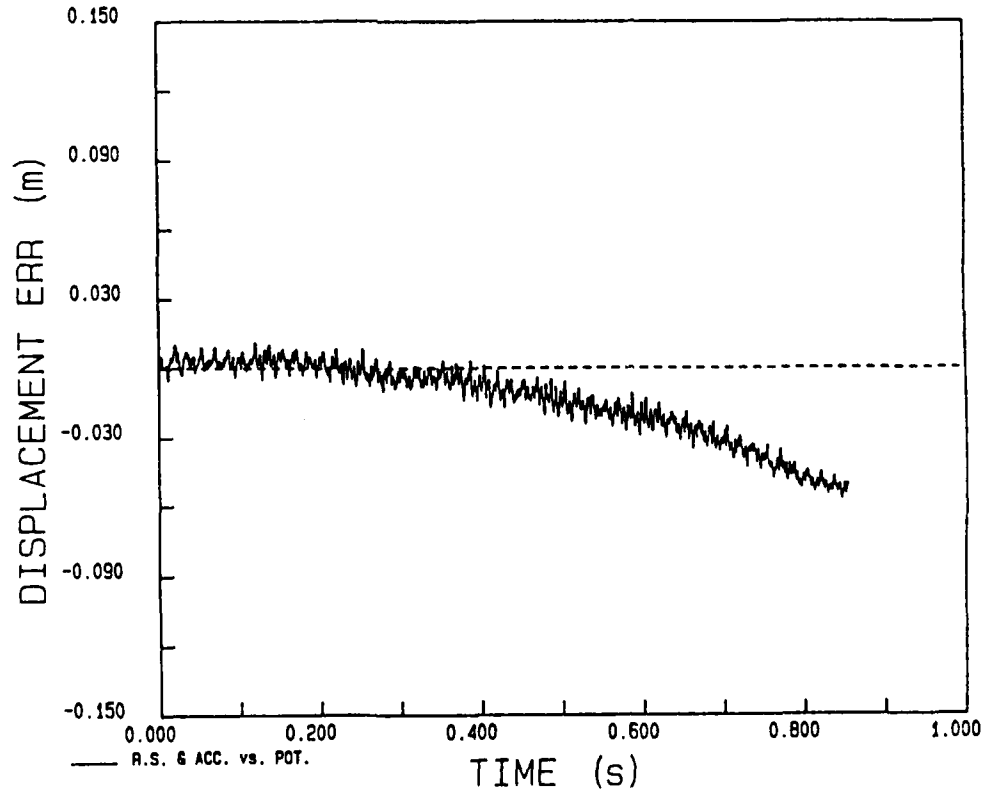


Figure 75. Vertical displacement error versus time of the sensor array for Test 45.

POTENTIOMETER - 45

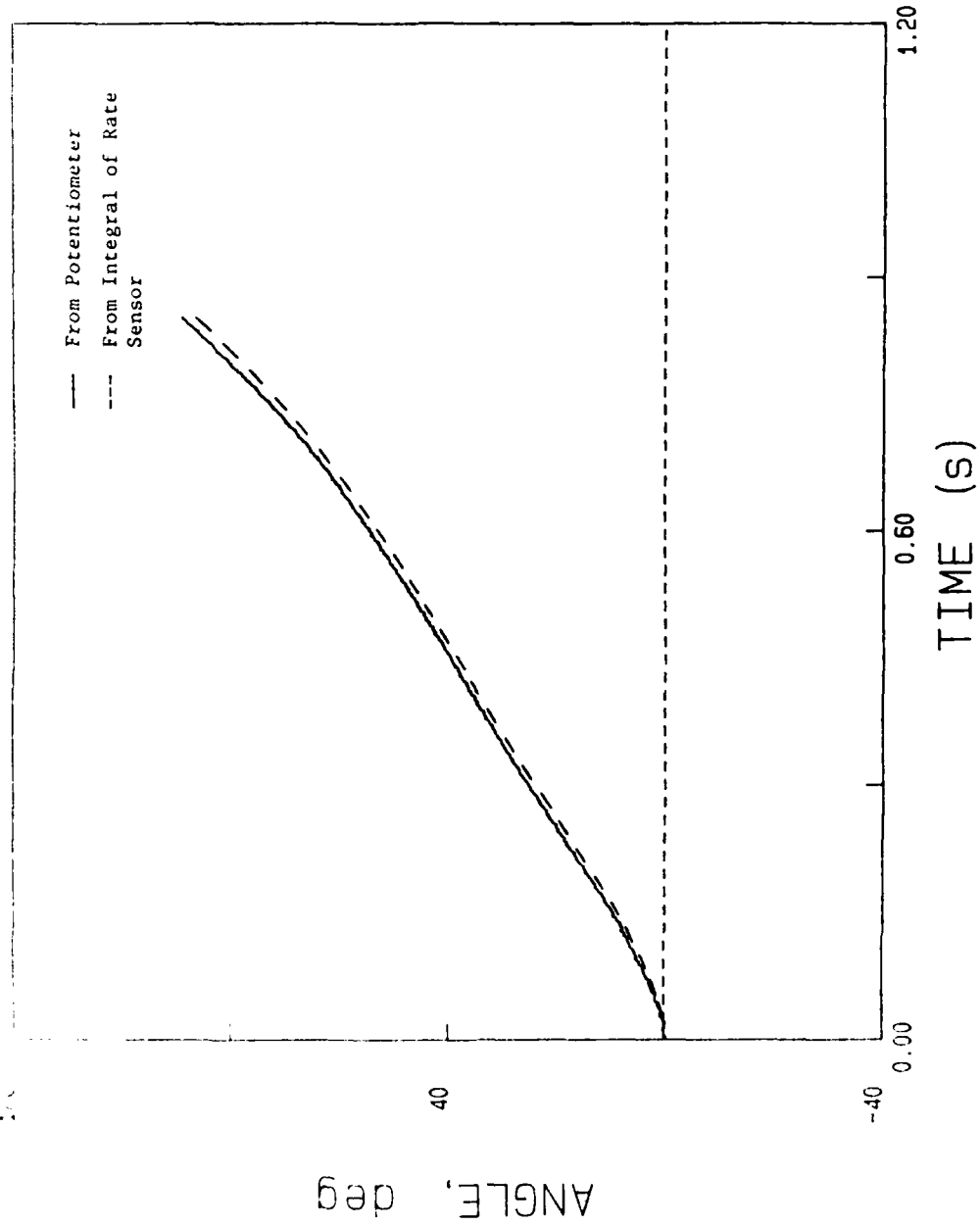


Figure 76. Comparison of the rotation angle obtained by integration of the rate sensor record with that derived from the potentiometer record for Test 45.

potentiometer record. Figure 77 shows the error in angle versus time. For most of the time, the error is less than 2 degrees in magnitude. It is a maximum of -2.60 degrees at impact.

4. Test 46

This test was performed using the Schaevitz accelerometers. The total force in the cable at initiation of the test was 1334 Newtons, and a peak acceleration of about 7.4 g's was produced.

Figures 78 through 93 show unfiltered and filtered records for the accelerometers, rate sensor, potentiometer, and load cell. The oscillations on the accelerometer waveforms are lower in magnitude than those that occur on the Endevco accelerometer records.

Figure 94 shows the trajectory of the accelerometers. The dashed curve is that derived from the accelerometer and rate sensor records using the computer program of Appendix A. The solid reference curve is that derived using the radius and the potentiometer record. Here the disagreement is large. Figures 95 and 96 show the horizontal and vertical displacement errors. The horizontal displacement error is small and acceptable. The vertical displacement error increases in time to an ultimate value of 0.16 metres.

Figure 97 compares the angle of rotation as determined by integrating the rate sensor record with that derived from the potentiometer record. Figure 98 shows the error in angle versus time. For most of the time the error is about one degree in magnitude. It increases to -2.4 degrees at impact.

5. Tests 28, 30, 31, and 35

These tests were performed using the Endevco accelerometers.

For Tests 28 and 30, the total force in the cable at initiation was 712 Newtons. For Tests 31 and 35, the force was 1334 Newtons.

The peak accelerations were about 4 g's for Tests 28 and 30, and about 8.5 g's for Tests 31 and 35.

Figures 99 through 118 show the comparisons of the trajectories derived from the inertial sensors with that derived from the potentiometer record and the radius, the horizontal and vertical displacement errors, the comparison of the rotation angle from the integral of the rate sensor record with that from the potentiometer, and the error in angle versus time.

6. Tests 43 and 48

These tests were performed using the Schaevitz accelerometers.

For Test 43, the total force in the cable at initiation was 712 Newtons. The peak acceleration was about 3.5 g's.

ANGULAR ERROR - 45

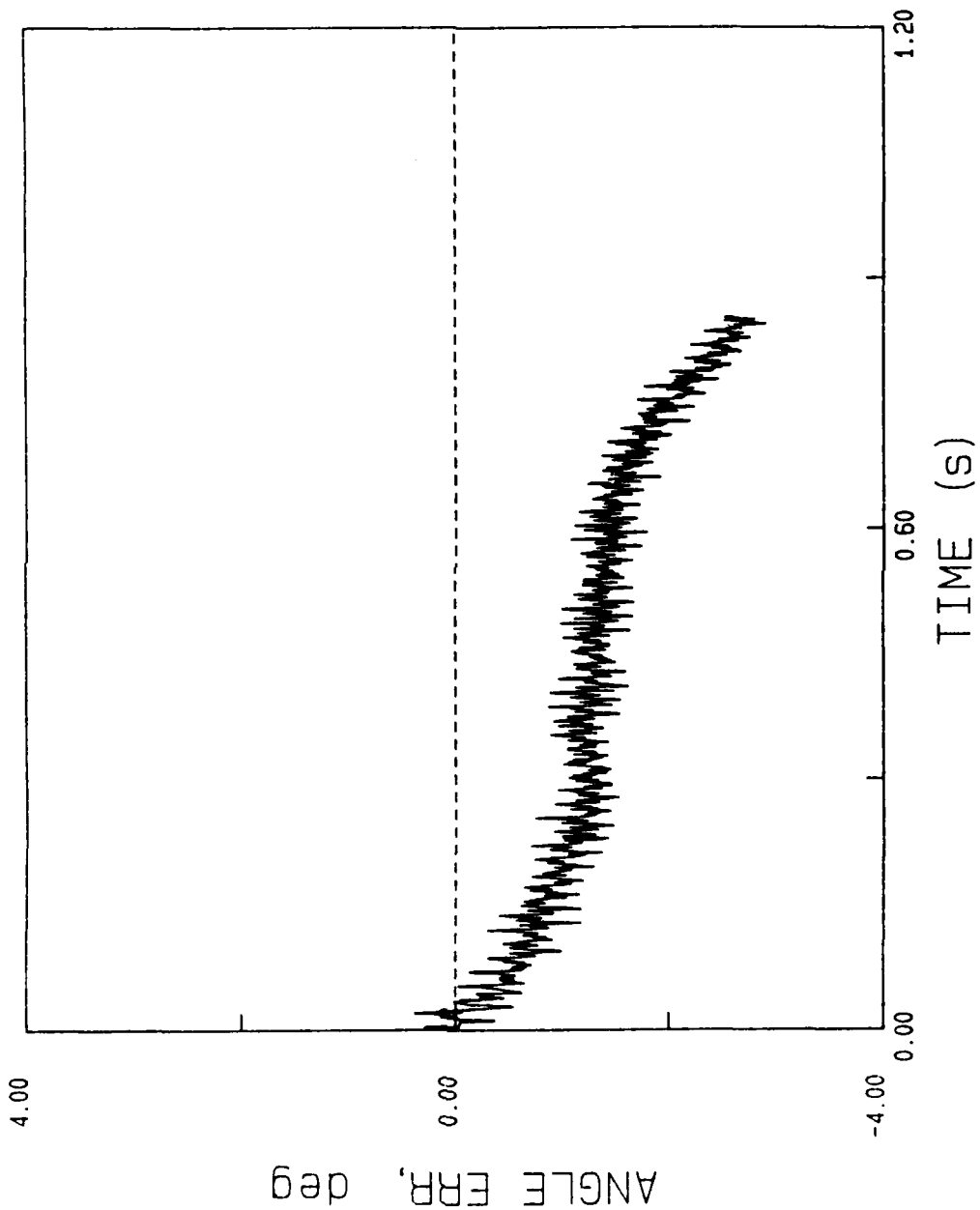


Figure 77. Error in the rotation angle obtained by integration of the rate sensor record for Test 45.

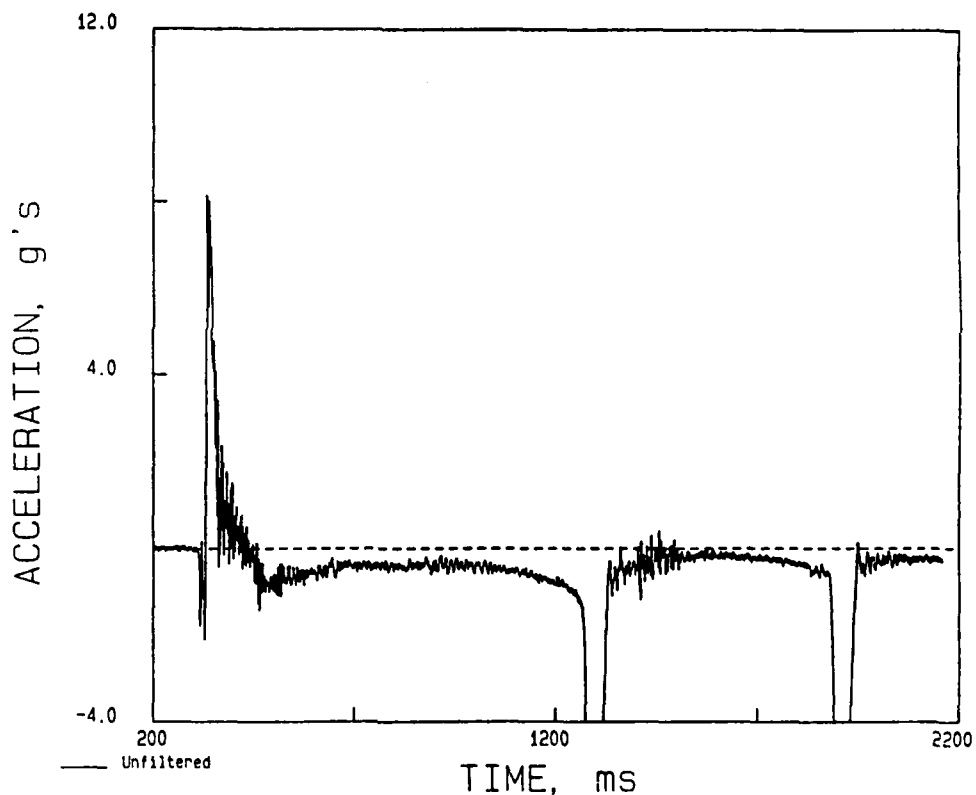


Figure 78. Unfiltered acceleration versus time from the initially vertical Schaevitz accelerometer on Test 46.

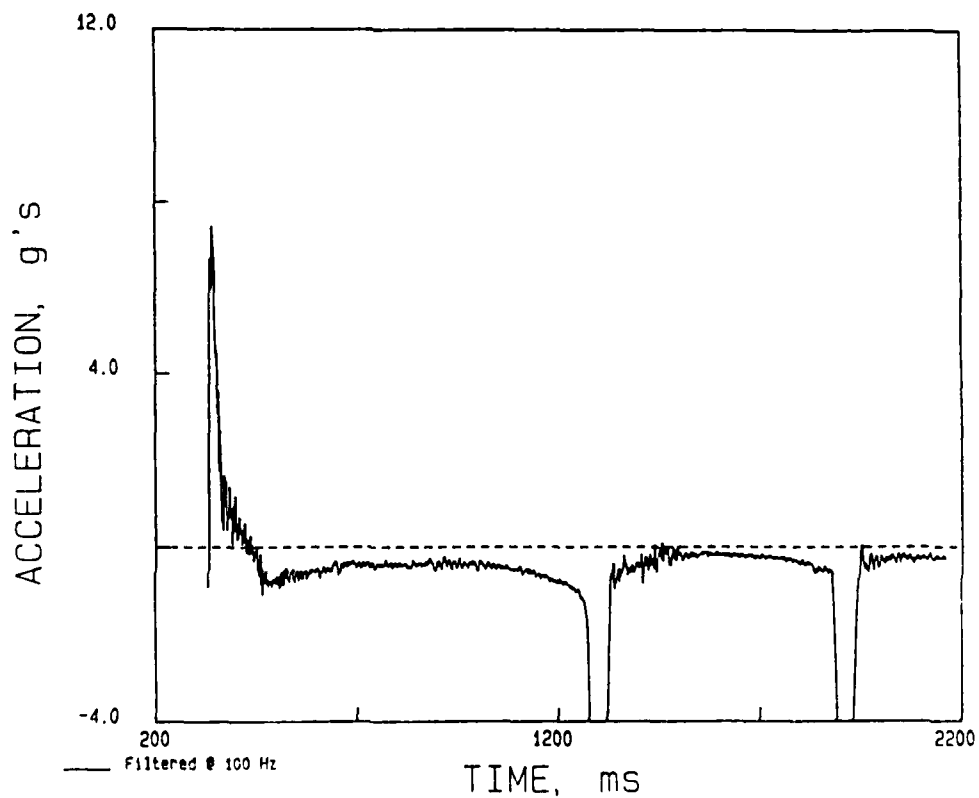


Figure 79. Filtered acceleration versus time from the initially vertical Schaevitz accelerometer on Test 46.

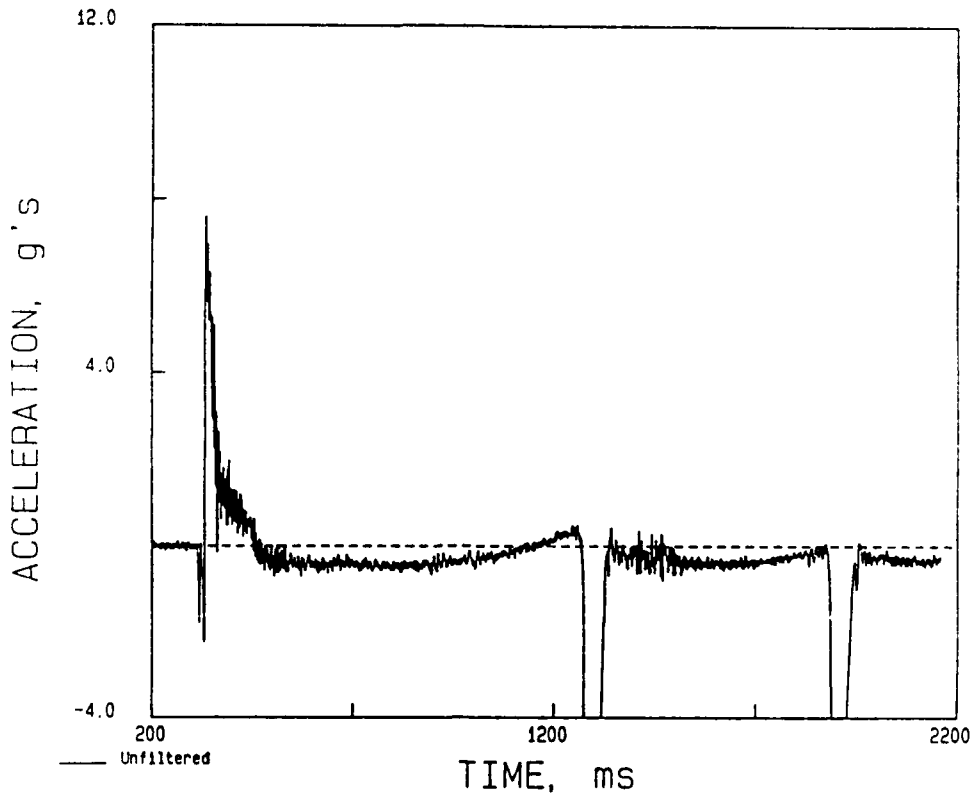


Figure 80. Unfiltered acceleration versus time from the initially horizontal Schaevitz accelerometer on Test 46.

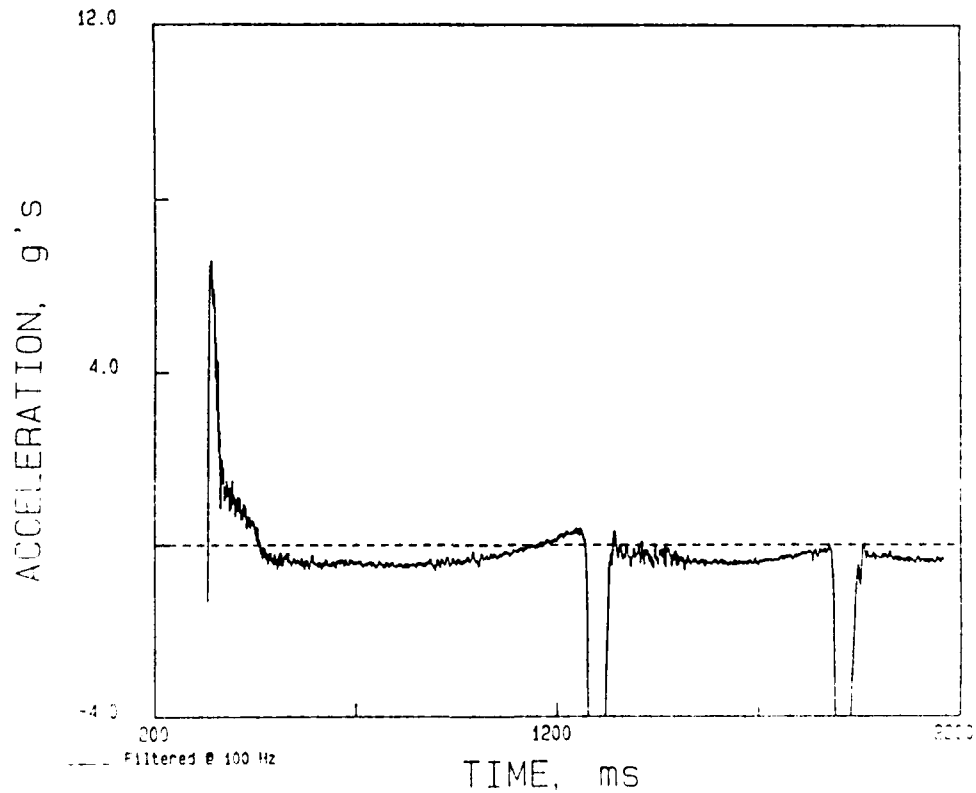


Figure 81. Filtered acceleration versus time from the initially horizontal Schaevitz accelerometer on Test 46.

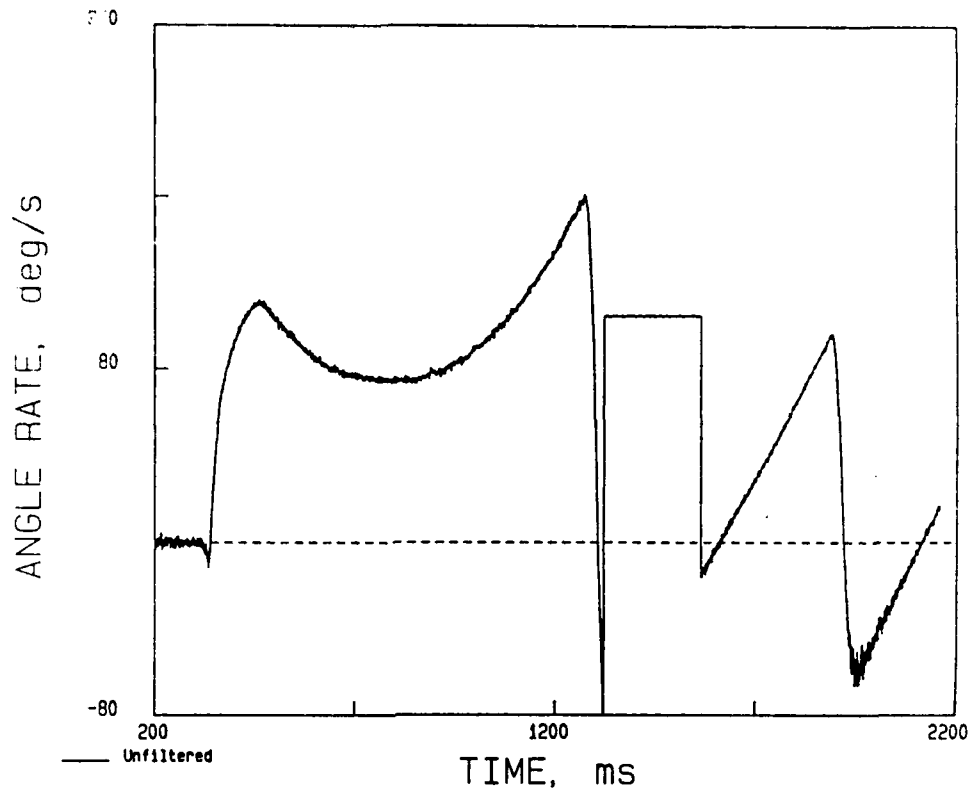


Figure 82. Unfiltered angular velocity versus time from the Humphrey rate sensor on Test 46.

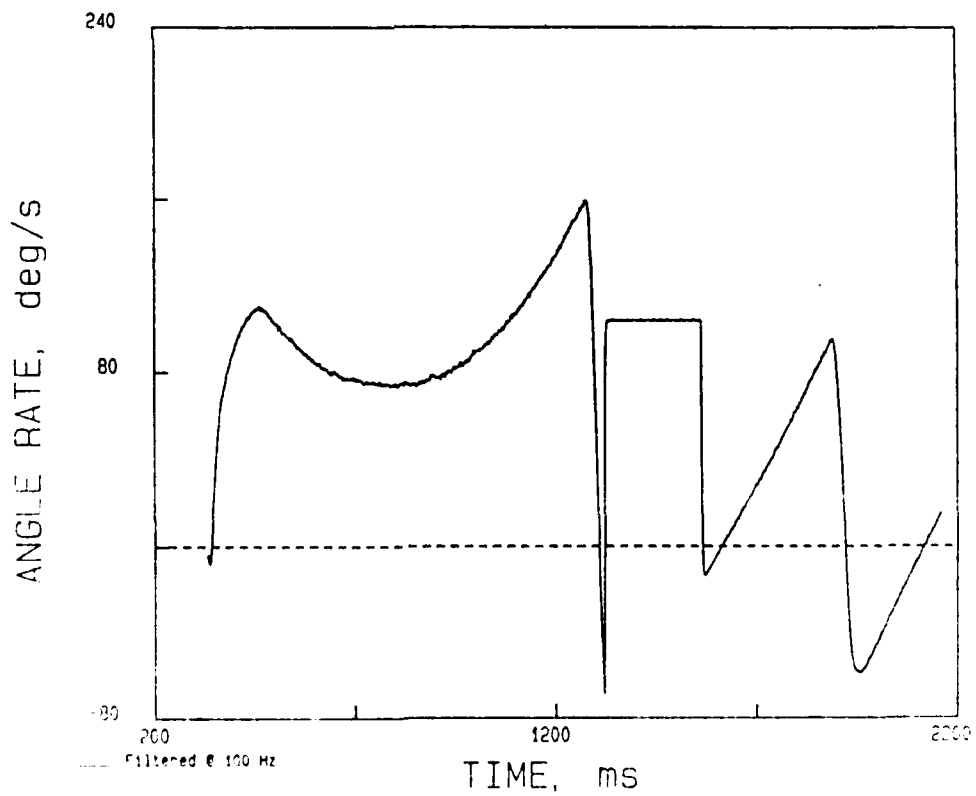


Figure 83. Filtered angular velocity versus time from the Humphrey rate sensor on Test 46.

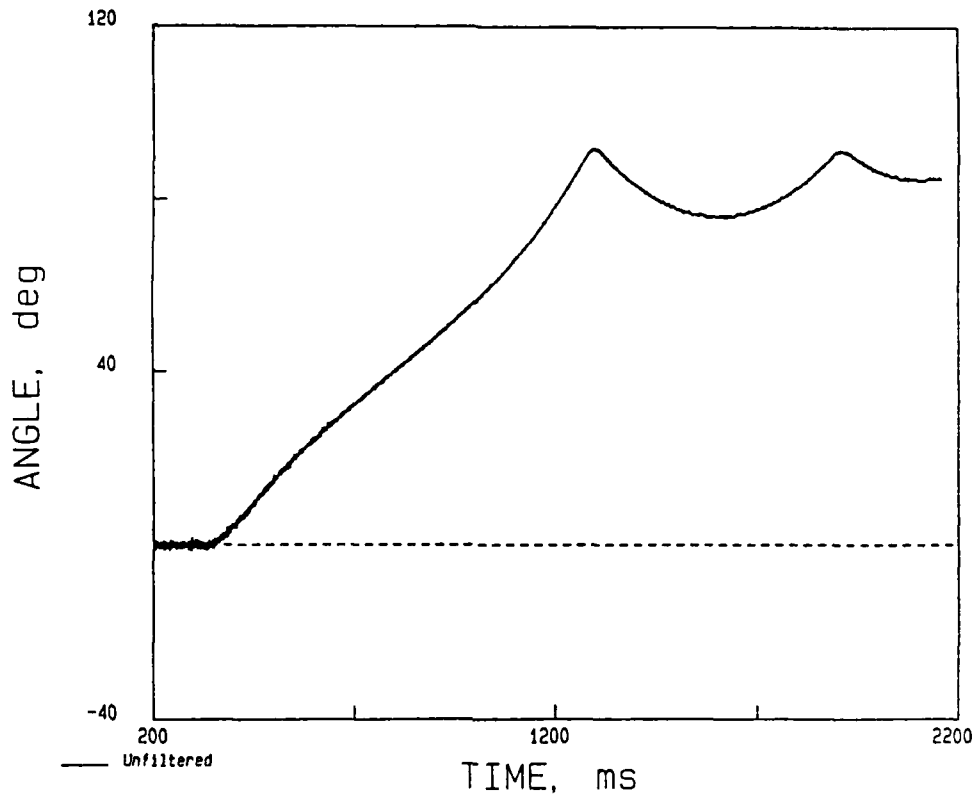


Figure 84. Unfiltered angle versus time derived from the potentiometer on the axle of the quarter wheel on Test 46.

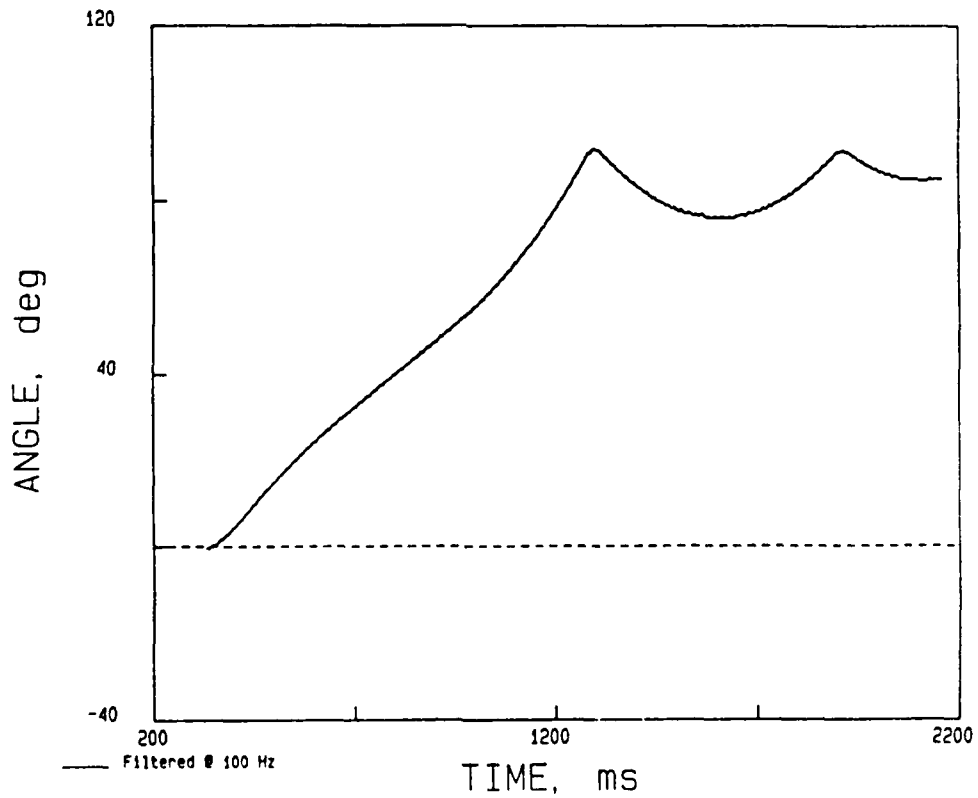


Figure 85. Filtered angle versus time derived from the potentiometer on the axle of the quarter wheel on Test 46.

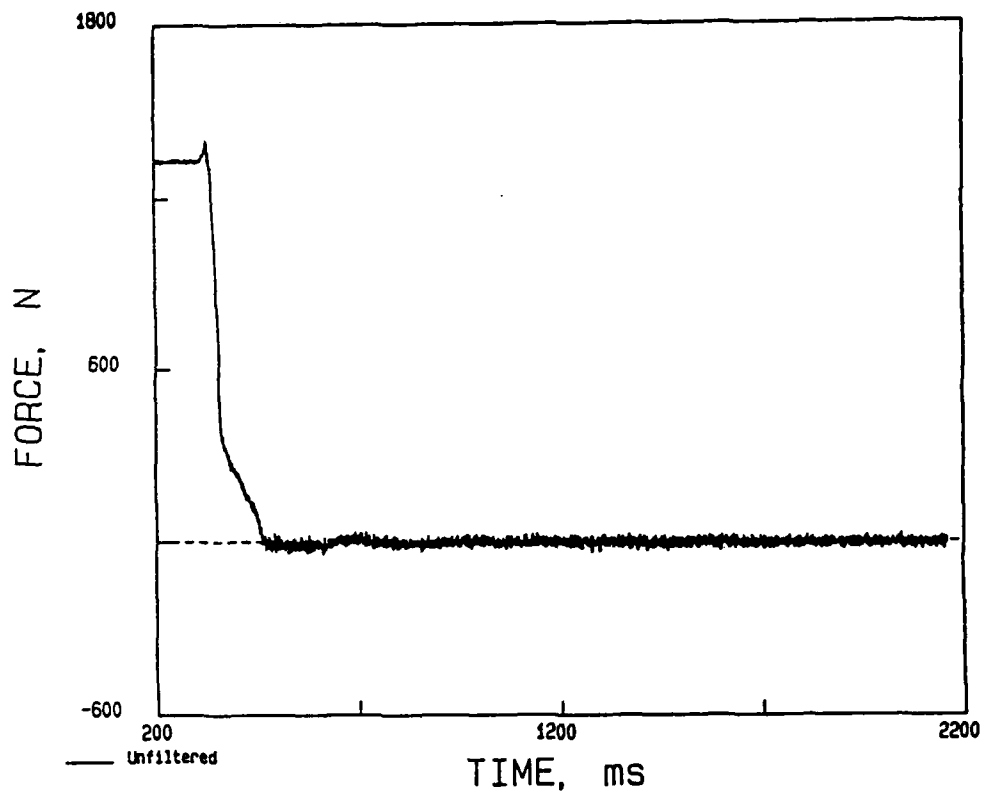


Figure 86. Unfiltered load cell record from Test 46.

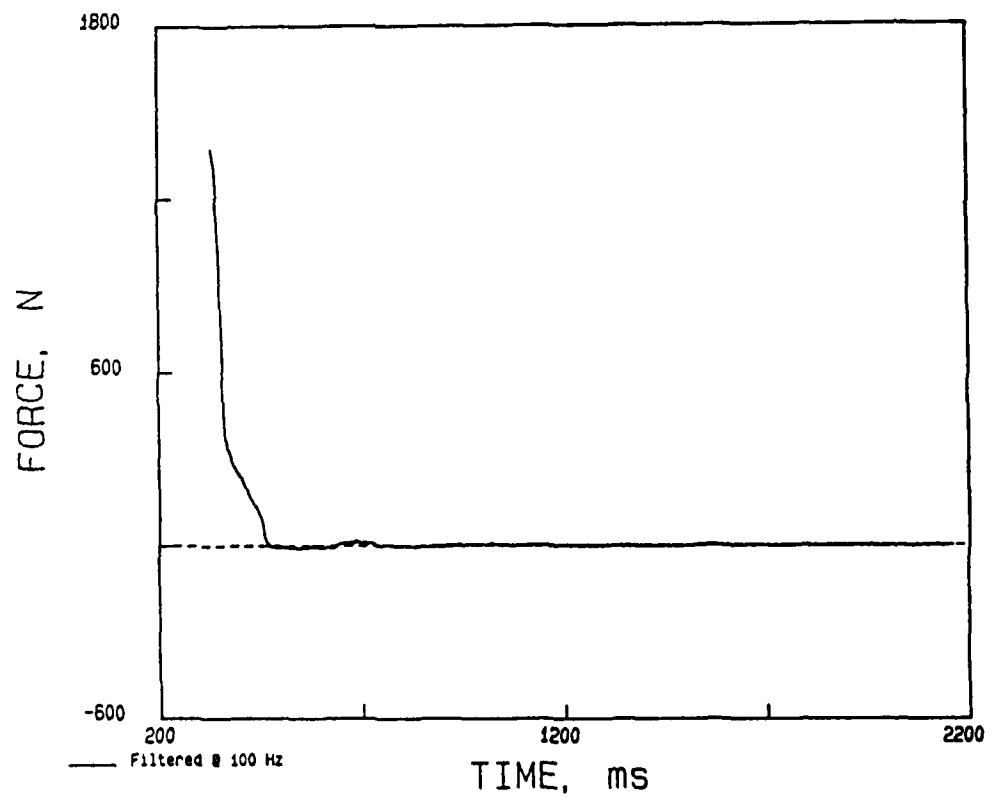


Figure 87. Filtered load cell record from Test 46.

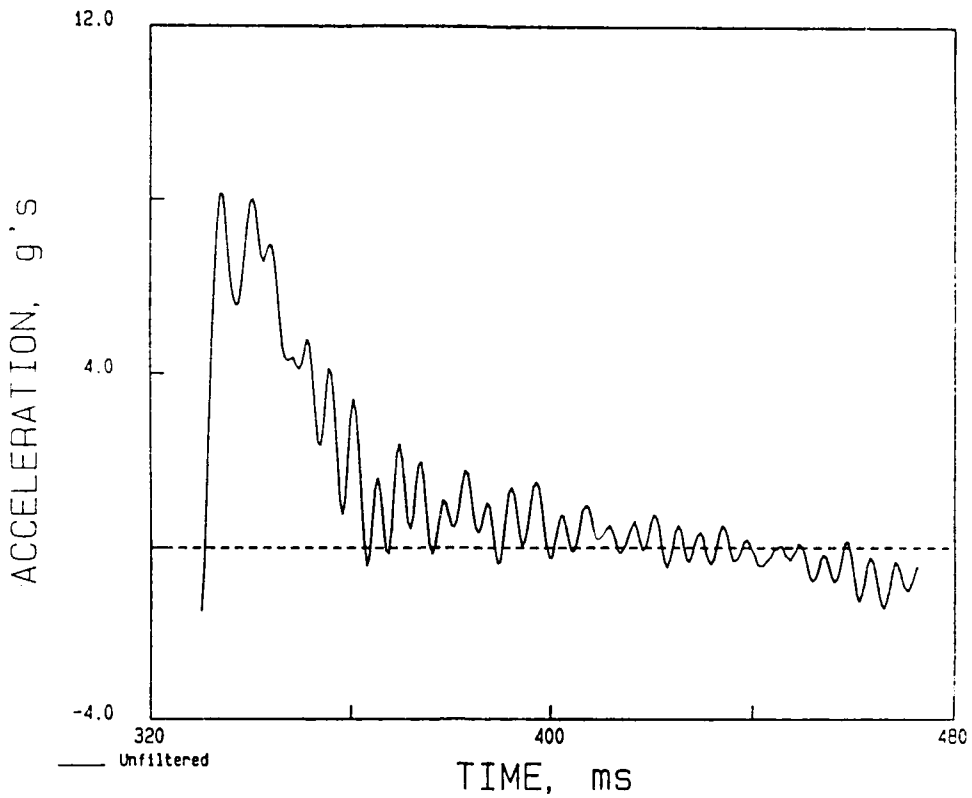


Figure 88. Unfiltered positive phase of acceleration versus time from the vertical accelerometer on Test 46.

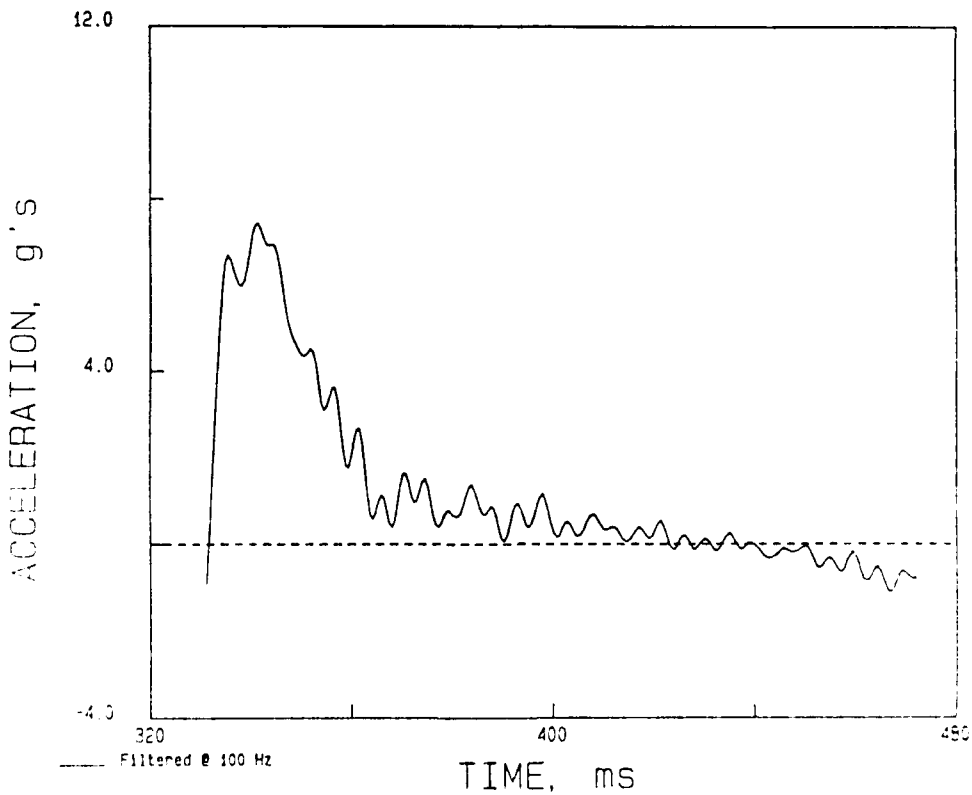


Figure 89. Filtered positive phase of acceleration versus time from the vertical accelerometer on Test 46.

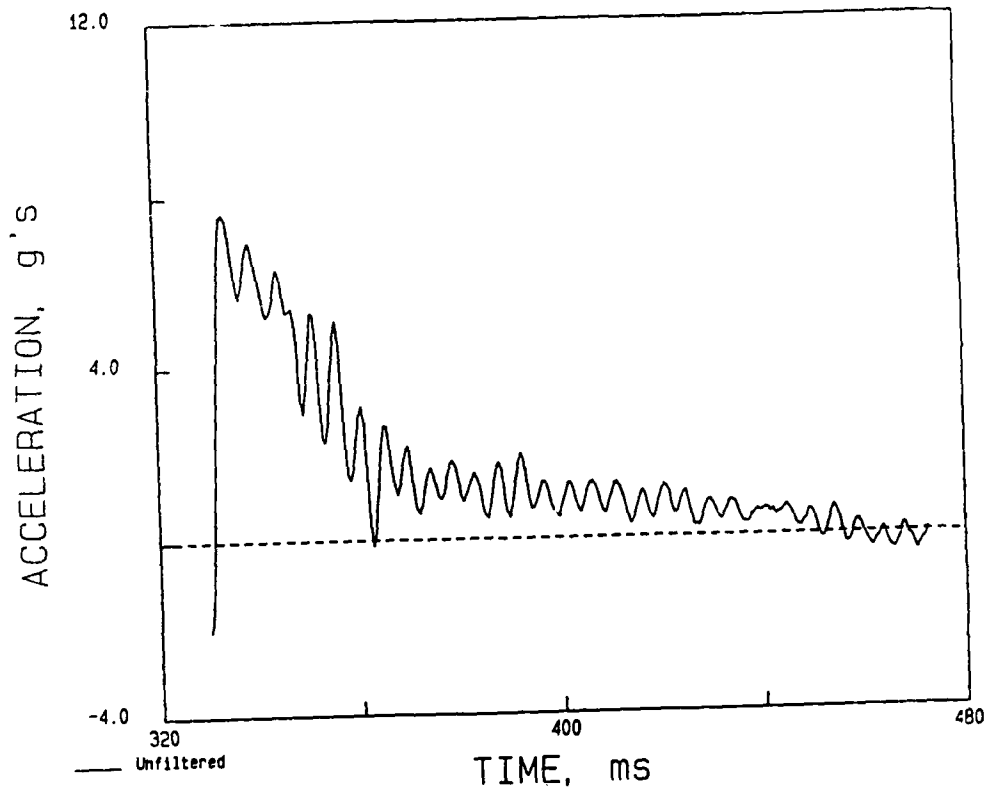


Figure 90. Unfiltered positive phase of acceleration versus time from the initially horizontal accelerometer on Test 46.

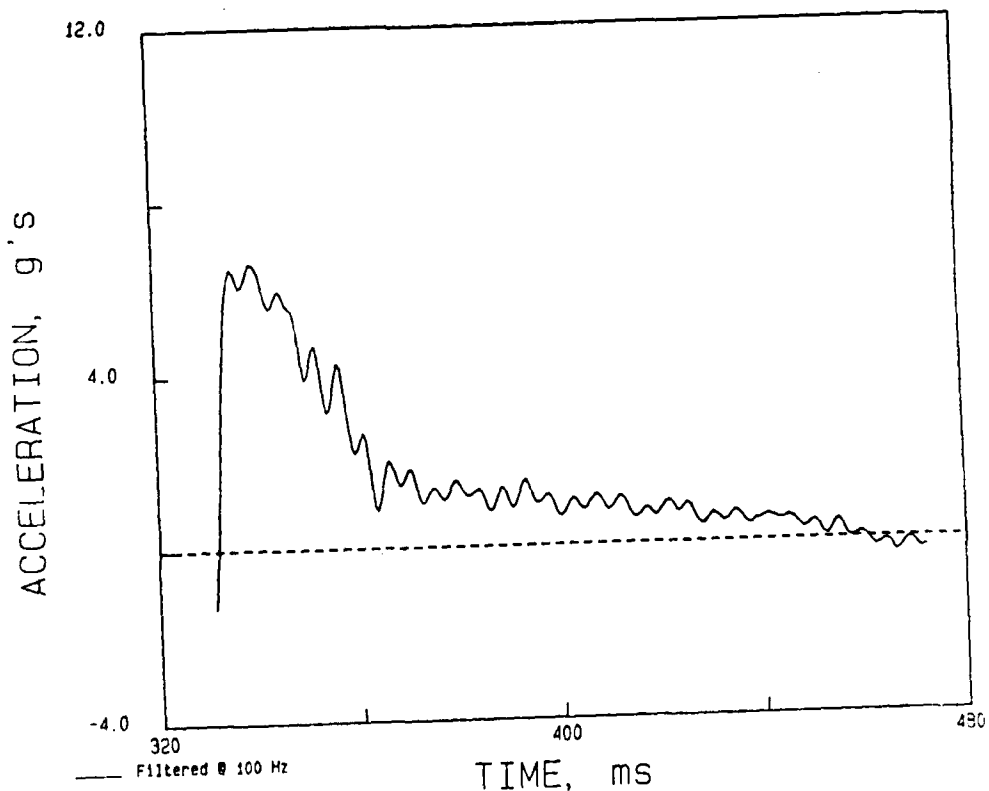


Figure 91. Filtered positive phase of acceleration versus time from the initially horizontal accelerometer on Test 46.

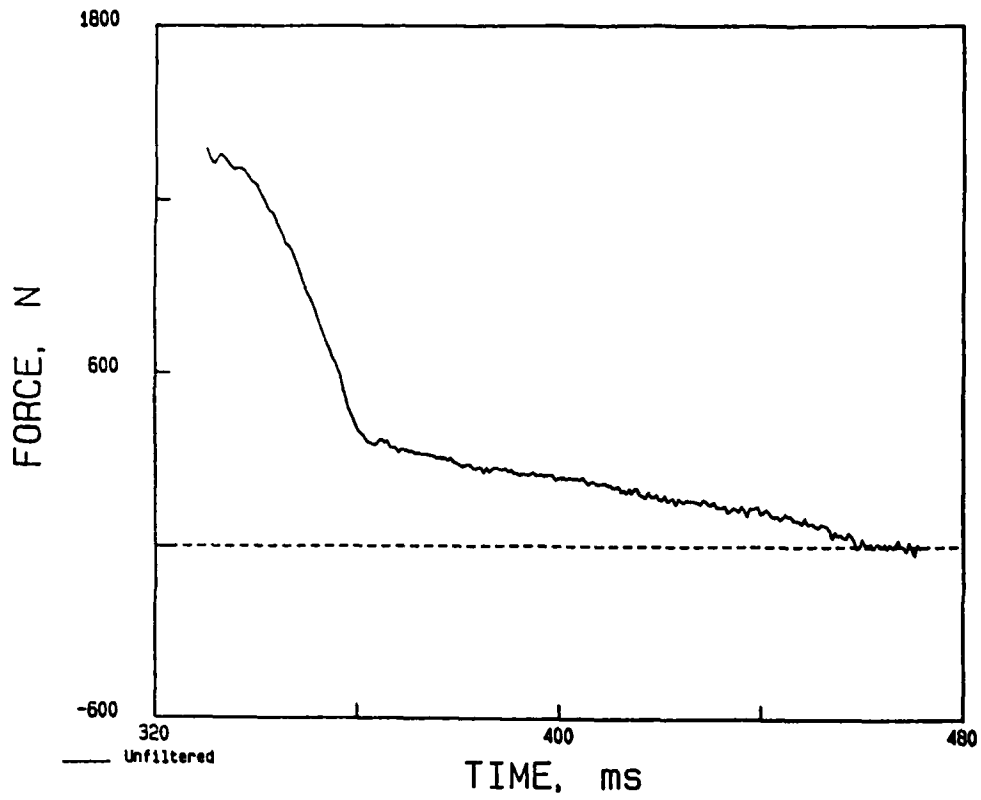


Figure 92. Unfiltered positive phase of the load cell record from Test 46.

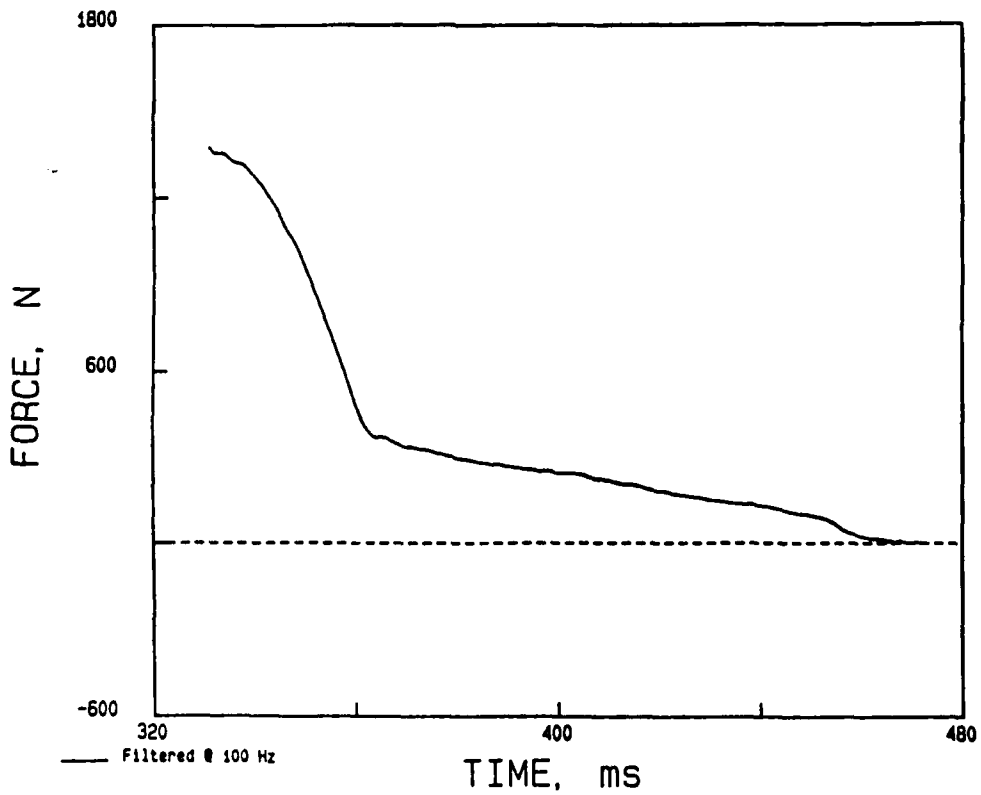


Figure 93. Filtered positive phase of the load cell record from Test 46.

TRAJECTORY OF SENSORS - 46

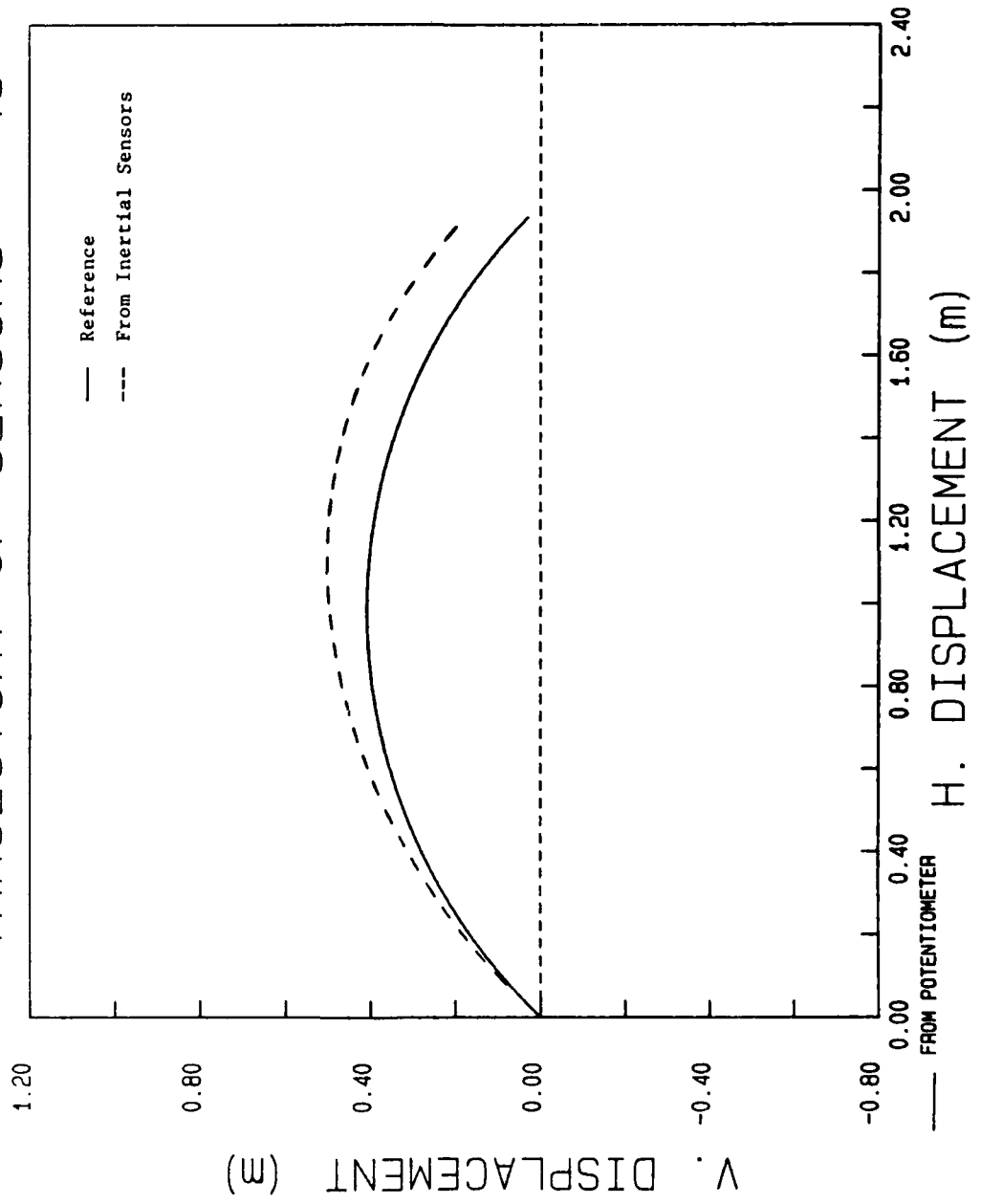


Figure 94. Comparison of the sensor array trajectory for Test 46 derived from the Schaevitz accelerometers and the Humphrey rate sensor with the reference trajectory derived from the potentiometer record.

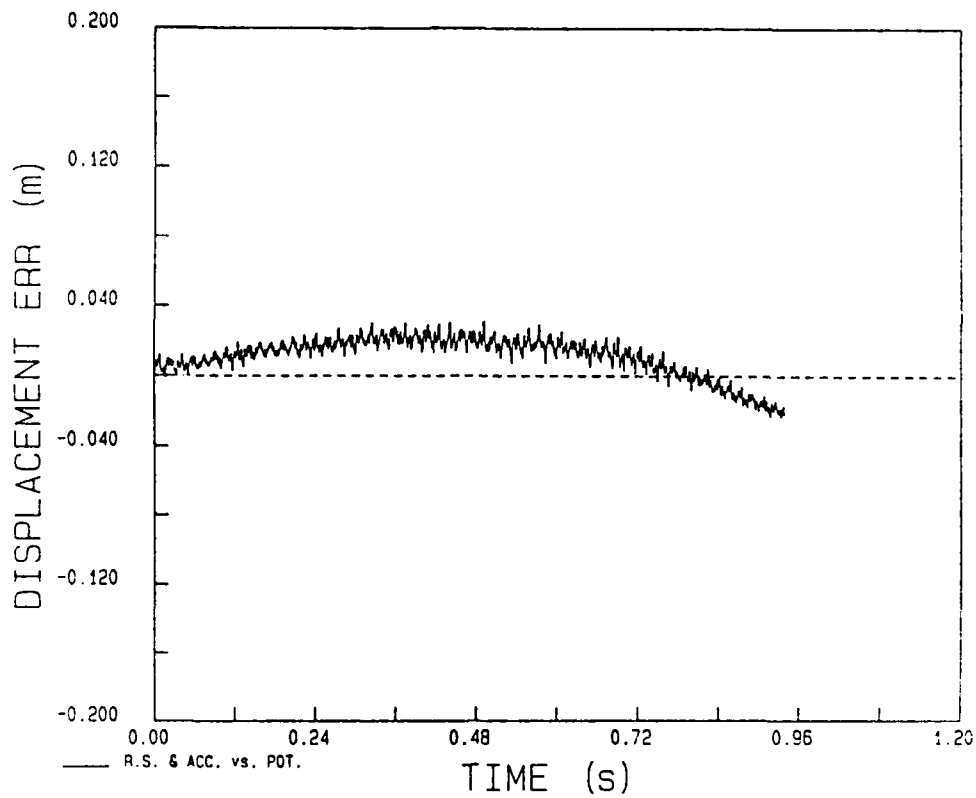


Figure 95. Horizontal displacement error versus time of the sensor array for Test 46.

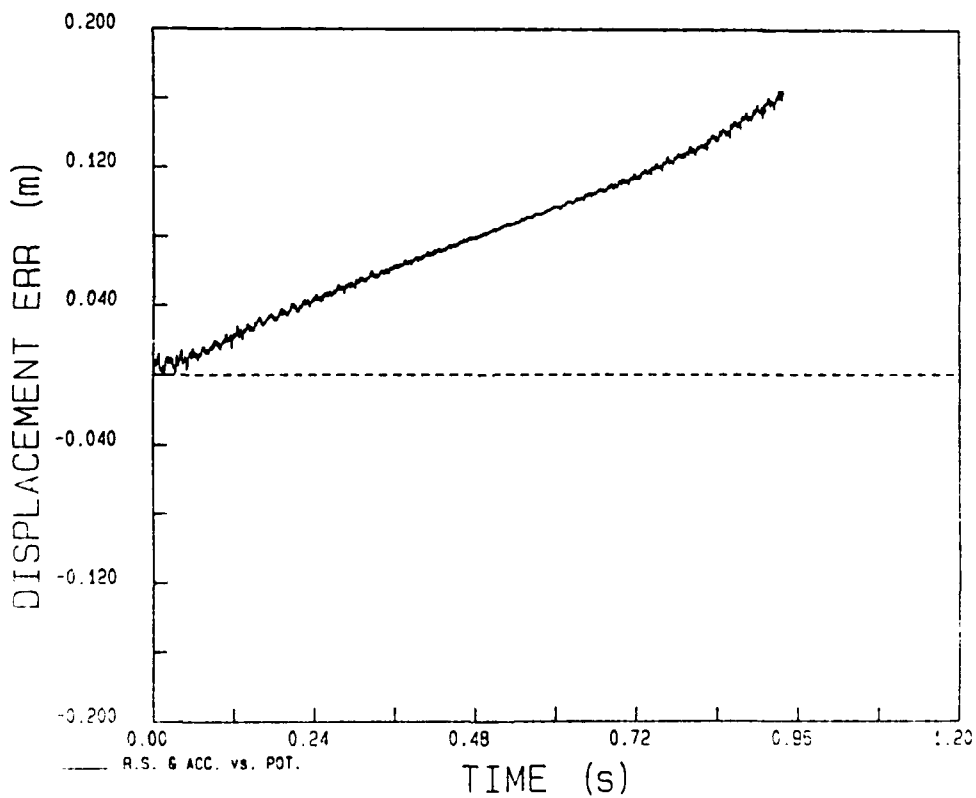


Figure 96. Vertical displacement error versus time of the sensor array for Test 46.

POTENTIOMETER - 46

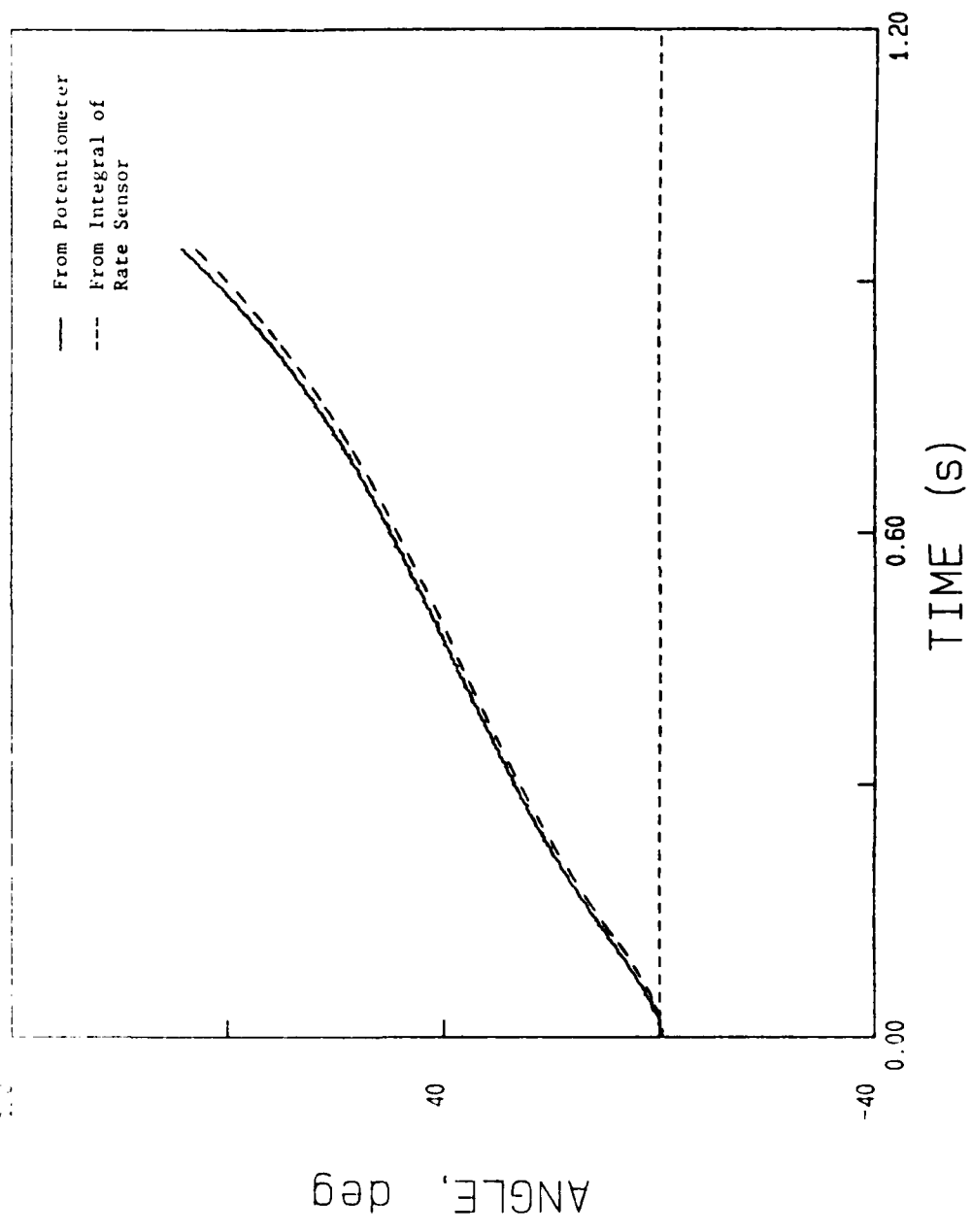


Figure 97. Comparison of the rotation angle obtained by integration of the rate sensor record with that derived from the potentiometer record for Test 46.

ANGULAR ERROR - 46

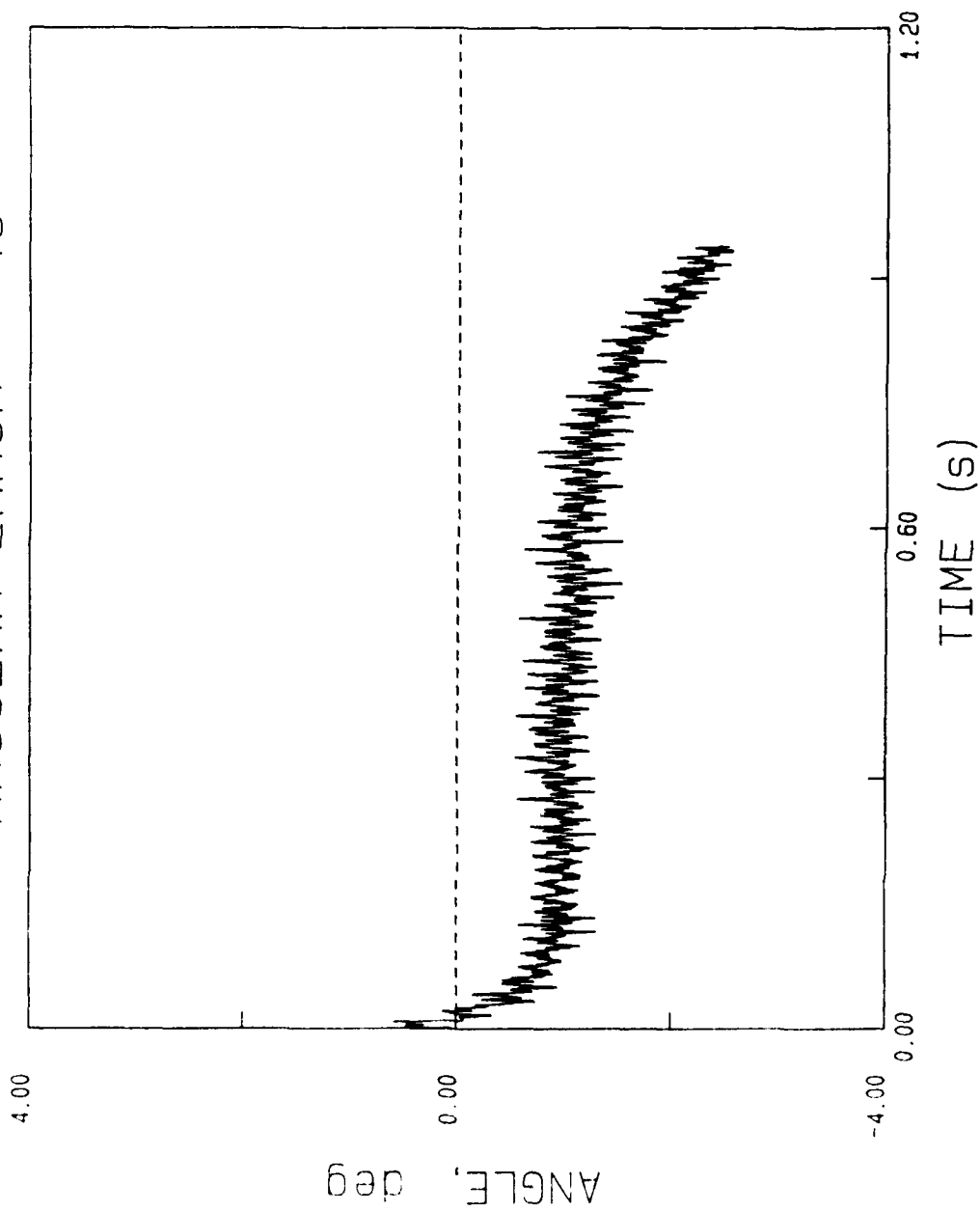


Figure 98. Error in the rotation angle obtained by integration of the rate sensor record for Test 46.

TRAJECTORY OF SENSORS - 28

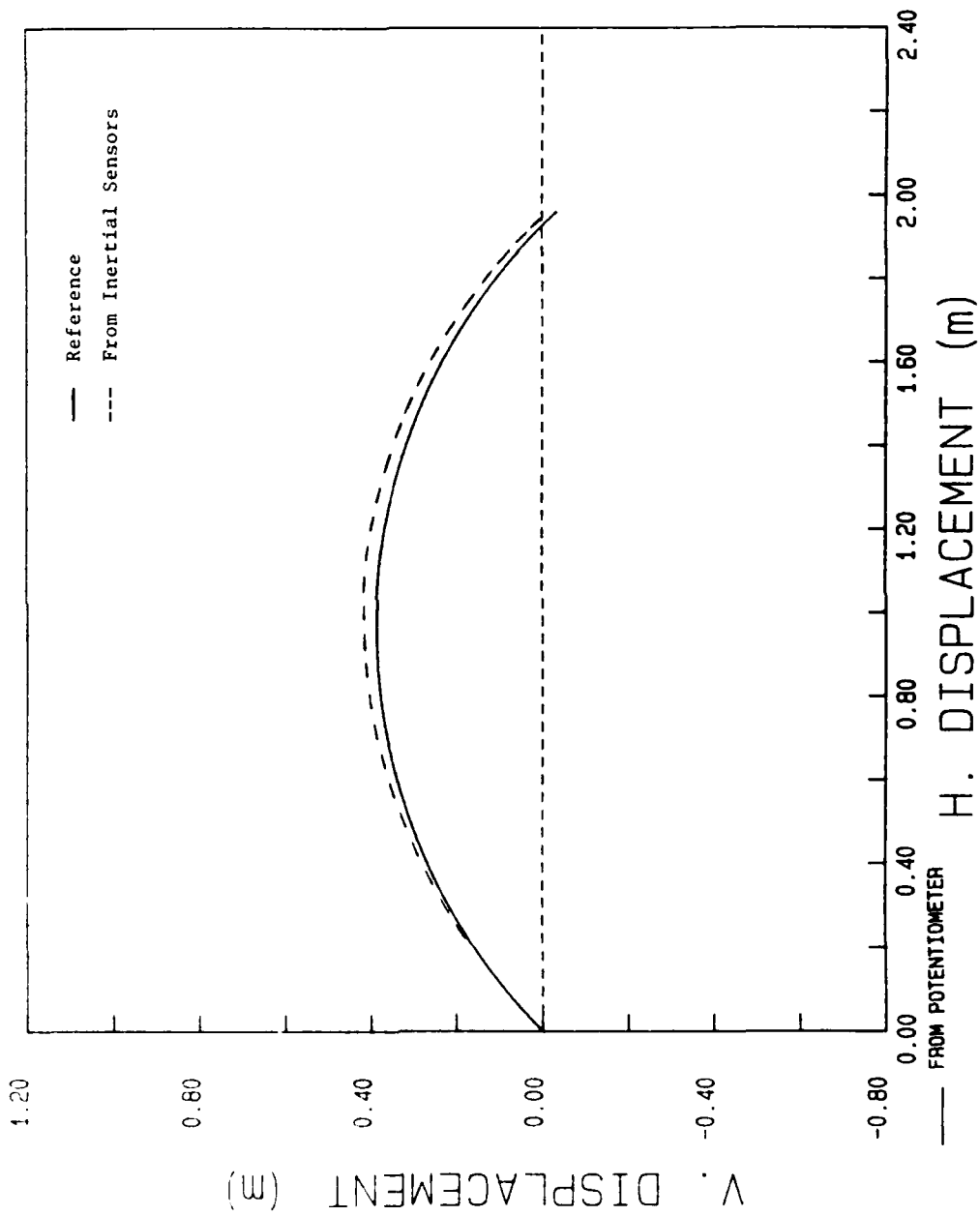


Figure 99. Comparison of the sensor array trajectory for Test 28 derived from the Endeavour accelerometers and the Humphrey rate sensor with the reference trajectory derived from the potentiometer record.

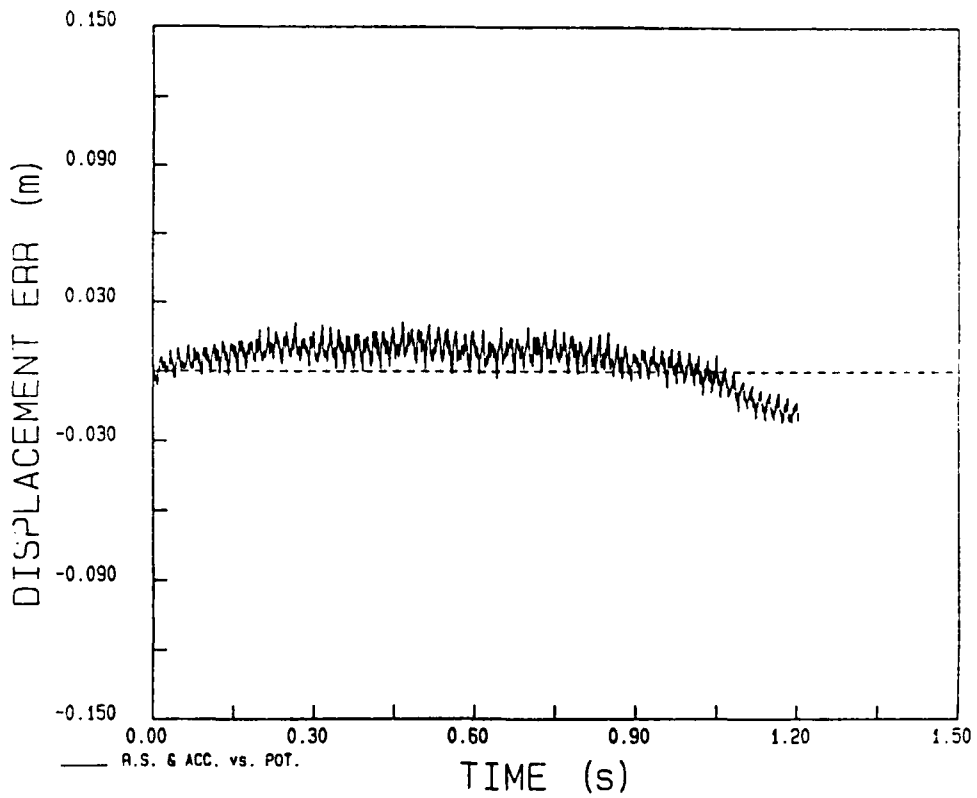


Figure 100. Horizontal displacement error versus time of the sensor array for Test 28.

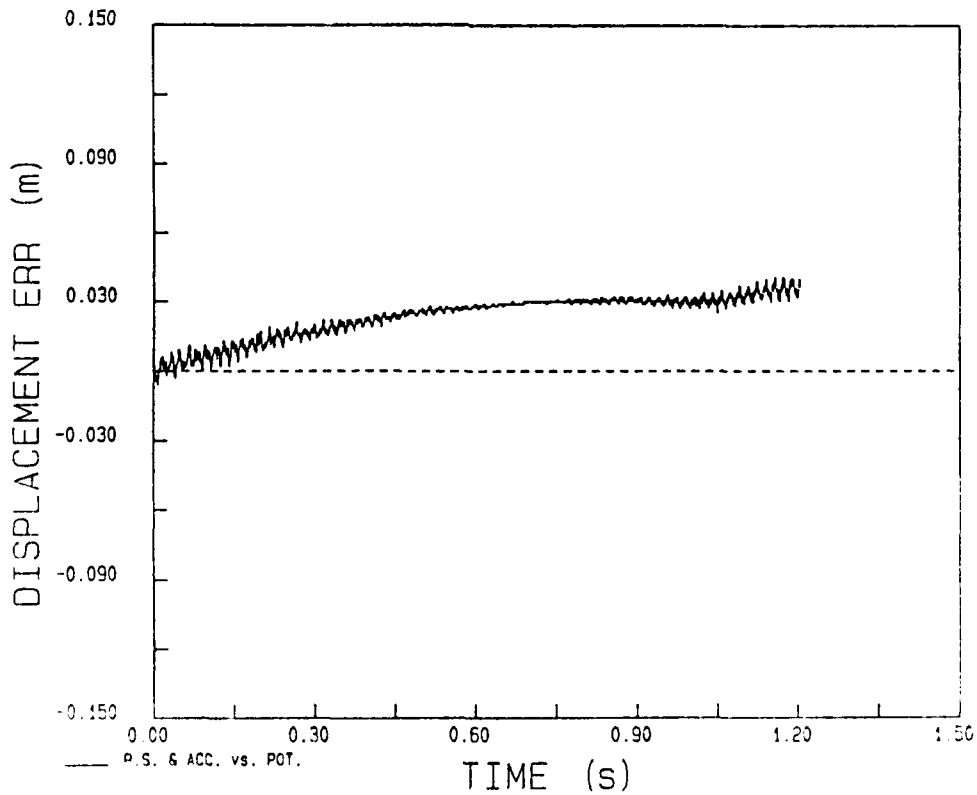


Figure 101. Vertical displacement error versus time of the sensor array for Test 28.

POTENTIOMETER -- 28

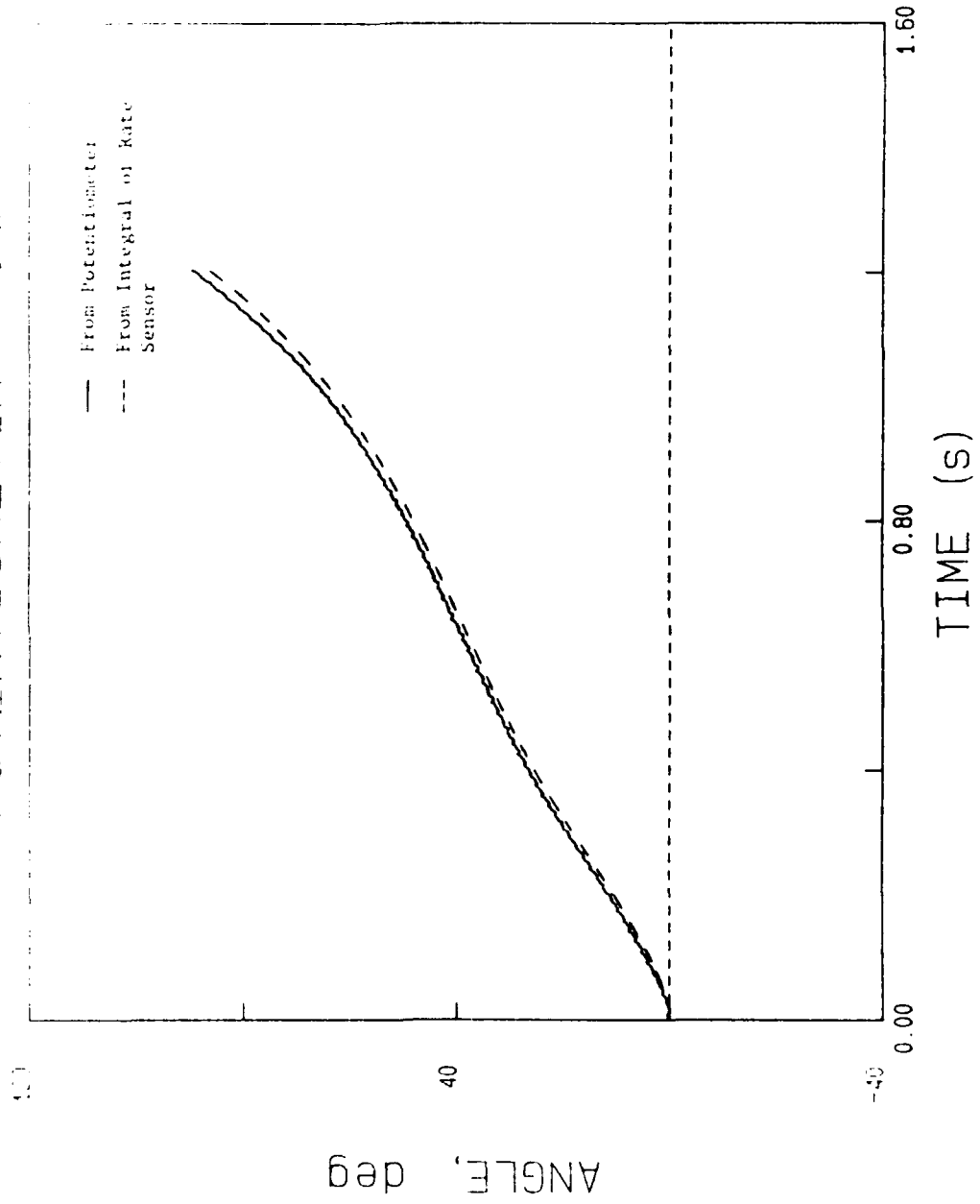


Figure 102. Comparison of the rotation angle obtained by integration of the rate sensor record with that derived from the potentiometer record for Test 28.

ANGULAR ERROR - 28

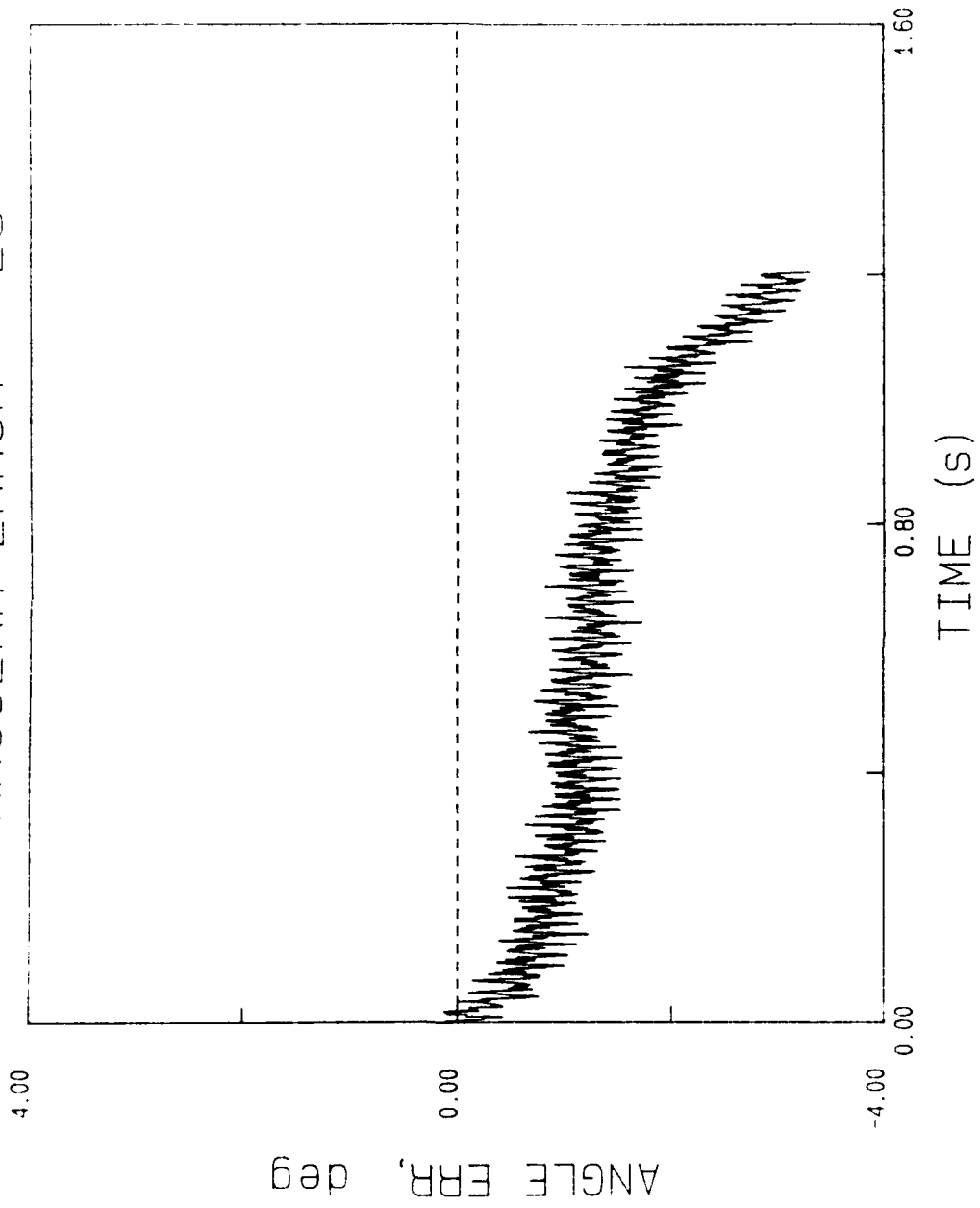


Figure 103. Error in the rotation angle obtained by integration of the rate sensor record for Test 28.

TRAJECTORY OF SENSORS - 30

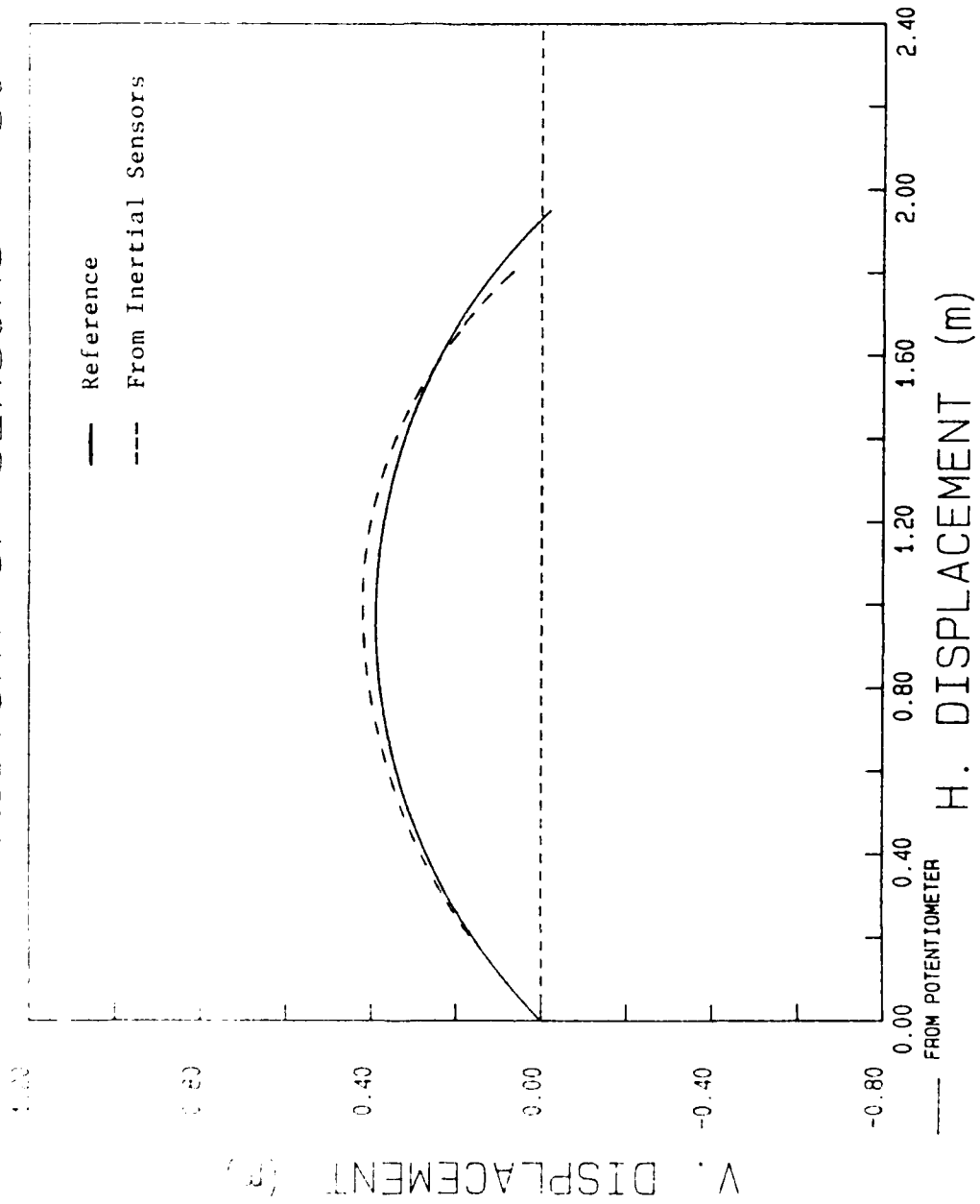


Figure 104. Comparison of the sensor array trajectory for Test 30 derived from the Endevo accelerometers and the Humphrey rate sensor with the reference trajectory derived from the potentiometer record.

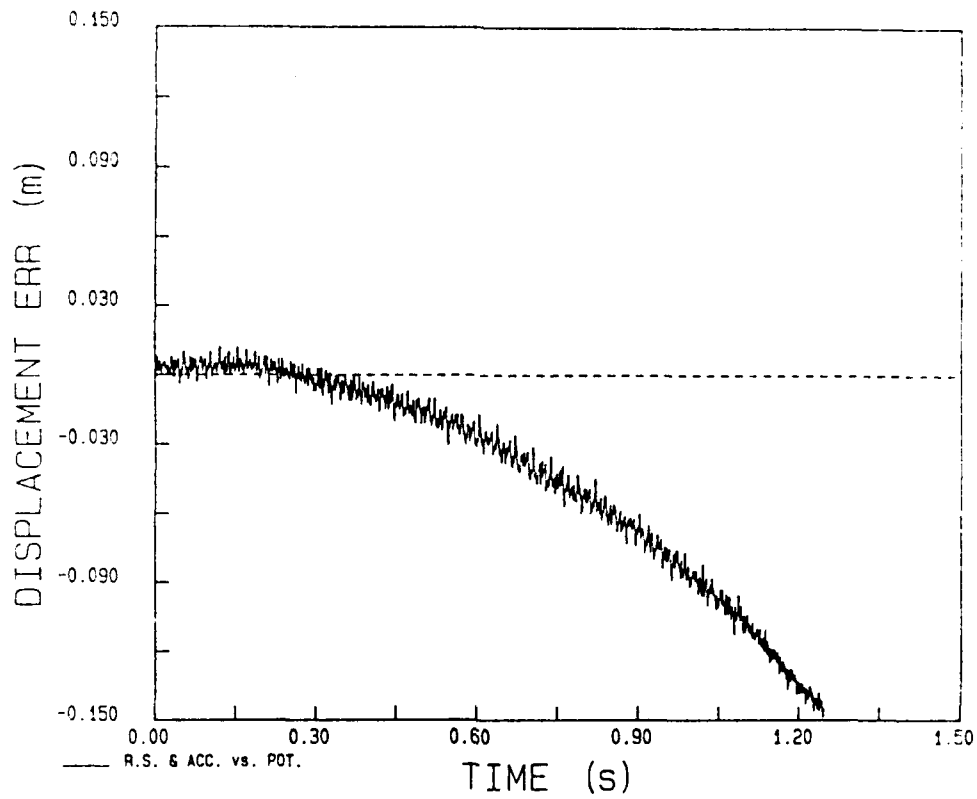


Figure 105. Horizontal displacement error versus time of the sensor array for Test 30.

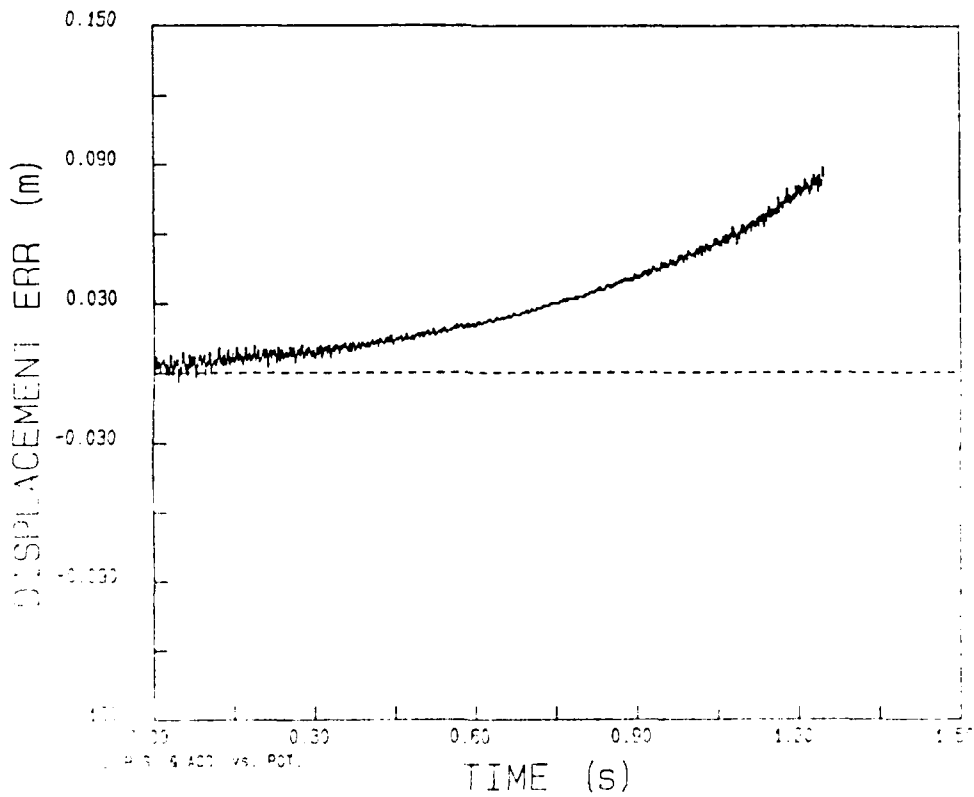


Figure 106. Vertical displacement error versus time of the sensor array for Test 30.

POTENTIOMETER - 30

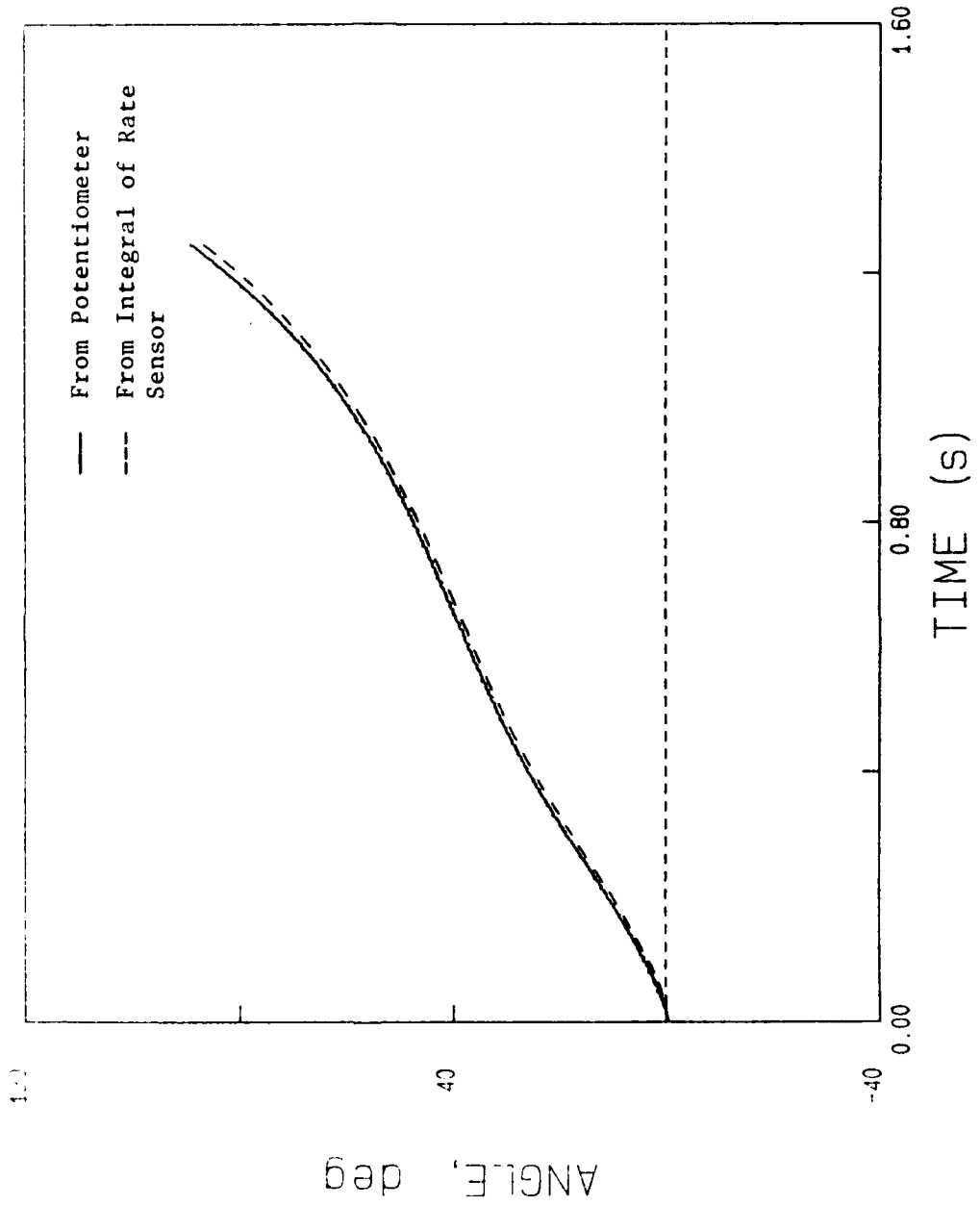


Figure 107. Comparison of the rotation angle obtained by integration of the rate sensor record with that derived from the potentiometer record for Test 30.

ANGULAR ERROR - 30

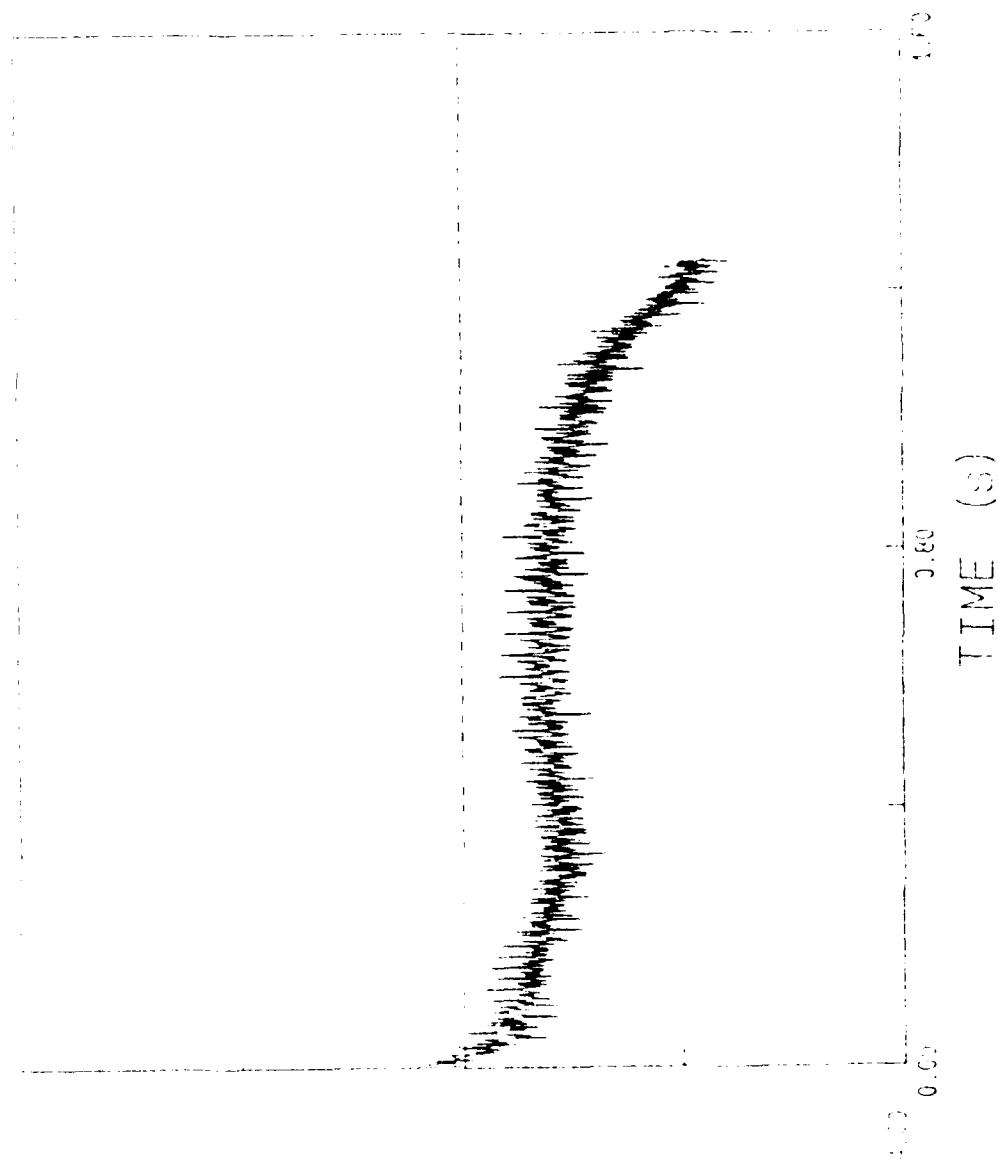


Figure 10. Error in the rotation angle obtained by integration of the rate sensor record for test 30.

TRAJECTORY OF SENSORS - 31

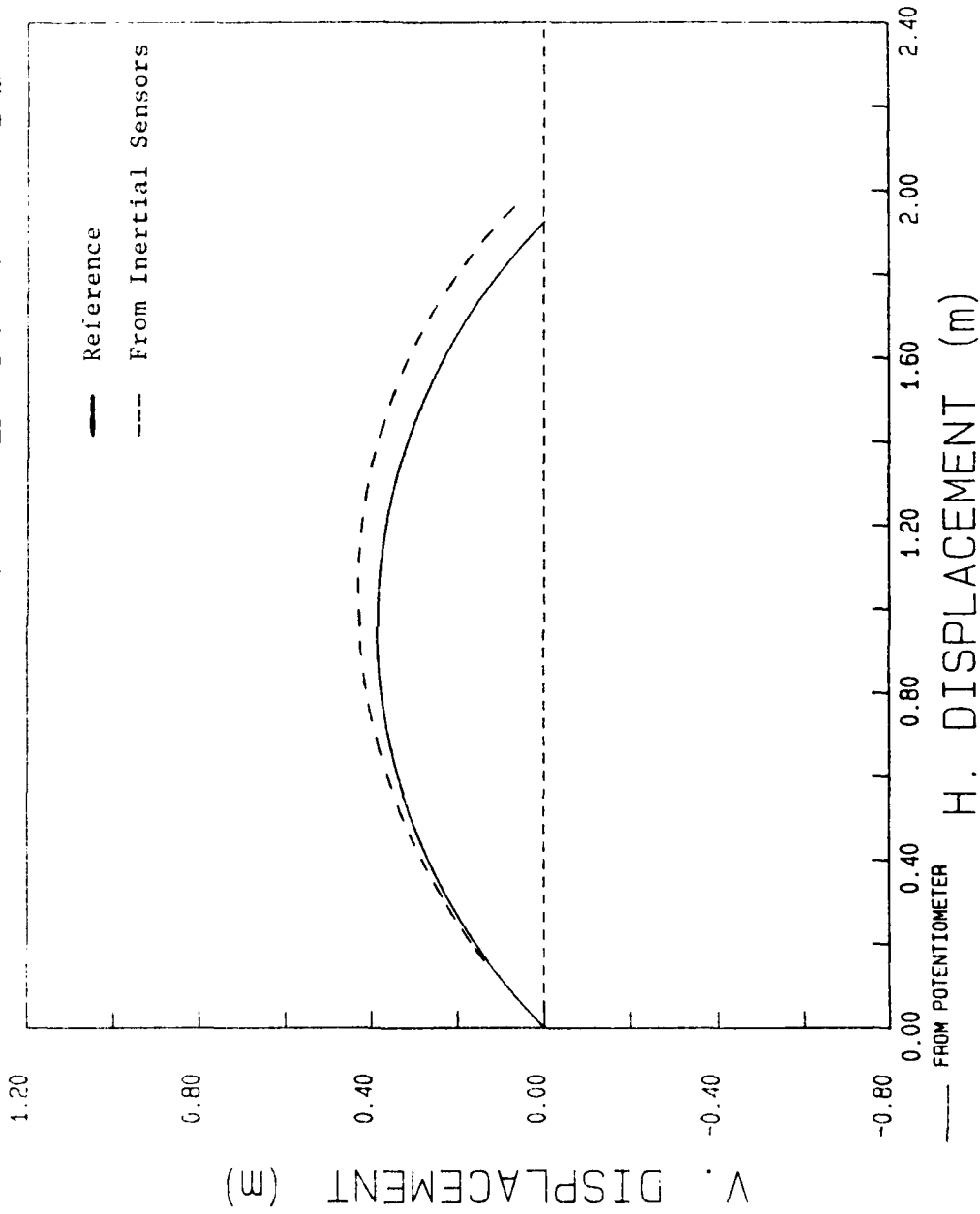


Figure 109. Comparison of the sensor array trajectory for Test 31 derived from the Endevo accelerometers and the Humphrey rate sensor with the reference trajectory derived from the potentiometer record.

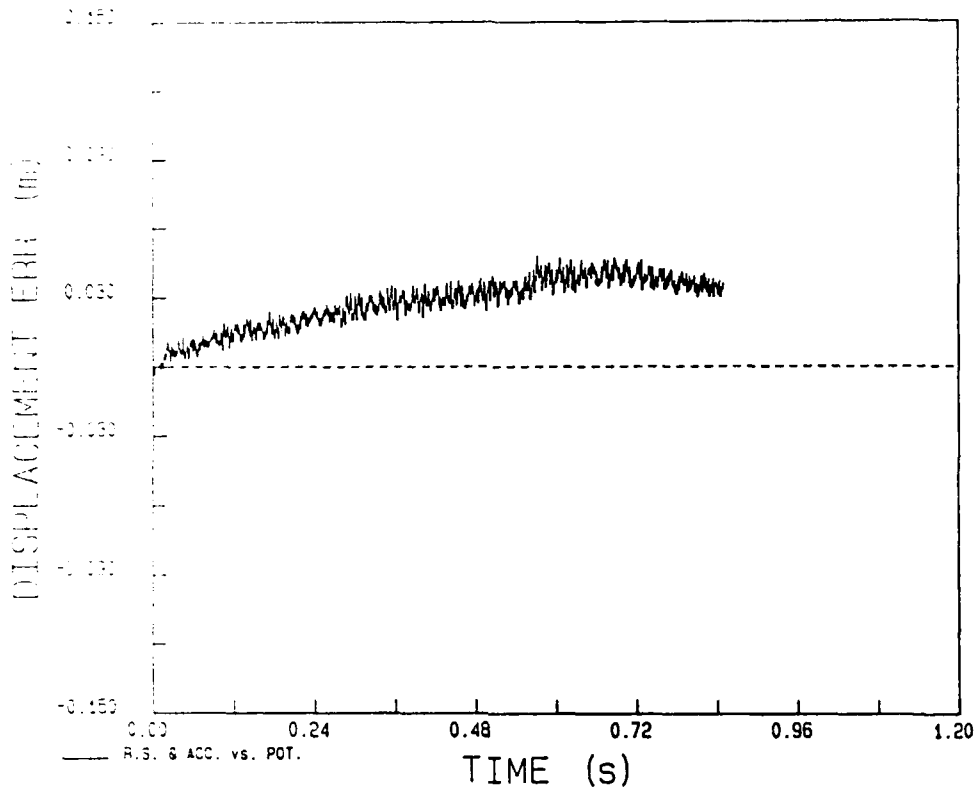


Figure 110. Horizontal displacement error versus time of the sensor array for Test 31.

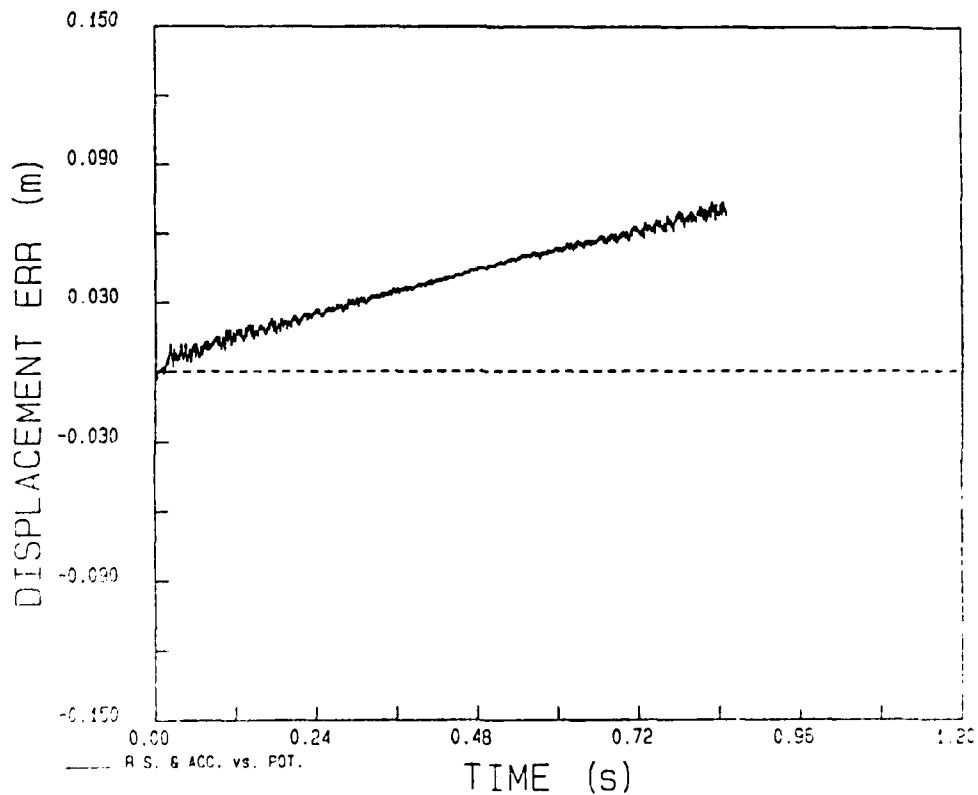


Figure 111. Vertical displacement error versus time of the sensor array for Test 31.

POTENTIOMETER - 31

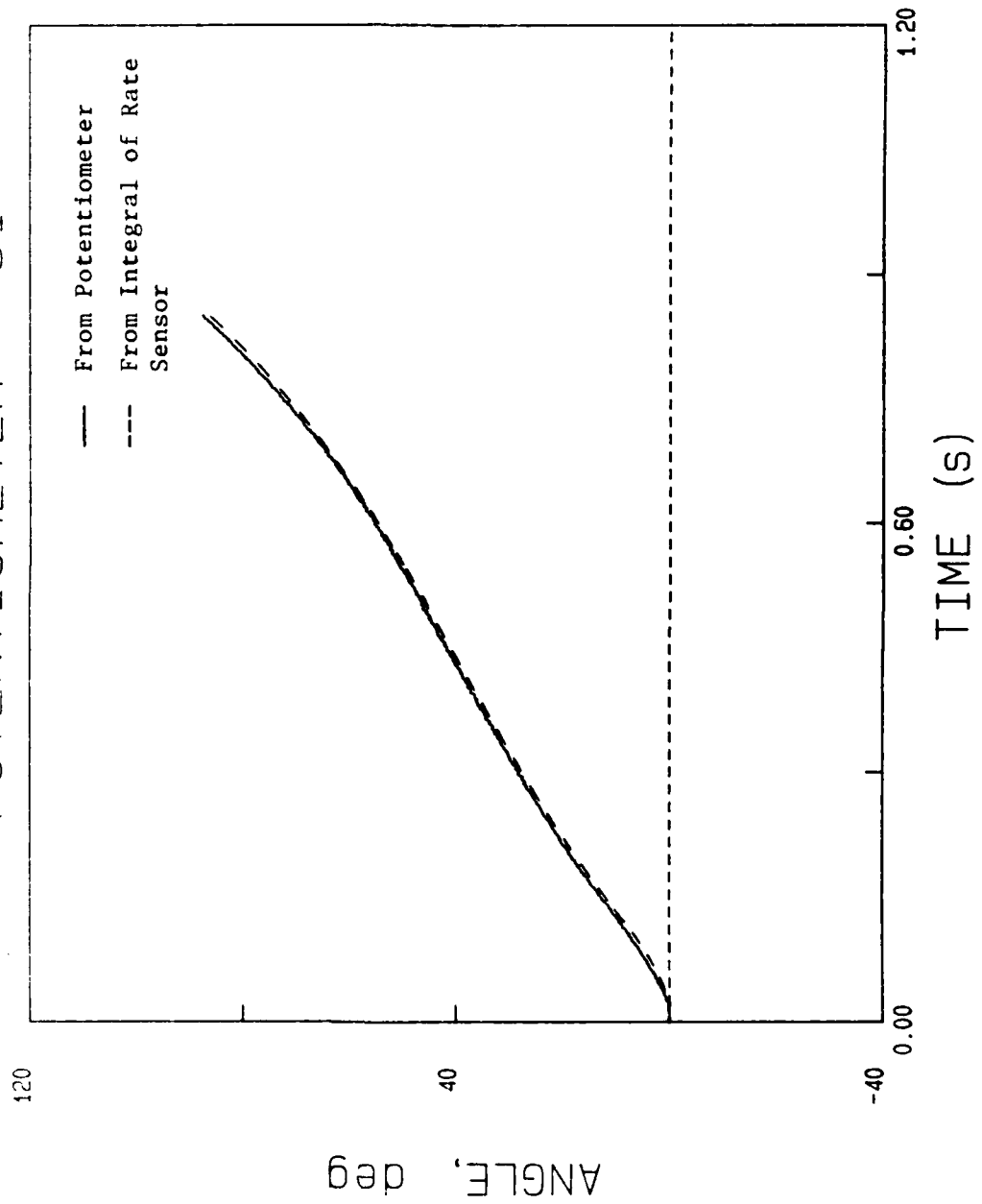


Figure 112. Comparison of the rotation angle obtained by integration of the rate sensor record with that derived from the potentiometer record for Test 31.

ANGULAR ERROR - 31

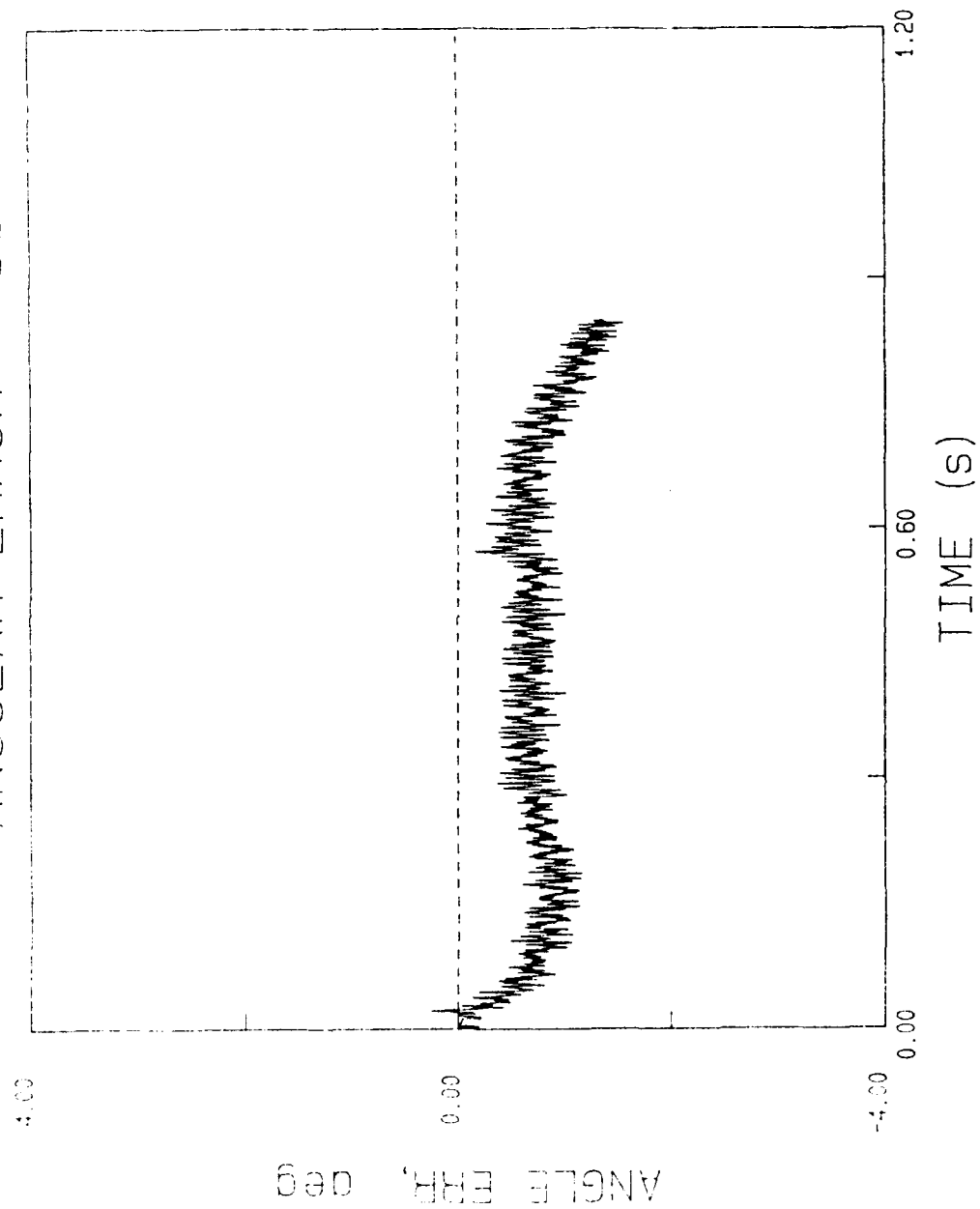


Figure 113. Error in the rotation angle obtained by integration of the rate sensor record for Test 31.

TRAJECTORY OF SENSORS - (3)

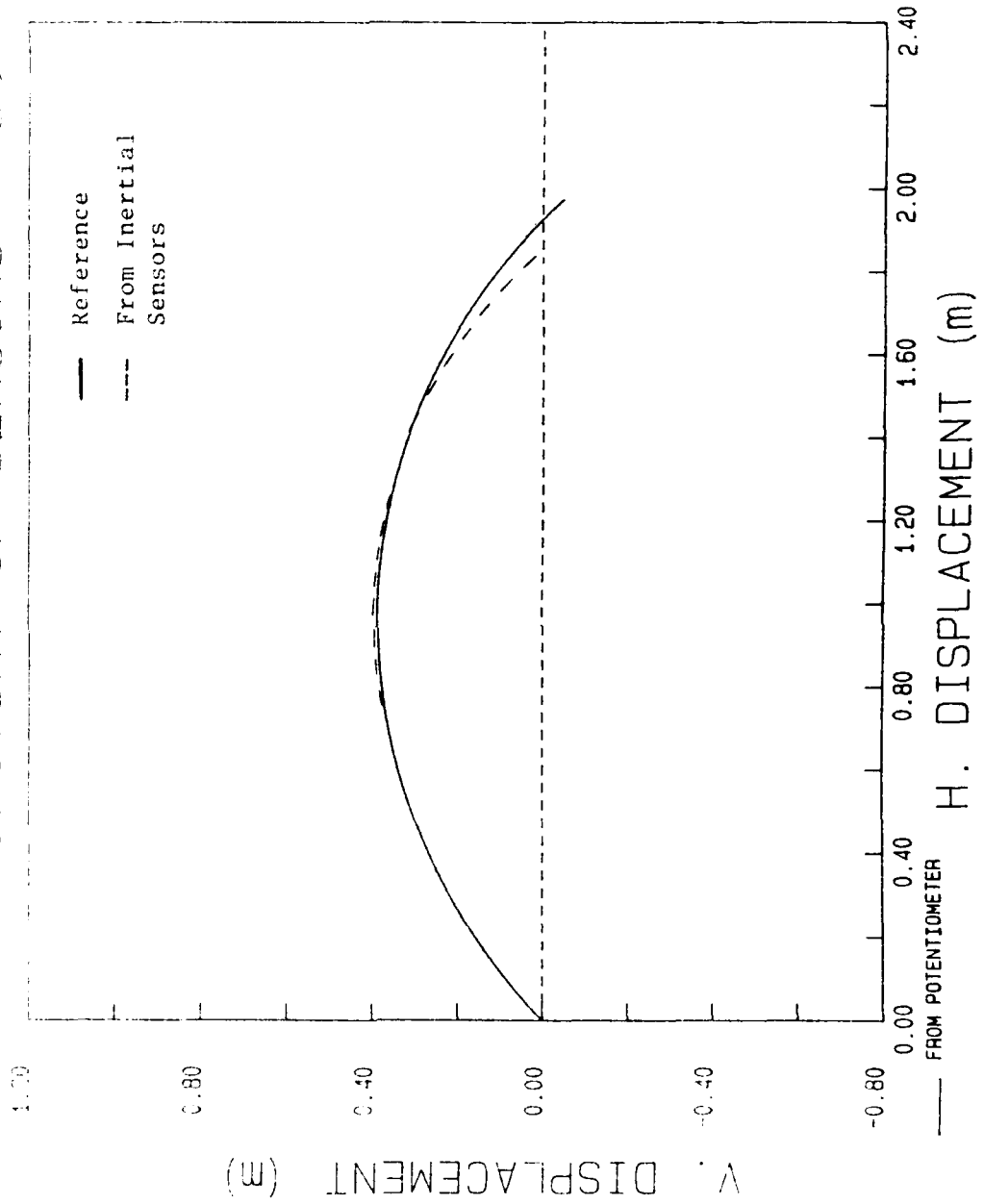


Figure 114. Comparison of the sensor array trajectory for Test 35 derived from the Endevco accelerometers and the Humphrey rate sensor with the reference trajectory derived from the potentiometer record.

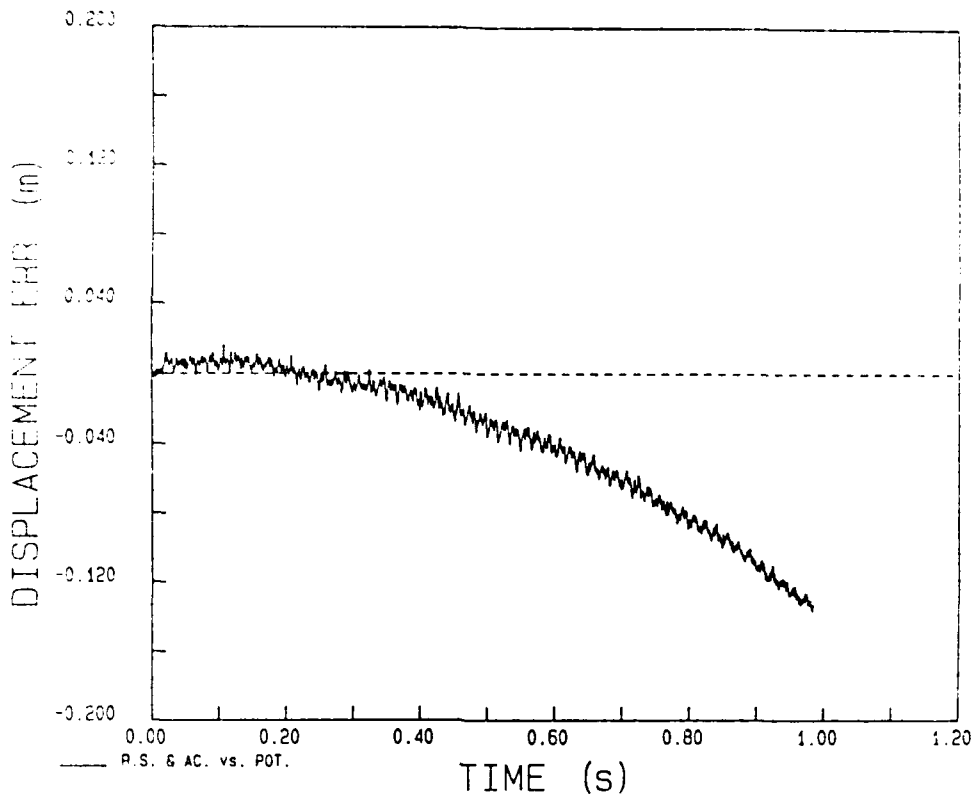


Figure 115. Horizontal displacement error versus time of the sensor array for Test 35.

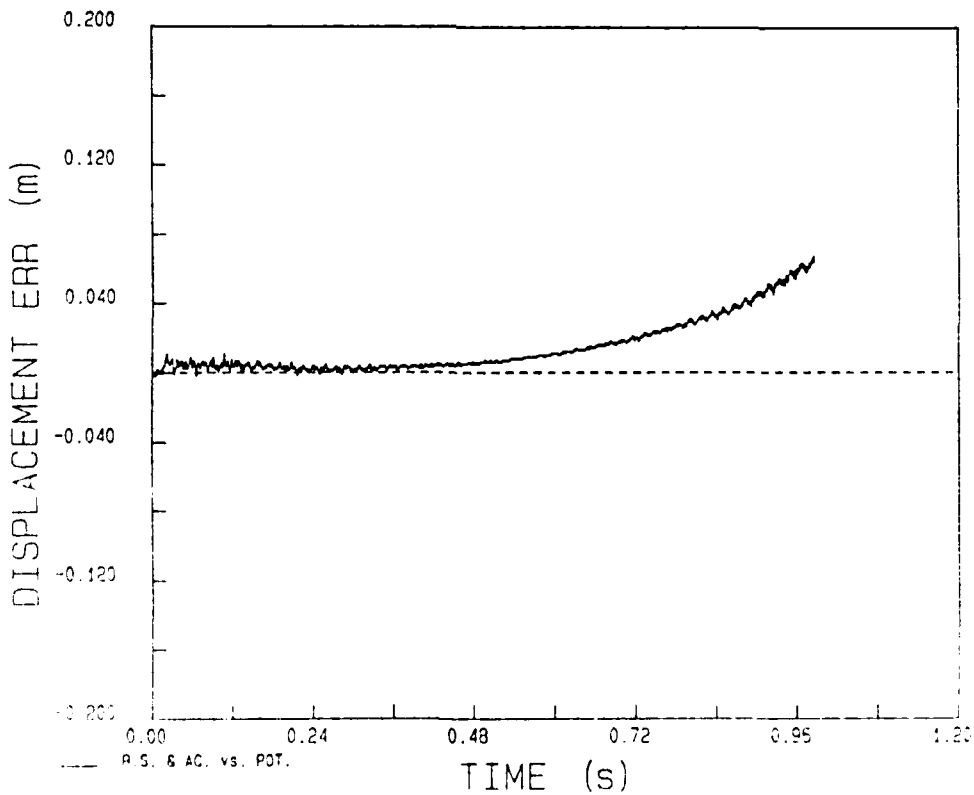


Figure 116. Vertical displacement error versus time of the sensor array for Test 35.

POTENTIOMETER - 35

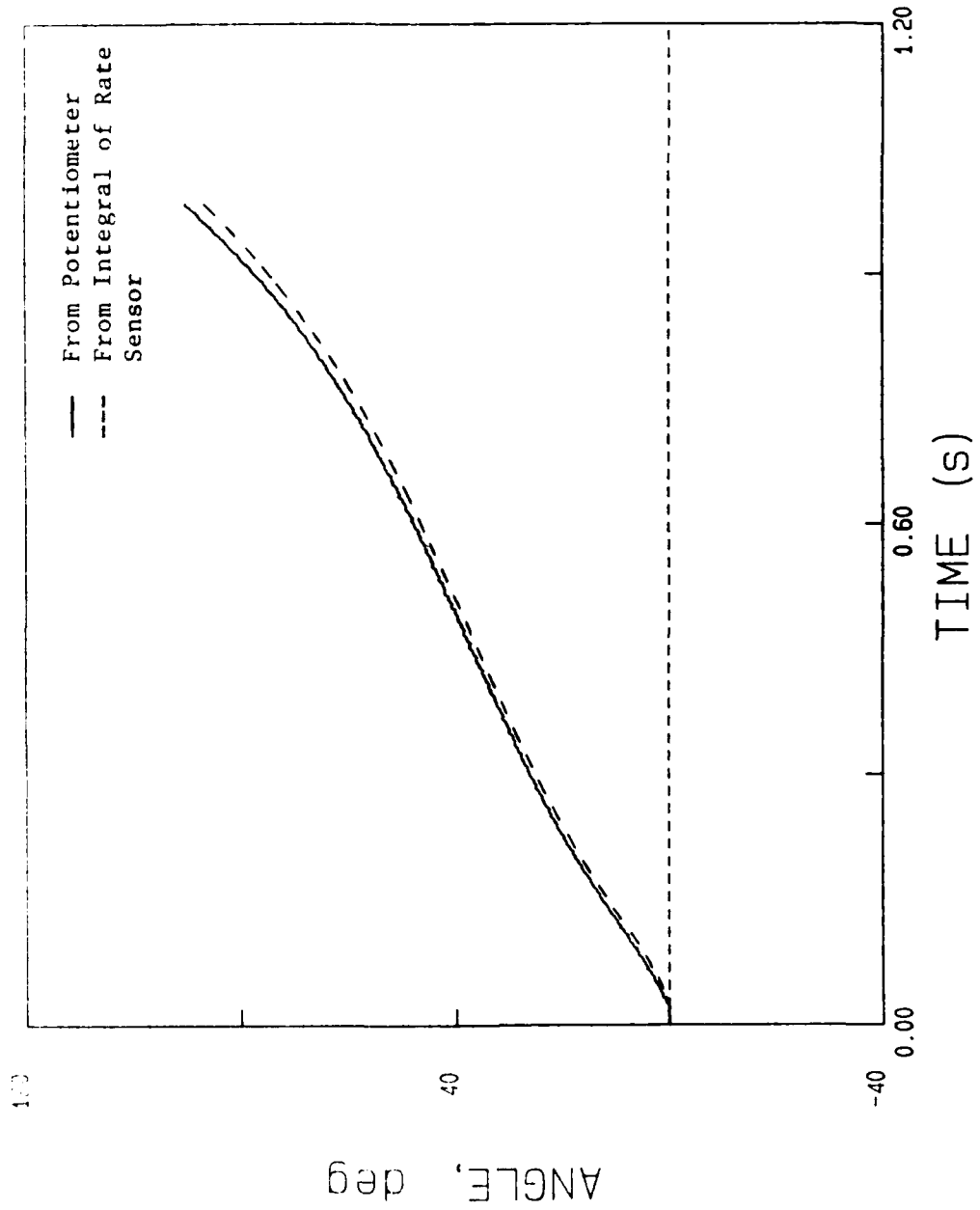


Figure 117. Comparison of the rotation angle obtained by integration of the rate sensor record with that derived from the potentiometer record for Test 35.

ANGULAR ERROR - 35

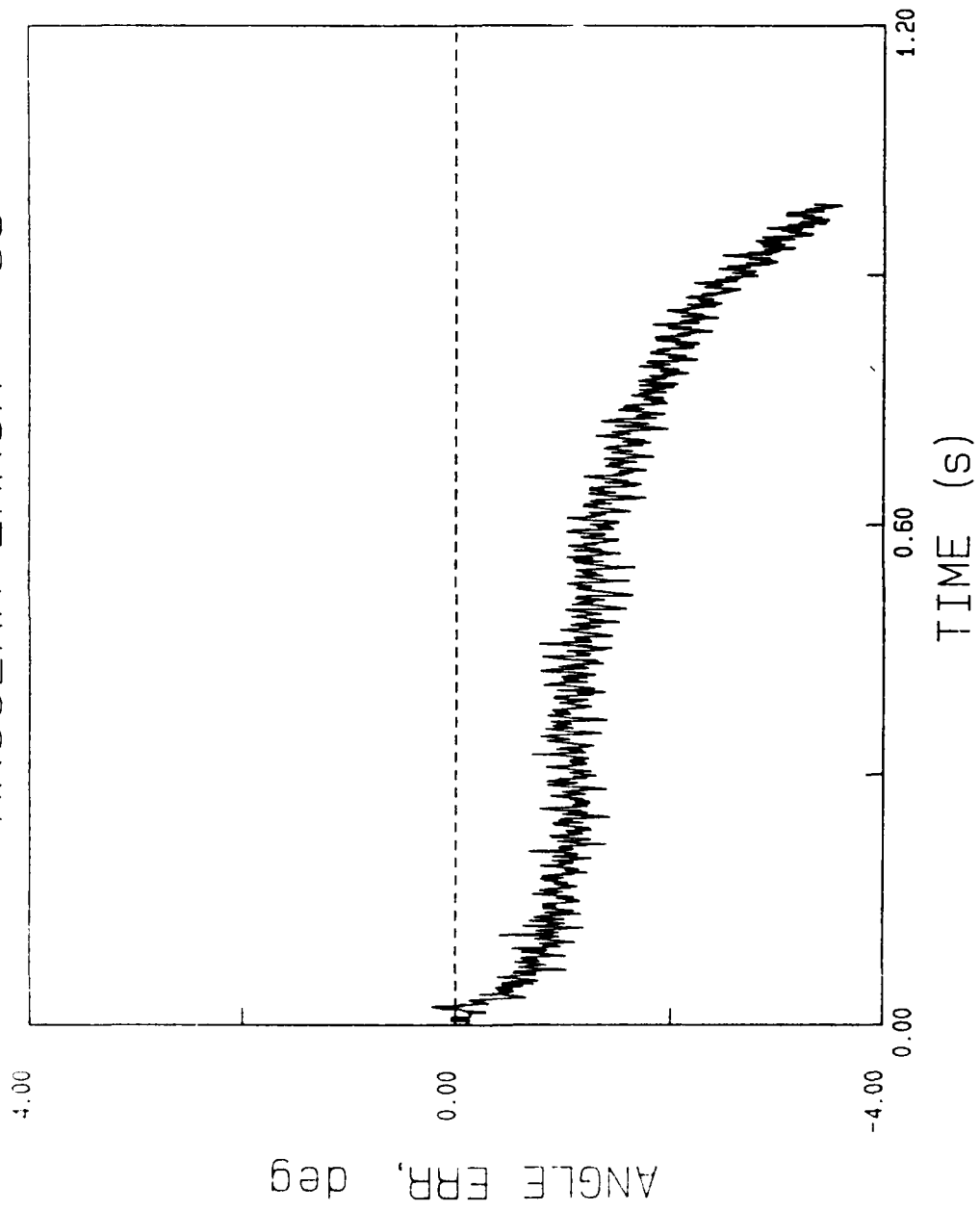


Figure 118. Error in the rotation angle obtained by integration of the rate sensor record for Test 35.

In test 28, the total force in the cable was 1472 Newtons. The peak acceleration was about 21.1 g's.

Figure 127 through 128 show the comparison of the trajectories derived from the potentiometer sensors with that derived from the potentiometer record and the rate sensor. The horizontal and vertical displacement errors, the error in the rotation angle from the integral of the rate sensor agree with that from the potentiometer record, and the error in angle is small.

The errors in the trajectories are large. The errors in rotation angle derived from the integration of the rate sensor record are also large for both tests.

129. Comparison of Curves

The test in Figure 128 produced overturning of the quarter wheel that resembled that of a truck-shelter system struck by blast. Figure 129 shows a comparison of the computed angular velocity of a truck-shelter system, shown in Figure 3, to that measured on Test 28. The initial peaks are about the same value, but the curve from Figure 3 has a faster rise and narrower peak because of faster and longer amplitude initial loading. Qualitatively the curves are the same.

Figure 130 shows the angle versus time curve corresponding to the angular velocity presented in Figure 3 compared to the angle versus time curve for Test 28. The curves agree fairly well. The response of the quarter wheel can be changed by using different springs with different strengths and extension capabilities.

The total force loading the quarter wheel can be adjusted by turning the threaded rods at the rear of the springs. The loads were easily adjusted to be within one unit of the display of the monitoring meter, and was one pound (.45 Newtons).

Tests 28, 29, and 30 had the same initial conditions. Figure 131 shows the comparison of the angular velocities obtained. The tests were performed in succession, and the slight delay in response between the curves indicates that the springs did not recover to their pretest condition after each test. Figure 132 shows a comparison between the angle versus time curves for the three tests. The curves agree very well, but the successive delays are evident, indicating some change in the characteristics of the springs.

The quarter wheel struck stiff plastic tape upon overturning 90 degrees. The angle versus time records from the potentiometer show that the wheel bounced several times. The accelerometers were over-ranged by a large negative acceleration, but recovered and operated during the bounces. The rate sensor immediately produced a negative spike at first impact, and appears not to be near recovery until late in the first bounce or after the second bounce. Therefore, tracking movement in the test facilities using the accelerometer and rate sensor records cannot be carried beyond first impact at about 90 degrees of rotation.

TRAJECTORY OF SENSORS 43

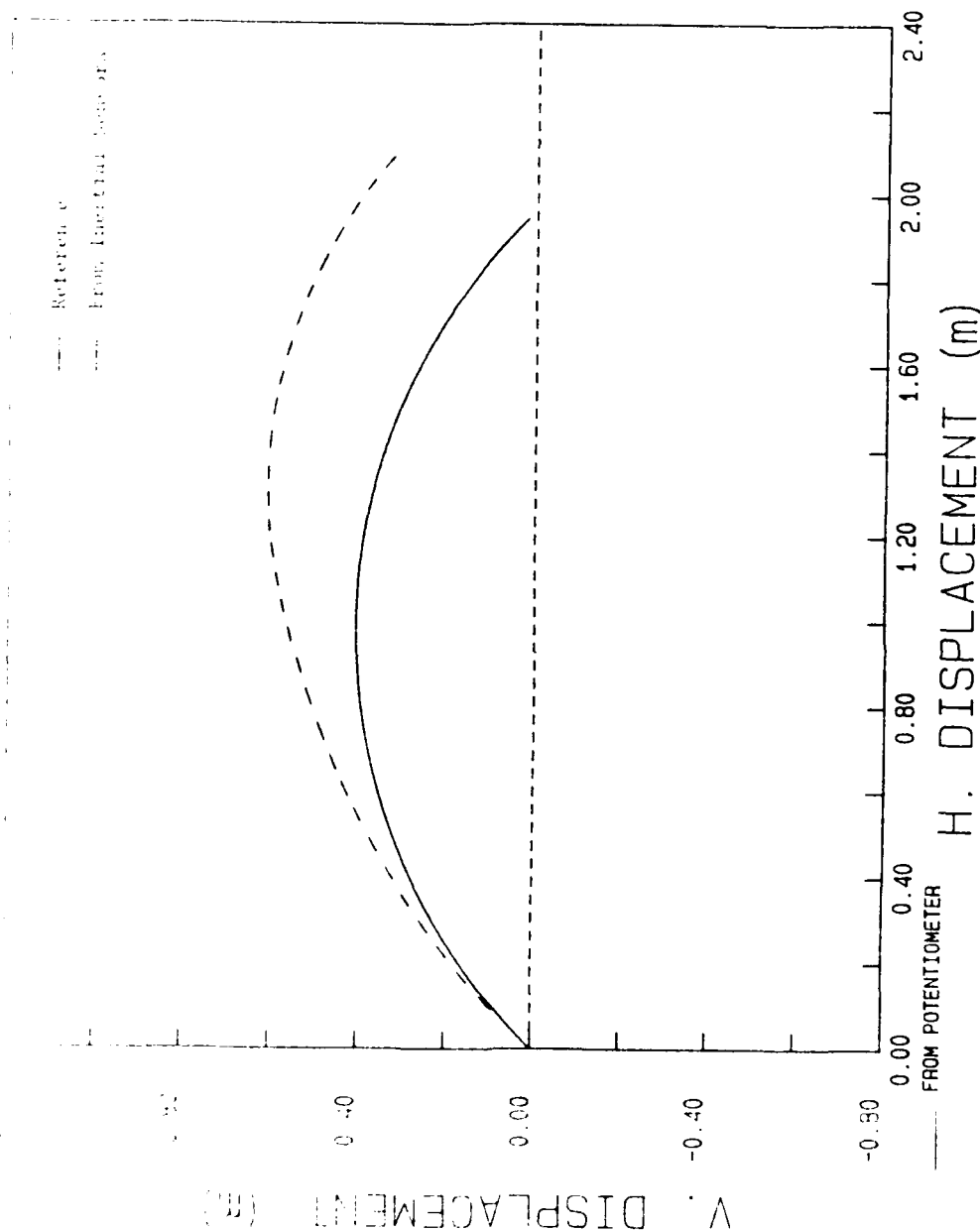


Figure 119. Comparison of the sensor array trajectory for Test 43 derived from the Schaevitz accelerometers and the Humphrey rate sensor with the reference trajectory derived from the potentiometer record.

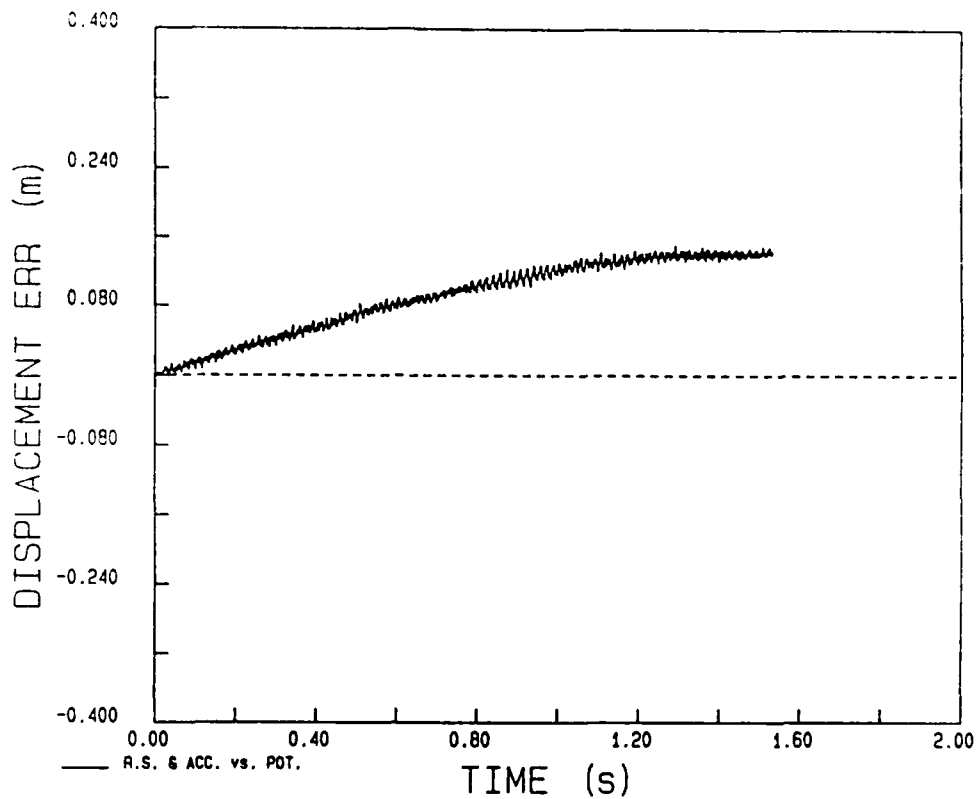


Figure 120. Horizontal displacement error versus time of the sensor array for Test 43.

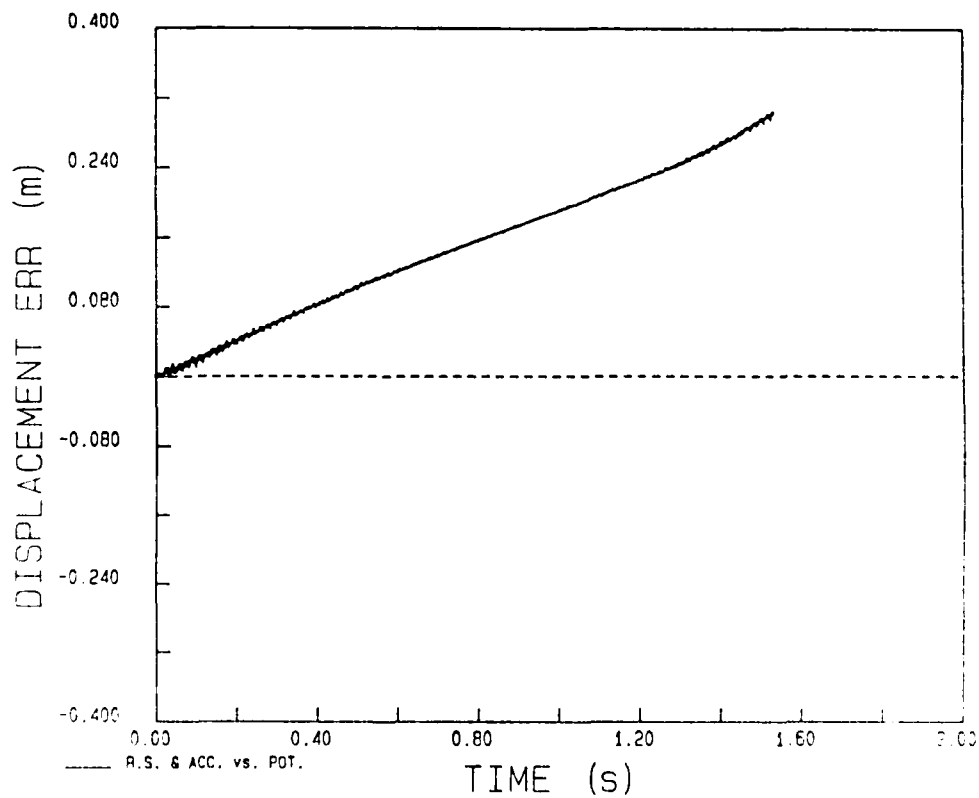


Figure 121. Vertical displacement error versus time of the sensor array for Test 43.

POTENTIOMETER - 43

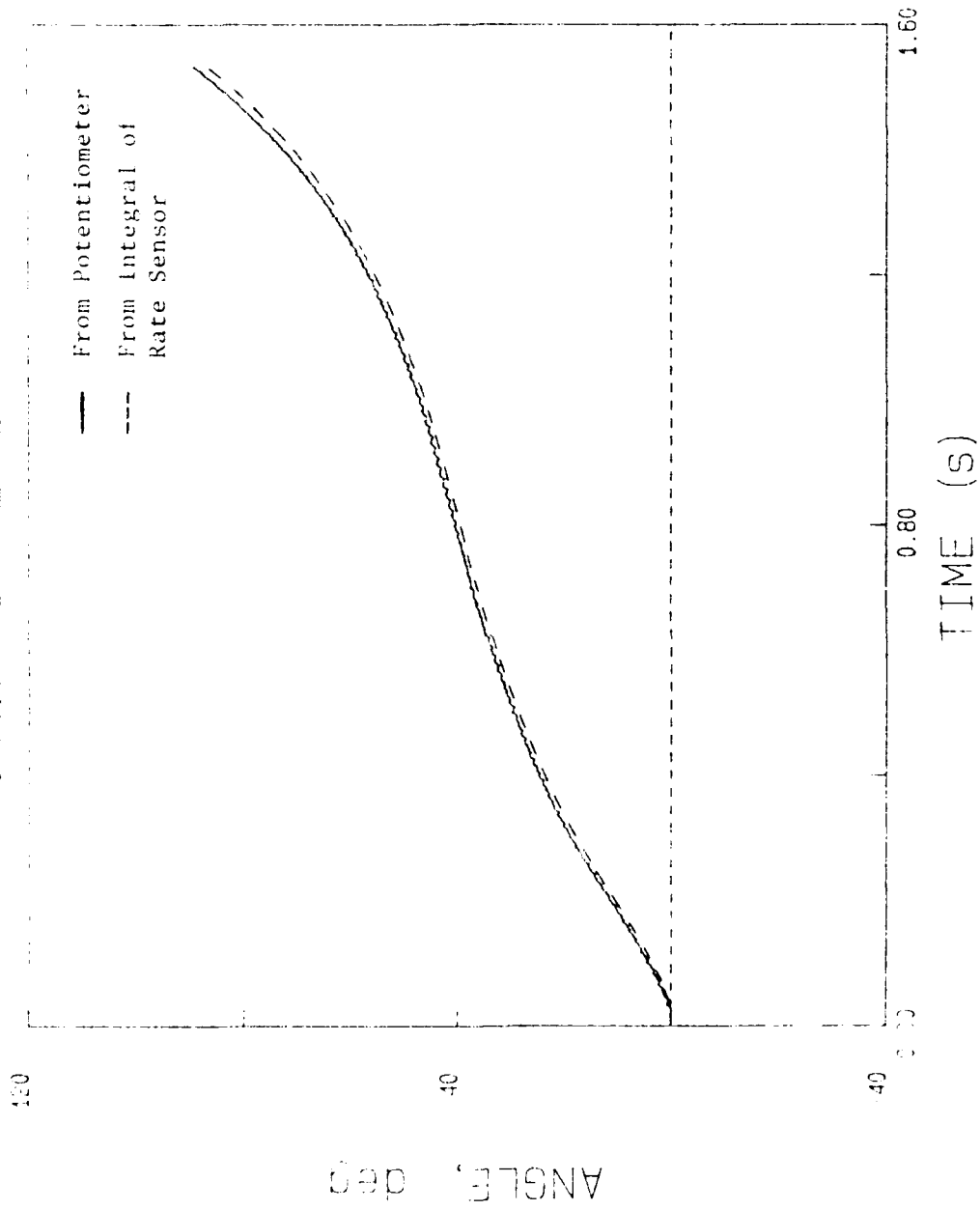


Figure 122. Comparison of the rotation angle obtained by integration of the rate sensor record with that derived from the potentiometer record for Test 43.

ANGULAR ERROR = 43

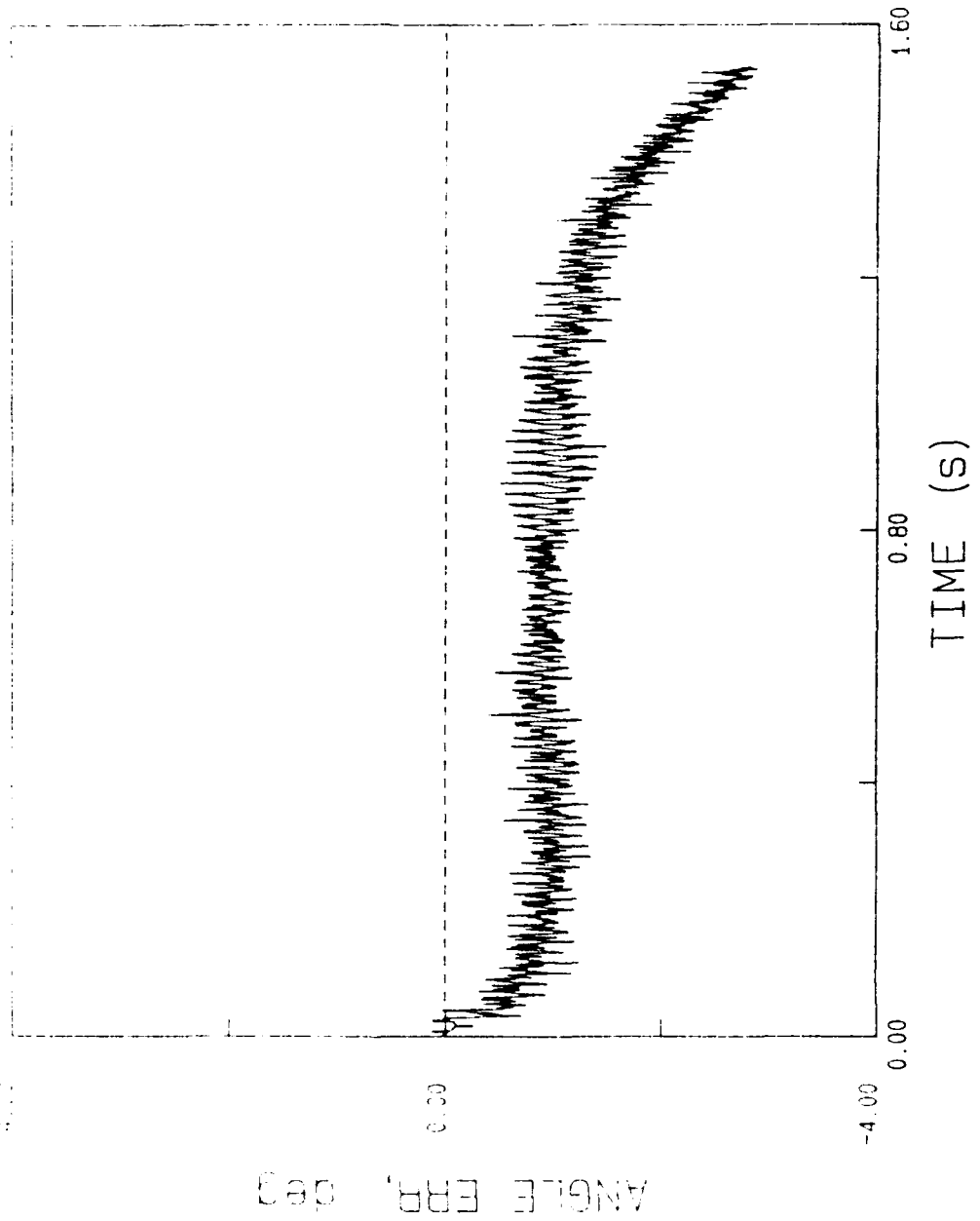


Figure 123. Error in the rotation angle obtained by integration of the rate sensor record for Test 43.

TRAJECTORY OF SENSORS - 48

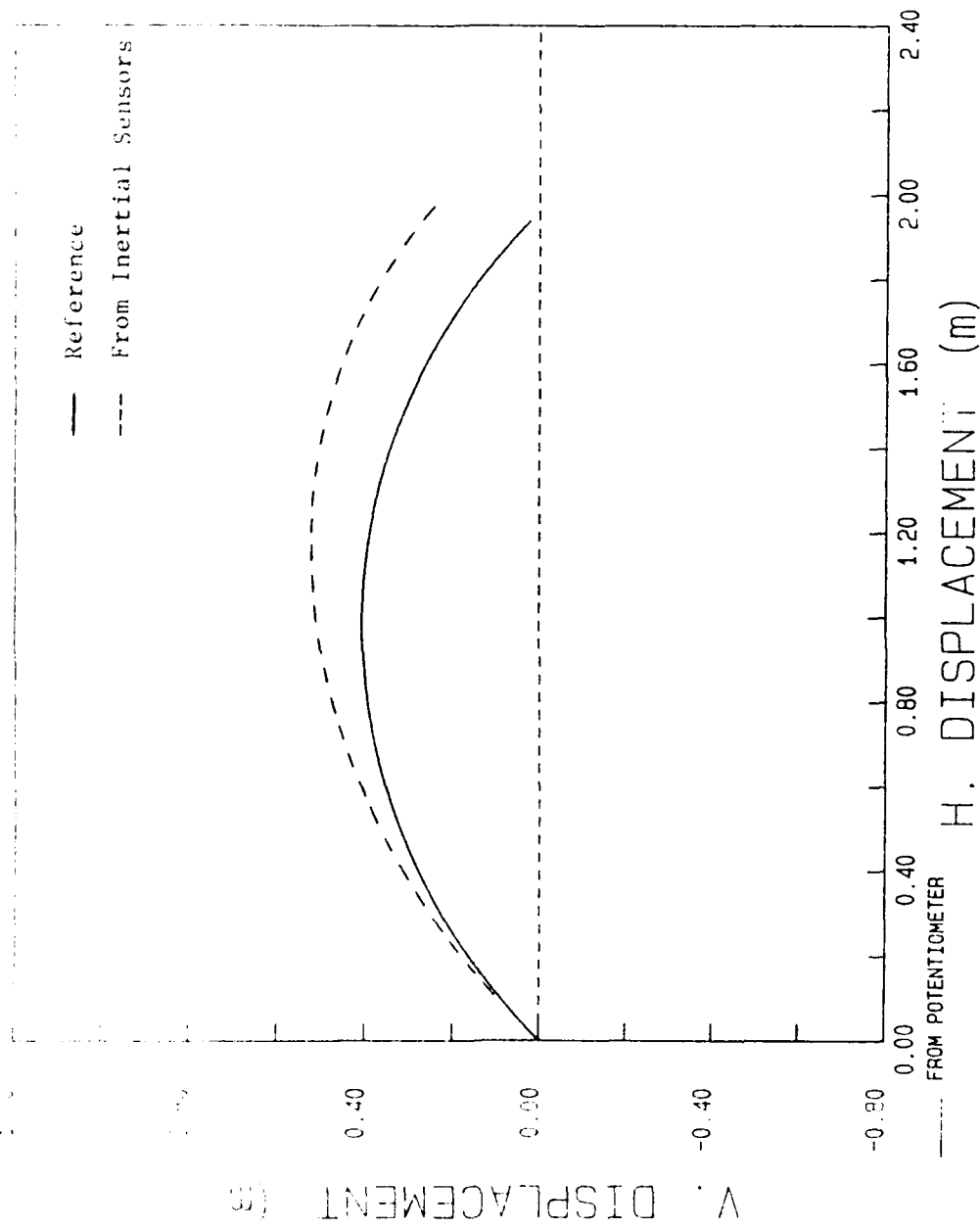


Figure 124. Comparison of the sensor array trajectory for Test 48 derived from the Schaevitz accelerometers and the Humphrey rate sensor with the reference trajectory derived from the potentiometer record.

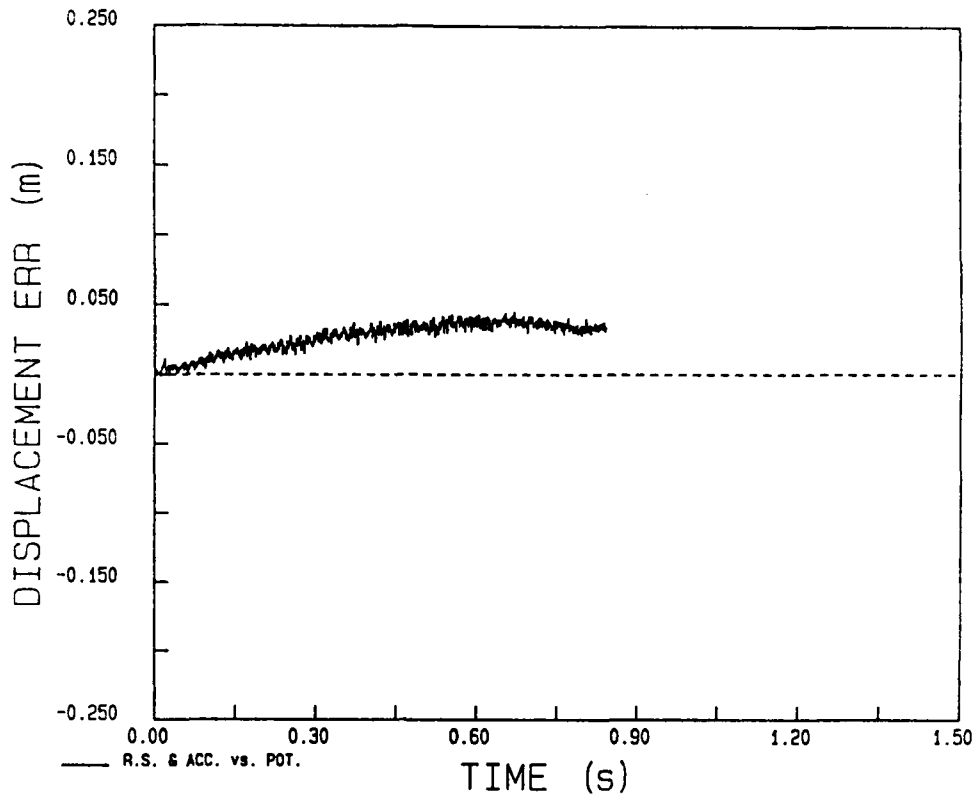


Figure 125. Horizontal displacement error versus time of the sensor array for Test 48.

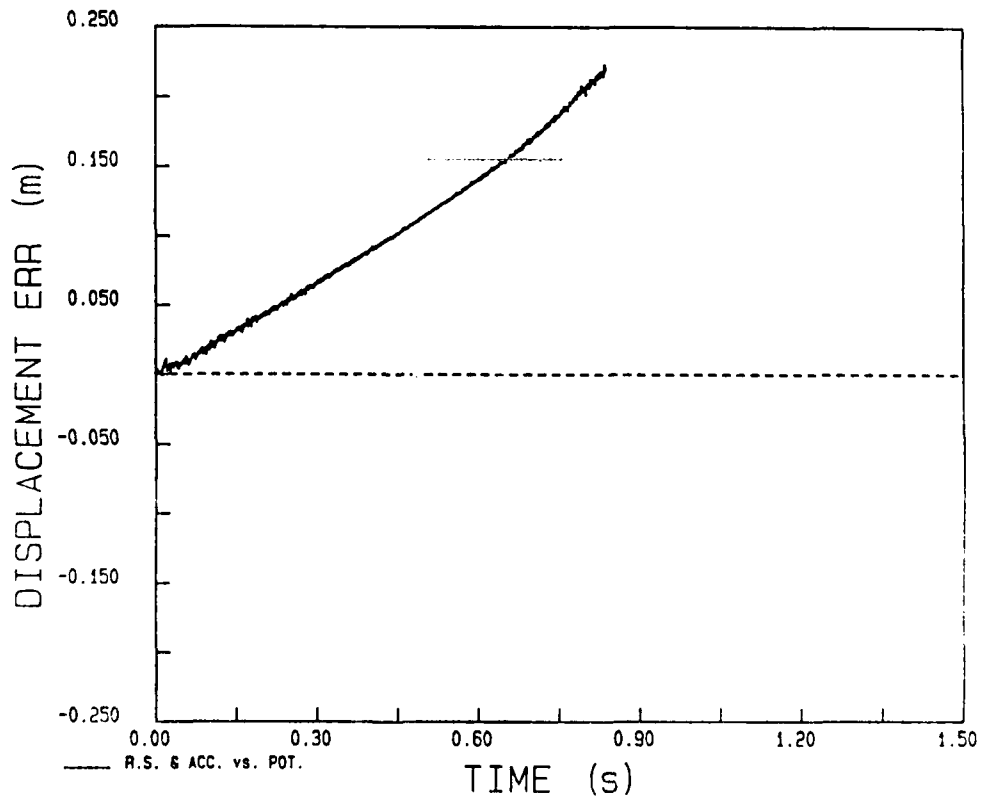


Figure 126. Vertical displacement error versus time of the sensor array for Test 48.

POTENTIOMETER - 48

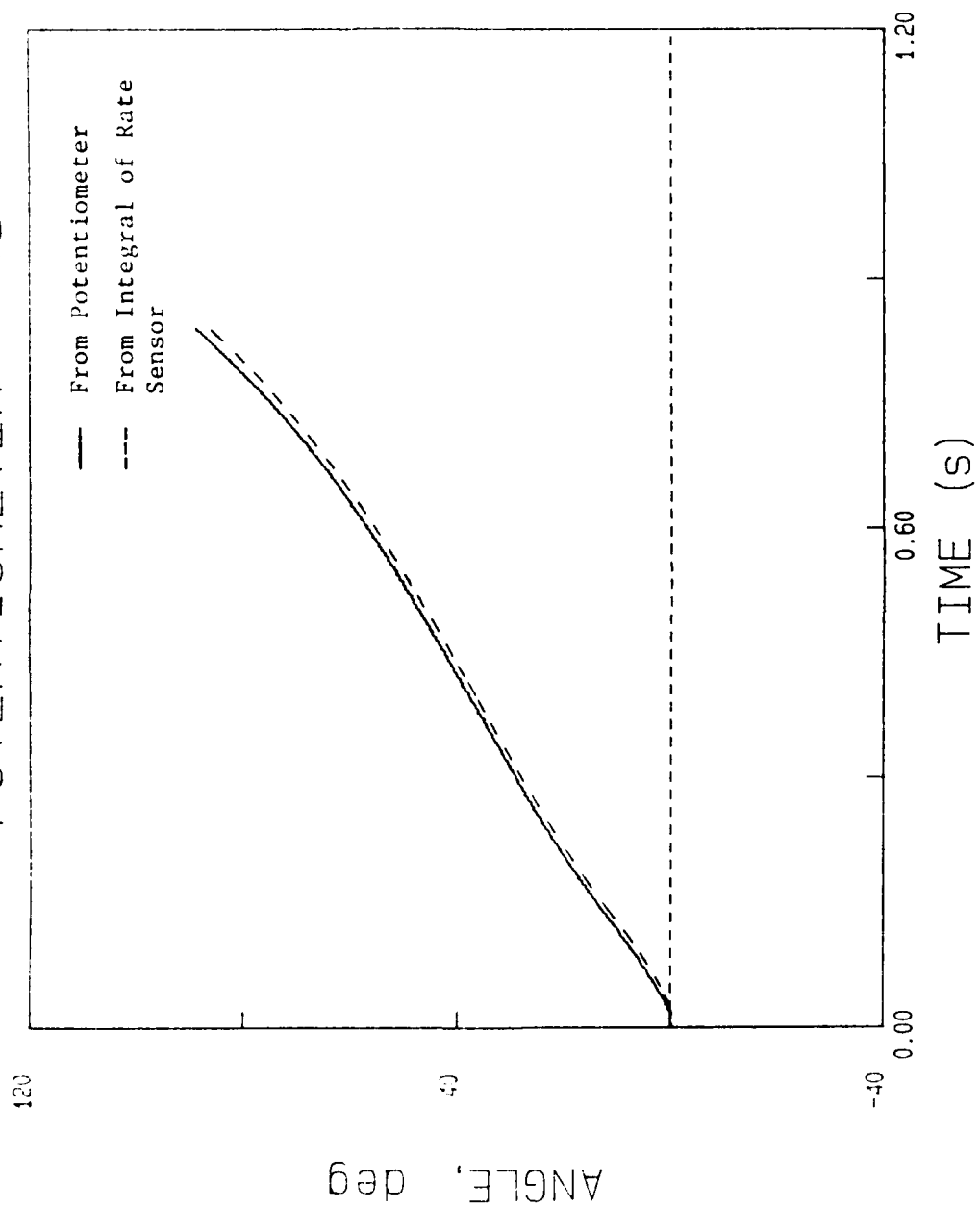


Figure 127. Comparison of the rotation angle obtained by integration of the rate sensor record with that derived from the potentiometer record for Test 48.

ANGULAR ERROR - 48

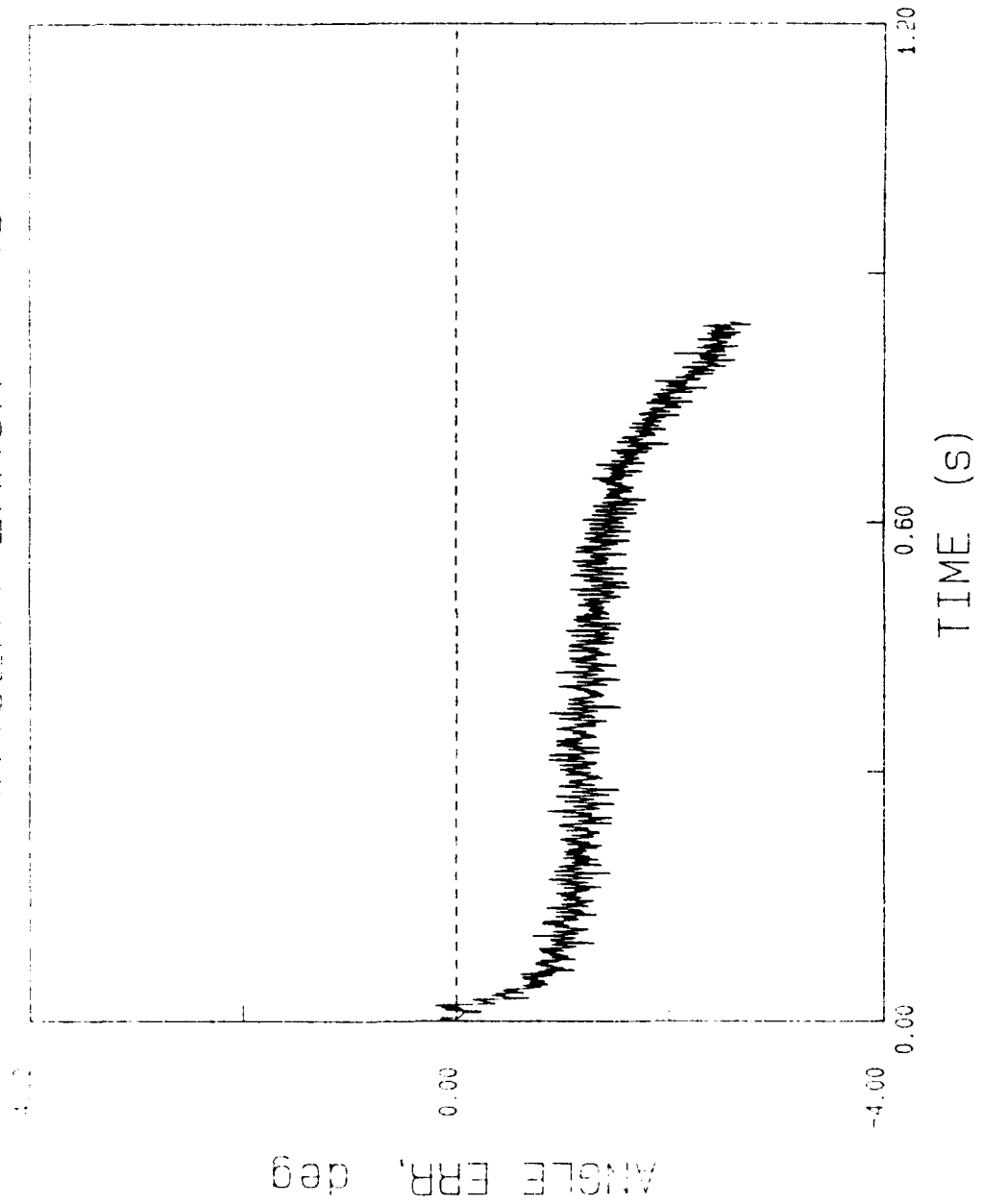


Figure 128. Error in the rotation angle obtained by integration of the rate sensor record for Test 48.

RATE SENSOR - SHOT 28

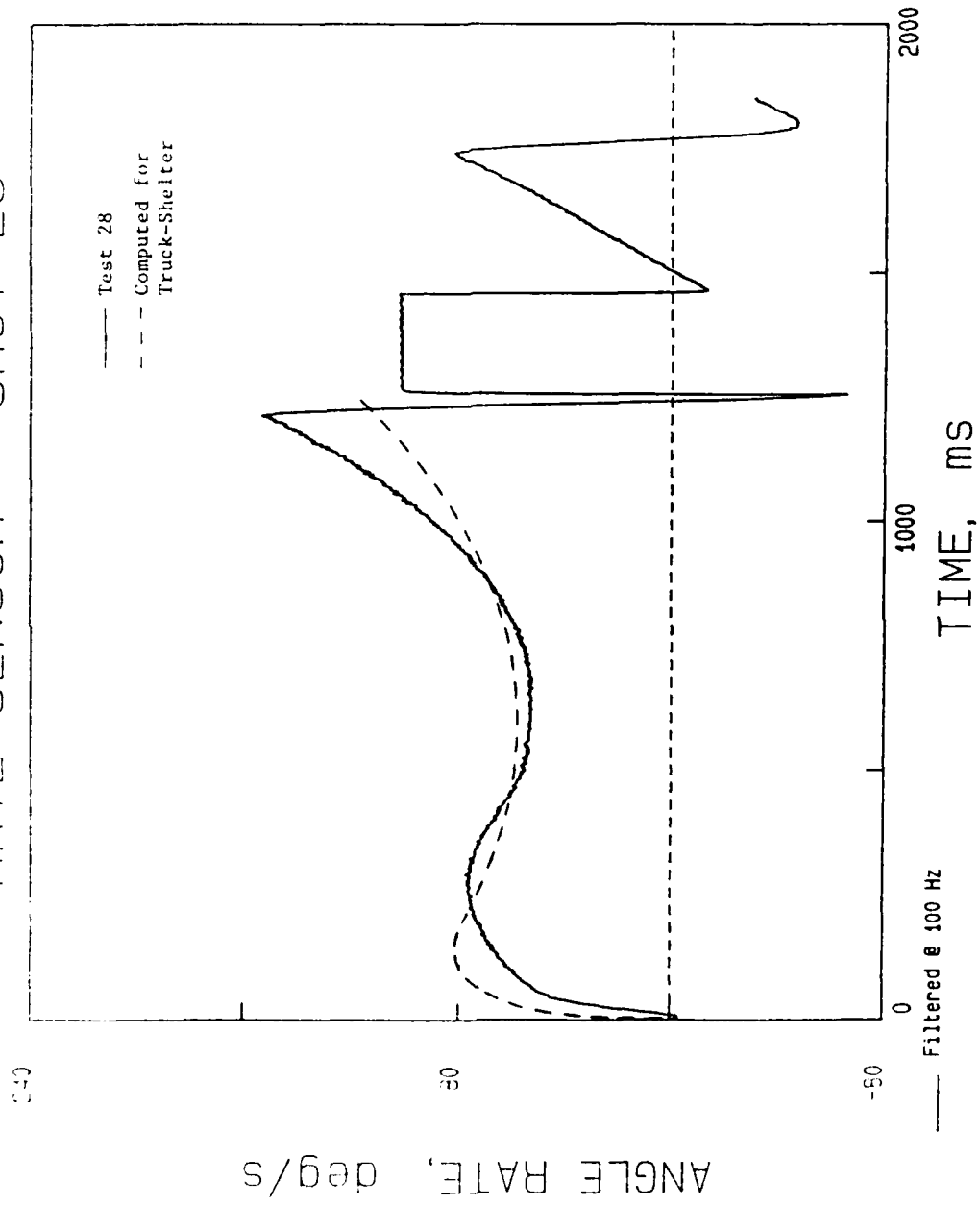


Figure 129. Comparison of computed angular velocity for a truck-shelter system struck by blast with that from Test 28 in the test facility.

POTENTIOMETER - 28

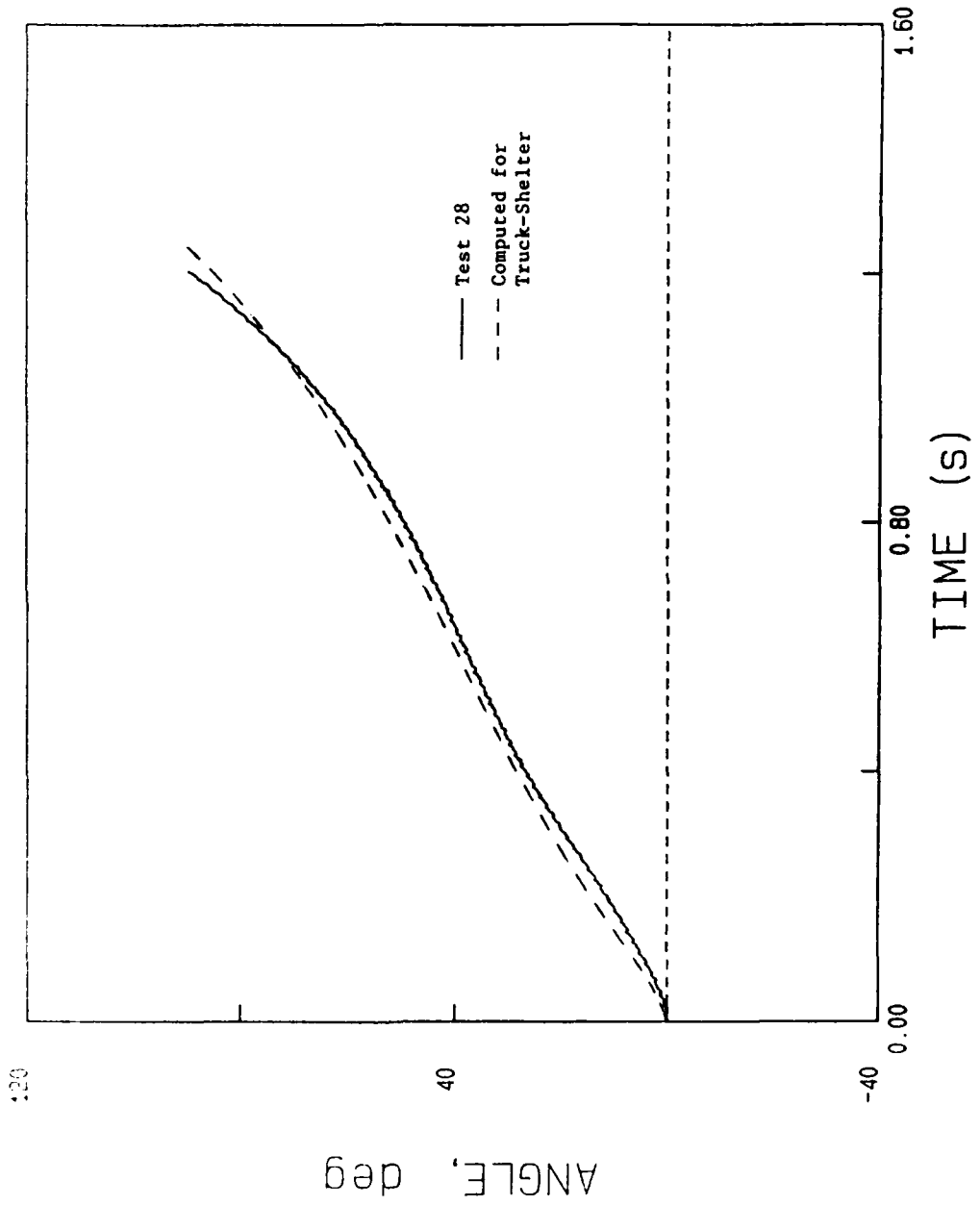


Figure 130. Comparison of computed angle versus time for a truck-shelter system struck by blast with that from Test 28 in the test facility.

RATE SENSOR - SHOT 28

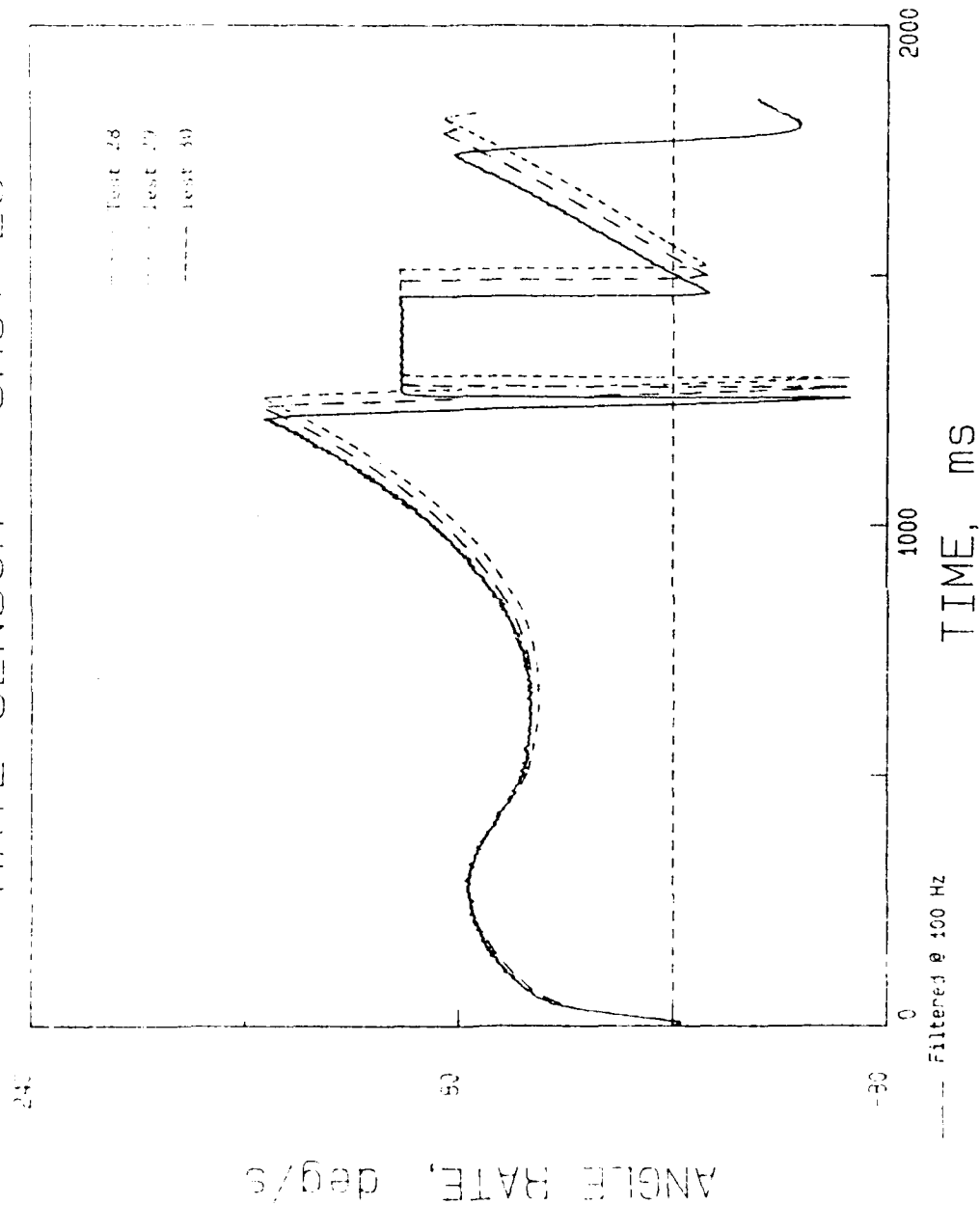


Figure 131. Comparison of measured angular velocities from Tests 28, 29, and 30 in the test facility with the same springs and initial load.

POTENTIOMETER - 28

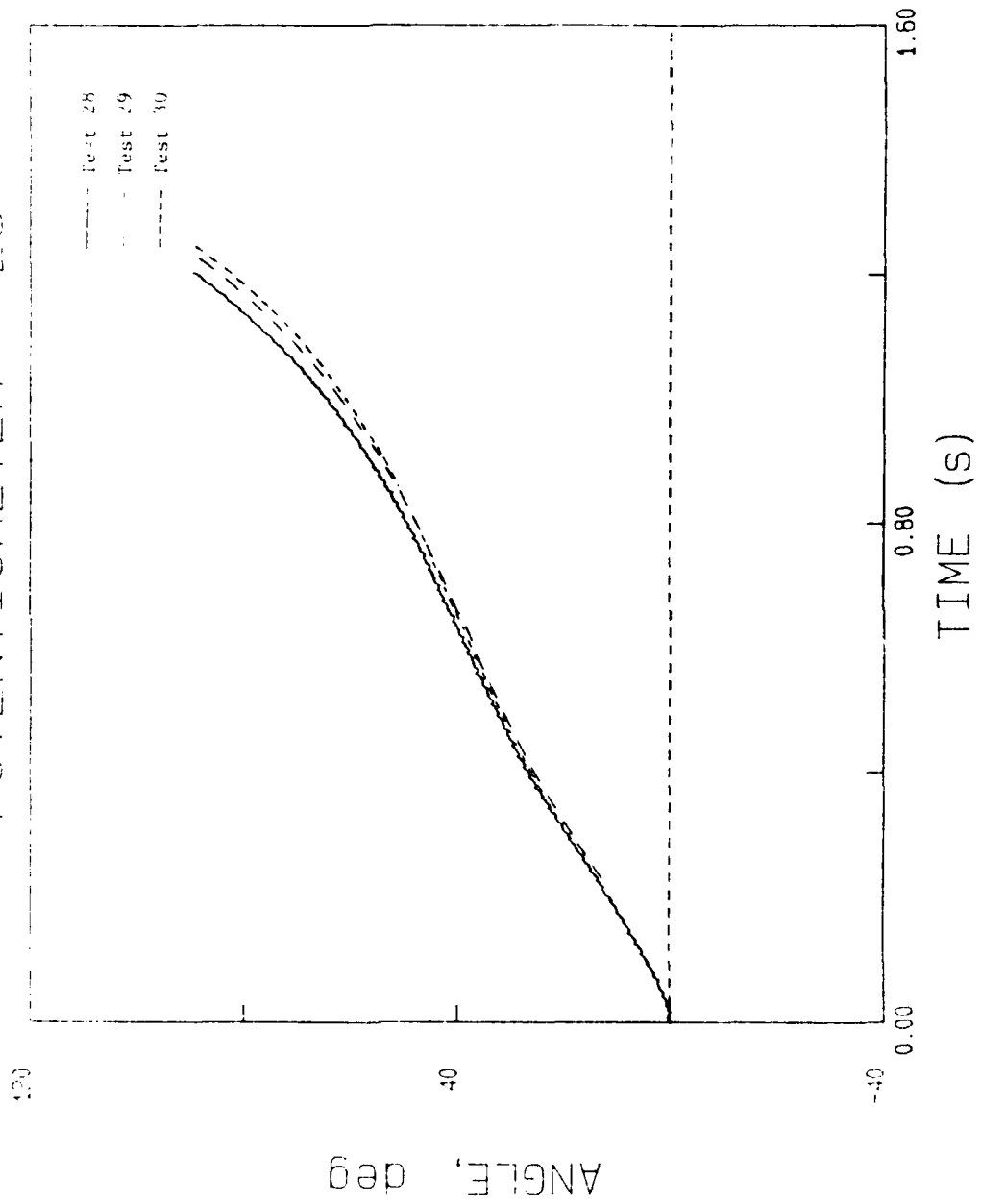


Figure 132. Comparison of measured angle versus time for Tests 28, 29, and 30 in the test facility with the same springs and initial load.

Table 6 lists the errors in the horizontal and vertical displacements at the end of the trajectories in the test facility. Also listed is the error in the rotation angle derived from the integral of the rate sensor record.

The error in the rotation angle at the end of the trajectory ranges from +1.27 to -3.51 degrees. The error could be reduced by correcting for the lag in response time that occurs where the angular velocity is changing rapidly.

There seems to be no distinction in errors between high and low g tests. The Schaevitz accelerometers produced X errors that are about the same as the Endevco X errors. However, the Schaevitz Y errors are larger than the Endevco Y errors. The outputs from both the vertical and horizontal accelerometers are used to obtain X or to obtain Y. At the end of the contract effort, no explanation had been found for these larger errors. The Schaevitz accelerometer has a much lower natural frequency than the Endevco accelerometer, but it is rated for higher accuracy.

The errors from the tests using the Endevco accelerometers seem small enough to warrant further pursuit of an inertial reference system for use on vehicles. The records in the tests reported here were obtained using off-the-shelf sensors, and were processed using a simple time-marching integration program. The accuracy of performance of a sensor array should improve if filters are matched to gage and input waveform characteristics, and if the distortions in the data produced by gage-response characteristics are removed or reduced.

It seems unlikely that a sensor array can track a vehicle struck by blast beyond first impact with the ground, whether the impact is due to overturning or to the return to ground after the vehicle has been airborne.

The sensor array will require packaging so that the arrival of the blast wave at the vehicle does not disable the accelerometers or the rate sensors for more than a few milliseconds, if at all. The test facility at present does not provide an impact at the start of rotation corresponding to that experienced by a vehicle struck by blast.

VIII. REQUIREMENTS FOR AN INERTIAL REFERENCE SYSTEM

The results of the test program indicate that the array of off-the-shelf sensors can track movement in a plane within acceptable error bounds. Figure 133 shows a block diagram of a system for use on a vehicle with six degrees-of-freedom of movement.

The array of accelerometers and rate sensors is packaged separately to minimize the size of the array and facilitate its mounting near the center of gravity of the vehicle.

TABLE 6. ERRORS IN HORIZONTAL X AND VERTICAL Y DISPLACEMENTS AND ROTATION ANGLE θ AT END OF TRAJECTORIES IN THE TEST FACILITY

Test Number	X Error (m)	Y Error (m)	θ Error (deg)
Two Endevco accelerometers, one Humphrey rate sensor			
28	-0.018	0.037	-3.14
29	-0.086	0.025	-1.81
30	-0.145	0.085	-2.20
31	0.036	0.068	-1.20
33	0.023	0.031	-3.37
35	-0.135	0.067	-3.51
Two Schaevitz accelerometers, one Humphrey rate sensor			
43	+0.149	0.305	-2.82
45	-0.051	0.108	-2.60
46	-0.021	0.163	-2.43
48	0.034	0.219	-2.57

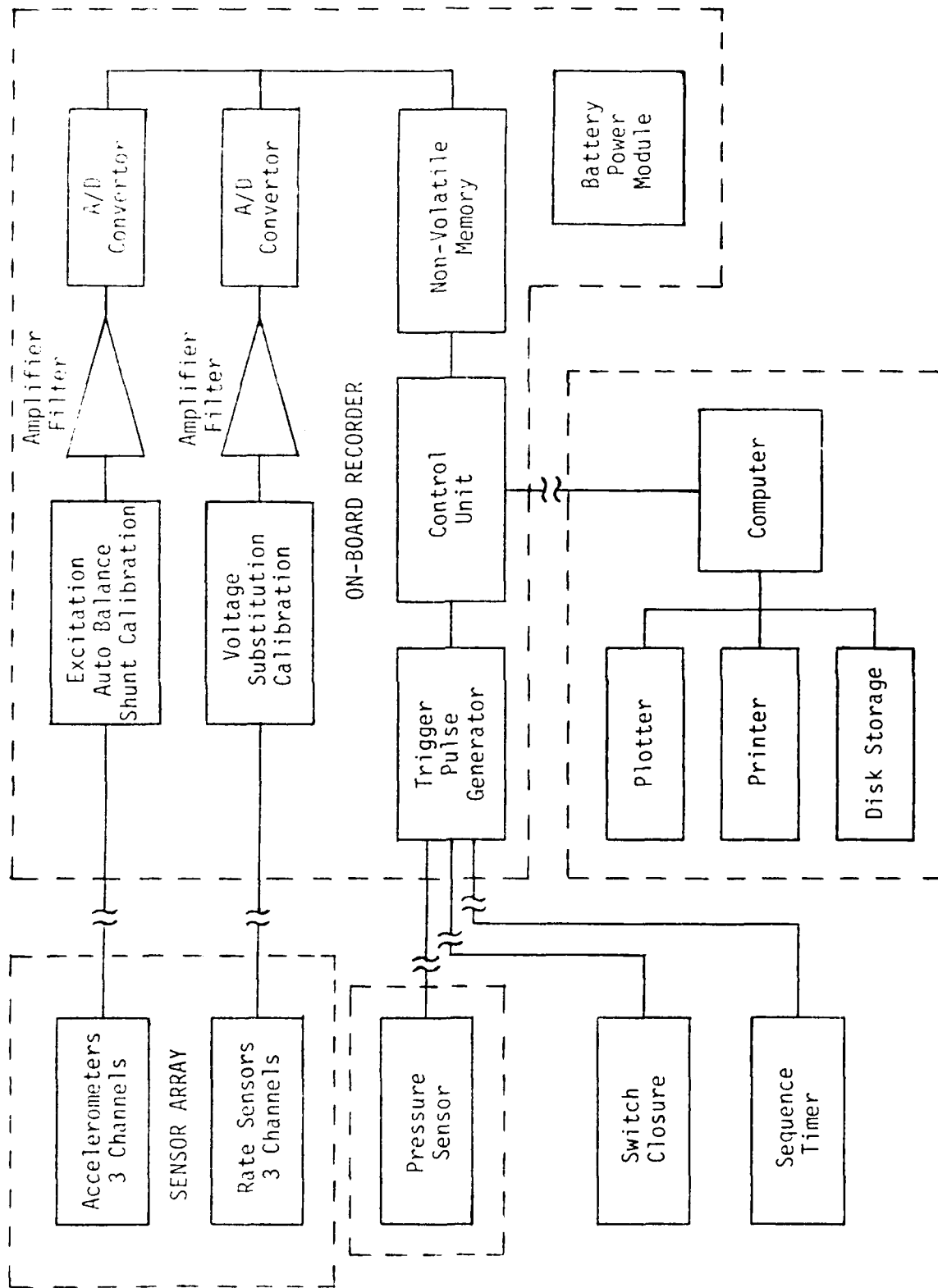


Figure 133. Block diagram of inertial reference system.

The system requires an arming signal prior to the test so that the equipment can warm-up and stabilize. This signal can be provided either by internal programming or hard wire from a sequence timer or manual switch.

A means of triggering the data storage mode at the desired time is required. The pressure sensor provides this signal when the blast wave arrives at its location. The sensor is to be placed on or near the outer surface of the vehicle facing the blast so that the data recording will commence before any sensor response takes place.

Once stored in memory, the data must remain unchanged until the retrieval process takes place. At this time the data is transferred in sequence to the computer where it is stored permanently on a magnetic disk.

An examination of vehicle overturning calculations that were made using the BLOM code showed that a 2 1/2 ton truck-shelter system, an M113 personnel carrier, and the Infantry Fighting Vehicle can require from 2.0 to 3.1 seconds to rotate to an angle at which they almost overturn. These times applied over the yield range for a nuclear explosion from 1 KT to 1000 KT. The time for fall back to the original position or to overturn 90 degrees will be approximately the same. Therefore, to track the full rotational movement of a vehicle under conditions where it is exposed near the threshold for overturning, a recording time of at least seven seconds is required.

The data from the gages are filtered before they are digitized. The filters and sampling rates are selected considering the frequency content of the sensor signals. The records from the Endevco and Schaevitz accelerometers used in the tests described in this report still retained significant oscillations at a frequency of about 250 Hz after passing through a 100 Hz low-pass filter. For reducing the error due to sampling rate to about one percent, the sampling rate should be 5000 Hz or more.

The minimum storage capacity for each channel, considering seven seconds of recording at a rate of 5000 Hz, is 35000 data points. With a storage capacity of 64000 12 bit words, eight seconds of recording could be obtained at a sampling rate of 8000 Hz. Such a sampling rate is fast enough to ensure that no information will be lost due to the sampling process. The sampling times are synchronized for all channels.

The system is computer driven. The computer is used to give directions to the system, insert calibration data, monitor system status, and retrieve data.

For use on a large-scale blast simulation in the field, the system should be capable of operating unattended for a period of 72 hours, where activation for a single event may occur within the first 48 hours, and data may not be retrieved for another 24 hours.

Table 7 lists characteristics of the system. There are several commercially available systems that may meet the hardware requirements after some modifications. However, the software must be developed.

XI. CONCLUSIONS

After a review of the literature, the conclusion was made that the best combination of sensors for an inertial reference system for tracking the movement of a vehicle struck by blast is three linear accelerometers and three angular rate sensors. This conclusion was made assuming that gages with satisfactory response characteristics can be found.

Before proceeding with building a complete six degrees-of-freedom inertial reference system, it is highly desirable to verify the tracking capability of sensor arrays for a simpler system.

It was found possible to construct a test facility that would simulate the overturning of a vehicle struck by blast. The required sensor array for tracking rotation in a plane is two linear accelerometers and one angular rate sensor.

Two arrays were assembled and tested on the test facility. One used Endevco accelerometers and the other used Schaevitz servo accelerometers. After testing the sensor arrays in the test facility, it was concluded that the sensor array with off-the-shelf Endevco accelerometers and a Humphrey rate sensor tracked displacement and rotation in a plane within acceptable error bounds.

Other than filtering with a 100 Hz low-pass filter, no preprocessing or modification of the gage records was performed. The accuracy of performance of the sensor array can be improved if filters are matched to gage and input waveform characteristics, and if the distortions in the data produced by gage response characteristics are removed or reduced.

The results of the tests show that the development of a complete inertial reference system is worth pursuing. The general requirements for such a system were determined.

Because of the large signals generated on the gage records by impact of the vehicle with the ground, an inertial reference system cannot be expected to track the vehicle after the first impact with the ground.

The sensor array with the Schaevitz accelerometers did not track displacement satisfactorily. At the time of the end of the contract, no explanation for the large error had been found. The Schaevitz accelerometer has a much lower natural frequency than the Endevco accelerometer, but is rated for higher accuracy.

The test facility was simple to use and performed well. The means of holding the restraint cable needs to be improved to minimize the distortion of the waveforms.

TABLE 7. CHARACTERISTICS OF INERTIAL REFERENCE SYSTEM
FOR TRACKING THE BLAST OVERTURNING OF VEHICLES

Physical Construction

- * Packaged as two components connected by electrical cable. One component is the sensor array, the other is the recording and power package.
- * Sensors mounted for mechanical filtering of vibration induced by blast
- * Both components of rugged, shock- and vibration-resistant construction

Gages

- * Three linear accelerometers (Endevco)
- * Three rate sensors (Humphrey, Inc.)

Memories

- * Non-volatile
- * Minimum 64K 12 bit words per channel

A/D Converters

- * 12 bit
- * 4000 and 8000 Hz sampling rates
- * Synchronized

Operating Modes

- * Activated by manual switch, sequence timer, or internal clock-controlled program
- * Armed by manual switch, sequence timer, or internal clock-controlled program
- * Triggered for data storage by pressure sensor signal, manual switch, sequence timer, or internal clock-controlled program

Control Unit

- * Controls operation of system components
- * Receives external signals and instructions
- * Has capability for internal clock-driven program

TABLE 7. CHARACTERISTICS OF INERTIAL REFERENCE SYSTEM FOR TRACKING BLAST OVERTURNING OF VEHICLES (CONTINUED)

Calibration

- * Control unit directed
- * Use of shunt resistor for accelerometer channels
- * Use of voltage substitution for rate sensor channels

Power Supply

- * Self-contained, rechargeable batteries
- * Adequate to support system for 72 hours for a single event test, with the single event occurring in the first 48 hours
- * Adequate to maintain memory for months

Computer

- * Delivers instructions to control unit
- * Interrogates system to monitor status
- * Reads data from system and stores data on disks
- * Processes records to remove noise and correct for sensor distortions
- * Computes movement of vehicle

Software

- * Available to perform filtering, noise removal, spectral analysis and waveform reconstitution, and corrections for sensor-introduced distortions
- * Program to utilize corrected records to derive displacement and orientation versus time of the vehicle

LIST OF REFERENCES

1. "Strap-Down Inertial Systems," AGARD Lecture Series No. 95, AGARD-LS-95, Advisory Group for Aerospace Research and Development, North Atlantic Treaty Organization, 7 rue Ancelle, 92200 Neuilly sur Seine, France, May 1978. ADA055778
2. Mital, N.K. and King, A.I., "Computation of Rigid-Body Rotation in Three-Dimensional Space From Body-Fixed Linear Acceleration Measurements," Transactions of the ASME, Journal of Applied Mechanics, Vol 46, December 1979, pp 925-930.
3. McMaster, D.K., "The Development of an Accelerometer System for Measuring Pelvic Motion During Walking," Ph.D. Dissertation, University of Oxford, 1979. AD-A088579.
4. Jeffers, Jr., M.F., "Analytical Methods for Determining the Motion of a Rigid Body Equipped with Internal Motion-Sensing Transducers," DTNSRDC-76-0041, David W. Taylor Naval Ship R&D Center, Bethesda, Maryland, October 1976.
5. Becker, E. and Willems, G., "An Experimentally Validated 3-D Inertial Tracking Package for Application in Biodynamic Research," Proceedings of the Nineteenth Stapp Car Crash Conference, San Diego, CA, 17-19 November 1975, pp 899-930.
6. Willems, G., "A Detailed Performance Evaluation of Subminiature Piezo-Resistive Accelerometers," Proceedings of the 23rd ISA International Instrumentation Symposium, 1-5 May 1977, pp 531-540.
7. Willems, G., "A Detailed Evaluation of the Endevco Model 7302 Angular Accelerometer," NBDL-83R009, Naval Biodynamics Laboratory, New Orleans, LA, August 1983.

APPENDIX A

DATA REDUCTION PROGRAM

The following program was written and compiled on the IBM PC AT using version 1.10 of the Ryan-McFarland RM/FORTRAN language compiler.

TEST FIXTURE DATA REDUCTION
ABERDEEN RESEARCH CENTER
NOEL H. ETHRIDGE

PROGRAM DESCRIPTION

THIS PROGRAM IS INTENDED TO COMPUTE THE VERTICAL AND HORIZONTAL MOVEMENT OF A SENSOR ARRAY ROTATING IN A VERTICAL PLANE ABOUT A FIXED AXIS. THE SENSOR ARRAY IS MOUNTED ON A FIXTURE THAT IS ESSENTIALLY A WHEEL. THE WHEEL IS LOADED BY A CABLE ATTACHED TO ITS PERIPHERY AND HELD IN PLACE BY ANOTHER CABLE. AT START THE RESTRAINT CABLE IS SUDDENLY RELEASED AND THE WHEEL ROTATES THROUGH APPROXIMATELY 90 DEGREES. THE SENSOR ARRAY MOVES THROUGH A KNOWN ARC. THE OBJECT OF THE TEST AND THIS COMPUTATION IS TO COMPARE THE TRAJECTORY OF THE SENSOR ARRAY AS DETERMINED FROM THE SENSOR RECORDS WITH THAT DETERMINED BY OTHER MEANS, SUCH AS A COMPUTATION USING THE MEASURED ANGLE OF ROTATION AND THE RADIUS FROM THE ROTATION AXIS TO THE SENSOR ARRAY.

THE ARRAY CONSISTS OF TWO LINEAR ACCELEROMETERS AND ONE ANGULAR RATE SENSOR. ONE ACCELEROMETER IS INITIALLY VERTICAL AND THE OTHER HORIZONTAL. OTHER SENSORS USED ARE A LOAD CELL TO MEASURE THE FORCE IN THE CABLE AND A PRECISION POTENTIOMETER ATTACHED TO THE ROTATION AXIS TO MEASURE ROTATION ANGLE.

THE ANGULAR VELOCITY FROM THE RATE SENSOR IS INTEGRATED TO OBTAIN THE ANGLE OF ROTATION. THIS ANGLE IS USED TO CORRECT THE READINGS OF THE ACCELEROMETERS FOR THE GRAVITY FIELD, AND TO CALCULATE THE HORIZONTAL X AND VERTICAL Y COMPONENTS OF ACCELERATION FROM THE CORRECTED ACCELEROMETER RECORDS. THE X AND Y COMPONENTS OF ACCELERATION ARE DOUBLE INTEGRATED TO OBTAIN X AND Y VELOCITIES AND DISPLACEMENTS.

AN ALTERNATIVE COMPUTATION IS PERFORMED IN WHICH THE ANGLE TO CORRECT THE GRAVITY FIELD AND TO DETERMINE THE X AND Y COMPONENTS IS OBTAINED FROM THE POTENTIOMETER RECORD. THE COMPUTED MOVEMENT DERIVED USING THE ROTATION ANGLE MEASURED BY THE POTENTIOMETER AND THE RADIUS TO THE SENSOR IS PRESENTED AS A REFERENCE FOR EVALUATION OF THE RESULTS DERIVED FROM THE SENSOR ARRAY. LAST RECORD IS 9999 9999 9999 9999 9999.

DEFINITIONS OF PARAMETERS

C ATITLE = IDENTIFICATION OF TEST, DATE
 C GAGES = GAGE DATA
 C SPRNGS = SPRING DATA
 C TSTEP = TIME STEP - SAMPLING INTERVAL (S)
 C NSTOP = NUMBER OF TIME STEP TO STOP COMPUTATIONS
 C RADIUS = RADIUS FROM AXIS OF ROTATION TO AXES OF ACCELEROMETERS (M)
 C XZERO = HORIZONTAL DISTANCE FROM AXIS TO ACCELEROMETER AXES (M)
 C AZERO = INITIAL ANGLE OF RADIUS WITH HORIZONTAL (RADIAN)
 C AZEROD = AZERO EXPRESSED IN DEGREES (DEG)
 C G = ACCELERATION DUE TO GRAVITY = 9.800 M/S**2 AT ABERDEEN
 C TIME = TIME FROM START OF LOADING (S)
 C ANGVEL = ANGULAR VELOCITY FROM RATE SENSOR (DEG/S)
 C ACH = ACCELERATION MEASURED BY ACCELEROMETER WITH AXIS
 C INITIALLY HORIZONTAL (G'S)
 C ACU = ACCELERATION MEASURED BY ACCELEROMETER WITH AXIS
 C INITIALLY VERTICAL (G'S)
 C ANGPD = ANGLE OF ROTATION FROM POTENTIOMETER (DEG)
 C FORCE = FORCE IN LOADING CABLE MEASURED BY LOAD CELL (NEWTONS)
 C ANGRSD = ANGLE ROTATED FROM START DERIVED BY INTEGRATING RATE
 C SENSOR RECORD (DEG)
 C ANGRS = ANGRSD EXPRESSED IN RADIAN (RADIAN)
 C ACKCG = ACCELERATION MEASURED BY HORIZONTAL ACCELEROMETER
 C CORRECTED FOR GRAVITATIONAL FIELD (G'S)
 C ACVCG = ACCELERATION MEASURED BY VERTICAL ACCELEROMETER
 C CORRECTED FOR GRAVITATIONAL FIELD (G'S)
 C ACXHU = X COMPONENT OF ACCELERATION OBTAINED BY COMBINING X
 C COMPONENTS FROM BOTH CORRECTED ACCELERATION RECORDS
 C (M/S**2)
 C ACYHU = Y COMPONENT OF ACCELERATION OBTAINED BY COMBINING Y
 C COMPONENTS FROM BOTH CORRECTED ACCELERATION RECORDS
 C (M/S**2)
 C VELACX = FIRST INTEGRAL OF ACXHU (M/S)
 C VELACY = FIRST INTEGRAL OF ACYHU (M/S)
 C XACRS = X DISPLACEMENT OF SENSOR ARRAY DERIVED USING ANGLE FROM
 C RATE SENSOR, SECOND INTEGRAL OF ACXHU (M)
 C YACRS = Y DISPLACEMENT OF SENSOR ARRAY DERIVED USING ANGLE FROM
 C RATE SENSOR, SECOND INTEGRAL OF ACYHU (M)
 C XRPT = X DISPLACEMENT OF SENSOR ARRAY DERIVED USING ANGLE FROM
 C POTENTIOMETER AND RADIUS TO SENSOR ARRAY (M)
 C YRPT = Y DISPLACEMENT OF SENSOR ARRAY DERIVED USING ANGLE FROM
 C POTENTIOMETER AND RADIUS TO SENSOR ARRAY (M)
 C ANGPOT = ANGPD EXPRESSED IN RADIAN (RADIAN)
 C ACKCGP = HORIZONTAL ACCELEROMETER READING ACH CORRECTED FOR
 C GRAVITATIONAL FIELD USING ANGLE FROM POTENTIOMETER (G'S)
 C ACVCGP = VERTICAL ACCELEROMETER READING ACU CORRECTED FOR GRAVI-
 C TATIONAL FIELD USING ANGLE FROM POTENTIOMETER (G'S)
 C ACKHUP = X COMPONENT OF ACCELERATION OBTAINED BY COMBINING X
 C COMPONENTS FROM BOTH CORRECTED ACCELERATION RECORDS
 C WHERE CORRECTION WAS MADE USING ANGLE FROM POTENTIOMETER
 C (M/S**2)
 C ACYHUP = Y COMPONENT OF ACCELERATION OBTAINED BY COMBINING Y
 C COMPONENTS FROM BOTH CORRECTED ACCELERATION RECORDS
 C WHERE CORRECTION WAS MADE USING ANGLE FROM POTENTIOMETER
 C (M/S**2)

```

C      VELAXP = FIRST INTEGRAL OF ACXHUP (M/S)
C      VELAYP = FIRST INTEGRAL OF ACYHUP (M/S)
C      XACPOT = X DISPLACEMENT OF SENSOR ARRAY DERIVED USING ANGLE FROM
C              POTENTIOMETER AND ACCELEROMETER RECORDS (M)
C      YACPOT = Y DISPLACEMENT OF SENSOR ARRAY DERIVED USING ANGLE FROM
C              POTENTIOMETER AND ACCELEROMETER RECORDS (M)

```

```

C      *****

```

```

C      MAIN PROGRAM

```

```

C      DIMENSION TIME(4000)  ANGVEL(4000), ACH(4000), ACU(4000),
1  ANGPJ(4000), FORCE(4000), ANGRSD(2), ANGRS(2), ACUCG(2), ACHCG(2)
2  , ACXHV(2), ACYHV(2), VELACX(2), VELACY(2), XACRS(2), YACRS(2),
3  XRPOT(4000), YRPOT(4000), ANGPOT(2), ACHCGP(2), ACUCGP(2),
4  ACXHUP(2), ACYHUP(2), VELAXP(2), VELAYP(2), XACPOT(2), YACPOT(2)
C      CHARACTER*80 ATITLE
C      CHARACTER*80 GAGES
C      CHARACTER*80 SPRNGS
C      PI = 3.141592654
C      DGTORAD = PI/180.

```

```

C      READ IN TITLE OF TEST

```

```

C      READ(5,1) ATITLE
1  FORMAT (A80)

```

```

C      READ IN GAGE DATA

```

```

C      READ (5,1) GAGES

```

```

C      READ IN SPRING DATA

```

```

C      READ (5,1) SPRNGS

```

```

C      READ IN RADIUS AND XZERO

```

```

C      READ (5,2) RADIUS, XZERO
2  FORMAT (F10.5,F11.4)

```

```

C      READ TIME STEP - SAMPLING INTERVAL, AND NUMBER OF TIME STEP FOR
C      STOPPING COMPUTATION

```

```

C      READ (5,3) TSTEP, NSTOP
3  FORMAT (F12.6,I5)

```

```

C      READ IN ACCELEROMETER, RATE SENSOR, POTENTIOMETER, AND FORCE
C      RECORDS

```

```

C      DO 5 I=1, NSTOP
4  READ (5,4) ACH(I), ACU(I), ANGVEL(I), ANGPJ(I), FORCE(I)
C      FORMAT (SF10.4)
C      IF (ACH(I).EQ.9999) GOTO 20

```

```

        TIME(I) = FLOAT(I-1) * TSTEP
        FORCE(I) = FORCE(I) * 4.448222
5      CONTINUE
20     NSTOP = I - 1

C
C
C     DEFINE GRAVITATIONAL CONSTANT (M/S**2) AT ABERDEEN
C
C     G = 9.800
C
C     COMPUTE INITIAL ANGLE
C
C     AZERO = ACOS(XZERO/RADIUS)
C     AZEROD = AZERO * (1./DGTORAD)
C
C     DEFINE INITIAL VALUES
C
C     ANGRS(1) = 0.
C     ANGRSD(1) = 0.
C     UELACX(1) = 0.
C     UELACY(1) = 0.
C     XACRS(1) = 0.
C     YACRS(1) = 0.
C     UELAXP(1) = 0.
C     UELAYP(1) = 0.
C     XACPOT(1) = 0.
C     YACPOT(1) = 0.
C     I = 1
C
C     COMPUTE START VALUES ASSUMING ACCELEROMETERS ARE HORIZONTAL AND
C     VERTICAL
C
C     ACHCG(1) = ACH(1)
C     ACVCG(1) = ACV(1)
C     ACXHV(1) = (ACVCG(1)*SIN(0.) + ACHCG(1)*COS(0.))*G
C     ACYHV(1) = (ACVCG(1)*COS(0.) - ACHCG(1)*SIN(0.))*G
C
C     COMPUTE SECOND STEP VALUES AND PERFORM INTEGRATIONS,
C     INTEGRATE ANGULAR VELOCITY
C
100    ANGRSD(2) = 0.5*(ANGVEL(I+1) + ANGVEL(I))*(TIME(I+1)-TIME(I)) +
1     ANGRSD(1)
        ANGRS(2) = ANGRSD(2)*DGTORAD
C
C     CORRECT ACCELEROMETER RECORDS FOR GRAVITY FIELD USING ANGLE
C     OBTAINED BY INTEGRATING ANGULAR VELOCITY
C
C     ACHCG(2) = ACH(I+1) + SIN(ANGRS(2))
C     ACVCG(2) = ACV(I+1) + 1. - COS(ANGRS(2))
C
C     COMPUTE COMBINED X AND Y ACCELERATIONS FROM ACCELEROMETER
C     RECORDS USING ANGLE OBTAINED BY INTEGRATING ANGULAR VELOCITY
C
C     ACXHV(2) = (ACVCG(2)*SIN(ANGRS(2)) + ACHCG(2)*COS(ANGRS(2)))*G
C     ACYHV(2) = (ACVCG(2)*COS(ANGRS(2)) - ACHCG(2)*SIN(ANGRS(2)))*G

```

```

C
C   INTEGRATE X AND Y ACCELERATIONS TO OBTAIN X VELOCITY AND DISPLAC
C   MENT AND Y VELOCITY AND DISPLACEMENT
C
C   VELACX(2) = 0.5*(ACXHUP(2) + ACXHUP(1))*(TIME(I+1)-TIME(I)) +
1  VELACX(1)
C   VELACY(2) = 0.5*(ACYHUP(2) + ACYHUP(1))*(TIME(I+1)-TIME(I)) +
1  VELACY(1)
C   XACRS(2) = 0.5*(VELACX(2) + VELACX(1))*(TIME(I+1)-TIME(I)) +
1  XACRS(1)
C   YACRS(2) = 0.5*(VELACY(2) + VELACY(1))*(TIME(I+1)-TIME(I)) +
1  YACRS(1)
C
C   REPEAT COMPUTATION USING ANGLE FROM POTENTIOMETER RECORD
C
C   IF (I.GT.1) GO TO 105
C   ANGPOT(1) = ANGPD(1)*DGTORAD
C
C   CORRECT ACCELERATION RECORDS FOR G FIELD
C
C   ACHCGP(1) = ACH(1) + SIN(ANGPOT(1))
C   ACUCGP(1) = ACU(1) + 1. - COS(ANGPOT(1))
C
C   COMPUTE COMBINED X AND Y ACCELERATIONS FROM BOTH ACCELEROMETER
C   RECORDS USING ANGLE FROM POTENTIOMETER
C
C   ACXHUP(1) = (ACUCGP(1)*SIN(ANGPOT(1)) + ACHCGP(1))*
1  COS(ANGPOT(1))*G
C   ACYHUP(1) = (ACUCGP(1)*COS(ANGPOT(1)) - ACHCGP(1))*
1  SIN(ANGPOT(1))*G
C
C   COMPUTE SECOND STEP VALUES AND PERFORM INTEGRATIONS
C
105  ANGPOT(2) = ANGPD(I+1)*DGTORAD
C
C   CORRECT ACCELEROMETER RECORDS FOR GRAVITY FIELD
C
C   ACHCGP(2) = ACH(I+1) + SIN(ANGPOT(2))
C   ACUCGP(2) = ACU(I+1) + 1. - COS(ANGPOT(2))
C
C   COMPUTE COMBINED X AND Y ACCELERATIONS FROM BOTH ACCELEROMETER
C   RECORDS USING ANGLE OBTAINED FROM POTENTIOMETER
C
C   ACXHUP(2) = (ACUCGP(2)*SIN(ANGPOT(2)) + ACHCGP(2))*
1  COS(ANGPOT(2))*G
C   ACYHUP(2) = (ACUCGP(2)*COS(ANGPOT(2)) - ACHCGP(2))*
1  SIN(ANGPOT(2))*G
C
C   INTEGRATE X AND Y ACCELERATIONS TO OBTAIN X VELOCITY AND
C   DISPLACEMENT AND Y VELOCITY AND DISPLACEMENT
C
C   VELAXP(2) = 0.5*(ACXHUP(2) + ACXHUP(1))*(TIME(I+1)-TIME(I)) +
1  VELAXP(1)
C   VELAYP(2) = 0.5*(ACYHUP(2) + ACYHUP(1))*(TIME(I+1)-TIME(I)) +

```

```

1  UELAYP(1)
   XACPOT(2) = 0.5*(UELAXP(2) + UELAXP(1))*(TIME(I+1)-TIME(I)) +
1  XACPOT(1)
   YACPOT(2) = 0.5*(UELAYP(2) + UELAYP(1))*(TIME(I+1)-TIME(I)) +
1  YACPOT(1)

C
C   CALCULATE X AND Y DISPLACEMENTS FROM RADIUS AND ANGLE
C
   IF (I.GT.1) GO TO 106
   XRPOT(1) = RADIUS*(COS(AZERO)-COS((ANGPD(1)*DGTORAD)
1  + AZERO))
   YRPOT(1) = RADIUS*(SIN((ANGPD(1)*DGTORAD) + AZERO) -
1  SIN(AZERO))
106  XRPOT(I+1) = RADIUS*(COS(AZERO) - COS((ANGPD(I+1)*(PI/
1  180.)) + AZERO))
   YRPOT(I+1) = RADIUS*(SIN((ANGPD(I+1)*DGTORAD) + AZERO)
1  - SIN(AZERO))

C
C   PRINT RESULTS
C
   IF(I.GT.1) GO TO 101
   WRITE (6,6)
6  FORMAT (1H1)
   WRITE (6,7)
7  FORMAT (/)
   WRITE (6,8) ATITLE
8  FORMAT (5X,A80)
   WRITE (6,7)
   WRITE (6,8) GAGES
   WRITE (6,7)
   WRITE (6,8) SPRNGS
   WRITE (6,7)
   WRITE (6,7)
   WRITE (6,8) RADIUS
9  FORMAT (10X, 9HRADIUS = , F10.4, 8H METRES)
   WRITE (6,10) XZERO
10  FORMAT (11X, 8HXZERO = ,F10.4, 8H METRES)
   WRITE (6,11) AZEROD
11  FORMAT (10X, 9HAZEROD = ,F10.4, 9H DEGREES)
   WRITE (6,12) G
12  FORMAT (15X, 4HG = , F10.4, 8H M/S**2)
   WRITE (6,6)
   WRITE (6,7)
   WRITE (6,13)
13  FORMAT (1X, 6H TIME ,4X, 5HANGPD, 2X, 6HANGRSD, 2X, 6HANGVEL, 4X, 3HACH,
1  5X, 3HACV, 3X, 5HFORCE, 4X, 5HACHCG, 3X, 5HACVCG, 3X, 5HACHXHU, 3X, 5HACYHU,
2  2X, 5HXACRS, 1X, 6HXACPOT, 2X, 5HXRPT, 2X, 5HYACRS, 1X, 6HYACPOT, 2X,
3  5HYPPOT)
   WRITE (6,14)
14  FORMAT (1X, 4H (S), 6X, 5H(DEG), 2X, 5H(DEG), 2X, 7H(DEG/S), 3X, 5H(G'S),
1  3X, 5H(G'S), 3X, 3H(N), 5X, 5H(G'S), 3X, 5H(G'S), 1X, 7H(M/S**2, 1X,
2  7H(M/S**2), 3X, 3H(M), 4X, 3H(M), 4X, 3H(M), 4X, 3H(M), 4X, 3H(M))
   WRITE (6,7)
   WRITE (6,15) TIME(I), ANGPD(1), ANGRSD(1), ANGVEL(1), ACH(1), ACV(1),

```

```

1  FORCE(1),ACHCG(1),ACUCG(1),ACXHU(1),ACYHU(1),XACRS(1),
2  XACPOT(1),XRPOI(1),YACRS(1),YACPOT(1),YRPOI(1)
15  FORMAT (F8.5,SF8.3,F8.2,4F8.3,6F7.3)
101 WRITE (6,15) TIME(I+1),ANGPD(I+1),ANGRSD(2),ANGVEL(I+1),ACH(I+1),
1  ACV(I+1),FORCE(I+1),ACHCG(2),ACUCG(2),ACXHU(2),ACYHU(2),
2  XACRS(2),XACPOT(2),XRPOI(I+1),YACRS(2),YACPOT(2),YRPOI(I+1)
C
C  SET COMPUTED VALUES AS INITIAL VALUES FOR THE NEXT ITERATION
C
  ANGRSD(1) = ANGRSD(2)
  ANGRS(1) = ANGRS(2)
  ACHCG(1) = ACHCG(2)
  ACUCG(1) = ACUCG(2)
  ACXHU(1) = ACXHU(2)
  ACYHU(1) = ACYHU(2)
  VELACX(1) = VELACX(2)
  VELACY(1) = VELACY(2)
  XACRS(1) = XACRS(2)
  YACRS(1) = YACRS(2)
  ANGPOT(1) = ANGPOT(2)
  ACHCGP(1) = ACHCGP(2)
  ACUCGP(1) = ACUCGP(2)
  ACXHUP(1) = ACXHUP(2)
  ACYHUP(1) = ACYHUP(2)
  VELAXP(1) = VELAXP(2)
  VELAYP(1) = VELAYP(2)
  XACPOT(1) = XACPOT(2)
  YACPOT(1) = YACPOT(2)
  IF (I.EQ.NSTOP) STOP
  I = I+1
  GO TO 100
  END

```


LIST OF SYMBOLS

- $\underline{a}, \underline{a}$ = acceleration (underlining denotes a vector quantity)
- a_H = acceleration output of the initially horizontal accelerometer
- a_{HR} = acceleration due to rotation sensed by initially horizontal accelerometer
- a_{H1} = starting acceleration for the horizontal accelerometer
- a_{Hg1} = a_{H1} corrected for gravity
- a_{H2} = acceleration at time t_2 for the horizontal accelerometer
- a_{Hg2} = a_{H2} corrected for gravity
- a_N = acceleration magnitude due to rotation at radius R_2 that is along radius R_2 and normal to the path of movement
- a_T = acceleration magnitude due to rotation at radius R_2 that is perpendicular to the radius and tangent to the path of movement
- a_V = acceleration output of initially vertical accelerometer
- a_{VR} = acceleration due to rotation sensed by initially vertical accelerometer
- a_{V1} = starting acceleration for the vertical accelerometer
- a_{Vg1} = a_{V1} corrected for gravity
- a_{V2} = acceleration at time t_2 for the vertical accelerometer
- a_{Vg2} = a_{V2} corrected for gravity
- A_{X1} = starting horizontal (X) component of acceleration at accelerometers in fixed coordinate system
- A_{X2} = horizontal (X) component of acceleration at accelerometer at time t_2 in fixed coordinate system
- A_{Y1} = starting vertical (Y) component of acceleration at accelerometers in fixed coordinate system
- A_{Y2} = vertical (Y) component of acceleration at accelerometer at time t_2 in fixed coordinate system
- a_g = acceleration due to gravity
- l = constant length of force moment arm
- I_{axis} = moment of inertia about axis of quarter wheel and sensors

- k_1 = spring constant for high force spring
- k_2 = spring constant for low force spring
- m = mass of quarter wheel and sensors
- ω = wheel in revolutions per minute of spin table
- p = position of point P as measured in the body-centered system
- r = radius to the seismic mass in inches on a spin table
- r_0 = position of point P in fixed coordinate system
- r_0^0 = initial position of point P in fixed coordinate system
- \ddot{r}_0 = acceleration of point P in fixed coordinate system
- r_1 = radius from axis to sensitive masses of the accelerometers on the quarter wheel
- R = position in fixed coordinate system of origin of body-centered coordinate system
- r_2 = radius from axis to center of gravity of quarter wheel
- r_3 = radius from axis to accelerometers
- \ddot{R} = acceleration of the origin of the body-centered system
- t = time
- t_1 = start time
- t_2 = second time value
- v_{x1} = X component of velocity at accelerometers at start time
- v_{x2} = X component of velocity at accelerometers at time t_2
- v_{y1} = Y component of velocity at accelerometers at start time
- v_{y2} = Y component of velocity at accelerometers at time t_2
- v = velocity of point P in a rigid body relative to fixed coordinate system
- v_0 = initial velocity of point P in fixed coordinate system
- w = weight, mg, of the quarter wheel and sensors
- x = starting horizontal displacement of the accelerometers in fixed coordinate system

- X_2 = horizontal displacement of the accelerometers at time t_2 in fixed coordinate system
 Y_1 = starting vertical displacement of the accelerometers in fixed coordinate system
 Y_2 = vertical displacement of the accelerometers at time t_2 in fixed coordinate system
 Z_1 = initial extension in length beyond its rest position of high force spring in test facility model
 Z_2 = initial extension in length beyond its rest position of low force spring in test facility model
 θ = angle of rotation from an initial position
 θ_0 = initial angle of R with respect to the horizontal
 θ_1 = initial value of rotation angle θ ($\theta_1 = 0$), or initial angle of R_1 with respect to the horizontal
 θ_2 = initial angle of R_2 with respect to the horizontal
 θ_{RS1} = initial angle of rotation of rate sensor
 θ_{RS2} = integrated value for angle of rotation at time t_2 using angular velocity from rate sensor
 θ_{p2} = rotation angle at time t_2 derived from potentiometer record
 $\dot{\theta}$ = $\frac{d\theta}{dt}$, angular velocity
 $\dot{\theta}_{RS1}$ = initial angular velocity from rate sensor
 $\dot{\theta}_{RS2}$ = angular velocity at time t_2 from rate sensor
 $\ddot{\theta}$ = $\frac{d^2\theta}{dt^2}$, angular acceleration
 ω = angular velocity of the body-centered system relative to the fixed system
 $\dot{\omega}$ = time rate of change of angular velocity

<u>pies</u>	<u>Organization</u>	<u>Copies</u>	<u>Organization</u>
12	Administrator Defense Technical Information Center ATTN: DTIC-FDAC Cameron Station, Bldg 5 Alexandria, VA 22304-6145	9	Director Defense Nuclear Agency ATTN: DDST TIPL/Tech Lib SPSS/K. Goering SPTD/T. Kennedy SPAS/P.R. Rohr G. Ullrich STSP/COL Kovel NATD NATA Washington, DC 20305
1	Director of Defense Research & Engineering ATTN: DD/TWP Washington, DC 20301	2	Commander Field Command Defense Nuclear Agency ATTN: FCPR FCTMOF Kirtland AFB, NM 87115
1	Asst. to the Secretary of Defense (Atomic Energy) ATTN: Document Control Washington, DC 20301	1	Commander Field Command, DNA Livermore Branch ATTN: FCPRL P.O. Box 808 Livermore, CA 94550
1	Director Defense Advanced Research Projects Agency ATTN: Tech Lib 1400 Wilson Boulevard Arlington, VA 22209	1	HQDA (DAMA-ART-M) Washington, DC 20310
2	Director Federal Emergency Management Agency ATTN: D. A. Bettge Technical Library Washington, DC 20472	10	C.I.A. OIR/DB/Standard GE47 HQ Washington, D.C. 20505
1	Director Defense Intelligence Agency ATTN: DT-2/Wpns & Sys Div Washington, DC 20301	1	Program Manager US Army BMD Program Office ATTN: John Shea 5001 Eisenhower Avenue Alexandria, VA 22333
1	Director National Security Agency ATTN: E. F. Butala, R15 Ft. George G. Meade, MD 20755	2	Commander US Army BMD Advanced Technology Center ATTN: CRDABH-X CRDABH-S P.O. Box 1500 Huntsville, AL 35807
1	Director Joint Strategic Target Planning Staff JCS Offut AFB Omaha, NB 68113		

DISTRIBUTION LIST

<u>No. of Copies</u>	<u>Organization</u>	<u>No. of Copies</u>	<u>Organization</u>
1	Commander US Army BMD Command ATTN: BDMSC-TFN/N.J. Hurst P.O. Box 1500 Huntsville, AL 35807	1	U.S. Army Armament, Munitions and Chemical Command ATTN: AMSMC-IMP-L Rock Island, IL 61299-7300
1	Commander US Army Engineer Division ATTN: HNDED-FD P.O. Box 1500 Huntsville, AL 35807	1	Commander US AMCCOM ARDEC CCAC Benet Weapons Laboratory ATTN: SMCAR-CCB-TL Watervliet, NY 12189-4050
2	Deputy Chief of Staff for Operations and Plans ATTN: Technical Library Director of Chemical & Nuc Operations Department of the Army Washington, DC 20310	1	Commander U.S. Army Aviation Systems Command ATTN: AMSAV-ES 4300 Goodfellow Blvd. St. Louis, MO 63120-1798
3	Director US Army Engineer Waterways Experiment Station ATTN: Technical Library Jim Watt Jim Ingram P.O. Box 631 Vicksburg, MS 39180-0631	1	Director U.S. Army Aviation Research and Technology Activity Ames Research Center Moffett Field, CA 94035-1099
1	Commander US Army Materiel Command ATTN: AMCDRA-ST 5001 Eisenhower Avenue Alexandria, VA 22333-0001	1	Commander US Army Communications - Electronics Command ATTN: AMSEL-ED Fort Monmouth, NJ 07703-5301
1	Commander US Army Armament Research, Development and Engineering Center ATTN: SMCAR-MSI Dover, NJ 07801-5001	1	Commander US Army Communications Rsch and Development Command ATTN: DRSEL-ATDD Fort Monmouth, NJ 07703
1	Commander US Army Armament Research, Development and Engineering Center ATTN: SMCAR-TDC Dover, NJ 07801	1	Commander CECOM R&D Technical Library ATTN: AMSEL-IM-L (Reports Section) B.2700 Fort Monmouth, NJ 07703-5301
		2	Commander US Army Electronics Research and Development Command ATTN: DELEW-E, W. S. McAfee DELSA-EI, J. Roma Fort Monmouth, NJ 07703-5301

DISTRIBUTION LIST

<u>No. of Copies</u>	<u>Organization</u>	<u>No. of Copies</u>	<u>Organization</u>
6	Director US Army Harry Diamond Labs ATTN: Mr. James Gaul Mr. L. Belliveau Mr. J. Meszaros Mr. J. Gwaltney Mr. Bill Vault Mr. R. J. Bostak 2800 Powder Mill Road Adelphi, MD 20783-1197	1	Commander US Army Logistics Management Center ATTN: ATCL-O, Mr. Robert Cameron Fort Lee, VA 23801
		2	Commander US Army Materials Technology Laboratory ATTN: AMXMR-ATL Eugene de Luca Watertown, MA 02172-0001
4	Director US Army Harry Diamond Labs ATTN: SLCHD-TA-L DRXDO-TI/002 DRXDO-NP SLCHD-RBA/J. Rosado 2800 Powder Mill Road Adelphi, MD 20783-1197	1	Commander US Army Research Office ATTN: SLCRO-D P.O. Box 12211 Research Triangle Park NC 27709-2211
1	Commander US Army Missile Command ATTN: AMSMI-RD Redstone Arsenal, AL 35898-5245	4	Commander US Army Nuclear & Chemical Agency ATTN: ACTA-NAW MONA-WE Technical Library LTC Finno 7500 Backlick Rd, Bldg. 2073 Springfield, VA 22150
1	Director US Army Missile and Space Intelligence Center ATTN: AIAMS-YDL Redstone Arsenal, AL 35898-5500		
2	Commander US Army Natick Research and Development Center ATTN: AMDNA-D/Dr. D. Sieling STRNC-UE/J. Calligeros Natick, MA 01762	1	Commander US Army TRADOC ATTN: DCST&E Fort Monroe, VA 23651
		2	Director US Army TRADOC Systems Analysis Activity ATTN: LTC John Hesse ATOR-TSL White Sands Missile Range, NM 88002-5502
1	Commander US Army Tank-Automotive Command ATTN: AMSTA-TSL Warren, MI 48397-5000		
1	Commander US Army Foreign Science and Technology Center ATTN: Research and Data Br 220 7th Street, NE Charlottesville, VA 22901	2	Commandant U.S. Army Infantry School ATTN: ATSH-CD-CS-OR Fort Benning, GA 31905-5400

DISTRIBUTION LIST

<u>No. of Copies</u>	<u>Organization</u>	<u>No. of Copies</u>	<u>Organization</u>
1	Commander U.S. Army Development and Employment Agency ATTN: MODE-ORO Fort Lewis, WA 98433-5000	1	Commander Naval Sea Systems Command ATTN: Code SEA-62R Department of the Navy Washington, DC 20362-5101
1	Commandant Interservice Nuclear Weapons School ATTN: Technical Library Kirtland AFB, NM 87115	3	Officer-in-Charge(Code L31) Civil Engineering Laboratory Naval Construction Battalion Center ATTN: Stan Takahashi R. J. Odello Technical Library Port Hueneme, CA 93041
1	Chief of Naval Material ATTN: MAT 0323 Department of the Navy Arlington, VA 22217	1	Commander David W. Taylor Naval Ship Research & Development Command ATTN: Lib Div, Code 522 Bethesda, MD 20084-5000
2	Chief of Naval Operations ATTN: OP-03EG OP-985F Department of the Navy Washington, DC 20350	1	Commander Naval Surface Weapons Center ATTN: DX-21, Library Br. Dahlgren, VA 22448-5000
1	Chief of Naval Research ATTN: N. Perrone Department of the Navy Arlington, VA 22217	2	Commander Naval Surface Weapons Center ATTN: Code WA501/Navy Nuclear Programs Office Code WX21/Tech Library Silver Spring, MD 20902-5000
1	Director Strategic Systems Projects Ofc ATTN: NSP-43, Tech Library Department of the Navy Washington, DC 20360	1	Commander Naval Weapons Center ATTN: Code 533, Tech Lib China Lake, CA 93555-6001
1	Commander Naval Electronic Systems Com ATTN: PME 117-21A Washington, DC 20360	1	Commander Naval Weapons Evaluation Fac ATTN: Document Control Kirtland AFB, NM 87117
1	Commander Naval Facilities Engineering Command Washington, DC 20360	1	Commander Naval Research Laboratory ATTN: Code 2027, Tech Lib Washington, DC 20375

DISTRIBUTION LIST

<u>No. of</u> <u>Copies</u>	<u>Organization</u>	<u>No. of</u> <u>Copies</u>	<u>Organization</u>
1	Superintendent Naval Postgraduate School ATTN: Code 2124, Technical Reports Library Monterey, CA 93940	1	Director Lawrence Livermore Lab. ATTN: Tech Info Dept L-3 P.O. Box 808 Livermore, CA 94550
1	AFSC/SDOA Andrews Air Force Base MD 20334	2	Director Los Alamos Scientific Lab. ATTN: Doc Control for Rpts Lib P.O. Box 1663 Los Alamos, NM 87545
1	AFWL/SUL Kirtland AFB, NM 87117	2	Director Sandia National Laboratories ATTN: Doc Control for 3141 Sandia Rpt Collection L. J. Vortman P.O. Box 5800 Albuquerque, NM 87185-5800
1	AFATL/DOIL (Tech Info Center) Eglin AFB, FL 32542-5438	1	Director Sandia Laboratories Livermore Laboratory ATTN: Doc Control for Technical Library P.O. Box 969 Livermore, CA 94550
1	AFESC/RDCS ATTN: Paul Rosengren Tyndall AFB, FL 32403	1	Director National Aeronautics and Space Administration Scientific & Tech Info Fac P.O. Box 8757 Baltimore/Washington International Airport MD 21240
1	AFATL (DLYV) Eglin AFB, FL 32542-5438	1	Director NASA-Ames Research Center Applied Computational Aerodynamics Branch MS 202-14, Dr. T. Holtz Moffett Field, CA 94035
1	RADC (EMTLD/Docu Library) Griffiss AFB, NY 13441		
1	AFWL/NTES, R. Henny Kirtland AFB, NM 87117-6008		
1	AFWL/NTED, J. W. Aubrey Kirtland AFB, NM 87117-6008		
2	Commander-in-Chief Strategic Air Command ATTN: NRI-STINFO Lib Offutt AFB, NB 68113		
1	AFIT (Lib Bldg. 640, Area B) Wright-Patterson AFB Ohio 45433		
1	FTD/NIIS Wright-Patterson AFB Ohio 45433		

DISTRIBUTION LIST

<u>No. of</u> <u>Copies</u>	<u>Organization</u>	<u>No. of</u> <u>Copies</u>	<u>Organization</u>
3	Aberdeen Research Center ATTN: N.H. Ethridge J. Keefer Library P.O. Box 548 30 Diamond Street Aberdeen, MD 21001	1	California Research & Technology, Inc. ATTN: M. Rosenblatt 20943 Devonshire Street Chatsworth, CA 91311
1	Aerospace Corporation ATTN: Tech Info Services P.O. Box 92957 Los Angeles, CA 90009	1	Carpenter Research Corporation ATTN: H. Jerry Carpenter Suite 424 904 Silver Spur Road Rolling Hills Estates, CA 90274
1	Applied Physics Inc ATTN: Paul H. Frisch 31 Highview Avenue Manuet, NY 10954	3	EG&G Idaho, Inc. ATTN: W. C. Reed W. H. Landman, Jr R. A. Berry P.O. Box 1625 Idaho Falls, ID 83415
1	Applied Research Associates, Inc. ATTN: Robert L. Guice 7114 West Jefferson Ave., Suite 305 Lakewood, Colorado 80235	1	Goodyear Aerospace Corp ATTN: R. M. Brown, Bldg 1 Shelter Engineering Litchfield Park, AZ 85340
1	The BDM Corporation ATTN: Richard Hensley P.O. Box 9274 Albuquerque International Albuquerque, NM 87119	6	Kaman Avidyne ATTN: Dr. R. Reutenick (4 cys) Mr. S. Criscione Mr. R. Milligan 83 Second Avenue Northwest Industrial Park Burlington, MA 01830
1	Black & Veatch Engineers-Architects ATTN: John L. Evans P.O. Box 8405 Kansas City, MO 64114	1	Kaman Sciences Corporation ATTN: Frederic W. Balicki 1613 University Blvd., N.E. Albuquerque, NM 87102
1	The Boeing Company ATTN: Aerospace Library P.O. Box 3707 Seattle, WA 98124	3	Kaman Sciences Corporation ATTN: Library P. A. Ellis F. H. Shelton 1500 Garden of the Gods Road Colorado Springs, CO 80907
1	California Research and Technology ATTN: F. Sauer Suite B 130 11875 Dublin Blvd Dublin, CA 94568		

DISTRIBUTION LIST

<u>No. of Copies</u>	<u>Organization</u>	<u>No. of Copies</u>	<u>Organization</u>
3	Kaman-TEMPO ATTN: DASIAC Don Sachs P.O. Drawer QQ 316 State Street Santa Barbara, CA 93102	2	Science Applications, Inc. ATTN: W. Layson John Cockayne PO BOX 1303 1710 Goodridge Drive McLean, VA 22102
1	Lockheed Missiles & Space Co. ATTN: J. J. Murphy, Dept. 81-11, Bldg. 154 P.O. Box 504 Sunnyvale, CA 94086	1	Science Applications, Inc. ATTN: Technical Library 1250 Prospect Plaza La Jolla, CA 92037
1	Martin Marietta Aerospace Orlando Division ATTN: G. Fotieo P.O. Box 5837 Orlando, FL 32805	1	Sparta, Inc. Los Angeles Operations ATTN: Irving B. Osofsky 3440 Carson Street Suit 300 Torrance CA 90503
2	McDonnell Douglas Astronautics Corporation ATTN: Robert W. Halprin K.A. Heinly 5301 Bolsa Avenue Huntington Beach, CA 92647	1	Sverdrup Technology Inc. ATTN: R. F. Starr P.O. Box 884 Tullahoma, TN 37388
1	New Mexico Engineering Research Institute (CERF) ATTN: J. Leigh P.O. Box 25 UNM Albuquerque, NM 87131	2	Systems, Science and Software ATTN: C. E. Needham Lynn Kennedy PO Box 8243 Albuquerque, NM 87198
2	Physics International Corp 2700 Merced Street San Leandro, CA 94577	3	Systems, Science and Software ATTN: Technical Library R. Duff K. Pyatt PO Box 1620 La Jolla, CA 92037
2	R&D Associates ATTN: Technical Library Allan Kuhl P.O. Box 9695 Marina del Rey, CA 90291	1	Texas Engineering Experiment Station ATTN: Dr. D. Anderson 301 Engineering Research Center College Station, TX 77843
1	R&D Associates ATTN: G.P. Ganong P.O. Box 9335 Albuquerque, NM 87119	2	TRW Systems Group ATTN: Benjamin Sussholtz Stanton Fink One Space Park Redondo Beach, CA 90278

DISTRIBUTION LIST

<u>No. of Copies</u>	<u>Organization</u>	<u>No. of Copies</u>	<u>Organization</u>
1	TRW Ballistic Missile Division ATTN: H. Korman, Mail Station 526/614 P.O. Box 1310 San Bernadino, CA 92402	1	Stanford University ATTN: Dr. D. Bershader Durand Laboratory Stanford, CA 94305
			<u>Aberdeen Proving Ground</u>
1	Battelle Memorial Institute ATTN: Technical Library 505 King Avenue Columbus, OH 43201		Dir, USAMSAA ATTN: AMXSJ-D AMXSJ-MP, H. Cohen
1	California Inst of Tech ATTN: T. J. Ahrens 1201 E. California Blvd. Pasadena, CA 91109		Cdr, USATECOM ATTN: AMSTE-SI-F Cdr, CRDC, AMCCOM ATTN: SMCCR-RSP-A SMCCR-MJ SMCCR-SPS-IL
2	Denver Research Institute University of Denver ATTN: Mr. J. Wisotski Technical Library PO Box 10127 Denver, CO 80210		
1	Massachusetts Institute of Technology Aeroelastic and Structures Research Laboratory ATTN: Dr. E. A. Witmer Cambridge, MA 02139		
1	Northrop University Mechanical Engineering Dept. ATTN: Frederick B. Safford 5800 W. Arbor Vitae St. Los Angeles, CA 90045		
2	Southwest Research Institute ATTN: Dr. W. E. Baker A. B. Wenzel 8500 Culebra Road San Antonio, TX 78228		
1	SRI International ATTN: Dr. G. R. Abrahamson 333 Ravenswood Avenue Menlo Park, CA 94025		

USER EVALUATION SHEET/CHANGE OF ADDRESS

This Laboratory undertakes a continuing effort to improve the quality of the reports it publishes. Your comments/answers to the items/questions below will aid us in our efforts.

1. BRL Report Number _____ Date of Report _____
2. Date Report Received _____
3. Does this report satisfy a need? (Comment on purpose, related project, or other area of interest for which the report will be used.) _____

4. How specifically, is the report being used? (Information source, design data, procedure, source of ideas, etc.) _____

5. Has the information in this report led to any quantitative savings as far as man-hours or dollars saved, operating costs avoided or efficiencies achieved, etc? If so, please elaborate. _____

6. General Comments. What do you think should be changed to improve future reports? (Indicate changes to organization, technical content, format, etc.) _____

CURRENT ADDRESS

Name _____

Organization _____

Address _____

City, State, Zip _____

7. If indicating a Change of Address or Address Correction, please provide the New or Correct Address in Block 6 above and the Old or Incorrect address below.

OLD ADDRESS

Name _____

Organization _____

Address _____

City, State, Zip _____

(Remove this sheet, fold as indicated, staple or tape closed, and mail.)

FOLD HERE

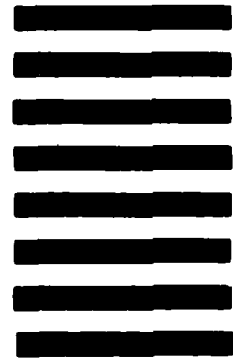
Director
US Army Ballistic Research Laboratory
ATTN: DRXBR-OD-ST
Aberdeen Proving Ground, MD 21005-5066



NO POSTAGE
NECESSARY
IF MAILED
IN THE
UNITED STATES

OFFICIAL BUSINESS
PENALTY FOR PRIVATE USE, \$300

BUSINESS REPLY MAIL
FIRST CLASS PERMIT NO 12062 WASHINGTON, DC
POSTAGE WILL BE PAID BY DEPARTMENT OF THE ARMY



Director
US Army Ballistic Research Laboratory
ATTN: DRXBR-OD-ST
Aberdeen Proving Ground, MD 21005-9989

FOLD HERE

ENVI

DATED

FILM

8-88

otic